Polarized partons in hadrons at high energy

The structure of hadrons from single and double parton interactions

Sabrina Cotogno

Leescommissie: prof.dr. D. Boer (Rijksuniversiteit Groningen)
prof.dr. E.L.M.P. Laenen (Universiteit van Amsterdam)
dr. C. Lorcé (École Polytechique, CPHT)
dr. T. Kasemets (Johannes Gutenberg Universität Mainz)
prof.dr. B. Pasquini (Università degli Studi di Pavia)
prof.dr. H.G. Raven (Vrije Universiteit Amsterdam)

ISBN: 978-94-9301-440-4
Printed by: Gildeprint - Enschede
Front cover: Illustration and layout by Marta Comito

This work is part of the European Research Council (ERC) under the program QWORK (contract no. 320389). The scientific research described in this thesis has been accomplished at the department of Physics and Astronomy of the Vrije Universitetit Amsterdam (VU) and the National Institute for subatomic Physics (Nikhef).

VRIJE UNIVERSITEIT

Polarized partons in hadrons at high energy

The structure of hadrons from single and double parton interactions

ACADEMISCH PROEFSCHRIFT

ter verkrijging van de graad Doctor aan
de Vrije Universiteit Amsterdam,
op gezag van de rector magnificus
prof.dr. V. Subramaniam,
in het openbaar te verdedigen
ten overstaan van de promotiecommissie
van de Faculteit der Bètawetenschappen
op maandaag 15 oktober 2018 om 11.45 uur
in het auditorium van de universiteit,
De Boelelaan 1105

door

Sabrina Cotogno

geboren te Enna, Italië

promotor:	prof.dr. P.J.G. Mulders
copromotor:	prof.dr. A. Bacchetta

“ [...] Quel che nel cuore resta a meraviglia
è sempre l’immagine della mia famiglia”
R. C.

To my dear dad

Contents

Scientific publications

This thesis is partially based on the following publications:

1. Daniël Boer, Sabrina Cotogno, Tom van Daal, Piet J. Mulders, Andrea Signori, and Yajin Zhou
   Gluon and Wilson loop TMDs for hadrons of spin ≤ 1
   JHEP 1610 (2016) 013 - `arXiv:1607.01654 [hep-ph]`.

2. Alessandro Bacchetta, Sabrina Cotogno, and Barbara Pasquini
   The transverse structure of the pion in momentum space inspired by the Ad-S/QCD correspondence
   Phys.Lett. B771(2017) 546-552 - `arXiv:1703.07669 [hep-ph]`.

3. Sabrina Cotogno, Tom van Daal, and Piet. J. Mulders
   Positivity bounds on gluon TMDs for hadrons of spin ≤ 1
   JHEP 11 (2017) 185 - `arXiv:1709.07827 [hep-ph]`.

4. Sabrina Cotogno, Tomas Kasemets, and Miroslav Myska
   Parton correlations in same sign W boson pair production at the LHC
   In preparation.

Conference proceedings

1. Alessandro Bacchetta, Sabrina Cotogno, Barbara Pasquini
   Internal Structure of the Pion Inspired by the AdS/QCD Correspondence
   contribution to the Light Cone Conference, Frascati 2015
   Few Body Syst. 57 (2016) no.6, 443-447

2. Daniël Boer, Sabrina Cotogno, Tom van Daal, Piet J. Mulders, Andrea Signori, and Yajin Zhou
   Gluon transverse momentum dependent correlators in polarized high energy processes
   Proceedings of the 24$^{\text{th}}$ International Workshop on Deep-Inelastic Scattering and Related Subjects (DIS 2016)
   PoS DIS2016 (2016) 207 - `arXiv:1609.02788 [hep-ph]`.

3. Sabrina Cotogno
   Parametrization of the Transverse Momentum Dependent Light-Front correlator for gluons
   contribution to the Light Cone Conference, Lisbon 2016
   Few Body Syst. 58 (2017) no.2, 92

Chapter 1

Introduction

1.1 Inside hadrons

An outstanding problem in particle physics is the description of the structure of hadrons in terms of their elementary degrees of freedom, quarks and gluons (collectively called *partons*). The most common hadrons are protons and neutrons, which build the atomic nuclei and make up almost all the visible mass of the universe.

The fundamental theory that governs the interactions between partons is called Quantum Chromo-Dynamics (QCD). This is a non-abelian gauge theory with local gauge group $SU(3)$. Similarly to the theory of electrodynamics (QED), where the electric charge is defined with respect to the $U(1)$ symmetry, in QCD we associate the so-called color charges to the symmetry group $SU(3)$. The peculiarity of QCD is that the strength of the interaction between partons through their color charges, varies considerably with the energy scales, being strong at low energies and progressively becoming weaker as the energy increases, as shown in Fig. 1.1.

Hadrons at very short distances correspond to an infinite number of almost free partons, only weakly interacting through their color (and electroweak) charges. The appropriate degrees of freedom in the description are no longer the hadrons themselves, but the elementary fields. This regime of QCD is called *asymptotic freedom* [1, 2]. Perturbative QCD (pQCD) methods are valid tools, because the coupling constant of the color interaction is weak, and the interacting theory can be com-

puted as a perturbation of the free theory. As soon as the energy gradually decreases, asymptotically free partons are replaced by strongly coupled constituents [3,4], which are effectively described as a cloud of gluons and quark-antiquark pairs. The partons appear *confined* inside the hadrons, and the theoretical tools available to describe hadronic structure cannot rely any longer upon perturbation theory.

As a matter of fact, a colored particle has never been detected, and only hadrons can eventually be observed in the detectors. It is impossible to tear them apart to measure the constituents directly, without creating new colorless hadrons, inside which the color interaction is contained. Information on the constituents is derived indirectly and a consistent framework needs to be developed.

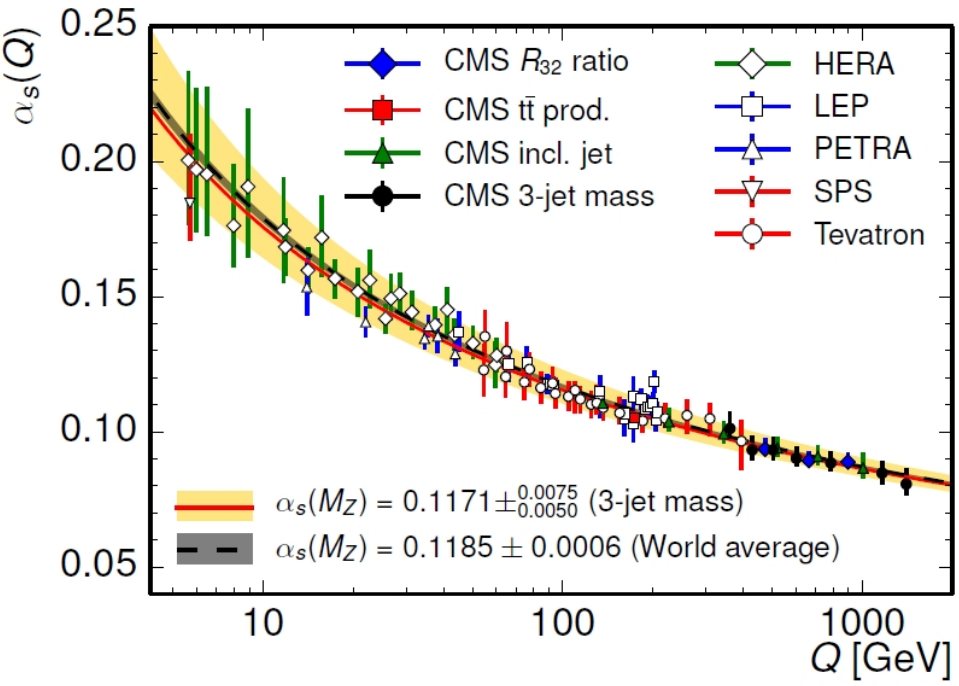

Figure 1.1: The QCD coupling constant $\alpha_s(Q)$ from different measurements, as a function of the energy scale Q. Figure taken from ref. [5].

1.2 Multidimensional imaging of hadrons

Several properties of hadrons, such as their mass and spin, are intimately connected to the dynamics of partons and their distributions in position and momentum space.

High-energy processes are the perfect tools to access indirect information on quarks and gluons at different energy and distance scales. Since both the long- and short-distances are probed, the description of such processes contains a perturbative (calculable) part and a nonperturbative part. Extracting information on the latter from experiments must rely on a solid theoretical framework.

Parton distributions

The fundamental objects which contain the nonperturbative information about the hadron structure in terms of the constituents are called correlators. They are not calculable directly and can be parametrized in terms of multidimensional parton distribution functions, each of them related to different portions of the hadron phase space.

For instance, the information about the longitudinal fraction of momentum, carried by the partons, is encoded in the parton distribution functions (PDFs), while the complete information on the motion of partons in the three-dimensional (longitudinal and transverse) momentum space is contained in the transverse momentum dependent parton distributions (TMDPDFs or TMDs). A complementary picture to the TMDs, in a different three-dimensional portion of the hadron phase-space, is given by the Generalized Parton Distributions (GPDs). The combined knowledge encoded in TMDs and GPDs provides information on the transverse structure of the hadron in momentum and coordinate space.

To reach a thorough description of the hadron structure, we also need to look at multiple partons at the same time. If we restrict ourselves to the simplest two-parton correlations, this information is encoded in the double parton distributions (DPDs), which are functions of the longitudinal momentum carried by two partons and their relative separation in the transverse plane. DPDs are accessible in experiments in which two high-energetic scatterings occur simultaneously (double parton scatterings).

All the functions mentioned above include the information on the parton spin, and, in the DPDs case, on the other quantum numbers of the partons. If the target spin states are also included in the description, the number of functions increases and the information acquired comprehends several kind of spin correlations between the partons and the hadron. However, not all the functions are involved at the same time

in the computation of the cross-section of high energy processes. Depending on the specific process, the polarization state of the hadron, and the detected final states, different projections of the hadron structure become accessible.

Combining the different parton distributions is similar to a mosaic: each piece comes from a different place and occupies a relevant position on its own, but the final picture is complete only once all the tiles are assembled. Aiming for such a complete knowledge is indispensable to address the fundamental questions about the origin of hadron mass and spin, and the mechanism of confinement.

Light-front wave functions

When dealing with nonperturbative quantities, one needs to select the most suitable framework carefully. It is especially convenient to use the light-front quantization of QCD, i.e. a formulation of the theory of QCD obtained by using a different time component (light-cone time) than the usual one. Light-front QCD is widely employed in the field of high-energy physics, as it represents a very natural choice of frame for describing the hadron in this kinematic regime. In addition, the use of the light-front formulation allows to express the hadron state in terms of frame-independent quantities called light-front wave functions (LFWFs), that have a semiclassical interpretation. Similarly to the correlators, the LFWFs are nonperturbative objects, whose form cannot be precisely determined. In practice, the LFWFs are not directly extracted from experiments, they rather represent a powerful tool in model calculations: modeling the LFWFs allows in principle to formally derive an explicit expression for many parton distributions at the same time. Because of their central theoretical role, they are considered the fundamental objects to describe the hadron [6].

1.3 This thesis

In this thesis we present a selection of topics that explore and develop certain aspects of the hadron structure. We shortly discuss the motivations behind the choice of the material included in the next chapters and the existing connections. We conclude this section with an outline of the content of the manuscript.

As previously mentioned, one of the fundamental questions that arise in hadronic physics concerns the origin of the proton spin, and how it generates in terms of parton spin and angular momentum [7, 8]. Spin-dependent parton functions become therefore the relevant observable to be after. The polarization of partons can be studied in inclusive processes only if the polarization of the parent hadron is included

as well. This is directly connected to the fact that spin-dependent PDFs only exist if the hadron is polarized.

One might wonder whether additional degrees of freedom enable the study of spin-dependent distributions, both in polarized and unpolarized hadrons. Despite not being the only possibilities, in this thesis we analyze two directions that lead to the description of polarized partons:

1. *Inclusion of parton transverse momenta.* By extending the treatment to the transverse momenta a wide range of possibilities opens up. For instance, it is possible to probe the spin of partons in the transverse plane with respect to the target momentum, even if no direction for the spin of the parent hadron has been chosen. Also, many more spin-dependent effects arise when polarized hadrons are considered. The functions encoding this information are the TMDs, defined for quarks and gluons in unpolarized and polarized targets.

2. *Double parton interactions.* Since partons carry spin, their polarization states can be correlated inside the proton. When two of them are selected simultaneously they can be described in terms of spin-dependent functions, also when the parent hadron is unpolarized. This kind of inter-parton spin correlations are encoded in the DPDs, and are typical of double parton scattering (DPS) processes.

TMDs and DPDs are particularly interesting because they allow for the study of polarized partons in hadrons in a complementary way: from the TMDs we can extract information on the spin-spin and spin-orbit correlations between the parton and the hadron. On the other hand, the analysis of double parton interactions allows to access the spin correlations between the two partons. More in general, they both enable to study the spin of the partons, even in the absence of hadron polarization.

The outline of the thesis is as follows:

In Chapter 2 we discuss the correlation functions as arising from the factorized formula of the cross section of hadron-hadron collision. We define the relevant matrix elements for quarks and gluons, in single and double parton scattering. We characterize the general features of correlators, such as their symmetry properties. We discuss the concept of universality, i.e. the property of correlators to appear (or not) identically in all process calculations. This is in particular linked to the presence of

transverse gauge links, introduced in the definition of the operators to ensure gauge invariance, which will also be discussed. The common choice of using light-front variables in high-energy process description is extensively motivated in the second part of the chapter, and we discuss the advantages of using the Light-Front Wave Functions (LFWFs) to modeling the hadronic state. The convenient features of the LFWFs will be recalled in Chapter 5, where we present an explicit example of the use of LFWFs as unifying framework to model hadronic observables.

In Chapter 3 we devote our efforts entirely to the study of TMDs, for quarks and gluons in hadrons of spin up to 1. In particular, gluons are of utmost importance at very high-energy, corresponding to small momentum fractions carried by the partons, where they dominate over the valence quarks. Being massless spin-1 objects inside the hadrons, their dynamics is described by many spin-dependent functions. We present the complete parametrization of the correlator for unpolarized targets, as well as vector and tensor polarized one, in fact allowing the descriptions of gluons in momentum space of hadrons (and nuclei) of spin up to 1. We also derive positivity bounds, i.e. relations between the TMDs that allow to relate the functions and to estimate their magnitude.

In Chapter 4 we consider the picture of the proton resulting from the two-partons interactions. Particular attention is given to spin and kinematic correlations between the two quarks. We chose a process that is particularly suitable to look at double parton scatterings: the production of a pair of same-sign W boson at the LHC. Hence, the effects of parton polarization are investigated, not only at the level of partonic interactions but also including the analysis of final states.

In Chapter 5 we analyze a simpler case, and we present a study of the transverse structure of the pion in terms of its valence quarks. We use an attractive approach based on the calculation of the LFWFs from the AdS/QCD correspondence to calculate the valence quark TMDs. The pion is a spin-0 hadron, and by definition, it has no polarization degrees of freedom. Thanks to the inclusion of the transverse momentum, one can access both unpolarized and polarized quark TMDs in the pion. However, the spin structure is not included in the theoretical formulation of AdS/QCD, and it is therefore not discussed. Being the AdS/QCD correspondence a theory whose validity lies in the intersection between the perturbative and nonperturbative QCD domain we also discuss the QCD running coupling behavior in this context.

The covered material aims to give a contribution to the current description of hadronic physics, especially towards less investigated and explored aspects such as the gluonic content of spin-1 hadrons and nuclei, the multiparton correlations in the proton, and the study of quark TMDs in the pion.

We conclude the dissertation with some discussions and possible outlook in Chapter 6.

Chapter 2

QCD and hadronic interactions

2.1 Introduction

In this Chapter, we introduce the relevant concepts that will be developed throughout the dissertation. In particular, we dedicate the first part of the chapter to the parton correlation functions, or correlators. These are general objects: they can be defined for quarks and gluons, in single and double parton scattering. They are used in all high-energy process formulae that involve hadrons and contain the full information on partonic correlations, in a way that will be specified in the next sections and complemented in Chapter 3 and 4. Assuming always factorization between the high and low energy scales, we first discuss the concept of transverse momentum dependent (TMD) single parton correlator in Drell-Yan process. As a straightforward generalization, the concept of double parton correlator is introduced. The latter is the relevant quantity that enters the cross section of a double parton scattering (DPS) process.

From the analysis of the kinematics of high-energy processes, it appears natural to adopt light-cone coordinates. Besides being a very convenient choice in practice, using light-cone coordinates can provide unique insights into the description of the hadron

state. In the second part of the chapter, we summarize the advantages deriving from the quantization of quantum field theories on the light-cone and focus on the special features acquired by the relativistic hadronic wave functions in this framework.

2.2 Hadronic collisions

High-energy processes are powerful tools to investigate the hadron internal structure. Loosely speaking, they consist of the interaction of a probe with point-like partons extracted from the hadron, followed by the production of final states.

There are two energy scales involved: the hadron mass scale, of the order of ~ 1 GeV, and the partonic scattering mass scale, typically much higher (e.g., ~ 80 GeV if a W boson is produced). The two regimes are well-separated in energies and they occur at distances (and time) which are substantially different. This allows one to write the cross section formula as a convolution of two distinct pieces: the partonic cross section, calculable with standard perturbation theory methods (Feynman rules involving free fields), convoluted with a nonperturbative object representing the probability for the parton to be "selected" from the hadron to enter the process. This picture constitutes the basic idea of the parton model [9,10]. We distinguish a *hard* part, containing all the perturbative contributions, from a *soft* part, where the low-energy hadronic physics is contained. The *factorization* between the hard and soft physics implies that all the contributions that connect the two regions either cancel out or they are absorbed into the definition of the nonperturbative quantities in a well-defined way.

In the early stages of the theoretical and experimental investigation of hadrons only the components of the parton momenta collinear to the parent hadron were considered. It is possible to directly generalize the parton model in order to include transverse partonic momenta. A further generalization was introduced by Politzer [11] and is referred to as diagrammatic approach. It introduces in a field theoretical language the more structured concept of correlator, also accounting for the extraction of more than one parton from the hadron. Thanks to this approach the cross section for a generic scattering process can be derived and the factorized formulae will contain correlators instead of free external fields.

The correlators defined in the factorized cross section formulae contain all the nonperturbative information about hadrons and can be used to describe both the distribution of partons inside the hadron and the fragmentation of parton into hadrons, in coordinate and momentum space. In this thesis we will not discuss fragmentation processes and the term correlator will refer to the distributions, unless otherwise specified.

Most common high-energy processes involving hadrons

Experiments involving hadrons give access to a variety of different partonic functions. Including fragmentation processes only for completeness, the most important categories of processes are:

- Inclusive deep inelastic scattering (DIS): inclusive lepton scattering off a proton $lp \to l'X$.
- Semi-inclusive deep inelastic scattering (SIDIS): one-particle inclusive lepton scattering off a proton $lp \to l'h\,X$.
- Proton-proton collision (pp) and Drell-Yan process (DY): production of W, Z, γ^* boson and subsequent leptonic decay $pp \to l\bar{l}X$. We include within this category also the Higgs boson or heavy quark pair production through the gluon fusion.
- Electron-positron annihilation (e^+e^-): lepton anti-lepton annihilation and production of hadrons $l\bar{l} \to hX$. This process involves the nonperturbative physics in the fragmentation region (i.e. in the production of hadrons in the final state).
- Deeply virtual Compton scattering (DVCS): exclusive process of a virtual photon off a proton and consequent production of a real photon and the proton with momentum changed into p', namely $\gamma^* p \to \gamma p'$.
- Elastic processes: low-energy scattering between an electron and the proton, such that the proton remains intact, with final momentum changed into p'.

Each process is relevant to the extraction of hadronic observables. For instance, inclusive DIS can give information on the distribution of the partons along the same direction of the proton momentum, but it is not suitable to access multi-dimensional distributions. On the other hand, SIDIS, e^+e^-, and DY can be implemented such that the transverse motion of the partons, both in the initial proton and in the fragmented final hadrons, can be accessed. Elastic and exclusive processes are sensitive to the distribution of partons in the transverse coordinate space and longitudinal momenta. The processes are schematically depicted in Fig. 2.1 and Fig. 2.2.

The study of these processes relies on the validity of factorization, rigorously demonstrated in all cases when the longitudinal momentum of the partons are considered [12]. Inclusion of transverse momenta requires a generalized form of the collinear factorization theorems [13–15]. Factorization holds true in most of the process above [14–16]. Examples of factorization-breaking contributions regard those processes in which color plays a nontrivial role in the production of the final states [17–21].

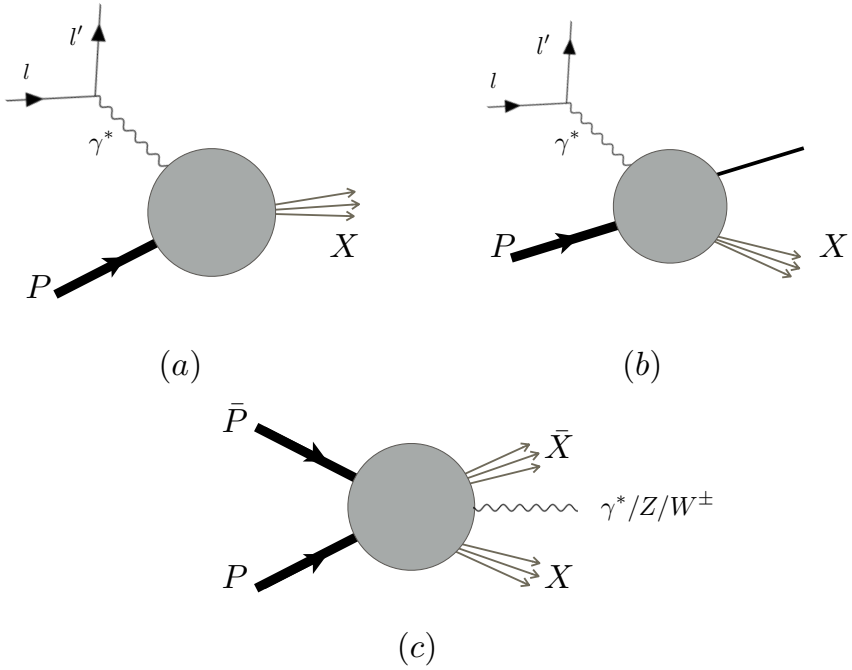

Figure 2.1: Pictorial representation of the high energy processes described in the text. The grey area generically represents the nonperturbative physics. (a) DIS: access to quark and gluon PDFs; (b) SIDIS: access to PDFs and TMDs, both for quarks and gluons; (c) *pp* collisions (e.g. DY): access to PDFs, TMDs, DPDs for quarks and gluons.

In the context of *pp* collision it has been shown that factorization holds true also in the case of two hard scatterings occurring independently, when the longitudinal momenta of the partons are considered. The same result hold true for transverse momenta but only in the context of the production of colorless final states [22, 23]. Finally, the DVCS exclusive process has been proven to factorize in [24]. Factorized formulae for the DY cross section calculations will be employed in the rest of this thesis.

Light-cone coordinates and Sudakov decomposition

Throughout the thesis, light-cone coordinates will be used. As will be discussed in Section 2.6 this has more meaning than a simple choice of frame. In fact, the theory of high-energy processes is naturally quantized on the light-front (LF).

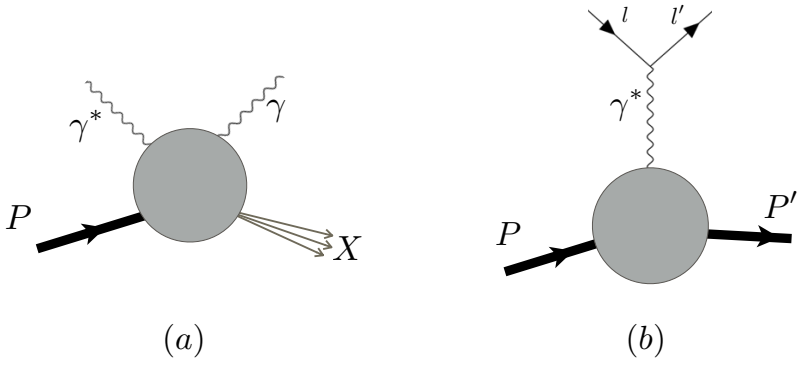

Figure 2.2: Pictorial representation of the high energy processes desrcribed in the text. The grey area generically represents nonperturbative physics. (a) DVCS: access to quark and gluon GPDs at the amplitude level; (b) elastic scattering: access to electromagnetic form factors.

Choosing a light-like basis corresponds to having two light-like vectors n_+^μ and n_-^μ satisfying:

$$n_+ \cdot n_- = 1, \quad n_+^2 = n_-^2 = 0, \tag{2.1}$$

such that any four-vector a can be written as:

$$a^\mu = a^+ n_+^\mu + a^- n_-^\mu + a_T^\mu, \tag{2.2}$$

where the transverse four-vector a_T^μ has non-vanishing components a^1, a^2. For instance, the momentum of the proton traveling along the z-direction, satisfying the constraint $P^2 = M^2$, reads:

$$P^\mu = P^+ n_+^\mu + \frac{M^2}{2P^+} n_-^\mu, \tag{2.3}$$

while the parton extracted from the proton with fraction of longitudinal momentum x and value of transverse momentum k_T is:

$$k^\mu = xP^+ n_+^\mu + k_T^\mu + k^- n_-^\mu. \tag{2.4}$$

If P^+ becomes very large, the proton momentum probes the light-cone, namely the minus component becomes insignificant and the mass is negligible compared to the hard scale of the process.

Alternatively, one can employ a Sudakov-like decomposition for the vectors, which is a more general choice of basis. That is, we choose the momentum of the proton P^μ as being one element of the basis. The other element is a four-vector n^μ that satisfies $P\cdot n = 1$, which forces n^μ to have dimension $[\text{mass}]^{-1}$ (since P^μ has mass dimensions). Further demanding $P^2 = M^2$, any four-vector in this frame can be written using a Sudakov decomposition:

$$a^\mu = (a\cdot n)P^\mu + a_T^\mu + \left[a\cdot P - (a\cdot n)M^2\right]\, n^\mu, \tag{2.5}$$

where the transverse vector a_T^μ is now defined in the transverse directions with respect to n and P. In particular, the parton momentum is expressed in terms of the proton momentum as:

$$k^\mu = xP^\mu + k_T^\mu + (k\cdot P - xM^2)\, n^\mu, \tag{2.6}$$

where we have defined $x = k\cdot n$.

The Sudakov decomposition has the advantage that n can be specified each time depending on the kinematics of the process. This will be preferred as far as the parametrizations and definitions in Chapter 3 are concerned. The vector decompositions in terms of the light-like basis, as in eq. (2.2), is useful in process calculations and will be used extensively in Section 2.3 and 2.4 and other explicit cross section calculations.

2.3 TMD correlator from Drell-Yan process

As originally conceived by Drell and Yan [25], the Drell-Yan process consists of the production, in pp collisions, of a pair of lepton-antilepton as the result of a virtual photon decay. Processes in which any of the electroweak gauge bosons are produced will be also referred to as Drell-Yan processes. As an extension, we call *double* Drell-Yan process the production of two electroweak bosons in the context of double parton scattering (see Section 2.4). The final state distributions of these types of processes are sensitive to the proton structure.

The cross section is calculated using the diagrammatic approach, following the simplified procedure outlined in [26]. We choose a frame where the two protons collide along the z-direction, and they have a large and opposite component of the momentum along this axes. This means that the momentum P of the (conventionally) left-moving proton is dominated by the plus component P^+, while the momentum $\bar{P}$ of the right-moving proton has large minus component $\bar{P}^-$ (see eq. (2.3)). The produced electroweak boson has momentum q that defines the hard scale of the process $q^2 = Q^2$.

The latter is much higher than a typical hadronic scale Λ of the order of the proton mass, i.e. $Q^2 \gg \Lambda^2$ in the high-energy limit. The square of the centre of mass (CM) energy is $(P + \bar{P})^2 = s$, and in the deep inelastic limit one has $Q^2, s \to \infty$, keeping the ratio $\tau = Q^2/s$ finite. The cross section reads:

$$d\sigma = \frac{1}{\mathcal{F}} \prod_f \frac{d^3 P_f}{(2\pi)^3 2P_f^0} \left|\mathcal{M}\right|^2 (2\pi)^4 \delta^{(4)}(P + \bar{P} - \sum_f P_f), \tag{2.7}$$

where $\mathcal{F}$ is the flux factor, and the subscript f generically labels all the momenta of the final states crossing the final state cut in Fig. 2.3.

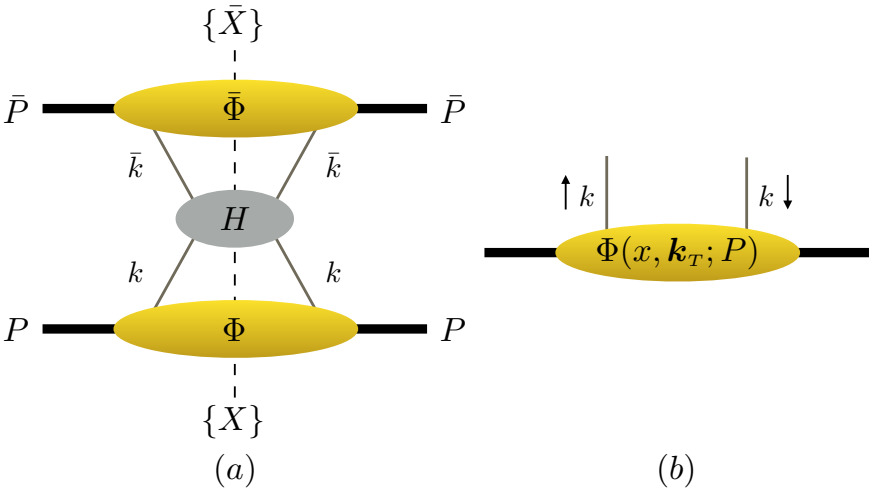

Figure 2.3: Left-side: diagram of a Drell-Yan process. Right-side: pictorial representation of the quark TMD correlator.

One must bear in mind that there are no free fields ultimately involved: the spinors that enter the hard scattering are extracted from the proton through a nonperturbative process. Therefore, we substitute free spinors (or polarization vectors in the gluon case) with hadronic matrix elements in the scattering amplitude $\mathcal{M}$. Assuming factorization between the three blobs in Fig. 2.3(a), and introducing the complete set of intermediate states $\{|X\rangle\}, \{|\bar{X}\rangle\}$ one has:

$$\begin{aligned}\frac{d\sigma}{d\mathcal{R}} =& \frac{(2\pi)^4}{2s}\sum_X \int \frac{d^3P_X}{(2\pi)^3 2P_X^0}\int \frac{d^4k}{(2\pi)^4}\frac{d^4k'}{(2\pi)^4} d^4\xi d^4\xi' e^{ik\cdot\xi - ik'\cdot\xi'} \\ &\times \sum_{\bar{X}} \int \frac{d^3P_{\bar{X}}}{(2\pi)^3 2P_{\bar{X}}^0}\int \frac{d^4\bar{k}}{(2\pi)^4}\frac{d^4\bar{k}'}{(2\pi)^4} d^4\bar{\xi} d^4\bar{\xi}' e^{i\bar{k}\cdot\bar{\xi} - i\bar{k}'\cdot\bar{\xi}'} \\ &\times \langle P|\,\overline{\psi}(\xi')\,|X\rangle\,\langle X|\,\psi(\xi)\,|P\rangle\,\langle \bar{P}|\,\overline{\psi}(\bar{\xi}')\,|\bar{X}\rangle\,\langle \bar{X}|\,\psi(\bar{\xi})\,|\bar{P}\rangle \\ &\times H(k,k',\bar{k},\bar{k}')\delta^{(4)}(P+\bar{P}-P_X-P_{\bar{X}}-q), \end{aligned} \tag{2.8}$$

where, for the sake of simplicity, we temporarily omit the dependence on the hadron spin and write the state simply as $|P\rangle$. We denote the hard part as $H(k,k',\bar{k},\bar{k}')$ and leave it unspecified, as not relevant for the present discussion. Also the Dirac indices on the fermion fields and in the hard part are understood. The flux factor is $\mathcal{F} = 4\sqrt{(P\cdot\bar{P})^2 - M^4} \approx 2s$, the n-particle phase factor is:

$$d\mathcal{R} = \prod_{f=1}^{n}\frac{d^4q_f}{(2\pi)^4}, \tag{2.9}$$

and the completeness condition on the intermediate sets:

$$\sum_X \int \frac{d^3P_X}{(2\pi)^3 2P_X^0}\,|X\rangle\,\langle X| = 1. \tag{2.10}$$

We skip the details of the derivation of the cross section formula and list the main steps towards the definition of the quantities relevant to our discussion. Using the completeness (2.10) of the intermediate states one can get rid of the transition matrix elements that appear in (2.8), such that the only matrix elements that are left contain the expectation values of the fermion fields between the proton state. Moreover, translational invariance allows us to shift the position of the fields, as the matrix elements only depend on the difference of the positions. Finally, using the momentum conservation relations one can write the cross section in terms of the hard part and the *correlation functions* as:

$$\frac{d\sigma}{d\mathcal{R}} \sim \int d^4k\, d^4\,\bar{k}\delta^{(4)}(k+\bar{k}-q) H_{\alpha\beta\gamma\delta}(k,\bar{k},q)\Phi_{\alpha\beta}(k,P)\bar{\Phi}_{\gamma\delta}(\bar{k},\bar{P}), \tag{2.11}$$

where we have reinserted the Dirac indices $\alpha,\beta,\gamma,\delta$ and defined the *fully unintegrated*

quark correlation function as:

$$\Phi_{\alpha\beta}(k;P) \equiv \int \frac{d^4\xi}{(2\pi)^4} e^{ik\cdot\xi} \langle P| \overline{\psi}_\beta(0)\psi_\alpha(\xi) |P\rangle , \tag{2.12}$$

and for the antiquark:

$$\overline{\Phi}_{\gamma\delta}(\bar{k};P) \equiv \int \frac{d^4\xi}{(2\pi)^4} e^{-i\bar{k}\cdot\bar{\xi}} \langle P| \overline{\psi}_\delta(0)\psi_\gamma(\bar{\xi}) |P\rangle , \tag{2.13}$$

The (2.12) is a matrix in Dirac space which depends on the momentum of the parton, the momentum and the spin of the proton. A trace over color is understood and we will later give further details on the color structure of the correlators. The quantity in (2.12) is a fundamental object that encodes all the nonperturbative physics in the high-energy processes. Choosing the light-like basis as in (2.2), the hierarchies of the momentum components, dictated by the high-energy kinematics, become the guiding criteria to identify the relevant components and rewrite the delta function in (2.11). As already mentioned, the dominant component of the proton P ($\bar{P}$) is the plus (minus). The components of momenta in (2.11) scale like (*hard scattering approximation*):

$$\begin{aligned} P^+ \sim k^+ \sim q^+ \sim Q, \quad \bar{P}^- \sim \bar{k}^- \sim q^- \sim Q, \\ P^- \sim k^- \sim \frac{\Lambda^2}{Q}, \quad \bar{P}^+ \sim \bar{k}^+ \sim \frac{\Lambda^2}{Q}. \end{aligned} \tag{2.14}$$

We assume that the partons entering the hard scattering are *almost* collinear to the incoming hadrons, therefore all the transverse momenta are of the order of the hadronic scale Λ, i.e.

$$|\boldsymbol{k}_T| \sim |\bar{\boldsymbol{k}}_T| \sim |\boldsymbol{q}_T| \sim \Lambda. \tag{2.15}$$

Neglecting momenta of order Λ^2/Q, the delta function can be written as:

$$\begin{aligned} \delta^{(4)}(k+\bar{k}-q) &= \delta(k^+ + \bar{k}^+ - q^+)\delta(k^- + \bar{k}^- - q^-)\delta^{(2)}(\boldsymbol{k}_T + \bar{\boldsymbol{k}}_T - \boldsymbol{q}_T) \\ &\approx \delta(k^+ - q^+)\delta(\bar{k}^- - q^-)\delta^{(2)}(\boldsymbol{k}_T + \bar{\boldsymbol{k}}_T - \boldsymbol{q}_T). \end{aligned} \tag{2.16}$$

As a consequence, one can deduce $k^+ \approx q^+$ and $\bar{k}^- \approx q^-$ and define the light-cone longitudinal momentum fractions and the hard momenta as:

$$x = \frac{k^+}{P^+} \approx \frac{q^+}{P^+}, \quad \bar{x} = \frac{\bar{k}^-}{\bar{P}^-} \approx \frac{q^-}{\bar{P}^-}, \quad q^2 \approx 2q^+q^- \approx x\bar{x}s. \tag{2.17}$$

Substituting in (2.11) gives:

$$\frac{d\sigma}{d\mathcal{R}} \sim \int d^2\boldsymbol{k}_T d^2\bar{\boldsymbol{k}}_T \delta^{(2)}(\boldsymbol{k}_T + \bar{\boldsymbol{k}}_T - \boldsymbol{q}_T) H_{\alpha\beta\gamma\delta}(k, \bar{k}, q) \times \int dk^- \Phi_{\alpha\beta}(k, P) \int d\bar{k}^+ \bar{\Phi}_{\gamma\delta}(\bar{k}, \bar{P}) + \{\text{corrections}\}. \tag{2.18}$$

We can define the *transverse momentum dependent* (TMD) correlator for quarks (and similarly for antiquarks) as follows:

$$\Phi_{\alpha\beta}(x, \boldsymbol{k}_T; P) = \int dk^- \Phi_{\alpha\beta}(k, P) = \int \frac{d\xi^- d^2\boldsymbol{\xi}_T}{(2\pi)^3} e^{ik\cdot\xi} \langle P| \overline{\psi}_\beta(0)\psi_\alpha(\xi) |P\rangle \Big|_{\xi^+=0}, \tag{2.19}$$

which is a matrix in Dirac space that contains the information on the transverse motion and spin of the partons. It is parametrized in terms of TMD parton distribution functions (TMD PDFs or TMDs[1]).

In the collinear limit, one can perform the integration over the transverse momentum of the produced particle $\boldsymbol{q}_T$ in (2.19) and obtain a factorized formula containing the collinear correlator for quark, the relevant quantity in inclusive DY processes. The integrated correlator reads:

$$\Phi_{\alpha\beta}(x; P) = \int \frac{d\xi^-}{2\pi} e^{ik\cdot\xi} \langle P| \overline{\psi}_\beta(0)\psi_\alpha(\xi) |P\rangle \Big|_{\xi^+=\boldsymbol{\xi}_T=0}, \tag{2.20}$$

which is parametrized in terms of parton distributions PDFs. A trace over color is understood and the dependence on the hadron spin will be later specified.

Gluon correlator

In *pp* collisions the hard scattering can be initiated by gluons (see Fig. 2.4(a)), such as in Higgs boson production, heavy quark pair or quankonium production [27–30]. Accordingly, the relevant correlator that needs to be introduced in this equation is:

$$\Gamma^{\mu\nu;\rho\sigma}(x, \boldsymbol{k}_T; P) \equiv \int \frac{d\xi^- d^2\boldsymbol{\xi}_T}{(2\pi)^3} e^{ik\cdot\xi} \langle P| F^{\mu\nu}(0) F^{\rho\sigma}(\xi) |P\rangle \Big|_{\xi^+=0}, \tag{2.21}$$

[1] In this thesis the TMD fragmentation functions are not treated, therefore unless otherwise specified the name TMDs simply refers to the TMD PDFs distributions and is not ambiguous.

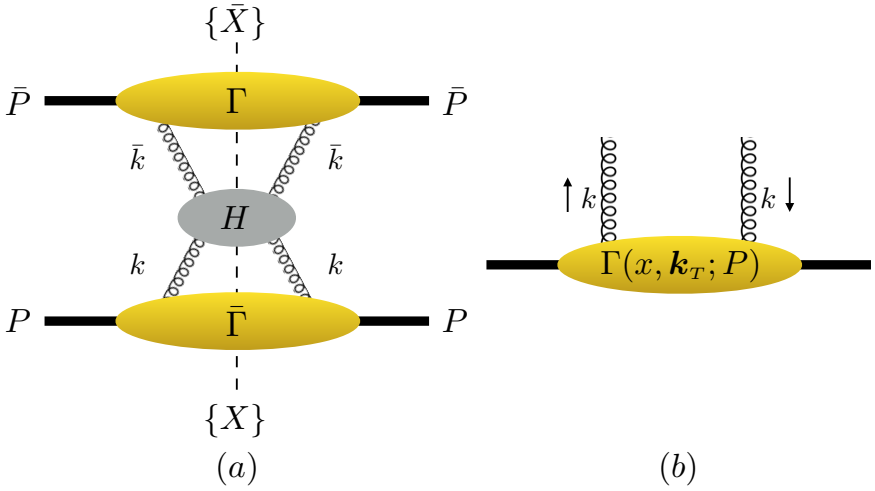

Figure 2.4: Left-side: Gluon fusion in pp collisions. Right-side: pictorial representation of the gluon TMD correlator.

where once again we implicitly assume a trace over color. The quantity (2.21) is the *transverse momentum dependent* (TMD) correlator for gluons. The presence of the gauge field-strength tensor rather than the field is dictated by gauge invariance, and the definition needs to be further completed with the Wilson lines, as explained in Section 2.5. The quantity (2.21) is parametrized by gluon TMDs. Integration over transverse momenta gives the definition of the collinear gluon correlator:

$$\Gamma^{\mu\nu;\rho\sigma}(x;P) \equiv \int \frac{d\xi^-}{2\pi}\, e^{ik\cdot\xi} \left\langle P\right| F^{\mu\nu}(0) F^{\rho\sigma}(\xi) \left|P\right\rangle \Big|_{\xi^+=\boldsymbol{\xi}_T=0}, \tag{2.22}$$

which is parametrized in terms of gluon PDFs. The dominant terms in (2.21) and (2.22) are the ones that contain one plus and one transverse index in the field-strength tensor, as extensively explained in Chapter 3.

The correlators of eq. (2.19) and (2.21) are diagonal operators in momentum space and they represent the probability of extracting a parton from the proton with longitudinal and transverse momentum x and $\boldsymbol{k}_T$. They are usually schematically represented as in Fig.2.3(b) and 2.4(b).

2.4 Double parton correlator

The concept according to which, in pp collisions, only one parton from each proton participate in the hard scattering can be extended to multipartonic interactions. In particular, two hard scatterings can occur simultaneously, defining this process as a double parton scattering (DPS), at variance with the usual single parton scattering (SPS). In this Section, we consider the double Drell-Yan process (dDY), in which two electroweak gauge bosons are produced in two distinct hard processes. The two-parton correlation functions can be defined in a similar way as in the single parton ones. Assuming the general validity of factorization for the DPS processes that we consider, the double parton correlators enter the cross section calculations in an analogous way as the correlator (2.19), with the due modifications.

2.4.1 Double Drell-Yan cross section

We start by writing the factorized cross section for the double parton scattering at tree level. We generalize the result in Section 2.2 as in [31, 32]. The diagram we are about to calculate is displayed in Fig. 2.5.

Without any particular choice of hierarchy, one can set hard scales of the two hard processes to a common scale $Q^2 \sim q_1^2 \sim q_2^2$.

Naming the momenta as l_1, l_2 for the outgoing parton in the left moving proton and $\bar{l}_1, \bar{l}_2$ the ones in the right moving proton, the cross section reads:

$$
\begin{aligned}
\frac{d\sigma}{d\mathcal{R}} =& \frac{1}{C}\frac{1}{4P\bar{P}}\sum_{X,\bar{X}}\left[\prod_{j=1}^{m}\int\frac{d^3P_{Xj}}{(2\pi)^3 2P^0_{Xj}}\right]\left[\prod_{j=1}^{n}\int\frac{d^3P_{\bar{X}j}}{(2\pi)^3 2P^0_{\bar{X}j}}\right] \\
&\times (2\pi)^4\delta^{(4)}\left(\sum_{i=1}^{2}q_i+\sum_{j=1}^{m}P_{Xj}+\sum_{j=1}^{n}P_{\bar{X}j}-P-\bar{P}\right) \\
&\times \prod_{i=1}^{2}\int\frac{d^4l_i}{(2\pi)^4}\frac{d^4\bar{l}_i}{(2\pi)^4}\prod_{i=1}^{2}\int\frac{d^4l'_i}{(2\pi)^4}\frac{d^4\bar{l}'_i}{(2\pi)^4}\prod_{i=1}^{2}H_i(q_i,l_i,\bar{l}_i,l'_i,\bar{l}'_i) \\
&\times (2\pi)^4\delta^{(4)}(q_i-l_i-\bar{l}_i)(2\pi)^4\delta^{(4)}(q_i-l'_i-\bar{l}'_i) \\
&\times \prod_{i=1}^{2}\int d^4\xi_i d^4\bar{\xi}_i d^4\xi'_i d^4\bar{\xi}'_i\, e^{i(\xi_i l_i-\xi'_i l'_i)+i(\bar{\xi}_i\bar{l}_i-\bar{\xi}'_i\bar{l}'_i)} \\
&\times \langle P|\,\bar{T}[\bar{\psi}(\xi'_1)\bar{\psi}(\xi'_2)]\,|X\rangle\,\langle X|\,T[\psi(\xi_2)\psi(\xi_1)]\,|P\rangle \\
&\times \langle \bar{P}|\,\bar{T}[\psi(\bar{\xi}'_1)\psi(\bar{\xi}'_2)]\,|\bar{X}\rangle\,\langle \bar{X}|\,T[\bar{\psi}(\bar{\xi}_2)\bar{\psi}(\bar{\xi}_1)]\,|\bar{P}\rangle\,,
\end{aligned}
\tag{2.23}
$$

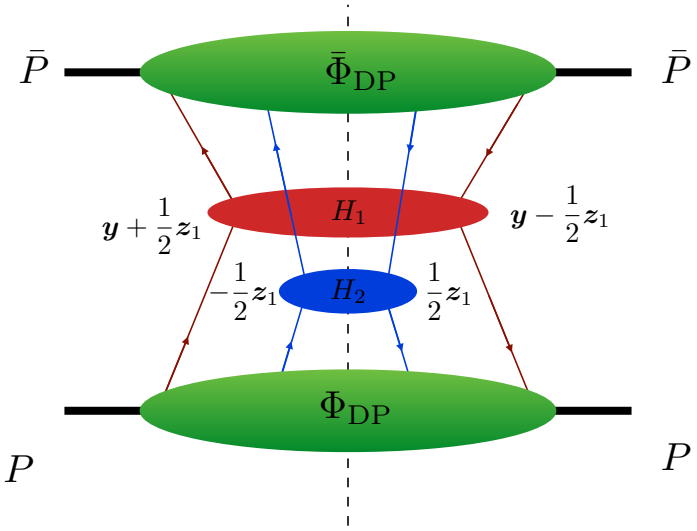

Figure 2.5: Representation of a DPS process (e.g. double Drell-Yan process).

where we have inserted the time and anti-time order operators as in [31] and:

$$d\mathcal{R} = \left[\prod_{i=1}^{2} \frac{d^4 q_i}{(2\pi)^4}\right]. \tag{2.24}$$

The factor C is set by combinatorics and it equals 1 (or 2) if the produced particles in the hard scatterings are different (or equal). As before, $H_{1,2}$ represent the hard part of the two processes and will be left unspecified. Let us define the symmetric momenta:

$$l_i = k_i - \frac{r_i}{2}, \qquad l_i' = k_i + \frac{r_i}{2}, \quad i = 1, 2, \tag{2.25}$$

which implies $r_1 = -r_2 = r$ from momentum conservation. Translational invariance allows us to introduce the position variables z_1, z_2, and y such that:

$$y + \frac{1}{2}z_1 = \xi_1 - \frac{1}{2}\xi_2, \qquad y - \frac{1}{2}z_1 = \xi_1' - \frac{1}{2}\xi_2, \qquad z_2 = \xi_2. \tag{2.26}$$

The cross section becomes:

$$\frac{d\sigma}{d\mathcal{R}} \sim \prod_{i=1}^{2} \int d^4k_i\, d^4\bar{k}_i \delta^{(4)}(q_i - k_i - \bar{k}_i) \int d^4\, r d^4\, \bar{r} \delta^{(4)}(r + \bar{r}) \\ \times \prod_{i=1}^{2} H_i(q_i, k_i, \bar{k}_i, r, \bar{r}) \Phi_{DP}(k_i, r) \bar{\Phi}_{DP}(\bar{k}_i, \bar{r}). \tag{2.27}$$

We define the *unintegrated double parton correlator*:

$$\Phi_{DP}(k_1, k_2, r) = \int \frac{d^4z_1}{(2\pi)^4} \frac{d^4z_2}{(2\pi)^4} \frac{d^4y}{(2\pi)^4} e^{iz_1k_1 + iz_2k_2 - iyr} \\ \times \langle P, S | \bar{T} \left[\bar{\psi}(y - \frac{1}{2}z_1) \bar{\psi}(-\frac{1}{2}z_2) \right] T \left[\psi(\frac{1}{2}z_2) \psi(y + \frac{1}{2}z_1) \right] | P, S \rangle \,. \tag{2.28}$$

which represents the emission of two quarks in the scattering amplitude and their reinsertion in the conjugate one. Once again, a trace over color is understood.

The *hard scattering approximation* described in Section 2.2 holds true also in the double parton case, complemented by some considerations. The components of momenta in (2.27) scale like (2.14). From the definition we also have $r^- \sim \bar{r}^+ \sim \Lambda^2/Q$, while r^+ and $\bar{r}^-$ could in principle be of order Q, but they are fixed by momentum conservation $r + \bar{r} = 0$ [31, 33]. Therefore one also has $r^+ \sim \bar{r}^- \sim \Lambda^2/Q$. All the transverse momenta are of the order of the hadronic scale, i.e.

$$|\boldsymbol{k}_{Ti}| \sim |\bar{\boldsymbol{k}}_{Ti}| \sim |\boldsymbol{r}_T| \sim |\bar{\boldsymbol{r}}_{\boldsymbol{T}}| \sim |\boldsymbol{q}_{Ti}| \sim \Lambda. \tag{2.29}$$

Reducing the delta functions as in (2.16), one has:

$$\frac{d\sigma}{d\mathcal{R}} \sim \prod_{i=1}^{2} H_i(q_i^2) \int dk_1^- dk_2^- \int dr^- \Phi_{DP}(k_i, r)\Big|_{k_i^+ \approx q_i^+,\, r^+ \approx 0} \\ \times \int d\bar{k}_1^+ d\bar{k}_2^+ \int d\bar{r}^+ \bar{\Phi}_{DP}(\bar{k}_i, \bar{r})\Big|_{\bar{k}_i^- \approx q_i^-,\, \bar{r}^- \approx 0} + \{\text{corrections}\}. \tag{2.30}$$

A Fourier transform to the transverse position $\boldsymbol{y}$, conjugate to $\boldsymbol{r}$, brings us to the definition of the *transverse momentum dependent double parton correlator* for quarks:

$$\Phi_{DP}(x_1, x_2, \boldsymbol{k}_{T1}, \boldsymbol{k}_{T2}, \boldsymbol{y}) = 2P^+ \left[\prod_{i=1}^{2} \int \frac{dz_i^-}{2\pi} \frac{d^2\boldsymbol{z}_{Ti}}{(2\pi)^2} e^{iz_1k_1 + iz_2k_2} \right] \int dy^-$$

$$\times \langle P| \left[\bar{\psi}(y-\frac{1}{2}z_1)\bar{\psi}(-\frac{1}{2}z_2)\right] \left[\psi(\frac{1}{2}z_2)\psi(y+\frac{1}{2}z_1)\right] |P\rangle\big|_{z_i^+=y^+=0}\,, \tag{2.31}$$

where we define the fractions of longitudinal momentum x_1, x_2, $\bar{x}_1$, $\bar{x}_2$ as obvious extension of (2.17). The correlator (2.31) is parametrized in terms of TMD double parton distributions (TMD DPDs).

After integration over all the transverse momenta, we obtain:

$$\Phi_{DP}(x_1,x_2,\boldsymbol{y}) = \prod_{i=1,2}\int d^2\boldsymbol{k}_{Ti}\Phi_{DP}(x_i,\boldsymbol{k}_{Ti},\boldsymbol{y}) \tag{2.32}$$

$$= 2P^+\left[\prod_{i=1}^{2}\frac{dz_i^-}{2\pi}\,e^{iz_1k_1+iz_2k_2}\right]\int dy^- \times \langle P| \left[\bar{\psi}(-\frac{1}{2}z_2)\psi(\frac{1}{2}z_2)\right] \left[\bar{\psi}(y-\frac{1}{2}z_1)\psi(y+\frac{1}{2}z_1)\right] |P\rangle\Big|_{\substack{z_i^+=y^+=0,\\ \boldsymbol{z}_{T1}=\boldsymbol{0}_T,\,\boldsymbol{z}_{T2}=\boldsymbol{0}_T}}\,, \tag{2.33}$$

which is the *collinear double parton correlator*, parametrized in terms of double parton distributions DPDs. For later convenience we also define the non-local bilinear operators contained between square brackets in (2.33) as:

$$\mathcal{O}(y,z) = \bar{\psi}(y-\frac{1}{2}z)\psi(y+\frac{1}{2}z). \tag{2.34}$$

One can interpret (2.33) as the probability of finding two partons with momenta aligned with the parent hadron separated in the transverse plane by a distance $\boldsymbol{y}$. In order for the double scattering to take place, the transverse relative distance between the partons in the two hadrons must match. However the distance of the partons from the centre of the parent hadron can be different [31].

Finally, we define the double gluon correlator in analogy to Section 2.3, namely:

$$\Gamma_{DP}^{ij,i'j'}(x_1,x_2,\boldsymbol{y}) = \left[\prod_{i=1}^{2}\frac{1}{x_iP^+}\int\frac{dz_i^-}{2\pi}\,e^{iz_1k_1+iz_2k_2}\right]\int dy^- \times \langle P| \left[F^{+j'}(-\frac{1}{2}z_1)F^{+i'}(\frac{1}{2}z_2)\right] \left[F^{+j}(y-\frac{1}{2}z_2)F^{+i}(y+\frac{1}{2}z_1)\right] |P\rangle\big|_{z_i^+=y^+=0}\,, \tag{2.35}$$

in which the dominant plus component has been chosen to simplify the notation. However, in the rest of the thesis we will not discuss double gluon correlators and we will focus exclusively to double parton correlators with quark fields.

2.4.2 Single versus double parton scattering

We want to briefly discuss the impact of the double parton scattering in comparison with the single parton counterpart [31], restricting ourselves to a qualitative discussion based on a simple power counting argument, neglecting all the effects arising at higher orders.

If one does not integrate over transverse momenta, the relevant cross section for the production of two particles in double parton scattering takes the form:

$$\frac{d\sigma}{\prod_{i=1}^{2} dx_i\, d\bar{x}_i\, d^2\boldsymbol{q}_{Ti}} = \frac{1}{C}\left[\prod_{i=1}^{2} H_i(x_i\bar{x}_i s)\right]\left[\prod_{i=1}^{2}\int d^2\boldsymbol{k}_{Ti} d^2\bar{\boldsymbol{k}}_{Ti}\,\delta^{(2)}(\boldsymbol{q}_{Ti}-\boldsymbol{k}_{Ti}-\bar{\boldsymbol{k}}_{Ti})\right] \times \int d^2\boldsymbol{y}\,\Phi_{DP}(x_i,\boldsymbol{k}_i,\boldsymbol{y})\bar{\Phi}_{DP}(\bar{x}_i,\bar{\boldsymbol{k}}_{Ti},\boldsymbol{y}). \tag{2.36}$$

The hard cross section parts have a power behavior $H \sim Q^{-2}$, while $\Phi_{DP}(x_i,\boldsymbol{k}_i,\boldsymbol{y}) \sim \Lambda^{-2}$ by definition. The terms $d^2\boldsymbol{k}_{Ti}d^2\bar{\boldsymbol{k}}_{Ti}\delta^{(2)}(\boldsymbol{q}_{Ti}-\boldsymbol{k}_{Ti}-\bar{\boldsymbol{k}}_{Ti}) \sim \Lambda^2$ and the transverse distance $|\boldsymbol{y}|$ is of the order $1/\Lambda$. Putting all together one has:

$$\left.\frac{d\sigma}{\prod_{i=1}^{2} dx_i\, d\bar{x}_i\, d^2\boldsymbol{q}_{Ti}}\right|_{\text{double}} \sim \frac{1}{\Lambda^2 Q^4}. \tag{2.37}$$

On the other hand, for a more inclusive process, where the transverse momenta are integrated over, the cross section reads:

$$\frac{d\sigma}{\prod_{i=1}^{2} dx_i\, d\bar{x}_i} = \frac{1}{C}\left[\prod_{i=1}^{2} H_i(x_i\bar{x}_i s)\right]\int d^2\boldsymbol{y}\,\Phi_{DP}(x_i,\boldsymbol{y})\bar{\Phi}_{DP}(\bar{x}_i,\boldsymbol{y}), \tag{2.38}$$

and it scales as:

$$\left.\frac{d\sigma}{\prod_{i=1}^{2} dx_i\, d\bar{x}_i}\right|_{\text{double}} \sim \frac{\Lambda^2}{Q^4}. \tag{2.39}$$

With a similar logic, one can study the power behavior of the production of the same two final states by means of single parton scattering processes. The result is:

$$\left.\frac{d\sigma}{\prod_{i=1}^{2} dx_i\, d\bar{x}_i\, d^2\boldsymbol{q}_{Ti}}\right|_{\text{single}} \sim \frac{1}{\Lambda^2 Q^4}, \qquad \left.\frac{d\sigma}{\prod_{i=1}^{2} dx_i\, d\bar{x}_i}\right|_{\text{single}} \sim \frac{1}{Q^2}. \tag{2.40}$$

It turns out that, for transverse momentum dependent cross sections, the power behavior of single and double parton scattering is the same, i.e. there is no suppression of the latter. For more inclusive quantities there is, in general, a power suppression

of the double parton scattering with respect to the single parton one. However, there are very interesting cases where the double parton scattering is not suppressed with respect to the single counterpart, such as the production of a pair of W bosons with the same electric charge. We will investigate this process in details in Section 4.5.

2.5 General properties of correlation functions

There are general properties which are common to all the correlation functions. In this Section, we discuss some of them, focusing on gauge invariance, discrete symmetries, and universality.

Gauge invariance

A fundamental requirement for all the correlators entering a cross section formula is that they must be *color gauge invariant* objects. The definitions provided in eqs. (2.19), (2.20), (2.21), (2.31) and (2.33) need to be modified accordingly.

The field operators for the extraction and reinsertion of the partons in the amplitude and in its conjugate are located at two distinct space-time points. Consequently, acting on them with a local gauge transformation would leave space-dependent phase factors that do not cancel out. Let us consider the transformation of the quark fields under a local gauge transformation:

$$\begin{aligned} &\psi(\xi) \to V(\xi)\psi(\xi), \\ &\overline{\psi}(\xi) \to \overline{\psi}(\xi)V^\dagger(\xi), \end{aligned} \tag{2.41}$$

where V is the unitary matrix of the SU(3) color gauge transformation. Similarly, the transformation for the gauge field strength tensor reads:

$$F^{\mu\nu}(\xi) \to V(\xi)F^{\mu\nu}(\xi)V^\dagger(\xi). \tag{2.42}$$

To restore the gauge invariance, we insert the operator $U(0,\xi)$ and demand the new product to transform as (a trace over color is understood):

$$\overline{\psi}(0)U(0,\xi)\psi(\xi) \to \overline{\psi}(0)V^\dagger(0)V(0)U(0,\xi)V^\dagger(\xi)V(\xi)\psi(\xi), \tag{2.43}$$

and a similar transformation is required for the product $F^{\mu\nu}(0)U(0,\xi)F^{\rho\sigma}U'(\xi,0)$.

We deduce that the transformation property for the U reads:

$$U(0,\xi) \to V(0)U(0,\xi)V^\dagger(\xi). \tag{2.44}$$

The operators U are called Wilson line. They are also called *gauge links* because they restore gauge invariance by "transporting" the color gauge transformation property from one point to the other. The expression for the gauge link in a non-abelian theory was first introduced by Wilson in [34], mimicking the structure of a path dependent phase formulated in QED for the description of the Aharonov-Bohm effect [35]. In QCD it reads:

$$U_{[C]} = \mathcal{P}\left\{\exp\left(-ig\int_C d\eta^\mu A_\mu(\eta)\right)\right\}, \tag{2.45}$$

where $A_\mu = A^a_\mu t_a$, where t^a are the generators of the color algebra $SU(3)$, satisfying $[t^a, t^b] = if^{abc}t_c$, with f_{abc} structure constants. C is the path connecting two space-time points (the path can also reduce to a loop) and $\mathcal{P}\{\cdots\}$ is the path-ordering operator [36]. In the case of the correlators defined in the previous sections, the links have to connect the two space-time points at which the fields are defined. The dominant paths are the ones along the lightlike direction n, hence the (2.45) becomes:

$$U(0,\xi) \equiv U^{[n]}_{[0,\xi]} = \mathcal{P}\left\{\exp\left(-ig\int_0^\xi d\eta^- A^n(\eta)\right)\right\}, \tag{2.46}$$

where we use the notation $A^n = A\cdot n$, which is A^+ in the light-cone basis (2.2). We can now define the color gauge invariant unintegrated correlators as the ones containing the operators U as follows[2]:

$$\Phi^{[U]}(x, \boldsymbol{k}_T; P) \equiv \int \frac{d\xi^- d^2\boldsymbol{\xi}_T}{(2\pi)^3} e^{ik\cdot\xi} \langle P|\, \overline{\psi}(0)U(0,\xi)\psi(\xi)\,|P\rangle \Big|_{\xi^+=0}, \tag{2.47}$$

$$\Gamma^{[U,U']\mu\nu;\rho\sigma}(x, \boldsymbol{k}_T; P) \equiv \int \frac{d\xi^- d^2\boldsymbol{\xi}_T}{(2\pi)^3} e^{ik\cdot\xi} \langle P|\, F^{\mu\nu}(0)U(0,\xi)F^{\rho\sigma}(\xi)U'(\xi,0)\,|P\rangle \Big|_{\xi^+=0}. \tag{2.48}$$

On a diagrammatic perspective, the inclusion of such objects in the definition of

[2]The superscript $[U]$ indicates that the correlator's structure does depend on the presence and on the structure of the gauge link. When not necessary, it will be understood in the notation.

the correlators corresponds to resumming gluons emitted from the correlator to the hard scattering, such as the contributions represented in Fig. 2.6. This realization dates back to the work of Efremov and Radyushkin [37]. Most importantly, these links need to involve transverse gluons at light cone infinity, a missing ingredient in the earlier treatments. Later in [38–40] the complete derivation of color-gauge invariant operators for TMD and integrated distribution was achieved, and the importance of the transverse gluons was unravelled. The presence of gauge links is connected to a wide variety of effects in TMD phenomenology, such as single spin asymmetry and process dependence. They are also responsible for the survival of the T-odd functions (as shortly discussed). The dominant gauge link structures appearing in the TMD operators are *staple-like*:

$$U^{[\pm]}_{[0,\xi]} \equiv U^{n}_{[0,\mathbf{0}_T;\pm\infty,\mathbf{0}_T]}\, U^{T}_{[\pm\infty,\mathbf{0}_T;\pm\infty,\boldsymbol{\xi}_T]}\, U^{n}_{[\pm\infty,\boldsymbol{\xi}_T;\xi^-,\boldsymbol{\xi}_T]}, \tag{2.49}$$

where $\pm$ indicates whether the path is future/past pointing along the direction of light-cone infinity, as depicted in Fig. 2.7(a-b). From the basic structures $U^{[\pm]}$ it is possible to construct all the relevant gauge links that are involved in the processes. For the DY process that we have discussed, the gauge link is due to initial-state interactions (see, e.g., the top-right diagram of Fig. 2.6) and is given by the past-pointing staple-like structure (see Fig. 2.7(a)):

$$U^{[-]}_{[0,\xi]} \equiv U^{n}_{[0^-,\mathbf{0}_T;-\infty^-,\mathbf{0}_T]}\, U^{T}_{[-\infty^-,\mathbf{0}_T;-\infty^-,\boldsymbol{\xi}_T]}\, U^{n}_{[-\infty^-,\boldsymbol{\xi}_T;\xi^-,\boldsymbol{\xi}_T]}, \tag{2.50}$$

where:

$$U^{n}_{[0^-,\mathbf{0}_T;-\infty^-,\mathbf{0}_T]} \equiv \mathcal{P}\left\{\exp\left(-ig\int_0^{-\infty} d\eta^- A^+(\eta^+=0,\eta^-,\boldsymbol{\eta}_T=\mathbf{0}_T)\right)\right\}, \tag{2.51}$$

$$U^{T}_{[-\infty^-,\mathbf{0}_T;-\infty^-,\boldsymbol{\xi}_T]} \equiv \mathcal{P}\left\{\exp\left(-ig\int_0^{\boldsymbol{\xi}_T} d\boldsymbol{\eta}\cdot\boldsymbol{A}(\eta^+=0,\eta^-=-\infty,\boldsymbol{\eta}_T)\right)\right\}, \tag{2.52}$$

and similarly for the third piece of (2.50).

As far as the gluons TMDs are concerned, one needs a gauge link in the adjoint representation or two gauge links in the fundamental representation. This allows for a bigger number of structures that describe the color flow in the processes initiated by gluons. In Fig. 2.7(c-f) some possibilities are sketched. For a review of the gauge link structures, see e.g. [41, 42].

Integration over transverse momenta produce the collinear non-local matrix elements in (2.20) and (2.22). Once the transverse momentum is integrated over, the

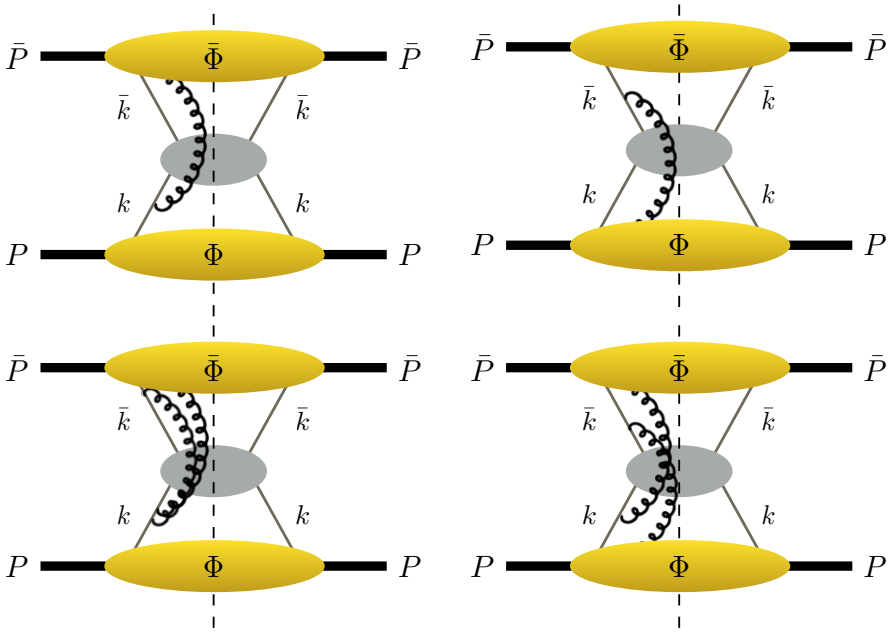

Figure 2.6: Diagrammatic interpretation of the gauge links of eq. (2.46), thanks to which the gluons in the picture are included in the correlators.

transverse direction (conjugated to the momentum) vanishes, and the gauge links reduce to a single line that connects two points along the n direction. The much simpler structure and the absence of the transverse pieces make the PDFs free from effects typical of TMDs, such as the non-universality feature that we will discuss in the next subsection.

The considerations that bring to the definition of the Wilson lines for quarks and gluons in single parton scattering remain valid for the double parton correlators as well, because they involve one hard scattering process at a time [31]. The procedure is rather general and it can be repeated in the case of double and multiparton correlators. Each operator of the type (2.34), that enters multiple times in a multiparton correlator, is gauge invariant upon the insertion of gauge links as before, namely:

$$\mathcal{O}^{[U]}(y,z) = \overline{\psi}\left(y - \frac{1}{2}z\right) U\left(y - \frac{1}{2}z, y + \frac{1}{2}z\right) \psi\left(y + \frac{1}{2}z\right), \tag{2.53}$$

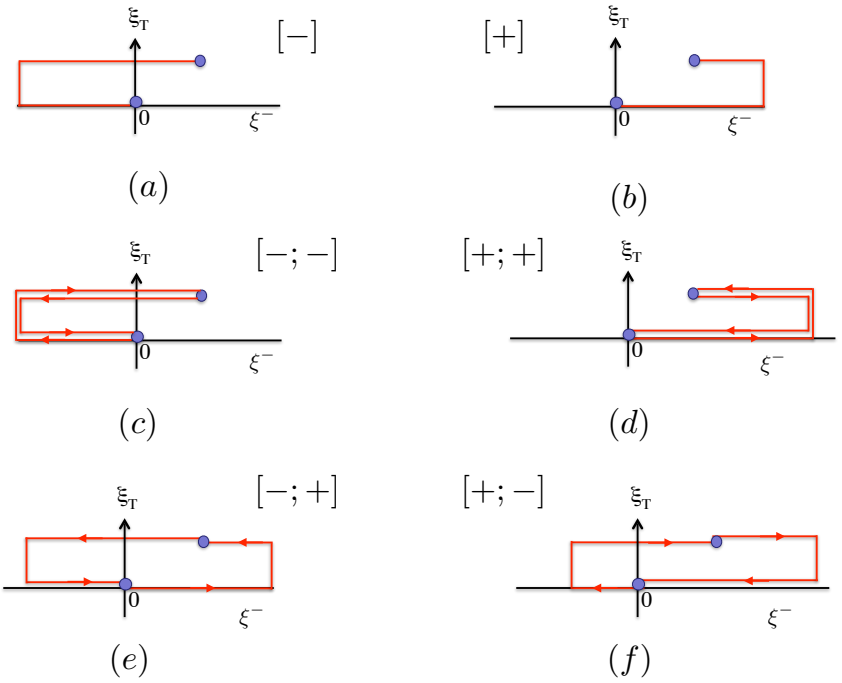

Figure 2.7: Fundamental gauge link structures for quarks and gluon correlators. The symbols [+] and [-] refer to the staple-like gauge links that are past (a) or future-pointing (b). All the other structures (c)-(f) are built from staple-like gauge links.

and the gauge invariant version of the collinear double parton correlator reads:

$$\Phi_{DP}^{[U,U']}(x_1,x_2,\boldsymbol{y}) = 2P^+ \left[\prod_{i=1}^{2}\int d^2\boldsymbol{k}_{Ti}\frac{dz_i^-}{2\pi}\frac{d^2\boldsymbol{z}_{Ti}}{(2\pi)^2}\,e^{iz_1k_1+iz_2k_2}\right]\int dy^- \times \langle P,S|\,\mathcal{O}^{[U]}(0,z)\mathcal{O}^{[U']}(y,z)\,|P,S\rangle\Big|_{\substack{z_i^+=y^+=0,\\ \boldsymbol{z}_{T1}=\boldsymbol{0}_T,\,\boldsymbol{z}_{T2}=\boldsymbol{0}_T}} . \quad (2.54)$$

In the relevant case for our purposes, each of the extracted parton and its conjugate partner are in a color singlet (no color octets and interference terms are present), thus the double collinear correlator reduces to straight lines connecting the two pairs of space-time points, in precisely the same way as the single collinear case. However, it

is worth mentioning that the color structure of the double parton correlators is, in general situations, more complicated than the single case also in the collinear case, see e.g., refs. [23, 31].

Discrete symmetries

The quark and gluon operators contained in the correlators are tensors in Dirac and Lorentz space, respectively. The matrix elements in addition depend on the kinematic variables of the partons and of the parent hadron. It is possible to find a decomposition of the correlators in terms of the elements of the basis of Dirac and Lorentz space combined with

$$\{k^\mu, P^\mu, S^\mu, \cdots\}, \tag{2.55}$$

where the "$\cdots$" represent other Lorentz structures (scalar, vector and tensor) the correlator can possibly depend on. Each term is weighted with multidimensional functions that depend on the kinematic variables and quantum numbers of the partons and will be generically called *parton distributions*. The number of terms one can construct in this way would quickly increase once the extra degrees of freedom are included.

Some constraints on the allowed structures come from symmetry arguments. Accordingly, we demand that this expansion is such that the correlator respects parity and hermiticity invariance, namely for quarks:

$$\text{Hermiticity:} \quad \Phi^{[U]\dagger}(k; P, S) = \gamma^0 \Phi^{[U]}(k; P, S)\gamma^0, \tag{2.56}$$

$$\text{Parity:} \quad \Phi^{[U]}(k; P, S) = \gamma^0 \Phi^{[U]}(\hat{k}; \hat{P}, -\hat{S})\gamma^0, \tag{2.57}$$

and for gluons:

$$\text{Hermiticity:} \quad \Gamma^{[U,U']\,\rho\sigma;\mu\nu *}(k; P, S) = \Gamma^{[U,U']\,\mu\nu;\rho\sigma}(k, P, S), \tag{2.58}$$

$$\text{Parity:} \quad \Gamma^{[U,U']\,\mu\nu;\rho\sigma}(k; P, S) = \Gamma^{[U,U']}_{\mu\nu;\rho\sigma}(\hat{k}, \hat{P}, -\hat{S}, \cdots), \tag{2.59}$$

where the vector $\hat{a} = \mathcal{P}a = (a, -\boldsymbol{a})$ is the parity transformed of vector a, that has a flipped sign in all the spatial coordinates [3]. The transformation properties (2.57) and (2.59) are valid for the double parton correlators as well.

The behavior of the Wilson lines under hermiticity and parity $\mathcal{P}$ transformations

[3] We do not use the barred notation for the vectors $\bar{a} = (a, -\boldsymbol{a}_T)$ as usually done in the literature, in order to avoid confusion with Section 2.3, where the bar indicates quantities belonging to the left-moving proton. The two vectors $\hat{a}, \bar{a}$ coincide when the transverse components are neglected.

is derived straightforwardly and reads:

$$U^{\dagger}_{[\alpha,\xi]} = U_{[\xi,\alpha]}, \quad \mathcal{P}U_{[\alpha,\xi]}\mathcal{P}^{\dagger} = U_{[\hat{\alpha},\hat{\xi}]}, \tag{2.60}$$

where $\hat{a}$ is defined as before.

The invariance under naive-time reversal transformation will instead not be imposed in the parametrization, as shortly explained.

Universality and process dependence

An important question about the correlators entering the factorized cross section formulae (and the functions in the parametrizations) is whether they are universal or they rather depend on the process under consideration. This matter is of utmost importance from a phenomenological point of view, as it determines whether the *same* partonic function can be eventually extracted from *different* processes. The answer to this question is connected to the gauge link structure of the correlators, which can vary from process to process. More precisely, the *lack* of universality can be related to the behavior of the transverse momentum dependent quantities under naive time reversal transformations. The complete treatment of this topic goes far beyond the purpose of this thesis. For a comprehensive set of references see, e.g., [39–48] and the dissertations in [26, 49, 50].

The quark and gluon correlators have the following behavior under naive time-reversal transformations $\mathcal{T}$:

$$\Phi^{[U]*}(k,P,S) = (-i\gamma_5 C)\Phi^{[U^{\mathcal{T}}]}(k,P,S)(-i\gamma_5 C), \tag{2.61}$$

$$\Gamma^{[U,U']\,\mu\nu;\rho\sigma *}(k,P,S) = \Gamma^{[U^{\mathcal{T}}U'^{\mathcal{T}}]}_{\mu\nu;\rho\sigma}(\hat{k},\hat{P},\hat{S}), \tag{2.62}$$

where $C = i\gamma^2\gamma^0$. From (2.62) the behavior of the Wilson lines under naive time reversal transformations is derived directly and it reads:

$$U^{\mathcal{T}} = \mathcal{T}U_{[\alpha,\xi]}\mathcal{T}^{\dagger} = U_{[-\hat{\alpha},-\hat{\xi}]}. \tag{2.63}$$

Time reversal transformations acting on the gauge links are such that future-pointing structures are transformed into past-pointing ones and viceversa (see part (a) and (b) of Fig. 2.7). For the TMD quark correlator this results in:

$$\Phi^{[+]}(x,\boldsymbol{k}_T;P,S) \xrightarrow{\mathcal{T}} \Phi^{[-]}(x,\boldsymbol{k}_T;P,S). \tag{2.64}$$

One can decompose each correlator into a T-even and a T-odd part as follows [51]:

$$\Phi^{[\text{T-even}]}(x, \boldsymbol{k}_T; P, S) = \frac{1}{2}\left[\Phi^{[+]}(x, \boldsymbol{k}_T; P, S) + \Phi^{[-]}(x, \boldsymbol{k}_T; P, S)\right], \tag{2.65}$$

$$\Phi^{[\text{T-odd}]}(x, \boldsymbol{k}_T; P, S) = \frac{1}{2}\left[\Phi^{[+]}(x, \boldsymbol{k}_T; P, S) - \Phi^{[-]}(x, \boldsymbol{k}_T; P, S)\right]. \tag{2.66}$$

In the parametrization of the correlator, naive time reversal symmetry does not impose constraints and T-odd structures do not vanish thanks to the presence of gauge links. We will see in Chapter 3 that one can parametrize the correlators in terms of quark distributions that multiply (Dirac and Lorentz) structures which flip sign under time reversal transformations. These functions, among which a famous one is the Sivers function (see Section 3.3.1), are non universal and depend on the process through the gauge link.

The scenario is more complex for gluons, for which there aretwo fundamental gauge-link structures that are not linked by any time-reversal transformation [47]. They are built from two past- or future-pointing staple-like links, called Weiszäcker-William (WW), and from one future- and one past-pointing staple-like gauge links, called dipole-type[4] (see Fig. 2.7(c)-(d) and Fig. 2.7(e)-(f) for WW and dipole-type of gauge links respectively). As pointed out in [47], due to the properties defined in (2.63), the WW structure $[++]$ is transformed to $[--]$ under time reversal transformations. Similarly, the dipole $[+-]$ becomes $[-+]$, whereas it is not possible to relate the WW-type with the dipole-type. It has been first discussed in [47] that, due to this complex color structure, the nonuniversality of gluon TMDs also involves the T-even part of the correlators.

From (2.66) it follows that the T-odd part vanishes when $\Phi^{[+]} = \Phi^{[-]}$. This is the case of the collinear correlators, where the gauge links reduce to a straight line, regardless of the light-cone direction. In the absence of the transverse direction no process dependence arises and PDFs are *universal* functions.

As a straightforward extension of the single parton case, the transverse momentum dependent DPDs, similarly as the single TMD PDFs, can be process dependent, although a precise expression for this dependence has never been derived. At variance with the single parton case, integration over transverse parton momenta does not lead, in principle, to the universality of collinear DPDs [31]. The universality is ensured in the cases when the two partons involved in each hard scatterings are in a color singlet configuration. In this case, the gauge link structures reduce to segments connecting the pairs of space-time point along the light-like direction. The lines are

[4]The latter nomenclature is not typically used in the field of TMD phenomenology, but it is rather common in the field of small-x physics.

thus invariant under time reversal symmetry and the relevant collinear DPDs are guaranteed to be universal, analogously to the single collinear PDFs [31, 52].

To summarize, the nonperturbative physics of high-energy processes is contained in the correlators, defined from the factorized cross section formulae. The operator definition can be easily extended to multiparton scattering processes. Without any further specification but the parton type, we can define the general symmetry properties of correlators, such as discrete space-time symmetries and gauge invariance. These aspects are fundamental to define the partonic functions that will be used to parametrize the correlators.

As discussed in Section 1.1, attempting an explicit calculation of the correlators is prohibitive with standard field theory formalism, because of the non smallness of the strong coupling in the low energy regime. In order to grasp information on the nonperturbative physics one can for instance seek help from lattice QCD calculations [34, 53–57], hamiltonian methods [6], model calculations [58–66], and extraction from experiments (see e.g. [67] and references therein). From a theoretical point of view, the hadronic matrix element contained in the definitions of the correlator can be formally expressed in terms of an expansion of wave functions, containing all the information about the parton dynamics and correlations. We will analyze this aspect in the next Section.

2.6 QCD on the light-front

Employing the light-cone coordinates to describe the kinematics of high energy processes is the natural and convenient choice, given that the dominant contribution to the deep inelastic kinematics comes from the light-cone. The numerous advantages of using the light-cone reference frame in the field of hadronic physics are extensively acknowledged[5] [6], and we discuss some of them in the present Section.

Field theories are quantized by introducing equal-time commutation and anti-commutation rules. In a covariant theory, it is possible to generalize the concept of time and space since what is called time-component is in some sense arbitrary. In 1949 Dirac [69] pointed out that there are three distinct ways to parametrize the 4-dimensional space, which are not connected by Lorentz transformations. Dirac defined three *forms of relativistic dynamics*, characterized by different definitions of the equal-time hyperplane where the fields are initialized. These three forms correspond to

[5] On the other hand, it is under debate whether this also represents an intrinsic simplification of QCD itself, see e.g. [68]. In the following we will not discuss this controversy further.

different *time-like* components. The usual quantization choice is called "instant-form" (IF) and corresponds to a hypersurface located at $t = x^0 = 0$, while the "light-front" (LF), or front-form, is characterized by the initial condition $x^+ = (x^0 + x^3)/\sqrt{2} = 0$, that represents a tangent plane to the light-cone. Being equivalent to the infinite momentum frame [70–74], it was recognized that LF quantization is particularly suitable in the description of high-energy processes [75–77]. For instance, the kinematic regime described in (2.14) naturally implies the choice $\xi^+ = 0$, and (LF-)time-ordering is automatic. The third form is called "point-form" and it is characterized by a hyperboloid-shaped hypersurface always pointing inside the light-cone. The picture in Fig. 2.8 graphically summarizes the three forms.

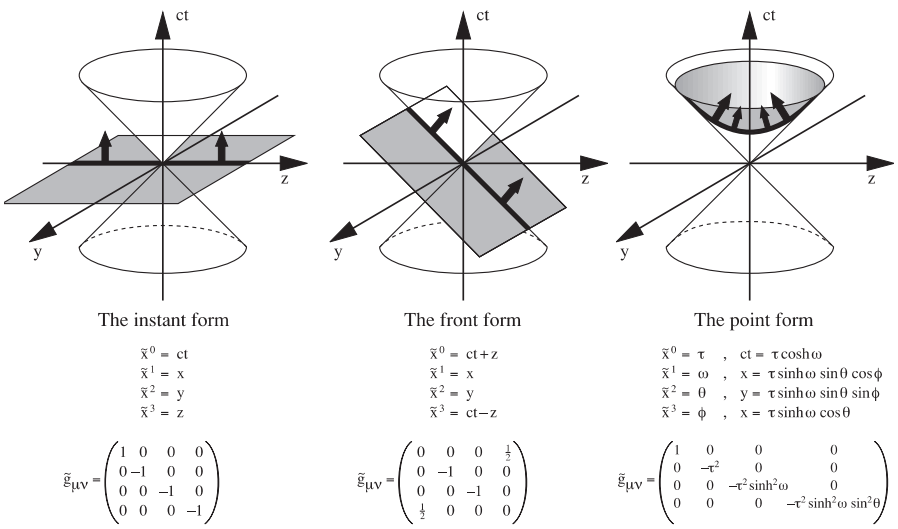

Figure 2.8: Graphic representation of the different forms of relativistic dynamics as formulated by Dirac [69]. The planes represent the hypersurface where the fields are initialized. Figure from ref. [6].

One can start by defining the four-vectors as in eq. (2.2) with components[6] [74]:

$$x^+ = \frac{1}{\sqrt{2}}\left(x^0 + x^3\right), \quad x^- = \frac{1}{\sqrt{2}}\left(x^0 - x^3\right), \quad \boldsymbol{x}_T = (x^1, x^2). \tag{2.67}$$

Therefore the following convention will be used:

$$x^\mu = (x^+, x^-, \boldsymbol{x}_T). \tag{2.68}$$

The metric tensor is[7]:

$$g_{\mu\nu} = g^{\mu\nu} = \begin{pmatrix} 0 & 1 & 0 & 0 \\ 1 & 0 & 0 & 0 \\ 0 & 0 & -1 & 0 \\ 0 & 0 & 0 & -1 \end{pmatrix}, \tag{2.69}$$

which is used to lower or raise indices, so that $x^+ = x_-$ and $x^- = x_+$. This means that $\partial_+ = \partial/\partial x^+ = \partial^-$ is a time-like derivative, while $\partial_- = \partial/\partial x^- = \partial^+$ is a space-like derivative. Scalar products reads:

$$x \cdot y = x^\mu y_\mu = g_{\mu\nu} x^\mu y^\nu = x^+ y^- + x^- y^+ - \boldsymbol{x}_T \cdot \boldsymbol{y}_T. \tag{2.70}$$

Other conventions and useful relations are collected in Appendix A.

Poincaré generators and Algebra

A remarkable feature of the LF quantization relies in the particular form of the Poincaré algebra [6, 74]. Dirac defines two classes of generators: dynamical and kinematic [69]. The latter are independent on the interaction, and they form a subgroup of the Poincaré group which transforms the hypersurface in itself. This is called *stability group*. The other Poincaré generators are called dynamical, as they contain the dynamics and transform the hypersurface into a different one. They play the role of hamiltonians in the sense of generators of time translations.

In any form of dynamics, the four-momentum P^μ and angular-momentum $M^{\mu\nu} = x^\mu P^\nu - x^\nu P^\mu$ obey the standard commutation relations which define the Poincaré group. Rotations and boosts are built as $J_i = \varepsilon_{ijk} M_{jk}$ and $M_{i0} = K_i$ (see Appendix A). In the instant form, the three components of the boost vector $M_{i0} = K_i$

[6] In the following the Kogut-Soper convention in [74] is used. A different choice of variables is the Brodsky-Lepage convention described in [6]

[7] We keep the same notation $g^{\mu\nu}$ as for the metric in IF, since this is not ambigous

are dynamical, and the three components of angular momentum $J_i = \varepsilon_{ijk} M_{jk}$ are kinematic. Let us define the combinations:

$$B_1 = \frac{1}{\sqrt{2}} (K_1 + J_2), \qquad B_2 = \frac{1}{\sqrt{2}} (K_2 - J_1), \tag{2.71}$$

$$S_1 = \frac{1}{\sqrt{2}} (K_1 - J_2), \qquad S_2 = \frac{1}{\sqrt{2}} (K_2 + J_1), \tag{2.72}$$

and analyze the generators in LF. Although the full set of generators must still obey the same Poincaré algebra, one can identify a subgroup of mutually commutant generators $P^-, P^+, P^1, P^2, J_3, B_1$ and B_2 that satisfy the commutation rules typical of a non-relativistic Galilean group in two-dimensions. This isomorphism between groups implies that the dynamics in the transverse plane is equivalent to a classical system. Moreover, the effect of the LF longitudinal boost leaves the transverse plane invariant. Denoting with β the dimensionless parameter of the boost, one has:

$$a^\mu \to a'^\mu = (\beta a^+, \frac{1}{\beta} a^-, \boldsymbol{a}_T). \tag{2.73}$$

Let us turn to the physical interpretation of the above discussion. During a high-energy scattering, an energetic probe scatters off a hadron along the longitudinal direction P^+. The hadron is highly boosted along this direction. In LF quantization, because of (2.73) the Lorentz contraction only occurs in the longitudinal direction, while the transverse plane remains unchanged. A parton inside the hadrons carries a fractions x of longitudinal momentum defined as $x = k^+/P^+$, which is a boost-invariant quantity in LF quantization. The following identifications are in order:

$$P^- \to \text{Hamiltonian};\ P^+ \to \text{Longitudinal momentum}; \tag{2.74}$$

$$\boldsymbol{P}_T \to \text{Transverse momenta};\ J_3 \to \text{Angular Momentum}; \tag{2.75}$$

$$\boldsymbol{B}_T \to \text{“Galilean” boosts along } x \text{ and } y. \tag{2.76}$$

The LF Hamiltonian P^- is the generator of the time evolution with respect to the LF time x^+, while the generators P^+ and $\boldsymbol{P}_T$ are kinematical. This identification explains why the notation $P = (P^-, P^+, \boldsymbol{P}_T)$ is very often preferred in the literature.

Dispersion relation

Given the momentum P of a massive particle of mass M, such that $P^\mu P_\mu = M^2$, one derives the LF dispersion relation:

$$P^- = \frac{(\boldsymbol{P}_\tau)^2 + M^2}{2P^+}. \tag{2.77}$$

The above dispersion relation is quite remarkable for the following reasons:

- It is a relativistic dispersion relation without any square root factors.
- The dependence of the energy P^- on the transverse momentum is the same as the nonrelativistic one.
- For P^+ positive (negative), P^- is positive (negative). This implies that it is possible to redefine negative momenta in order to always read $P^+ \geq 0$ both for particles and antiparticles. The latter constraint on the particle momenta has been referred to as responsible for the absence of vacuum diagrams and consequently the triviality of the QCD vacuum in LF. In [68], Collins explicitly shown that vacuum bubble diagrams do not actually vanish as often stated, and that the interacting QCD vacuum does not trivially coincide with the one of the free theory. However, the LF form still provides a number of advantages for the hadronic description as discussed in the rest of this Chapter.

2.6.1 Quantum field theories on the light-cone

An other significant feature of LF dynamics is that one can reduce the fermionic degrees of freedom from four to two. We shall see that the components of the fields are in fact not all independent and it is possible to define the *good* (*bad*) components of the fields, as the ones that are (not) dynamically independent. We define the Dirac gamma matrices in LF:

$$\gamma^+ = \frac{1}{\sqrt{2}}(\gamma^0 + \gamma^3), \qquad \gamma^- = \frac{1}{\sqrt{2}}(\gamma^0 - \gamma^3), \qquad \boldsymbol{\gamma}_\tau = \{\gamma^1, \gamma^2\}, \tag{2.78}$$

and the orthogonal projectors operators $P_\pm = \frac{1}{2}\gamma^\mp\gamma^\pm$:

$$P_- P_+ = P_+ P_- = 0, \qquad P_- + P_+ = 1, \tag{2.79}$$

which project out the good and bad field components as shortly explained. Rather than the Dirac representation of the gamma matrices, it is more convenient to choose

the Weyl or *light-cone* representation, where γ^0 is not diagonal while γ_5 is diagonal. In this choice of basis, the projectors (2.79) take the explicit form:

$$P_+ = \begin{pmatrix} 1 & 0 & 0 & 0 \\ 0 & 1 & 0 & 0 \\ 0 & 0 & 0 & 0 \\ 0 & 0 & 0 & 0 \end{pmatrix}, \quad P_- = \begin{pmatrix} 0 & 0 & 0 & 0 \\ 0 & 0 & 0 & 0 \\ 0 & 0 & 1 & 0 \\ 0 & 0 & 0 & 1 \end{pmatrix}. \tag{2.80}$$

The effect of the operators $P_\pm$ is to project out the two upper and lower components of the Dirac fields:

$$P_+\psi = \psi_+ = \phi = \begin{pmatrix} \phi^1 \\ \phi^2 \\ 0 \\ 0 \end{pmatrix}, \quad P_-\psi = \psi_- = \chi = \begin{pmatrix} 0 \\ 0 \\ \chi^1 \\ \chi^2 \end{pmatrix}. \tag{2.81}$$

Applying one projector at a time to the color Dirac equation, one obtains two coupled equations of motion for the upper and lower components:

$$i\gamma^- D^+ \psi_- - (\boldsymbol{\gamma}_T \cdot \boldsymbol{D}_T - m)\psi_+ = 0, \tag{2.82}$$

$$i\gamma^+ D^- \psi_+ - (\boldsymbol{\gamma}_T \cdot \boldsymbol{D}_T - m)\psi_- = 0. \tag{2.83}$$

where $D^\pm = \partial^\pm - igA^\pm$ is the covariant derivative and it is a matrix in color space.

From eq. (2.82) one can see that ψ_+ is the only independent field, since it has a non vanishing conjugate field. We refer to it as the *good* field and denote it with ϕ. The good fields describe a particle on its mass-shell [6]. At variance, the two components of ψ_- are not independent variables and they are constrained at any light-front time x^+ in terms of ϕ and A. The component A^- is also not independent, and one can usually fix a gauge where $A^+ = 0$ (*light-cone gauge*) [6,74]. Therefore ψ_- depends on the only dynamical fields ϕ and $\boldsymbol{A}_T$.

We refer to Appendix A for the explicit form of the good fields and to [6,70–74,78] for more details about LF quantization.

2.6.2 Light-Front Wave Functions (LFWFs)

As discussed earlier in this Chapter, the definition of the correlators contain matrix elements in which the hadron state $|P\rangle$ explicitly appears. Since $|P\rangle$ can formally be written as a bound-state of its constituents, the question is whether the formalism of LF quantization would simplify the description of bound-states. Let us consider the

relativistic bound-state problem:

$$H\,|\psi\rangle = \sqrt{M^2 + P^2}\,|\psi\rangle\,, \tag{2.84}$$

which corresponds to the eigenvalue problem for the QCD Hamiltonian, where M is the particle's mass and $|\psi\rangle$ is the hadronic wavefunction, expansion of multi-particle Fock eigenstates of the Hamiltonian $|n\rangle$, i. e. $|\psi\rangle = \sum_n \psi_n\,|n\rangle$. The treatment of such a relativistic bound-state represents a formidable challenge, both from a theoretical and practical point of view. The theoretical problem is related to the well-known nonperturbative nature of such an expression. The practical problems refer to the presence of the square root operator, which brings positive (negative) energies for particles (antiparticles), and the fact that the vacuum state is not an eigenstate of the full Hamiltonian. Moreover, in the standard instant form quantization, one should deal with the difficulties related to the presence of dynamical boost operators and nontrivial QCD vacuum.

It has been argued in refs. [6,79,80] that the situation highly simplifies in the light-front, although a firm preference for this approach in the hadronic physics community is not unanimous (see, e.g. [81]). The hadronic eigenvalue problem simplifies in light-front, and the hamiltonian eigenvalue problem reads:

$$H\,|\psi\rangle = \frac{M^2 + \boldsymbol{P}_T^2}{2P^+}\,|\psi\rangle = P^-\,|\psi\rangle\,, \tag{2.85}$$

which is a simplification because: 1) the boosts are kinematic, 2) from the on-shell condition follows that P^+ has only positive eigenvalues, and 3) the square-root operator is absent[8].

The state $|\psi\rangle$ is eigenstate of a complete set of mutually commuting operators: the mass, the three space-like momenta $P^+, \boldsymbol{P}_T$, the spin four-vector squared S^2 and its longitudinal projection S_z. Namely:

$$|\psi\rangle = \left|h; M, P^+, \boldsymbol{P}_T, S^2, S_z\right\rangle, \tag{2.86}$$

where we indicate with the index h everything that specifies the hadron, such as charge, parity, baryon number. The $|\psi\rangle$ is expanded in terms of a complete basis of Fock states of the type:

$$|N; x_i, \boldsymbol{k}_{Ti}, \beta_i\rangle\,,$$

[8]It is commonly added to this list that the QCD vacuum is trivially an eigenstate of the Hamiltonian. This statement is lively debated in the community and was formally proved to be incorrect in [68]. The considerations on the light-front wave functions remain valid and correct even in the absence of the vacuum triviality assumption.

which represent the N-partons states. The indices β_i includes all the other indices, such as parton-type, helicity, etc., and $(x_i, \boldsymbol{k}_{Ti})$ are the momentum components of each parton. Each parton in the state (quark, antiquark, gluon) with momentum components $k^+, \boldsymbol{k}_T$ and helicity β is created from the vacuum state due to the action of creation operators $(b^\dagger,\ d^\dagger, a^\dagger)$ whose commutation and anticommutation rules are listed in Appendix A. Namely[9]:

$$|q; k^+, \boldsymbol{k}_T, \beta\rangle = b^\dagger(k^+, \boldsymbol{k}_T, \beta)\,|0\rangle\,, \tag{2.87}$$

$$|\bar{q}; k^+, \boldsymbol{k}_T, \beta\rangle = d^\dagger(k^+, \boldsymbol{k}_T, \beta)\,|0\rangle\,, \tag{2.88}$$

$$|g; k^+, \boldsymbol{k}_T, \beta\rangle = a^\dagger(k^+, \boldsymbol{k}_T, \beta)\,|0\rangle\,. \tag{2.89}$$

The state of a hadron with momentum P and LF helicity Λ can therefore be written as a sum over all the Fock states:

$$|P, \Lambda\rangle = \sum_{N,\beta} \int \left[\frac{dx}{\sqrt{x}}\right]_N \left[d^2\boldsymbol{k}_T\right]_N \psi^\Lambda_{N,\beta}(r)\,|N; k_1, \cdots, k_N, \beta_1, \cdots, \beta_N\rangle\,, \tag{2.90}$$

where the projection of the hadron state onto the N-parton Fock states $\psi^\Lambda_{N,\beta}(r)$ are called *light-front wave functions* LFWFs. We define:

$$r = (r_1, \ldots, r_N)\,, \quad \text{with} \quad r_i = (x_i, \boldsymbol{k}_{Ti})\,. \tag{2.91}$$

The LFWFs are normalized as follows:

$$\sum_N \int \left[\frac{dx}{\sqrt{x}}\right]_N \left[d^2\boldsymbol{k}_T\right]_N \left|\psi_{n/h}(N, x_i, \boldsymbol{k}_{Ti}, \beta_i)\right|^2 = 1, \tag{2.92}$$

with the integration measures:

$$\left[\frac{dx}{\sqrt{x}}\right]_N \equiv \prod_{i=1}^N \frac{dx_i}{\sqrt{x_i}} \delta\left(1 - \sum_{i=1}^N x_i\right), \tag{2.93}$$

$$\left[d^2\boldsymbol{k}_T\right]_N \equiv \frac{1}{(16\pi^3)^{N-1}} \prod_{i=1}^N d^2\boldsymbol{k}_{Ti}\delta^{(2)}\left(\sum_{i=1}^N \boldsymbol{k}_{Ti}\right). \tag{2.94}$$

The LFWFs are frame independent quantities that only depend on relative coordi-

[9]The following property is typical of LF quantization and it is usually ascribed to the fact that, ignoring zero-modes, the perturbative vacuum is trivial in QCD and therefore $a\,|0\rangle = 0$. It has been shown in ref. [68] that the perturbative vacuum in LF actually satisfies $a\,|0\rangle = 0$ and allows the LFWF overlap representation, without any (wrong) assumption on the vacuum triviality.

nates x_i and $\boldsymbol{k}_{T_i}$, but not on the hadron momentum. This ultimately means the centre of mass motion can be separated from the relative motion of the partons [69].

The LFWFs are nonperturbative quantities. In practice, the expansion (2.90) can be used to model simultaneously several hadronic observables within a unifying framework, such as the matrix elements defining the TMDs, DPDs, PDFs, etc. [82].

2.7 Summary

We have presented an overview of selected topics relevant to the study of the hadron structure. This will serve as introductory material for the rest of the dissertation. An important consideration arising from the previous sections regards the versatility of the concept of parton correlators inside hadrons. The definition in terms of hadronic matrix element containing fields operators is extremely general, and it is indeed used in many contexts where one needs to specify the hadronic part in the factorized cross section formulae.

The operator definition derived from the diagrammatic approach needs to be complemented with Wilson lines to ensure gauge invariance, and this affects the universality of the correlator, which becomes process dependent in the TMD and DPS cases.

The correlators can be decomposed and parametrized in terms of functions that encode all the nonperturbative aspects of parton dynamics inside the hadron. These functions are related to the final state distributions and can be extracted in several processes.

Each correlator entering a hard scattering contains a hadron state. This is a cumbersome complication because an explicit procedure to derive the hadronic wave function is not know. A convenient formalism is then the use of the LFWFs, frame-independent quantities in terms of which all the partonic functions can be expressed. This would represent a unifying way of describing the hadronic observables in the seek of complete knowledge of hadron structure.

Chapter 3

Quarks and gluons in polarized hadrons and nuclei of spin ≤ 1

3.1 Introduction

In this Chapter, we discuss the parametrization of the TMD correlator of quarks and gluons in terms of transverse momentum-dependent parton distributions (TMDs), starting from the matrix elements (2.47) and (2.48).

The decomposition of the correlators in terms of relevant structures allowed by symmetry, multiplied by nonperturbative functions (TMDs), is an advantageous procedure. In fact, it enables us to single out the relevant quantities that contribute to the cross section of a selected process. The complete parametrization of the TMD correlator for quarks, including the T-odd structure, was given in [83] for spin-$1/2$ hadrons, and complemented in [84, 85] with the tensor polarization part (relevant for spin-1 and higher). As far as gluons are concerned, the first parametrization was performed in [86], followed by [87]. The latter focused on spin-$1/2$ targets, and we recently extended the parametrization for the complete spin-1 case in [88].

The study of the gluonic content of hadrons of spin higher than $1/2$ and nuclei

has been recently attracting attention also from the experimental and lattice community [89–91]. Looking at new gluon distributions, which are not related to the ones in the nucleons, can become very interesting for instance to study *exotic* (non-nucleonic) effects in the binding of nuclei.

The results we present on gluons are based on [88,92,93]. In particular, we include the definition and parametrization of a different type of correlator, the Wilson loop correlator, which is connected to the gluon correlator in the small-x domain [88]. For completeness, we also include the well-known results on quarks.

3.2 TMD correlators for polarized hadrons

We present the leading-twist expansion of the TMD correlator. The dependence on the transverse components of the parton momentum and the additional degrees of freedom linked to the polarization of the target are responsible for the significant number of functions appearing in the parametrization. We consider targets of spin up to 1. We begin by reviewing the general features of the parametrization valid both for quarks and gluons. Throughout this Chapter, a Sudakov type of decomposition for the four-vectors is employed, as explained in Section 2.2.

Target spin: 0, 1/2, and 1

In quantum mechanics we describe mix states by means of the density matrix ρ, defined as follows:

$$\rho = \sum_i p_i \, |i\rangle \, \langle i| \, , \tag{3.1}$$

where $|i\rangle$ are pure states and p_i is the probabilities of finding the particle in the spin state $|i\rangle$. The density matrix of a spin-$1/2$ hadron which is not in a pure state can be written as:

$$\rho = \frac{1}{2}(I + \boldsymbol{S} \cdot \boldsymbol{\sigma}), \tag{3.2}$$

where $\boldsymbol{\sigma} = (\sigma^1, \sigma^2, \sigma^3)$ are Pauli matrices and the vector $\boldsymbol{S} = (S^1, S^2, S^3)$ is identified as the spin vector of the particle in cartesian coordinates. A generalization of spin vectors into a covariant form can be obtained by defining the spin in the rest frame as space-like four-vector $S^\mu = (0, \boldsymbol{S})$. In the rest frame (and in any frame) one has $P \cdot S = 0$. A possible parametrization is:

$$S^\mu = S_L \frac{P^\mu}{M} + S_T^\mu - M S_L \, n^\mu. \tag{3.3}$$

The decomposition of the density matrix for a spin-1/2 particle can be generalized for spin-1 particles. In fact, one needs a Cartesian basis of 3×3 matrices formed by the identity matrix, the three-dimensional representation of the Pauli matrices Σ^i (generalized Pauli matrices), and the five bilinear combinations $\Sigma^{ij} = \frac{1}{2}(\Sigma^i\Sigma^j + \Sigma^j\Sigma^i) - \frac{2}{3}\delta^{ij}$. The density matrix has the form:

$$\rho = \frac{1}{3}\left(I + \frac{3}{2}S^i\Sigma^i + 3T^{ij}\Sigma^{ij}\right), \tag{3.4}$$

where the components S^i of the vector $\boldsymbol{S}$ are defined as previously and represent the vector part of the spin. The tensor part of the spin state is represented by the symmetric traceless tensor T^{ij}. The generalization into a covariant form is achieved by demanding $P_\mu T^{\mu\nu} = 0$. The parametrization reads:

$$\begin{aligned} T^{\mu\nu} = \frac{1}{2}\Bigg[&\frac{2}{3}S_{LL}\, g_T^{\mu\nu} + \frac{4}{3}S_{LL}\frac{P^\mu P^\nu}{M^2} + \frac{S_{LT}^{\{\mu}P^{\nu\}}}{M} + S_{TT}^{\mu\nu} \\ &- \frac{4}{3}S_{LL}P^{\{\mu}n^{\nu\}} - MS_{LT}^{\{\mu}n^{\nu\}} + \frac{4}{3}M^2 S_{LL}\, n^\mu n^\nu\Bigg]. \end{aligned} \tag{3.5}$$

The density matrix takes the form:

$$\rho(S,T) = \begin{pmatrix} \frac{1}{3} + \frac{S_L}{2} + \frac{S_{LL}}{3} & \frac{S_T^x - iS_T^y}{2\sqrt{2}} + \frac{S_{LT}^x - iS_{LT}^y}{2\sqrt{2}} & \frac{S_{TT}^{xx} - iS_{TT}^{xy}}{2} \\ \frac{S_T^x + iS_T^y}{2\sqrt{2}} + \frac{S_{LT}^x + iS_{LT}^y}{2\sqrt{2}} & \frac{1}{3} - \frac{2S_{LL}}{3} & \frac{S_T^x - iS_T^y}{2\sqrt{2}} - \frac{S_{LT}^x - iS_{LT}^y}{2\sqrt{2}} \\ \frac{S_{TT}^{xx} + iS_{TT}^{xy}}{2} & \frac{S_T^x + iS_T^y}{2\sqrt{2}} - \frac{S_{LT}^x + iS_{LT}^y}{2\sqrt{2}} & \frac{1}{3} - \frac{S_L}{2} + \frac{S_{LL}}{3} \end{pmatrix}. \tag{3.6}$$

The use of the spin density matrix allows one to include the target spin in the description in a Lorentz invariant way. The procedure is very general and can be extended to higher spin in an analogous way [94].

Symmetric traceless tensors

Both for quarks and gluons we write parametrizatons for target spin up to one, and employ symmetric and traceless tensors (STT) $k_T^{i_1\cdots i_n}$ that are built from the partonic momentum k_T. We use the metric tensor in transverse space defined as $g_T^{\mu\nu} \equiv g^{\mu\nu} - P^{\{\mu}n^{\nu\}}$ (curly brackets denote symmetrization of the indices), with nonvanishing elements $g_T^{11} = g_T^{22} = -1$. Up to rank $n = 4$, the tensorial structures are given by:

$$k_T^{ij} \equiv k_T^i k_T^j + \frac{1}{2}\boldsymbol{k}_T^2 g_T^{ij}, \tag{3.7}$$

$$k_T^{ijk} \equiv k_T^i k_T^j k_T^k + \frac{1}{4}\boldsymbol{k}_T^2 \left(g_T^{ij}k_T^k + g_T^{ik}k_T^j + g_T^{jk}k_T^i\right), \tag{3.8}$$

$$\begin{aligned} k_T^{ijkl} \equiv{}& k_T^i k_T^j k_T^k k_T^l + \frac{1}{6}\boldsymbol{k}_T^2 \left(g_T^{ij}k_T^{kl} + g_T^{ik}k_T^{jl} + g_T^{il}k_T^{jk} + g_T^{jk}k_T^{il} + g_T^{jl}k_T^{ik} + g_T^{kl}k_T^{ij}\right) \\ & - \frac{1}{8}\boldsymbol{k}_T^4 \left(g_T^{ij}g_T^{kl} + g_T^{ik}g_T^{jl} + g_T^{il}g_T^{jk}\right), \end{aligned} \tag{3.9}$$

satisfying

$$g_{T\,ij}k_T^{ij} = g_{T\,ij}k_T^{ijk} = g_{T\,ij}k_T^{ijkl} = 0. \tag{3.10}$$

From this decomposition of the Lorentz structures it follows that the functions involved in the parametrization are twist-2 TMDs of *definite rank*. This has the advantage that there is a one-to-one correspondence between the functions defined in $\boldsymbol{k}_T$ space and the correspondent ones that depend on the Fourier conjugate variable $\boldsymbol{b}_T$. This property turns out to be very convenient for the TMD evolution equations [95].

Twist expansion

Once the contributions allowed by symmetries are derived, the goal is to develop a tool to classify these terms, in order to recognize the important ones in the cross section calculation. In other words, one needs to identify the relevant expansion parameter that estimates the importance of each term of the correlator. This is why we need to introduce the concept of *twist*.

The twist expansion was first derived in the context of the Operator Product Expansion (OPE), proposed by Wilson in [96]. The OPE can be used to write a nonlocal operator $A(x)B(0)$ (e.g. the operator that enters the hadronic tensor) as an expansion on a basis of local operators $O_n(x)$ with (singular) coefficients that depend on the nonlocality, as long as the distance $|x|$ in spacetime is small [15], i.e.

$$\int d^4x e^{iq\cdot x} \langle P| A(x)B(0) |P\rangle = \sum_n C_n(q) \langle P| O_n |P\rangle . \tag{3.11}$$

The crucial point is to determine which operator in the expansion contribute the most. When applied to the DIS hadronic tensor, the singular coefficients are proportional to:

$$\left(\frac{M}{Q}\right)^{d_O - n - 2}, \tag{3.12}$$

where

$$t = d_O - n = \text{“dimension} - \text{spin”}, \tag{3.13}$$

is the *twist* of the local operator O, and governs the relevance of the operator in the expansion as powers of (M/Q).

Since the definition of twist is formally related to the validity of the OPE procedure, such expansion is in principle allowed only for the hadronic tensor of DIS, where $x^2 \sim 0$ (light-cone dominated) and e^+e^-, where $x \sim 0$ (short-distance dominated). In general, the formal derivation cannot be extended to all cases and, strictly speaking, it is not applicable to the Drell-Yan hadronic tensor.

However, the concept of twist can also be used in situations where the OPE does not hold true, and we hereby adopt a *working* definition of it. In [97] it is called twist the order in M/Q at which an operator contributes to the cross section of the high-energy process. It is based on the realization that one can order the operators by means of power counting, namely by counting the factors of mass M introduced in the parametrization in order to respect the mass dimension of the correlator. A twist t operator results in a contribution of the order

$$\left(\frac{M}{Q}\right)^{t-2} \tag{3.14}$$

to the cross section. The lowest order in the twist expansion is referred to as *twist-two*, while sub-leading terms are *twist-three* and higher. Throughout the Chapter, we only deal with twist-two contributions and omit any higher-twist structure in all the parametrizations we will present.

3.3 Parametrization for quarks

We denote the leading-twist TMD correlator as:

$$\begin{aligned}\Phi(x, \boldsymbol{k}_T) &\equiv \Phi^{[U]}(x, \boldsymbol{k}_T; n, P, S, T) \\ &\equiv \int \frac{d(\xi\cdot P) d^2\boldsymbol{k}_T}{(2\pi)^3} e^{ik\cdot\xi} \left\langle P, S, T \right| \overline{\psi}(0) U(0,\xi) \psi(\xi) \left| P, S, T \right\rangle \Big|_{\xi^+=0},\end{aligned} \tag{3.15}$$

where we indicate the dependence on the lightlike four-vector n, considering that in high energy processes one has staple-like gauge links running along the light-front $(\xi\cdot n = 0)$ via lightlike $\xi\cdot P = \pm\infty$.

We show the complete parametrization for quarks in hadrons of spin up to 1, using

symmetric traceless tensors [98], in a slightly different way as the original works [83–85], where the STT form was not employed. The correlator is organized in terms of target polarization, and schematically reads:

$$\Phi = \Phi_U + \Phi_L + \Phi_T + \Phi_{LL} + \Phi_{LT} + \Phi_{TT}, \tag{3.16}$$

with obvious meaning of the subscipts U, L, T, LL etc.. The decomposition reads:[1]

$$\Phi_U(x,\boldsymbol{k}_T) = \frac{1}{2}\left[\not{P} f_1(x,\boldsymbol{k}_T^2) + \frac{[\not{k}_T,\not{P}]}{2M} i\, h_1^\perp(x,\boldsymbol{k}_T^2)\right], \tag{3.17}$$

$$\Phi_L(x,\boldsymbol{k}_T) = \frac{1}{2} S_L \left[\gamma_5 \not{P} g_1(x,\boldsymbol{k}_T^2) + \frac{[\not{k}_T,\not{P}]}{2M}\gamma_5 h_{1L}^\perp\right], \tag{3.18}$$

$$\begin{aligned}\Phi_T(x,\boldsymbol{k}_T) = \frac{1}{2}\Bigg[&\frac{\epsilon_T^{S_T k_T}}{M}\not{P} f_{1T}^\perp(x,\boldsymbol{k}_T^2) + \frac{\boldsymbol{k}_T\cdot\boldsymbol{S}_T}{M}\gamma_5\not{P} g_{1T}(x,\boldsymbol{k}_T^2)\\ &+ \frac{[\not{S}_T,\not{P}]\gamma_5}{2} h_1(x,\boldsymbol{k}_T^2) - \frac{S_{T\rho}[\not{k}_T^\rho,\not{P}]\gamma_5}{2M^2} h_{1T}^\perp(x,\boldsymbol{k}_T^2)\Bigg],\end{aligned} \tag{3.19}$$

$$\Phi_{LL}(x,\boldsymbol{k}_T) = \frac{1}{2} S_{LL}\left[\not{P} f_{1LL} + \frac{[\not{k}_T,\not{P}]}{2M} i\, h_{1LL}^\perp(x,\boldsymbol{k}_T^2)\right], \tag{3.20}$$

$$\begin{aligned}\Phi_{LT}(x,\boldsymbol{k}_T) = \frac{1}{2}\Bigg[&\frac{\boldsymbol{k}_T\cdot\boldsymbol{S}_T}{M}\not{P} f_{1LT}(x,\boldsymbol{k}_T^2) + \frac{\epsilon_T^{S_{LT}k_T}}{M}\not{P}\gamma_5 g_{1LT}(x,\boldsymbol{k}_T^2)\\ &+ \frac{[\not{S}_{LT},\not{P}]}{2} i\, h_{1LT}(x,\boldsymbol{k}_T^2) - \frac{iS_{LT\rho}[\not{k}_T^\rho,\not{P}]}{2M^2} h_{1LT}^\perp(x,\boldsymbol{k}_T^2)\Bigg],\end{aligned} \tag{3.21}$$

$$\begin{aligned}\Phi_{TT}(x,\boldsymbol{k}_T) = \frac{1}{2}\Bigg[&\frac{k_T^{\mu\nu} S_{TT\mu\nu}}{M^2}\not{P} f_{1TT}(x,\boldsymbol{k}_T^2) - \frac{\epsilon_{T\mu\nu} k_T^{\mu\rho} S_{TT\rho\nu}}{M^2}\gamma_5\not{P} g_{1TT}(x,\boldsymbol{k}_T^2)\\ &- \frac{k_T^\rho[\not{S}_{TT\rho},\not{P}]}{M} i h_{1TT}(x,\boldsymbol{k}_T^2) + \frac{S_{TT\rho\sigma}[\not{k}_T^{\rho\sigma},\not{P}]}{M^3} i h_{1TT}^\perp(x,\boldsymbol{k}_T^2)\Bigg],\end{aligned} \tag{3.22}$$

where we use the notation $\not{k}^\rho S_\rho = \gamma_\mu k^{\mu\rho} S_\rho$, and analogously for the other contractions. The transverse antisymmetric tensor is defined as $\epsilon_T^{\mu\nu} \equiv \epsilon^{Pn\mu\nu}$, with nonzero components $\epsilon_T^{12} = -\epsilon_T^{21} = 1$. The f-type functions represent unpolarized parton structures, while g- and h-type functions are polarized distributions. Unless otherwise specified, the full dependence of the functions of the renormalization scale μ is understood. This aspect will be discussed in Chapter 5, where we implement the QCD evolution of the unpolarized TMD $f_1(x,\boldsymbol{k}_T)$, as well as the correspondent collinear function in

[1] We define the transverse four-vector a_T^μ to have light cone components $(0,0,\boldsymbol{a}_T)$, where $\boldsymbol{a}_T$ is a two-dimensional vector on the transverse plane. This implies e.g. that $a_T^2 = -\boldsymbol{a}_T^2$.

	Unpolarized	**Longitudinal**	**Transverse**
U	$\boldsymbol{f_1}$		$h_1^\perp$
L		$\boldsymbol{g_1}$	$h_{1L}^\perp$
T	$f_{1T}^\perp$	g_{1T}	$\boldsymbol{h_1}, h_{1T}^\perp$
LL	$\boldsymbol{f_{1LL}}$		$h_{1LL}^\perp$
LT	f_{1LT}	g_{1LT}	$h_{1LT}, h_{1LT}^\perp$
TT	f_{1TT}	g_{1TT}	$h_{1TT}, h_{1TT}^\perp$

Table 3.1: Summary table of the quark TMDs in polarized targets of spin up to 1. The rows display the target polarization (unpolarized, vector and tensor polarized) and the columns refer to the quark. Bold-face functions survive integration over transverse momenta and have a collinear correspondent. We do not display the collinear T-odd function h_{1LT} with bold-face, see main text.

a model calculation using AdS/QCD. In table 3.1 the functions are organized and divided according to the quark/hadron polarization.

Integration over transverse momenta

Integration over transverse momenta forces many functions to vanish. The collinear correlator can be parametrized as follows:

$$\Phi(x;P,S,T) = \frac{1}{2}\left[\not{P} f_1(x) + S_L\gamma_5\not{P} g_1(x) + \frac{[\not{S}_T,\not{P}]\gamma_5}{2} h_1(x) + S_{LL}\not{P} f_{1LL}(x) + \frac{[\not{S}_{LT},\not{P}]}{2} i\, h_{1LT}(x,\boldsymbol{k}_T^2)\right], \tag{3.23}$$

where $f_1(x) \equiv \int d^2\boldsymbol{k}_T\, f_1(x,\boldsymbol{k}_T^2)$, and similarly for the other functions. The quark PDFs for spin-1/2 target are historically the first quantities studied to investigate the hadronic structure. They represent the distribution of quarks in the longitudinal momentum space of unpolarized (f_1), longitudinally polarized (g_1, also called Δf), and transversely polarized (h_1) quarks in the proton. The spin-1 case has an extra collinear function, in our notation called f_{1LL}. This function is usually referred to as the b_1 function of [99] and is particularly attractive because it contains non-nucleonic degrees of freedom that are detectable in the nuclei. We include the collinear function

h_{1LT} which is T-odd and simultaneously survives integration over transverse momenta. At first order, in the framework where we operate the function h_{1LT} appears to vanish due to the gauge link structure and the behavior under naive time reversal transformations. However, the complete analysis of the gluonic pole matrix element associated with this function partially discussed in [50], might also contradict this statement.

3.3.1 Quark TMDs phenomenology

The intrinsic motion of partons inside the proton is responsible for the specific dependence of the cross section on an azimuthal angle. The various correlations encoded in the TMDs translate into azimuthal or spin *asymmetries* of the measured cross section, which are calculable assuming the validity of factorization theorems and whose measurement gives indirect access to a variety of TMDs (both distributions and fragmentation functions).

Experimental information on the TMD functions is restricted to few functions, and for unpolarized and vector polarized targets, while no data are available for the functions related to tensor polarization. We refer to the reviews [67, 100] and the dissertation [95] for a fairly complete overview of the status and perspectives of TMD phenomenology.

The unpolarized TMD f_1 is, at present, the best known TMD function. Reaching an increasingly better accuracy in the extraction of the unpolarized TMD is surely important on its own, but particularly because its value enters in the definition of all the asymmetries. Data on the unpolarized function are extracted from several processes in the facilities across the globe: from SIDIS at HERMES and COMPASS [101, 102], from DY at Fermilab, and from Z boson production at LHC and Tevatron [103]. The development of the formalism and the availability of experimental data on the nucleon led to recent extractions which are boosting the knowledge of the f_1 to the level of precision physics [104–109]. The second most known function is the Sivers function $f_{1T}^{\perp}$, followed by the transversity h_1, the Boer-Mulders $h_1^{\perp}$ and pretzelosity $h_{1T}^{\perp}$ [100]. Almost no experimental information is available for all the other functions. Worth mentioning is the history of the Sivers function $f_{1T}^{\perp}$. It was first introduced by Sivers [110], but later in [111] it was argued to be vanishing using time-reversal symmetry arguments. After the calculation in [112], it became clear that the Sivers function does not vanish thanks to the presence of the Wilson lines. The asymmetry arising in the angular distribution of the produced particles in processes involving transversely polarized targets was eventually calculated in [113], and this was subsequently called the Sivers effect. As a direct consequence of the presence of the gauge

link, the quark Sivers function (likewise all the other T-odd distributions) is not universal, as mentioned in Section 2.5. In particular, as a consequence of (2.64) one has:

$$f_{1T}^{\perp[+]}(x, \boldsymbol{k}_T^2) = -f_{1T}^{\perp[-]}(x, \boldsymbol{k}_T^2), \tag{3.24}$$

which is equivalent to saying that the Sivers function enters the cross section formula of SIDIS process (future-pointing gauge link) with an opposite sign than the Sivers function that enters the Drell-Yan (past-pointing gauge link). The first experimental measurements of the Sivers asymmetry were performed by the HERMES collaboration [114], and the measurements of the sign-change in (3.24) is at present one of the focus of the programs at the COMPASS-II experiment at CERN, at RHIC (BNL) [115] and at Fermilab [116, 117].

Similarly to the Sivers, the functions $h_1^\perp$, g_{1LT}, g_{1TT}, $h_{1LL}^\perp$, h_{1LT}, $h_{1LT}^\perp$, $h_{1TT}^\perp$, $h_{1TT}^{\perp\perp}$ are odd under naive time reversal transformations (T-odd). The Boer-Mulders function $h_1^\perp$, first defined in [51], is related to the density number of transversely polarized quarks in an unpolarized target in the current program of COMPASS. This T-odd function is a h-type function, which means that it is also chiral-odd because it describes a flip in the quark chirality. Likewise all the chiral-odd quark functions, their study is limited to those processes where they can couple with another chiral-odd structure, being a TMD PDF (double Boer-Mulders effect in Drell-Yan) or a TMD fragmentation function (the chiral-odd Collins function, for instance in SIDIS [118]) or with a mass term.

Almost no information is available for the tensor polarized functions, except in the collinear case. The function called here f_{1LL} is related to the structure function called b_1 in the deuteron. This was the object of a study by Hoodboy and Jaffe in [99], where, for the first time, was pointed out that in high-energy processes involving spin-1 hadrons one can define collinear quark structure functions (called $b_{1,2,3,4}$) that can be measured in experiments of inclusive deep inelastic scattering of an electron off a tensor polarized target. The extraction of the function b_1 for the deuteron was performed by the HERMES collaboration in 2005 [119]. The data collected and the parametrization proposed [120] deviate significantly from the standard theoretical predictions [99, 121–123], both for the x behavior and the magnitude, although the experimental uncertainties leave room for improvements. This suggests that, for the deuteron, dynamics beyond quarks and gluons confined within the individual nucleons is needed to describe it. More measurements of b_1 will be performed as part of the 12 GeV program at Jefferson Lab (JLab) [124]. Ideally, information on other spin-1 targets such as (virtual) ρ mesons would allow us to thoroughly study such different quark contributions and dynamics [65]. However, this is currently beyond

any experimental reach.

3.4 Gluons in polarized hadrons and nuclei

Whereas considerable knowledge has been acquired on the quarks over the past decades, understanding the gluonic content of hadrons is a challenging task far from being accomplished. Gluon observables are typically overwhelmed by the valence quark ones, as far as present experimental facilities are concerned. However, at higher energies, the gluon (and the quark sea) distributions become important, and they need to be studied in details [125].

The gluon TMDs are relevant for processes where the hard scattering is initiated by gluons rather than quarks. An example is the gluon-gluon fusion that leads to the production of a colorless final state (for example the Higgs boson). More generically one can have a partonic scattering involving gluons (or mixed quark/gluon distributions) resulting in the production of jets, or hadrons or photons at high transverse momentum.

The dominance of gluon quantities occurs in experiments which probe a region of low fraction of momentum x, as planned for the future Electron-Ion Collider (EIC) [126, 127]. Relevant small-x regions are accessible also when the centre of mass energy of the collisions increases, as expected for the LHC within the high-luminosity program. A new program of QCD precision physics will then be possible, in which the gluons will play a very important role.

An interesting and even less investigated aspect is the gluonic structure linked to the polarization of the target of spin ≤ 1, where non-nucleonic dynamics becomes accessible. The inclusion of tensor polarization, related to particles of spin larger than 1/2, could yield new insights into the internal dynamics of hadrons and nuclei.

3.4.1 Gluon correlation function

In 2001, Mulders and Rodrigues presented the first parametrization of the gluon TMD correlator at twist-two [86], considering both unpolarized and vector polarized hadrons, relevant for target of spin 0 and 1/2. In Ref. [88] we extended the analyses of refs. [86,87] by parametrizing the gluon correlator for unpolarized, vector polarized, as well as tensor polarized hadrons. In the same work, a connection between the gluon TMD operator, calculated at small-x, and the Wilson loop operator, that will be defined later in Section 3.4.3, was explored. A systematic way of naming the various TMDs was used, keeping and extending the notation proposed in Ref. [87].

The parametrization of the unintegrated correlator

$$\Gamma^{[U,U']\mu\nu;\rho\sigma}(k;P) \equiv \int \frac{d^4k}{(2\pi)^4} e^{ik\cdot\xi} \langle P| F^{\mu\nu}(0)U(0,\xi)F^{\rho\sigma}(\xi)U'(\xi,0) |P\rangle \tag{3.25}$$

is constrained by hermiticity and parity conservation and respects the relations induced by time reversal (see Section 2.5). This is a fundamental criterion to perform a first decomposition in terms of the allowed Loretz structures, which, in the unpolarized target case, explicitly reads:

$$\begin{aligned}
\Gamma^{[U,U']\,\mu\nu;\rho\sigma}(k;P,n) = {} & M^2 A_1\, \epsilon^{\mu\nu\alpha\beta}\epsilon^{\rho\sigma}{}_{\alpha\beta} + A_2\, P^{[\mu}g^{\nu][\rho}P^{\sigma]} + A_3\, k^{[\mu}g^{\nu][\rho}k^{\sigma]} \\
& + (A_4 + iA_5)\, P^{[\mu}g^{\nu][\rho}k^{\sigma]} + (A_4 - iA_5)\, k^{[\mu}g^{\nu][\rho}P^{\sigma]} \\
& + (A_6/M^2)\, P^{[\mu}k^{\nu]}P^{[\rho}k^{\sigma]} + M^4 A'_7\, n^{[\mu}g^{\nu][\rho}n^{\sigma]} \\
& + M^2(A'_8 + iA'_9)\, P^{[\mu}g^{\nu][\rho}n^{\sigma]} + M^2(A'_8 - iA'_9)\, n^{[\mu}g^{\nu][\rho}P^{\sigma]} \\
& + M^2(A'_{10} + iA'_{11})\, k^{[\mu}g^{\nu][\rho}n^{\sigma]} + M^2(A'_{10} - iA'_{11})\, n^{[\mu}g^{\nu][\rho}k^{\sigma]} \\
& + M^2 A'_{12}\, P^{[\mu}n^{\nu]}P^{[\rho}n^{\sigma]} + M^2 A'_{13}\, k^{[\mu}n^{\nu]}k^{[\rho}n^{\sigma]} \\
& + (A'_{14} + iA'_{15})\, P^{[\mu}k^{\nu]}P^{[\rho}n^{\sigma]} + (A'_{14} - iA'_{15})\, P^{[\mu}n^{\nu]}P^{[\rho}k^{\sigma]} \\
& + (A'_{16} + iA'_{17})\, P^{[\mu}k^{\nu]}k^{[\rho}n^{\sigma]} + (A'_{16} - iA'_{17})\, k^{[\mu}n^{\nu]}P^{[\rho}k^{\sigma]} \\
& + M^2(A'_{18} + iA'_{19})\, P^{[\mu}n^{\nu]}k^{[\rho}n^{\sigma]} \\
& + M^2(A'_{18} - iA'_{19})\, k^{[\mu}n^{\nu]}P^{[\rho}n^{\sigma]},
\end{aligned} \tag{3.26}$$

where $A_i = A_i(k\cdot n, k\cdot P, k^2)$. Relevant mass dimensions are $[\Gamma] = -2$ and $[A_i] = -4$. Terms with coefficients $A_5, A'_9, A'_{11}, A'_{15}, A'_{17}, A'_{19}$ are T-odd. A prime on the coefficient indicates that the corresponding Lorentz structure includes the four-vector n. These n-dependent structures give rise to higher twist TMDs (see ref. [128] for the analogous case for quarks) and will be omitted in the following, as we are only interested in leading-twist functions. For the same decomposition of the correlator when vector and tensor polarization are considered, we refer to Appendix B and [88].

Integrating eq. (3.25) over $k\cdot P$ leads to the TMD (light-front) correlator (2.48). By counting power of M/Q as explained earlier, the leading-twist terms are identified as the ones containing the contraction of the field strength tensor with n and one transverse index ($i, j = 1, 2$). Explicitly indicating the dependence of vector and tensor part of the spin, the correlator is then:

$$\Gamma^{ij}(x, \boldsymbol{k}_T) \equiv \Gamma^{[U,U']\,ni;nj}(x, \boldsymbol{k}_T; P, n, S, T)$$

$$\equiv \int \frac{d(\xi\cdot P)d^2\boldsymbol{k}_T}{(2\pi)^3} e^{ik\cdot\xi} \langle P,S,T|\, F^{\mu\nu}(0)\, U(0,\xi)\, F^{\rho\sigma}(\xi)\, U'(\xi,0)\,|P,S,T\rangle \Big|_{\xi^+=0}, \quad (3.27)$$

where a trace over color is understood and we omit the dependence on the gauge links unless needed. After the separation in terms of the possible hadronic polarization states, the correlator in eq. (3.27) can be schematically written as:

$$\Gamma^{ij} = \Gamma^{ij}_U + \Gamma^{ij}_L + \Gamma^{ij}_T + \Gamma^{ij}_{LL} + \Gamma^{ij}_{LT} + \Gamma^{ij}_{TT}. \quad (3.28)$$

The parametrization in terms of TMDs, separated in different polarization reads:

$$\Gamma^{ij}_U(x,\boldsymbol{k}_T) = \frac{x}{2}\left[- g_T^{ij}\, f_1(x,\boldsymbol{k}_T^2) + \frac{k_T^{ij}}{M^2}\, h_1^\perp(x,\boldsymbol{k}_T^2)\right], \quad (3.29)$$

$$\Gamma^{ij}_L(x,\boldsymbol{k}_T) = \frac{x}{2}\left[i\epsilon_T^{ij} S_L\, g_1(x,\boldsymbol{k}_T^2) + \frac{\epsilon_T^{\{i}{}_\alpha k_T^{j\}\alpha} S_L}{2M^2}\, h_{1L}^\perp(x,\boldsymbol{k}_T^2)\right], \quad (3.30)$$

$$\begin{aligned}\Gamma^{ij}_T(x,\boldsymbol{k}_T) = \frac{x}{2}\Bigg[& - \frac{g_T^{ij}\epsilon_T^{S_T k_T}}{M}\, f_{1T}^\perp(x,\boldsymbol{k}_T^2) + \frac{i\epsilon_T^{ij}\boldsymbol{k}_T\cdot\boldsymbol{S}_T}{M}\, g_{1T}(x,\boldsymbol{k}_T^2) \\ & - \frac{\epsilon_T^{k_T\{i} S_T^{j\}} + \epsilon_T^{S_T\{i} k_T^{j\}}}{4M}\, h_1(x,\boldsymbol{k}_T^2) - \frac{\epsilon_T^{\{i}{}_\alpha k_T^{j\}\alpha S_T}}{2M^3}\, h_{1T}^\perp(x,\boldsymbol{k}_T^2)\Bigg], \end{aligned} \quad (3.31)$$

$$\Gamma^{ij}_{LL}(x,\boldsymbol{k}_T) = \frac{x}{2}\left[- g_T^{ij} S_{LL}\, f_{1LL}(x,\boldsymbol{k}_T^2) + \frac{k_T^{ij} S_{LL}}{M^2}\, h_{1LL}^\perp(x,\boldsymbol{k}_T^2)\right], \quad (3.32)$$

$$\begin{aligned}\Gamma^{ij}_{LT}(x,\boldsymbol{k}_T) = \frac{x}{2}\Bigg[& - \frac{g_T^{ij}\boldsymbol{k}_T\cdot\boldsymbol{S}_{LT}}{M}\, f_{1LT}(x,\boldsymbol{k}_T^2) + \frac{i\epsilon_T^{ij}\epsilon_T^{S_{LT}k_T}}{M}\, g_{1LT}(x,\boldsymbol{k}_T^2) \\ & + \frac{S_{LT}^{\{i} k_T^{j\}}}{M}\, h_{1LT}(x,\boldsymbol{k}_T^2) + \frac{k_T^{ij\alpha} S_{LT\alpha}}{M^3}\, h_{1LT}^\perp(x,\boldsymbol{k}_T^2)\Bigg], \end{aligned} \quad (3.33)$$

$$\begin{aligned}\Gamma^{ij}_{TT}(x,\boldsymbol{k}_T) = \frac{x}{2}\Bigg[& - \frac{g_T^{ij} k_T^{\alpha\beta} S_{TT\alpha\beta}}{M^2}\, f_{1TT}(x,\boldsymbol{k}_T^2) + \frac{i\epsilon_T^{ij}\epsilon_{T\gamma}^{\beta} k_T^{\gamma\alpha} S_{TT\alpha\beta}}{M^2}\, g_{1TT}(x,\boldsymbol{k}_T^2) \\ & + S_{TT}^{ij}\, h_{1TT}(x,\boldsymbol{k}_T^2) + \frac{S_{TT\alpha}^{\{i} k_T^{j\}\alpha}}{M^2}\, h_{1TT}^\perp(x,\boldsymbol{k}_T^2) \\ & + \frac{k_T^{ij\alpha\beta} S_{TT\alpha\beta}}{M^4}\, h_{1TT}^{\perp\perp}(x,\boldsymbol{k}_T^2)\Bigg], \end{aligned} \quad (3.34)$$

where there is a implicit dependence of the TMDs on the gauge link, i.e. $f_1^{g[U,U']}(x,\boldsymbol{k}_T^2)$.

We omit any label on the functions that refers to gluons, being understood that we will only discuss the gluons in this Section. We also omit the dependence of the functions on the renormalization scale.

To be more precise, the polarized correlators that is parametrized in (3.30)-(3.34) are in fact defined as:

$$\Delta\Gamma^{\mu\nu;\rho\sigma}(x,\boldsymbol{k}_T;P,S) \equiv \frac{1}{2}\left[\Gamma^{\mu\nu;\rho\sigma}(x,\boldsymbol{k}_T;P,S) - \Gamma^{\mu\nu;\rho\sigma}(x,\boldsymbol{k}_T;P,-S)\right], \tag{3.35}$$

and

$$\Delta\Gamma^{\mu\nu;\rho\sigma}(x,\boldsymbol{k}_T;P,T) \equiv \frac{1}{2}\left[\Gamma^{\mu\nu;\rho\sigma}(x,\boldsymbol{k}_T;P,T) - \Gamma^{\mu\nu;\rho\sigma}(x,\boldsymbol{k}_T;P,-T)\right], \tag{3.36}$$

but we will not use the notation "$\Delta\Gamma$" throughout the thesis for the sake of simplicity.

The expressions of the TMDs in terms of the coefficients A_i can be found in appendix B. The functions $h_{1L}^{\perp}$, $f_{1T}^{\perp}$, g_{1LT}, g_{1TT}, h_1, and $h_{1T}^{\perp}$ are T-odd. The link to the more traditional parametrizations of [86, 87] is found in [88], and is based on the following identity:

$$\epsilon_T^{\{i}{}_{\alpha} k_T^{j\}\alpha\beta} S_{T\beta} = \epsilon_T^{k_T\{i} k_T^{j\}} \boldsymbol{k}_T\cdot\boldsymbol{S}_T + \frac{1}{4}\boldsymbol{k}_T^2\left(S_T^{\{j}\epsilon_T^{i\}k_T} + k_T^{\{j}\epsilon_T^{i\}S_T}\right). \tag{3.37}$$

The function h_1 is a rank-1 function, h_{1T} of [87] contains both rank-1 and rank-3 pieces, and $h_{1T}^{\perp}$ is a rank-3 function.

Integrating the TMD correlator in eq. (3.27) over transverse momentum, we obtain the collinear correlator:

$$\Gamma^{ij}(x) \equiv \int \frac{d\xi\cdot P}{2\pi}\, e^{ik\cdot\xi}\, \langle P,S,T|\, F^{ni}(0)\, U_{[0,\xi]} F^{nj}(\xi)\, U'_{[\xi,0]}\, |P,S,T\rangle\Big|_{\xi\cdot n=\boldsymbol{\xi}_T=0}. \tag{3.38}$$

The parametrization of this correlator in terms of collinear PDFs is given by

$$\Gamma^{ij}(x) = \frac{x}{2}\left[-g_T^{ij}\, f_1(x) + i\epsilon_T^{ij} S_L\, g_1(x) - g_T^{ij} S_{LL}\, f_{1LL}(x) + S_{TT}^{ij}\, h_{1TT}(x)\right]. \tag{3.39}$$

The surviving collinear PDF for vector polarization is the rank-0 function g_1, where we have omitted the subscript 'L' on $g_1 \equiv g_{1L}$, while in the tensor polarized case two more function $f_{1LL}(x)$ and $h_{1TT}(x)$ survive. The former function is analogous of what was called b_1 in the quark case, and the latter function shows up in the structure function $\Delta(x)$ discussed in ref. [129] and is called $\Delta_2 G(x)$ in ref. [130]. The gluon structure function $\Delta(x)$ and, equivalently, the PDF $h_{1TT}(x)$ are related to the

double-helicity flip scattering amplitude in processes involving hadrons of spin ≥ 1. At the parton level, $h_{1TT}(x)$ represents the distribution of linearly polarized gluons in a transversely tensor polarized target sometimes referred to as "gluon transversity" [89–91]. An overview of the functions in terms of target/gluon polarization is shown in Table 3.2

3.4.2 The gluon correlator at small-x

The gluon TMD correlator greatly simplifies in the small-x limit for the so-called dipole-type gauge link structure $[+,-]$, as shown in [88, 131]. In particular, in [88] we elaborated on the link between the gluon correlator at $x = 0$ and the operator depending on the same $[+,-]$ gauge link structure, where the gluon fields are absent.

The relation reads:

$$\begin{aligned}\Gamma^{[+,-]\,ij}(0,\boldsymbol{k}_T) &= \int \frac{d\xi{\cdot}P\, d^2\xi_T}{(2\pi)^3}\, e^{ik\cdot\xi}\, \langle P|\, F^{ni}(0)\, U^{[+]}_{[0,\xi]}\, F^{nj}(\xi)\, U^{[-]}_{[\xi,0]}\, |P\rangle \Big|_{\xi\cdot n=k\cdot n=0} \\ &= \frac{1}{2\pi L}\int \frac{d\xi{\cdot}P\, d^2\xi_T}{(2\pi)^3}\, e^{ik\cdot\xi}\, \langle P|\, F^{ni}(0)\, U^{[+]}_{[0,\xi]}\, F^{nj}(\xi)\, U^{[-]}_{[\xi,0]}\, |P\rangle \Big|_{\xi\cdot n=k\cdot n=0} \\ &= \frac{4}{2\pi L}\int \frac{d^2\xi_T}{(2\pi)^2}\, e^{ik_T\cdot\xi_T}\, \langle P|\, G^i_T(0)\, U^{[+]}_{[0,\xi]}\, G^j_T(\xi)\, U^{[-]}_{[\xi,0]}\, |P\rangle \Big|_{\xi\cdot n=0}\,. \end{aligned} \tag{3.40}$$

Eventually we can write [88]:

$$\Gamma^{[+,-]\,ij}(0,\boldsymbol{k}_T) = \frac{k_T^i k_T^j}{2\pi L}\, \Gamma_0^{[\Box]}(\boldsymbol{k}_T), \tag{3.41}$$

where $L \equiv \int d\xi{\cdot}P = 2\pi\,\delta(0)$ and we defined:

$$\Gamma_0^{[\Box]}(\boldsymbol{k}_T) = \int \frac{d^2\xi_T}{(2\pi)^2}\, e^{ik_T\cdot\xi_T}\, \langle P|\, U^{[+]}_{[0,\xi]}\,(\xi)\, U^{[-]}_{[\xi,0]}\, |P\rangle \Big|_{\xi\cdot n=0}\,. \tag{3.42}$$

The latter is called *Wilson loop correlator* and it will be properly defined in Section 3.4.3 (see eq. (3.46)). The loop is built from a future and a past pointing staple-like gauge link, that enter the rectangular Wilson loop $U^{[\Box]} \equiv U^{[+]}_{[0,\xi]} U^{[-]}_{[\xi,0]}$. More generically, one can write a loop as the square of the form $O(0)O^\dagger(\xi)$ for a specific nonlocal operator O as follows:

$$U^{[\Box]} = U^n_{[-\infty,0_T;\infty,0_T]} U^T_{[\infty,0_T;\infty,\xi_T]} U^n_{[\infty,\xi_T;-\infty,\xi_T]} U^T_{[-\infty,\xi_T;\infty,0_T]}$$

$$= \left(U^T_{[-\infty,\infty_T;-\infty,0_T]} U^n_{[-\infty,0_T;\infty,0_T]} U^T_{[\infty,0_T;\infty,\infty_T]}\right) \times \left(U^T_{[-\infty,\infty_T;-\infty,\xi_T]} U^n_{[-\infty,\xi_T;\infty,\xi_T]} U^T_{[\infty,\xi_T;\infty,\infty_T]}\right)^\dagger . \tag{3.43}$$

In the last step of (3.40), we use the results in eq. (15) of ref. [48] to calculate $k^i_T k^j_T \Gamma_0$. We performed one partial integration in 0 and the other in ξ and used the relevant gluonic pole factor $C^{[\Box]}_{GG} = 4$.

As will be shown in Section 3.4.4, the above results agree with the results in [47,131] and implies a relation between gluon TMDs at $x \to 0$ and the TMD functions that parametrize the Wilson correlator (see Section 3.4.3)

3.4.3 Wilson loop correlator

We define the fully unintegrated Wilson loop operator as:

$$\Gamma_0^{[U,U']}(k; P, n) \equiv \int \frac{d^4\xi}{(2\pi)^4}\, e^{ik\cdot\xi} \,\langle P|\, U_{[0,\xi]} U'_{[\xi,0]}\, |P\rangle\,, \tag{3.44}$$

where we implicitly include color tracing. The absence of the gluon fields and the structure of the loop on the light-front still allows integration over $k{\cdot}P$, and invariance in the $\xi{\cdot}P$ direction implies a delta function $\delta(k{\cdot}n)$:

$$\begin{aligned}\Gamma_0^{[U,U']}(x, \boldsymbol{k}_T; P, n) &\equiv \int \frac{d\xi{\cdot}P\, d^2\xi_T}{(2\pi)^3}\, e^{ik\cdot\xi} \,\langle P|\, U_{[0,\xi]} U'_{[\xi,0]}\, |P\rangle\Big|_{\xi\cdot n=0} \\ &= \delta(x)\, \Gamma_0^{[U,U']}(\boldsymbol{k}_T; P, n),\end{aligned} \tag{3.45}$$

where the loop correlator integrated over $k{\cdot}P$ and $k{\cdot}n$ is given by

$$\Gamma_0^{[U,U']}(\boldsymbol{k}_T; P, n) \equiv \int \frac{d^2\xi_T}{(2\pi)^2}\, e^{ik_T\cdot\xi_T} \,\langle P|\, U_{[0,\xi]} U'_{[\xi,0]}\, |P\rangle\Big|_{\xi\cdot n=0}. \tag{3.46}$$

Bearing in mind the proportionality to the longitudinal extent L of the loop, $L \equiv \int d\xi{\cdot}P = 2\pi\,\delta(0)$, the light-front correlator in eq. (3.46) is parametrized in terms of TMDs as follows (we suppress now the dependence on P and n) [88]:

$$\Gamma_0^{[\Box]}(\boldsymbol{k}_T) = \frac{\pi L}{M^2}\left[e(\boldsymbol{k}_T^2) + \frac{\epsilon_T^{S_T k_T}}{M}\, e_T(\boldsymbol{k}_T^2) + S_{LL}\, e_{LL}(\boldsymbol{k}_T^2)\right.$$

$$+\frac{\boldsymbol{k}_T\cdot\boldsymbol{S}_{LT}}{M}\,e_{LT}(\boldsymbol{k}_T^2)+\frac{k_T^{\alpha\beta}S_{TT\,\alpha\beta}}{M^2}\,e_{TT}(\boldsymbol{k}_T^2)\Bigg]. \tag{3.47}$$

An overview of the Wilson loop functions in terms of the target polarization is given in Table 3.2.

	Unpolarized	**Circular**	**Linear**	**Wilson loop**
U	$\boldsymbol{f_1}$		$h_1^\perp$	e
L		$\boldsymbol{g_1}$	$h_{1L}^\perp$	
T	$f_{1T}^\perp$	g_{1T}	$h_1, h_{1T}^\perp$	e_T
LL	$\boldsymbol{f_{1LL}}$		$h_{1LL}^\perp$	e_{LL}
LT	f_{1LT}	g_{1LT}	$h_{1LT}, h_{1LT}^\perp$	e_{LT}
TT	f_{1TT}	g_{1TT}	$\boldsymbol{h_{1TT}}$, $h_{1TT}^\perp$ $h_{1TT}^{\perp\perp}$	e_{TT}

Table 3.2: Gluon and Wilson loop TMD functions, divided in terms of target polarization. The bold-face functions survive integration over transverse momenta. The functions in column 2, 3, and 4 are gluon TMDs and have dependence $f \equiv f(x, \boldsymbol{k}_T^2)$, whereas in column 5 the functions read $e \equiv e(\boldsymbol{k}_T^2)$.

Similarly to the gluon case, the object that is parametrized is defined as:

$$\Delta\Gamma_0^{[U,U']}(\boldsymbol{k}_T;P,S,n)\equiv\frac{1}{2}\left[\Gamma_0^{[U,U']}(\boldsymbol{k}_T;P,S,n)-\Gamma_0^{[U,U']}(\boldsymbol{k}_T;P,-S,n)\right], \tag{3.48}$$

and

$$\Delta\Gamma_0^{[U,U']}(\boldsymbol{k}_T;P,T,n)\equiv\frac{1}{2}\left[\Gamma_0^{[U,U']}(\boldsymbol{k}_T;P,T,n)-\Gamma_0^{[U,U']}(\boldsymbol{k}_T;P,-T,n)\right], \tag{3.49}$$

but the notation "$\Delta\Gamma_0$" is once again discarded for simplicity.

3.4.4 The correspondence at small-x

The relation in eq. (3.41) between the gluon correlator (3.27) and the Wilson loop (3.46) is exact for $x = 0$. However, we can use this relation to infer the behavior of the gluon

TMDs at small-x, i.e.:

$$\lim_{x\to 0}\,\Gamma^{[+,-]\,ij}(x,\boldsymbol{k}_T) = \frac{k_T^i k_T^j}{2\pi L}\,\Gamma_0^{[\Box]}(\boldsymbol{k}_T). \tag{3.50}$$

In practice, we exploit the correspondence in (3.50) to obtain direct relations between the functions in the parametrization of Section 3.4.1 and 3.4.3. Since the correspondence must involve symmetric tensors, the functions related to longitudinally polarized target do not have any relation to the e-type of functions. This implies that g_1 and $h_{1L}^\perp$ are less divergent than $1/x$ in the limit of small x, given that an enhancement proportional to $1/x$ at small-x is predicted for the other functions. For each type of target polarization we find:

$$\lim_{x\to 0}\,xf_1(x,\boldsymbol{k}_T^2) = \frac{\boldsymbol{k}_T^2}{2M^2}\lim_{x\to 0}\,xh_1^\perp(x,\boldsymbol{k}_T^2) = \frac{\boldsymbol{k}_T^2}{2M^2}\,e(\boldsymbol{k}_T^2). \tag{3.51}$$

$$\begin{aligned}\lim_{x\to 0}\,xf_{1T}^\perp(x,\boldsymbol{k}_T^2) &= \lim_{x\to 0}\,xh_1(x,\boldsymbol{k}_T^2) = -\frac{\boldsymbol{k}_T^2}{2M^2}\lim_{x\to 0}\,xh_{1T}^\perp(x,\boldsymbol{k}_T^2)\\ &= \frac{1}{2}\lim_{x\to 0}\,xh_{1T}(x,\boldsymbol{k}_T^2) = \frac{\boldsymbol{k}_T^2}{2M^2}\,e_T(\boldsymbol{k}_T^2),\end{aligned} \tag{3.52}$$

$$\lim_{x\to 0}\,xf_{1LL}(x,\boldsymbol{k}_T^2) = \frac{\boldsymbol{k}_T^2}{2M^2}\lim_{x\to 0}\,xh_{1LL}^\perp(x,\boldsymbol{k}_T^2) = \frac{\boldsymbol{k}_T^2}{2M^2}\,e_{LL}(\boldsymbol{k}_T^2). \tag{3.53}$$

$$\lim_{x\to 0}\,xf_{1LT}(x,\boldsymbol{k}_T^2) = \lim_{x\to 0}\,xh_{1LT}(x,\boldsymbol{k}_T^2) = -\frac{\boldsymbol{k}_T^2}{4M^2}\lim_{x\to 0}\,xh_{1LT}^\perp(x,\boldsymbol{k}_T^2) = \frac{\boldsymbol{k}_T^2}{4M^2}\,e_{LT}(\boldsymbol{k}_T^2). \tag{3.54}$$

$$\begin{aligned}\lim_{x\to 0}\,xf_{1TT}(x,\boldsymbol{k}_T^2) &= \frac{2M^2}{3\boldsymbol{k}_T^2}\lim_{x\to 0}\,xh_{1TT}(x,\boldsymbol{k}_T^2) = -\frac{1}{2}\lim_{x\to 0}\,xh_{1TT}^\perp(x,\boldsymbol{k}_T^2)\\ &= \frac{\boldsymbol{k}_T^2}{6M^2}\lim_{x\to 0}\,xh_{1TT}^{\perp\perp}(x,\boldsymbol{k}_T^2) = \frac{\boldsymbol{k}_T^2}{6M^2}\,e_{TT}(\boldsymbol{k}_T^2).\end{aligned} \tag{3.55}$$

The relations (3.51)-(3.55) are valid modulo resummation of large logarithms in $1/x$ and higher twist effects.

The results (3.52) for the transversely polarized target are in agreement with [131], where the enhancement at small-x was investigated. For further discussion we refer

to [88] and reference therein. We mention that such a relation between matrix elements, which is made possible by specifically considering the dipole-type gauge link structure, has been extended to the GTMD correlator in [132].

For our purposes, it is relevant to notice that these relations serve as a guiding criteria in estimating the relative magnitude of functions. Combined with the information given by the positivity bounds discussed in Section 3.5, they allow to determine whether a function is enhanced or suppressed with respect to the other functions in the appropriate kinematical region. The latter consideration might become useful for applications especially in the future era of the EIC [126].

3.4.5 Gluon TMDs phenomenology

Currently, the experimental information on gluon distributions is scarce and almost completely restricted to the collinear gluon PDFs for spin-$1/2$ targets. Gluon TMDs are mostly unknown because the kinematical regions in which they are relevant are hardly accessible by present experiments.

As a matter of fact, most of the available information about gluons is at present delivered by LHC at CERN, even though it was not initially devised for accessing the desirable range of x-values, and from RHIC at Brookhaven National Lab. A proposal for implementing a fixed-target experiment within the LHC facilities is currently in progress. In fact, the realization of AFTER@LHC [133–135] would undoubtedly bring a significant improvement to the gluon and TMD physics program at the LHC.

Most of the phenomenological studies aim at characterizing the appropriate angular distribution to access gluon distributions. The extraction of these functions should rely on all-order TMD factorization, even though, for processes initiated by gluons, factorization breaking effects are often present [17–21], for instance for hadroproduction in pp collisions. In general cases, to avoid factorization breaking complications due to color entanglement, color-singlet configurations in the final states have often been considered.

On a different note, it is important to stress that the extraction of the gluon TMDs from different high energy processes requires to account for the appropriate gauge link structures, shown in the panels (c)-(f) of Fig. 2.7. Two fundamental gauge link structures exist for gluons (WW- and dipole-type), and different processes can probe either type or a mixture of them. For instance, the WW-type $[+,+]$ (Fig. 2.7(d)) is related to color flow into the final state, which is the case for e.g. quark-antiquark pair production in semi-inclusive deep-inelastic scattering [29]. The structure $[-,-]$ in Fig. 2.7(c) appears in processes with color flow annihilated within the initial state, such as the pp collision with Higgs production through gluon fusion ($gg \to h$) [136,

137]. When the color flow involves both initial and final states, the dipole-type gauge links $[-,+]$ and $[+,-]$ appear (see Fig. 2.7(e) and Fig. 2.7(f) respectively). This is, for instance, the case of the partonic processes with $qg \to qg$ and $\bar{q}g \to \bar{q}g$ contributions respectively. When more hadrons are involved, the gauge links can be combinations of future- and past-pointing Wilson lines, with the possibility of additional loops [42].

Thus far, a significant effort has been devoted to the study of unpolarized and linearly polarized gluon TMDs in unpolarized targets (f_1 and $h_1^\perp$). They have been studied through the $\boldsymbol{q}_\perp$-spectrum of the Higgs boson produced from gluon fusions [136–138]. More interestingly, it has been argued that the quark-antiquark pair and quarkonium production at the LHC [27, 29, 139–142] have an even more sizable dependence on linearly polarized gluons.

Among the other distributions, the gluon Sivers function occupies a special place. At present, it can be studied at RHIC and COMPASS, which can provide the transverse polarization of the target. The Sivers function can be accessed through the measurement of the Sivers asymmetry in $pp^\uparrow \to \pi X$ at RICH and COMPASS, even though the information in the region of small-x, that is expected to be the most important, is still mostly missing. The asymmetry measurements have the complication that they actually give indirect information on the Sivers function [143–145], rather than the function as arising from the proper definition in TMD factorization procedure. As far as the universality of the gluon Sivers function is concerned, we should expect a sign-change analogously to the quark case [30, 143], namely:

$$f_{1T}^{[++]}(x, \boldsymbol{k}_T^2) = -f_{1T}^{[--]}(x, \boldsymbol{k}_T^2); \quad f_{1T}^{[+-]}(x, \boldsymbol{k}_T^2) = -f_{1T}^{[-+]}(x, \boldsymbol{k}_T^2). \tag{3.56}$$

Among the most promising processes that can be used in the (near) future to access it, there are $ep^\uparrow \to e'Q\bar{Q}X$, which probes $f_{1T}^{[++]}$, $pp^\uparrow \to \gamma\gamma X$, which probes $f_{1T}^{[--]}$, and $pp^\uparrow \to \gamma \text{jet} X$, which probes $f_{1T}^{[+-]}$.

Being intrinsically different, the WW- and dipole-type structures probe in principle two distinct functions. Some of these gluon TMDs can be studied at RHIC, but especially the future electron-ion collider EIC [126] and the fixed target experiment AFTER@LHC will be ideal, because they will cover a kinematical region in which gluon functions are important [125, 127].

Being able to probe experimentally the low-x region dominated by gluons in its full richness would be extremely interesting in order for the theoretical predictions to find validations. The predictions about the reduction of the number of gluon TMDs in this region is very interesting from a theoretical point of view. In fact, as we have discussed in Section 3.40 and [88], the gluon correlator with dipole-type gauge links is related to the expectation value of a single Wilson loop, confirming the results of [47, 131]. It

turns out that only a few of the gluon TMDs survive in the small-x regime, among which the linear gluon polarization. Of course, it is crucial that any simplifications at small-x needs first to be tested for validity. Still on the small-x domain, there are theoretical indications that the partons undergo a BFKL type of dynamics, which only recently started to be considered in extractions of collinear quantities [146]. Effects like parton saturation could interestingly be measured as well [147].

Little information is available on spin-1 targets, mostly restricted to the Sivers asymmetry of the deuteron. No information is available on the tensor polarization. On this respect, the interest on the gluon content of nuclei is growing, even if restricted to the collinear quantities. The collinear structure function for gluons in spin-1 targets, called $\Delta(x)$, was first defined by Jaffe and Manohar in [129]. The authors pointed out that this observable is related to a transfer of two units of helicity to the nuclear target, and vanishes for any target of spin smaller than 1. They recognized that there must exist a tower of gluon operators contributing to the scattering amplitude with such a double-helicity flip that cannot be linked to single nucleons; instead, they are exclusive to hadrons and nuclei of spin ≥ 1. In the parton model language, $\Delta(x)$ describes linearly polarized gluons in targets with transverse tensor polarization, and it is related to the function that we called h_{1TT}. Aspects of this function (its first moment and a positivity bound) have recently been studied on the lattice in [89, 90], and also experimental interest has been shown [91].

3.5 Positivity bounds

The correlators in eq. (3.15) and (3.27) have been averaged over the target spin states. In order to single out the hadron spin, we can write the correlators as:

$$\Phi(x, \boldsymbol{k}_T; S, T) \equiv \mathrm{Tr}\left(\rho(S,T)\, F(x, \boldsymbol{k}_T)\right), \tag{3.57}$$

$$\Gamma^{ij}(x, \boldsymbol{k}_T; S, T) \equiv \mathrm{Tr}\left(\rho(S,T)\, G^{ij}(x, \boldsymbol{k}_T)\right), \tag{3.58}$$

where the information on the spin states of the parent hadron is encoded in the 3×3 density matrix $\rho(S,T)$ defined as (3.6) and the combined information on the hadron and parton spins is contained in the matrices $F(x, \boldsymbol{k}_T)$ and $G^{ij}(x, \boldsymbol{k}_T)$.

As is well known, one can impose positivity constraints on the hadronic tensor and find a probabilistic interpretation for some of the distribution functions [148]. In this Section we describe how to derive the positivity relations for gluons in spin-1 targets and eventually review the quark case. Some general considerations on the positivity bounds will follow.

3.5.1 Positivity bounds on gluon distributions

Positivity bounds on gluon TMDs were studied in [86] for spin-1/2 hadrons and, by applying the same strategy, we extended this analysis to spin-1 hadrons in [93]. The starting point is the idea that the correlator Γ can be seen as a 2×2 matrix in the two gluon polarizations, given by $\Gamma^{ij} = \rho_{s's} G^{ij}_{ss'}$ (see eq. (3.58)), where s, s' label the hadronic polarization states. The quantity G is a 6×6 matrix in the gluon $\otimes$ hadron spin space. As we will show explicitly, G turns out to be positive semidefinite, a property which allows for setting constraints on the gluon distributions. We will derive bounds for the TMD case and subsequently consider the transverse momentum integrated case. For completeness, we will also include the bounds that apply to spin-1/2 hadrons, completing the study of [86] where T-odd functions were not included.

Bounds on transverse momentum dependent functions

In this subsection, we derive bounds for the gluons TMDs that appear in the parametrization given in eq. (3.28). We choose the same basis for the matrix G as in [86], namely we use circular gluon polarizations, given by $|\pm\rangle = \mp \frac{1}{\sqrt{2}} (|x\rangle \pm i\,|y\rangle)$. At leading twist, this matrix is given by

$$G = \frac{x}{2} \begin{pmatrix} A & B \\ B^\dagger & C \end{pmatrix}, \tag{3.59}$$

where [93]:

$$A = \begin{pmatrix} f_1 + \frac{f_{1LL}}{2} - g_1 & \frac{e^{-i\phi}k}{\sqrt{2}M}\left(\tilde{f} - \tilde{g} + h_{1LT}\right) & \frac{e^{-2i\phi}k^2}{M^2}\left(f_{1TT} + i g_{1TT} - h^\perp_{1TT}\right) \\ \frac{e^{i\phi}k}{\sqrt{2}M}\left(\tilde{f}^* - \tilde{g}^* + h_{1LT}\right) & f_1 - f_{1LL} & -\frac{e^{-i\phi}k}{\sqrt{2}M}\left(\tilde{f}^* + \tilde{g}^* + h_{1LT}\right) \\ \frac{e^{2i\phi}k^2}{M^2}\left(f_{1TT} - i g_{1TT} - h^\perp_{1TT}\right) & -\frac{e^{i\phi}k}{\sqrt{2}M}\left(\tilde{f} + \tilde{g} + h_{1LT}\right) & f_1 + \frac{f_{1LL}}{2} + g_1 \end{pmatrix},$$

$$B = \begin{pmatrix} -\frac{e^{-2i\phi}k^2}{4M^2}\left(2h_1^\perp + h^\perp_{1LL} - 2i h^\perp_{1L}\right) & \frac{e^{-3i\phi}k^3}{2\sqrt{2}M^3}\left(h^\perp_{1LT} + i h^\perp_{1T}\right) & -\frac{e^{-4i\phi}k^4}{2M^4} h^{\perp\perp}_{1TT} \\ -\frac{e^{-i\phi}k}{\sqrt{2}M}\left(2h_{1LT} - i h_1\right) & -\frac{e^{-2i\phi}k^2}{2M^2}\left(h_1^\perp - h^\perp_{1LL}\right) & -\frac{e^{-3i\phi}k^3}{2\sqrt{2}M^3}\left(h^\perp_{1LT} - i h^\perp_{1T}\right) \\ -2h_{1TT} & \frac{e^{-i\phi}k}{\sqrt{2}M}\left(2h_{1LT} + i h_1\right) & -\frac{e^{-2i\phi}k^2}{4M^2}\left(2h_1^\perp + h^\perp_{1LL} + 2i h^\perp_{1L}\right) \end{pmatrix},$$

$$C = \begin{pmatrix} f_1 + \frac{f_{1LL}}{2} + g_1 & \frac{e^{-i\phi}k}{\sqrt{2}M}\left(\tilde{f} + \tilde{g} + h_{1LT}\right) & \frac{e^{-2i\phi}k^2}{M^2}\left(f_{1TT} - i g_{1TT} - h^\perp_{1TT}\right) \\ \frac{e^{i\phi}k}{\sqrt{2}M}\left(\tilde{f}^* + \tilde{g}^* + h_{1LT}\right) & f_1 - f_{1LL} & -\frac{e^{-i\phi}k}{\sqrt{2}M}\left(\tilde{f}^* - \tilde{g}^* + h_{1LT}\right) \\ \frac{e^{2i\phi}k^2}{M^2}\left(f_{1TT} + i g_{1TT} - h^\perp_{1TT}\right) & -\frac{e^{i\phi}k}{\sqrt{2}M}\left(\tilde{f} - \tilde{g} + h_{1LT}\right) & f_1 + \frac{f_{1LL}}{2} - g_1 \end{pmatrix},$$

where for convenience we have suppressed the argument $(x, \boldsymbol{k}_T^2)$ of the functions and defined $\tilde{f} \equiv f_{1LT} + i f_{1T}^{\perp}$ and $\tilde{g} \equiv g_{1T} + i g_{1LT}$. Furthermore, we have expressed $\boldsymbol{k}_T$ in terms of its polar coordinates (k, ϕ). From symmetry considerations it follows that the block C is the parity transformed of A and the off-diagonal blocks are Hermitian conjugates.

To make the properties of the matrix G more apparent, we write its elements in the following form:

$$\begin{aligned} G^{ij}_{ss'}(x, \boldsymbol{k}_T) &\equiv \int \frac{d\xi{\cdot}P\, d^2\boldsymbol{\xi}_T}{(2\pi)^3}\, e^{ik\cdot\xi}\, \langle P; s|\, F^{ni}(0)\, F^{nj}(\xi)\, |P; s'\rangle \Big|_{\xi\cdot n=0} \\ &= \sum_m \langle P_m|\, F^{ni}(0)\, |P; s\rangle^*\, \langle P_m|\, F^{nj}(0)\, |P; s'\rangle \\ &\quad \times \delta(P_m{\cdot}n - (1-x))\, \delta^{(2)}(\boldsymbol{P}_{mT} + \boldsymbol{k}_T), \end{aligned} \tag{3.60}$$

where we inserted a complete set of momentum eigenstates $\{|P_m\rangle\}$. Eq. (3.60) states that, in any basis, the diagonal elements are given by absolute squares. In particular, it follows that the eigenvalues of G in eq. (3.59) must be ≥ 0, or, equivalently, that G is positive semidefinite. This can be used to set constraints on the TMDs. Diagonalization of the full 6×6 matrix would involve a relation between all the functions at the same time and it would not be ideal for applications. We rather restrict ourselves to finding the eigenvalues of the 2×2 principal minors, a procedure which would provide less strict bounds. Due to the symmetry properties of G, some minors yield the same bounds. From the independent minors we derive 9 inequalities:

$$\frac{\boldsymbol{k}_T^2}{2M^2}\, |h_1^{\perp} - h_{1LL}^{\perp}| \leq f_1 - f_{1LL}, \tag{3.61}$$

$$\frac{\boldsymbol{k}_T^4}{16M^4}\, \left[4(h_{1L}^{\perp})^2 + (2h_1^{\perp} + h_{1LL}^{\perp})^2\right] \leq \left(f_1 + \frac{f_{1LL}}{2} + g_1\right)\left(f_1 + \frac{f_{1LL}}{2} - g_1\right), \tag{3.62}$$

$$\frac{\boldsymbol{k}_T^2}{2M^2}\, \left(h_1^2 + 4h_{1LT}^2\right) \leq (f_1 - f_{1LL})\left(f_1 + \frac{f_{1LL}}{2} + g_1\right), \tag{3.63}$$

$$\frac{\boldsymbol{k}_T^6}{8M^6}\, \left[(h_{1T}^{\perp})^2 + (h_{1LT}^{\perp})^2\right] \leq (f_1 - f_{1LL})\left(f_1 + \frac{f_{1LL}}{2} - g_1\right), \tag{3.64}$$

$$\frac{\boldsymbol{k}_T^2}{2M^2}\, \left[(f_{1T}^{\perp} + g_{1LT})^2 + (f_{1LT} + g_{1T} + h_{1LT})^2\right] \leq (f_1 - f_{1LL})\left(f_1 + \frac{f_{1LL}}{2} + g_1\right), \tag{3.65}$$

$$\frac{\boldsymbol{k}_T^2}{2M^2}\left[(f_{1T}^{\perp}-g_{1LT})^2+(f_{1LT}-g_{1T}+h_{1LT})^2\right]\leq(f_1-f_{1LL})\left(f_1+\frac{f_{1LL}}{2}-g_1\right), \tag{3.66}$$

$$|h_{1TT}|\leq\frac{1}{2}\left(f_1+\frac{f_{1LL}}{2}+g_1\right), \tag{3.67}$$

$$\frac{\boldsymbol{k}_T^4}{2M^4}\,|h_{1TT}^{\perp\perp}|\leq f_1+\frac{f_{1LL}}{2}-g_1, \tag{3.68}$$

$$\frac{\boldsymbol{k}_T^4}{M^4}\left[g_{1TT}^2+(f_{1TT}-h_{1TT}^{\perp})^2\right]\leq\left(f_1+\frac{f_{1LL}}{2}+g_1\right)\left(f_1+\frac{f_{1LL}}{2}-g_1\right). \tag{3.69}$$

Finally, we also include the bounds that apply to spin-1/2 hadrons. This case has been discussed already in [86] excluding the T-odd TMDs. The parametrization of the correlator for a spin-1/2 hadron is given by the sum of the terms (3.29)–(3.31). The density matrix is now parametrized in terms of the spin vector only and it is a 2×2 matrix in hadron spin space. Using the decomposition in eq. (3.58), G is a 4×4 matrix in gluon $\otimes$ hadron spin space and its explicit form (that *does* contain the T-odd functions) is given in [86]. From that matrix we can extract the following bounds from its 2×2 principal minors:

$$|g_1|\leq f_1, \tag{3.70}$$

$$\frac{\boldsymbol{k}_T^4}{4M^4}\left[(h_{1L}^{\perp})^2+(h_1^{\perp})^2\right]\leq(f_1+g_1)(f_1-g_1), \tag{3.71}$$

$$\frac{|\boldsymbol{k}_T|}{M}\,|h_1|\leq f_1+g_1, \tag{3.72}$$

$$\frac{|\boldsymbol{k}_T|^3}{2M^3}\,|h_{1T}^{\perp}|\leq f_1-g_1, \tag{3.73}$$

$$\frac{\boldsymbol{k}_T^2}{M^2}\left[(f_{1T}^{\perp})^2+g_{1T}^2\right]\leq(f_1+g_1)(f_1-g_1). \tag{3.74}$$

Upon omitting tensor polarization (and discarding all functions related to it) in bounds (3.61)–(3.92), which is mathematically equivalent to considering the spin-1/2 case, one obtains a set of bounds that is less strict (but consistent with) the bounds (3.70)–(3.74). In general, these less strict bounds can be sharpened upon considering the eigenvalues of higher-dimensional principal minors. We stress that the dependence on the gauge links and on the renormalization scale is understood. However, further comments on the consequences of these dependences on the bounds will be given in Section 3.6.

Bounds on transverse momentum integrated functions

We now turn to the transverse momentum integrated case, i.e. we will establish relations between the collinear PDFs appearing in eq. (3.39). This case was covered in [92]. The 3×3 blocks of the matrix G in eq. (3.59) are now given by:

$$A = \begin{pmatrix} f_1 + \frac{f_{1LL}}{2} - g_1 & 0 & 0 \\ 0 & f_1 - f_{1LL} & 0 \\ 0 & 0 & f_1 + \frac{f_{1LL}}{2} + g_1 \end{pmatrix}, \quad B = \begin{pmatrix} 0 & 0 & 0 \\ 0 & 0 & 0 \\ -2h_{1TT} & 0 & 0 \end{pmatrix},$$

$$C = \begin{pmatrix} f_1 + \frac{f_{1LL}}{2} + g_1 & 0 & 0 \\ 0 & f_1 - f_{1LL} & 0 \\ 0 & 0 & f_1 + \frac{f_{1LL}}{2} - g_1 \end{pmatrix},$$

where we have suppressed the argument (x) of the functions. From integration of eq. (3.60) over transverse momentum, it follows that G is positive semidefinite also in this case. In contrast to the TMD case, we can easily diagonalize the full matrix and we obtain the following three bounds:

$$|g_1| \leq f_1 + \frac{f_{1LL}}{2}, \tag{3.75}$$

$$f_{1LL} \leq f_1, \tag{3.76}$$

$$|h_{1TT}| \leq \frac{1}{2}\left(f_1 + \frac{f_{1LL}}{2} + g_1\right). \tag{3.77}$$

Including also the trivial relation $f_1 \geq 0$, these inequalities hold for *any* process, as PDFs are universal. In the spin-1/2 case, one simply has the bound $|g_1| \leq f_1$.

Recently in [89] the first moment of a bound analogous to (3.77) was studied on the lattice considering a ϕ meson ($s\bar{s}$). The bounds (3.75)–(3.77) will be relevant e.g. for the extraction of $\Delta(x)$, which has been proposed to occur at JLab using nitrogen targets [149], and which could also be achieved within the program of the EIC [126].

3.5.2 Positivity bounds on the Wilson loop correlator

In this Section, we will consider bounds on the gluon TMDs in the small-x kinematic region, by exploiting the correspondence (3.50). Let us derive positivity bounds for the Wilson loop operator. In fact, also the Wilson loop correlator $\Gamma_0^{[\Box]}$ is a spin-averaged correlator, given by $\Gamma_0^{[\Box]} = \rho_{s's}\, G_{0\, ss'}^{[\Box]}$ (analogously to eq. (3.58)). Inverting

this relation, we find that $G_0^{[\Box]}$ is given by

$$G_0^{[\Box]} = \frac{\pi L}{M^2} \begin{pmatrix} e + \frac{e_{LL}}{2} & \frac{e^{-i\phi}k}{\sqrt{2}M}\,(e_{LT} + ie_T) & \frac{e^{-2i\phi}k^2}{M^2}\,e_{TT} \\ \frac{e^{i\phi}k}{\sqrt{2}M}\,(e_{LT} - ie_T) & e - e_{LL} & -\frac{e^{-i\phi}k}{\sqrt{2}M}\,(e_{LT} - ie_T) \\ \frac{e^{2i\phi}k^2}{M^2}\,e_{TT} & -\frac{e^{i\phi}k}{\sqrt{2}M}\,(e_{LT} + ie_T) & e + \frac{e_{LL}}{2} \end{pmatrix}, \tag{3.78}$$

where we have suppressed the argument $(\boldsymbol{k}_T^2)$ of the functions. In analogy to eq. (3.60), we can write the elements of $G_0^{[\Box]}$ in the following form:

$$\begin{aligned} G_{0\,ss'}^{[\Box]}(\boldsymbol{k}_T) &\equiv \int \frac{d^2\boldsymbol{\xi}_T}{(2\pi)^2}\, e^{-i\boldsymbol{k}_T\cdot\boldsymbol{\xi}_T}\, \langle P; s|\, U^{[\Box]}\, |P; s'\rangle \Big|_{\xi\cdot n=0} \\ &= \sum_m \langle P_m|\, U^T_{[\infty,\boldsymbol{\infty}_T;\infty,\mathbf{0}_T]}\, U^n_{[\infty,\mathbf{0}_T;-\infty,\mathbf{0}_T]}\, U^T_{[-\infty,\mathbf{0}_T;-\infty,\boldsymbol{\infty}_T]}\, |P; s\rangle^* \\ &\quad \times \langle P_m|\, U^T_{[\infty,\boldsymbol{\infty}_T;\infty,\mathbf{0}_T]}\, U^n_{[\infty,\mathbf{0}_T;-\infty,\mathbf{0}_T]}\, U^T_{[-\infty,\mathbf{0}_T;-\infty,\boldsymbol{\infty}_T]}\, |P; s'\rangle \Big|_{\xi\cdot n=0} \\ &\quad \times \delta^{(2)}(\boldsymbol{P}_{m\,T} + \boldsymbol{k}_T), \end{aligned} \tag{3.79}$$

where we inserted a complete set a momentum eigenstates $\{|P_m\rangle\}$ and we used (3.43). From eq. (3.79) it follows that $G_0^{[\Box]}$ is positive semidefinite, thus its eigenvalues must be ≥ 0. To establish bounds for the Wilson loop TMDs, we again restrict ourselves to two-dimensional principal minors. We obtain the following two inequalities:

$$\frac{\boldsymbol{k}_T^2}{2M^2}\left(e_T^2 + e_{LT}^2\right) \leq (e - e_{LL})\left(e + \frac{e_{LL}}{2}\right), \tag{3.80}$$

$$\frac{\boldsymbol{k}_T^2}{M^2}\,|e_{TT}| \leq e + \frac{e_{LL}}{2}. \tag{3.81}$$

Applying the small-x limit to the bounds (3.61)–(3.92), one indeed recovers the bounds (3.80) and (3.81). Besides these two bounds, we also have $e \geq 0$ (this follows from eq. (3.43)).

The case of a spin-1/2 hadron follows straightforwardly. The parametrization of the Wilson loop correlator for spin-1/2 hadrons is given in terms of the two functions e and e_T. In this case $G_0^{[\Box]}$ reads:

$$G_0^{[\Box]} = \frac{\pi L}{M^2} \begin{pmatrix} e & \frac{ie^{-i\phi}k}{M}\,e_T \\ -\frac{ie^{i\phi}k}{M}\,e_T & e \end{pmatrix}, \tag{3.82}$$

from which we can derive the following upper bound for e_T:

$$\frac{|\boldsymbol{k}_T|}{M}\,|e_T| \le e. \tag{3.83}$$

Note that upon omitting tensor polarization and discarding all functions related to it (this is, in fact, mathematically equivalent to the reduction to a spin-½ description), the bounds (3.80) and (3.81) reduce to a bound that is consistent with but less strict than (3.83). We can also obtain (3.83) by applying the small-x limit to the bounds for spin-½ hadrons given in (3.70)–(3.74).

3.5.3 The quark case

Positivity bounds for quark TMDs and PDFs in hadrons up to spin-1 have been derived in [85,150,151]. Starting from (3.58), on similar lines as Section 3.5.1, one has to construct the 6×6 matrix $F(x,\boldsymbol{k}_T)$ in the quark $\otimes$ hadron polarization space. This matrix is positive semidefinite and an equation similar to (3.60) can be obtained for the quark case as well. Afterwards, the calculation of the bounds is straightforward. The 9 independent inequalities on quark TMDs read:

$$|\tilde{h}_1|^2 \le \frac{1}{2}\left(f_1+\frac{2f_{1LL}}{3}\right)\left(f_1+\tilde{g}_1-\frac{f_{1LL}}{3}\right), \tag{3.84}$$

$$\frac{\boldsymbol{k}_T^2}{2M^2}\,|g_{1T}+\tilde{f}_{1LT}|^2 \le \left(f_1+\frac{2f_{1LL}}{3}\right)\left(f_1+\tilde{g}_1-\frac{f_{1LL}}{3}\right), \tag{3.85}$$

$$\frac{\boldsymbol{k}_T^2}{2M^2}\,|g_{1T}-\tilde{f}_{1LT}|^2 \le \left(f_1+\frac{2f_{1LL}}{3}\right)\left(f_1-\tilde{g}_1-\frac{f_{1LL}}{3}\right), \tag{3.86}$$

$$\frac{\boldsymbol{k}_T^4}{2M^4}\,|\tilde{h}^{\perp}_{1T}| \le \left(f_1+\frac{2f_{1LL}}{3}\right)\left(f_1-\tilde{g}_1-\frac{f_{1LL}}{3}\right), \tag{3.87}$$

$$\frac{\boldsymbol{k}_T^6}{M^6}{h^{\perp}_{1TT}}^2 \le \left(f_1-\tilde{g}_1-\frac{f_{1LL}}{3}\right)^2, \tag{3.88}$$

$$\frac{\boldsymbol{k}_T^2}{M^2}\left(\tilde{h}^{\perp}_1+\frac{2h^{\perp}_{1LL}}{3}\right)^2 \le \left(f_1+\frac{2f_{1LL}}{3}\right)^2, \tag{3.89}$$

$$\frac{\boldsymbol{k}_T^2}{4M^2}h^2_{1TT} \le \frac{1}{4}\left(f_1+\tilde{g}_1-\frac{f_{1LL}}{3}\right)^2, \tag{3.90}$$

$$\frac{\boldsymbol{k}_T^2}{2M^2}\left[\left(h^{\perp}_1-\frac{h^{\perp}_{1LL}}{3}\right)^2+h^{\perp}_{1L}\right] \le \left(f_1+\tilde{g}_1-\frac{f_{1LL}}{3}\right)\left(f_1-\tilde{g}_1-\frac{f_{1LL}}{3}\right), \tag{3.91}$$

$$\frac{\boldsymbol{k}_T^4}{4M^4}|\tilde{f}_{1TT}|^2 \leq \left(f_1 + \tilde{g}_1 - \frac{f_{1LL}}{3}\right)\left(f_1 - \tilde{g}_1 - \frac{f_{1LL}}{3}\right), \tag{3.92}$$

where the following definitions have been employed for convenience in the notation:

$$\tilde{g}_1 \to g_1 - i f_{1T}^{\perp}, \tag{3.93}$$

$$\tilde{f}_{1LT} \to f_{1LT} - i g_{1LT}, \tag{3.94}$$

$$\tilde{f}_{1TT} \to f_{1TT} - i g_{1TT}^{\perp}, \tag{3.95}$$

$$\tilde{h}_1 \to h_1 + i h_{1LT}, \tag{3.96}$$

$$\tilde{h}_{1T}^{\perp} \to h_{1T}^{\perp} - i h_{1LT}^{\perp}. \tag{3.97}$$

These bounds reduce to the well-known relations between PDFs if one integrates over the transverse momenta.

3.6 Comments on the bounds

Positivity bounds are powerful tools in phenomenological studies, that have been employed in many context to pin down the magnitude or the shape of some unknown functions with respect to the known ones. However, some comments that apply irrespective of the parton type (both quark and gluons) are in order.

Since we look at TMDs, one must worry about the process dependence coming from the different types of gauge links [48]. In fact, the inequalities (3.61)–(3.92) and (3.70)–(3.74) do *not* hold generally true for any correlator. The matrices F (for quarks) and G (for gluons and Wilson correlator) is positive semidefinite only for field combinations, including gauge links, that factorize into the form $O^\dagger(0)O(\xi)$. The simplest gauge link structures for which this holds are $[+,+]$, $[-,-]$, $[+,-]$, and $[-,+]$. Additionally, the process dependence is not always directly calculable in the form of color factors, but it rather implies that the dependence of the distributions on $\boldsymbol{k}_T^2$ may require additional functions involving gluonic poles [152].

The results presented can be relevant for proposed experiments at JLab and a future EIC involving polarized targets. In practical situations, the bounds become useful in model and lattice calculations, or as a way to obtain an estimate on the order of magnitude of the functions. They are used to constrain the size of the less-known functions with respect to the better-known ones (e.g. polarized distributions with respect to the unpolarized ones). The latter is commonly done by saturating the bounds. These estimates for the functions can translate in estimates of specific measurement outcomes, e.g. azimuthal and spin asymmetries. Positivity bounds can

be defined for all the correlators that are positive semidefinite, therefore extensions to the double parton correlator are possible and interesting, as we shall see in Chapter 4.

In addition to these points, one might also worry about the effects of QCD evolution on the validity of the bounds. In the collinear case, the Soffer bound involving three quark functions [153] has been shown to be preserved up to next-to-leading order accuracy [154–156]. However, to our knowledge, there are no clear conclusions on the stability of bounds under TMD evolution equations.

The issue might be important for instance when the bound are used to compare functions that are extracted at different scales. The fact that the evolution kernel for TMDs is independent of spin [137, 157], might suggest that in the appropriate $\boldsymbol{k}_T$-regime where TMD factorization is valid, positivity bounds are respected also in this case. However, the latter could depend on the specific implementation of TMD evolution. This topic remains open to further investigation.

3.7 Discussion and conclusions

We have parametrized the quark and gluon correlation functions for target of spin up to 1, in terms of TMD functions of definite rank, reviewing the quark case and presenting the gluon results as originally derived in [88].

Concerning gluons, especially the small-x region is important, which is why we have also studied the gluon correlator in the small-x limit. To this end, we have derived and exploited the correspondence between the gluon correlator containing a dipole-type gauge link structure and a correlator containing a single Wilson loop [88]. The latter correlator can also be parametrized in terms of TMDs.

When only little information is available on the functions, useful tools to have in hands are the positivity bounds. These are model-independent relations that allows to relate one or more functions with each other. We have discussed positivity bounds on gluon correlators for hadrons of spin up to 1, thus looking at the unpolarized, vector polarized, and tensor polarized cases [92, 93]. The bounds have been derived using the fact that the correlators, even including gauge links that bridge the nonlocality, can be expressed as momentum densities. For both the TMD and collinear cases, we have obtained relations between the distribution functions that appear in the parametrization of the leading-twist gluon correlator.

These inequalities are relevant for the study of tensor polarized gluon TMDs at e.g. the EIC possibility at JLab (JLEIC) [125, 127, 158] or COMPASS [102] using tensor polarized deuterons. The proposed fixed-target experiment at LHC (AFTER@LHC) [133–135] would also allow to investigate the gluon TMDs, with the

possibility of including the ones related to tensor polarization.

Chapter 4

Pairs of polarized partons inside the proton

4.1 Introduction

In this Chapter, we discuss the possibility of studying interparton correlations through the double parton scattering (DPS) processes. The DPS factorized cross section leads to the definition of the double parton correlator of eq. (2.33). The latter is parametrized in terms of double parton distributions (DPDs), that are currently almost unknown because of the very limited experimental information on DPS compared to the single parton case. However, the experimental accessibility of many DPS processes is rapidly growing and their measurements will become more relevant in the future era of precision particle physics at high energies.

As a first approximation, the theoretical framework needed to describe double parton scatterings can be considered as an extension of the single parton description. However, this is often not sufficient, especially when dealing with physical concepts that are exclusive of multiparton interactions (such as the concept of quantum interference and correlation). A significant effort has been put into the formulation of a theory for double parton interactions. The complete review of this topic goes beyond the scope of this thesis and adequately comprehensive set of references that we point

out to the reader is [22, 23, 31, 159, 160].

The cross section formula for multiple hard scatterings has been derived in Section 2.4.1 using the standard factorized form, both for the TMD and collinear case, leading to the definition of TMD and collinear double parton correlator, respectively. Intriguing aspects, such as interference and correlation effects, are encoded in the tree-level expression of the cross section formulae.

The concept of quantum interference is remarkable and regards the fact that quantum numbers, such as the fermion and flavor number, have to be conserved globally (within the parton pair) in the amplitude and the conjugate one, but not necessarily between one parton and its conjugate partner. Interference terms of this sort would be forbidden in single parton scattering because of quantum number violation [31,33]. Some of these contributions, such as fermion number interference and color interference (see Section 4.4.2) are expected to be suppressed at high energy scales, even though a precise estimate of their magnitude has never been obtained, and usually they are excluded from phenomenological models.

The other peculiar feature of double parton theory is the presence of interparton correlation, extensively discussed in the rest of this Chapter. In the first part we mainly discuss two types of parton-parton correlations: quantum and kinematic. This information is formally entirely contained in the correlator and, consequently, in the DPDs. Therefore, different models for the DPDs, tailored to study correlations, are presented and discussed. In the second part of the Chapter, we present a study of correlation effects in the production of a pair of W bosons with the same charge at the LHC. In the hunt for possibilities to measure double parton scatterings, it has been recognized that this process is one of the most promising, thanks to its very clear signature. We focus on this process with the goal of characterizing signals of quark-quark correlations. In particular, we devote particular attention to studying the quantum correlation between the spin of the two partons and the kinematic correlation between their longitudinal momentum fractions.

Multiple interactions and interparton correlations change the structure of the final states. We discuss the modification of the final-state distributions due to the correlation effects at the level of partonic interactions and we subsequently extend the analysis to the final-state distributions at the LHC.

4.2 Double parton distributions

The phenomenology of double parton interactions relies on models that provide physically intuitive pictures but involve major simplifications. In fact, nearly nothing is

experimentally known about the double parton distributions, so we need to make assumptions based on the accessible theoretical and experimental information. In other words, one needs to find reasonable approximations that relate the double parton distributions to the single parton counterparts (about which much more information is known), postponing the detailed analysis to the moment when experiments will deliver more data.

To be able to deal with the single parton operator, we need to simplify the double parton correlator into a combination of multiple one-parton operators. Let us start from the definition (2.33) and insert a complete set of states. By recalling the notation (2.34), one reads:

$$\langle P|\,\mathcal{O}(0,z_2)\mathcal{O}(y,z_1)\,|P\rangle = \sum_X \langle P|\,\mathcal{O}(0,z_2)\,|X\rangle\,\langle X|\,\mathcal{O}(y,z_1)\,|P\rangle\,. \tag{4.1}$$

The usual choice taken in the literature is to assume that, among all the states $\{|X\rangle\}$, the dominant one is the proton state. We call it $|P'\rangle$ to indicate that this might (and actually is) a different momentum vector with respect to the original one. There is no theoretical motivation to reduce the sum over the intermediate states to a single proton state. However, in the absence of experimental data to test this hypothesis on, one can use it as a first approximation and exploit the knowledge on the single parton distributions. Omitting some details of the derivation (that are available in [31]), it turns out that:

$$\langle P|\,\mathcal{O}(0,z_2)\,|P'\rangle\,\langle P'|\,\mathcal{O}(y,z_1)\,|P\rangle \tag{4.2}$$

is related to the product of two generalized transverse momentum dependent correlation functions for a single parton.

These quantities depend on the collinear fraction of parton momentum x_1, the intrinsic transverse momentum $\boldsymbol{k}_{1T}$, and the unbalance of momenta (off-forwardness) between the initial and final-state proton. We define the transverse component of the difference between the proton momentum in the initial and final state as:

$$\boldsymbol{\Delta} = \boldsymbol{P'} - \boldsymbol{P}, \tag{4.3}$$

such that the DP correlator can be related to the single parton GTMD correlator [31].

The Fourier conjugate of the $\boldsymbol{\Delta}$ is the impact parameter $\boldsymbol{b}$, a transverse coordinate, which is related to the single GPD operator. The collinear double parton distributions,

like the ones entering eq. (2.38), can be written as follows[1]:

$$\Phi_{DP}(x_1, x_2, \boldsymbol{y}) \approx \int d^2\boldsymbol{b}\, \Phi_{SP}(x_1, \boldsymbol{b})\Phi_{SP}(x_2, \boldsymbol{b}+\boldsymbol{y}), \tag{4.4}$$

which relates the DPDs to two single parton distributions. Despite the fact that the validity of this approximation cannot be quantified in practice, the relation in (4.4) offers some indication and guidance to estimate the size and the interplay between longitudinal and transverse variables, otherwise unaccessible. Pushing further the simplifications, if one assumes that the $\boldsymbol{y}$-dependent part is universal and factorizes out, the collinear part is the product of single parton PDFs, i.e.:

$$\Phi_{DP}(x_1, x_2, \boldsymbol{y}) \approx \Phi_{DP}(x_1, x_2)G(\boldsymbol{y}) \approx \Phi_{SP}(x_1)\Phi_{SP}(x_2)G(\boldsymbol{y}). \tag{4.5}$$

Inserting (4.5) in (2.38) we can define the *effective cross section* as:

$$\frac{1}{\sigma_{\text{eff}}} = \int d^2\boldsymbol{y}\, G^2(\boldsymbol{y}) \tag{4.6}$$

such that the cross section of a double parton scattering process is factorized into the so-called *pocket formula*:

$$\sigma_{DP} = \frac{1}{C}\frac{\sigma_1\sigma_2}{\sigma_{\text{eff}}}, \tag{4.7}$$

where $\sigma_{1,2}$ are the cross sections of the single parton scattering process necessary to produce the final states, and σ_{eff} represents the "strength" of double parton contribution over the separated single parton ones. The expression (4.7) implies that all the correlations between partons in the proton are zero. One of the focus of this Chapter is to go beyond this approximation.

4.2.1 Effective cross section σ_{eff} and beyond

The approximations that lead to eq. (4.7) are quite drastic, and one can expect them to fail in many respects. We summarize the problem of having such a crude estimate of the cross section for double parton scattering.

The first part of the factorization (4.5) eliminates all possible correlations between collinear momenta and transverse separation, which is contradicted by the majority of model calculations [161–166]. The second part of (4.5) excludes in addition all pos-

[1] When necessary, we will use the subscript DP and SP to indicate the double and single parton operators respectively. When not ambiguous, we will drop this label and consistently refer to the double parton operators.

sible correlations between parton momenta. The validity of this approximation fails if one considers the natural kinematical constraint of double parton scattering, i.e. $x_1 + x_2 \leq 1$. In spite of its validity on the right-hand site of (4.7), the single parton quantities on the left-hand side are not constrained in the same way, but only as $x_1 \leq 1$ and $x_2 \leq 1$. Taking into account the conservation of momentum implies the introduction of longitudinal correlations and the breakdown of (4.5). This would imply the explicit x_i-dependence of the σ_{eff}, as predicted by several models [162, 165, 167]. The factorization between longitudinal momenta and transverse separation is also violated by the presence of longitudinal-transverse correlations of the type (4.4), although the identification of such correlations is challenging because $\boldsymbol{y}$ is not a measurable quantity and it is integrated over.

However, the definition of the effective cross section through (4.7), states the independence of this quantity on longitudinal momenta, type of partons involved and, consequently, processes. More generically, the factorization of the double parton quantities into a product of single parton distributions eliminates all correlations between partons, including the quantum-mechanical ones, i.e., correlations deriving from the pairwise quantum interactions of partons through their spin, color, fermion and flavor number. Despite its usefulness as a first approximation, the approach according to which the quantity σ_{eff} is a universal number, independent on all kinematical variable and quantum numbers, is theoretically unsatisfactory to describe double parton scattering. The next era of high luminosity at the LHC is undoubtedly an opportunity to refine and test the theory of DPS and to go beyond the σ_{eff} approximation. In this Chapter, we will contribute to this goal with a closer look at feasible ways to measure correlations and extend the factorized approach.

4.3 Experimental status of double parton scattering measurements

Double parton scattering raised interest in the experimental community quite soon after the first theoretical works appeared. The first DPS process probed experimentally is the production of 4 jets. First measurements were performed first at CERN at the Intersecting Storage Rings (ISR) and the Super Proton Synchrotron (SPS) [168, 169], and Fermilab [170], followed by more recent measurements at the LHC [171, 172]. To increase the cleanliness of the signal, the D0 collaboration at Tevatron has also used processes with the production of one (or two) photon accompanied by jets [173–176]. The direct photon is more easily detectable and it can be distinguished from the hadronic matter in the final-states [177].

On the other hand, at LHC processes with more clear signatures, with less number of jets or no jets involved, are preferred. The ATLAS, CMS, LHCb, and ALICE collaborations produced, in the first round of LHC, measurements on the following (subset of) processes:

- vector bosons and jets: $Z/W + jj$ [178, 179];
- vector bosons pair: $ZZ/W^{\pm}W^{\pm}/WZ$ [180];
- meson pair: J/ψ or open charm [181–184].

The σ_{eff} values derived in all these measurements are displayed in Figure 4.1, and in a summary Table 4.1 taken from ref. [185]. The numbers vary approximately between 10 and 20 mb. A commonly used value for applications is $\sigma_{\text{eff}} = 15$.

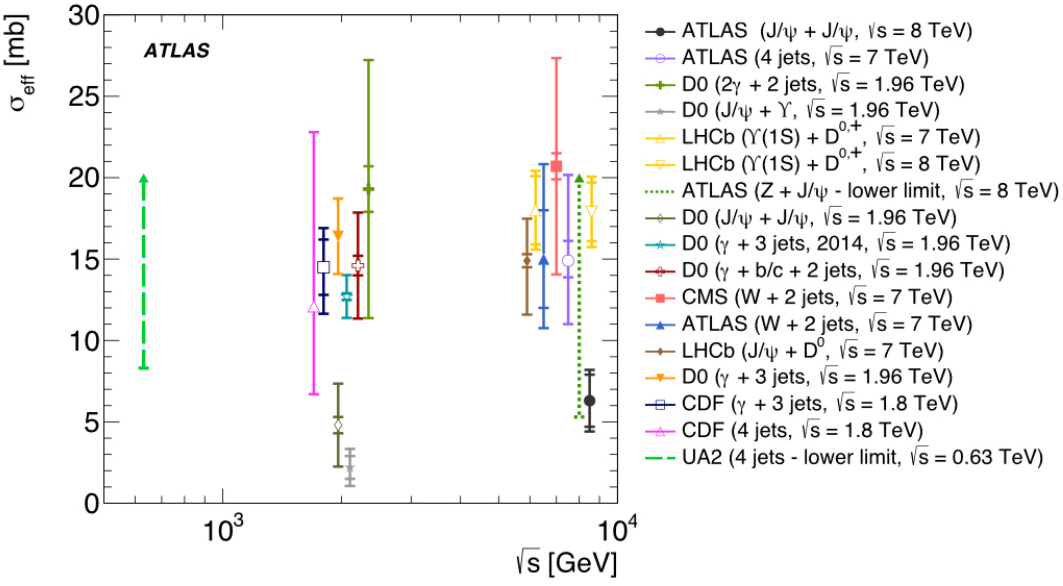

Figure 4.1: Schematic overview of the measurements of the effective cross sections as a function of the CM energy $\sqrt{s}$. Figure from ref [186].

DPS channel	$\boldsymbol{\sigma_{\text{eff}}}$(mb)	**Collaboration**	**Collider**	**Luminosity**
$jj \otimes jj$	$12.1^{+10.7}_{-5.4}$	CDF [170]	1.8 TeV Tevatron	325 nb^{-1}
$J/\Psi \otimes D$	$14.9^{+2.6}_{-3.1}$ $17.6^{+3.1}_{-4.0}$ $12.8^{+2.6}_{-3.2}$ $18.0^{+4.8}_{-5.5}$	LHCb [182]	7 TeV LHC	355 pb^{-1}
$W \otimes jj$	$15.0^{+5.8}_{-4.2}$	ATLAS [178]	7 TeV LHC	36 pb^{-1}
$W^{\pm} \otimes W^{\pm}$	> 5.91	CMS [187]	8 TeV LHC	19.7 fb^{-1}
$W \otimes jj$	$20.7^{+6.6}_{-6.6}$	CMS [179]	7 TeV LHC	5 fb^{-1}
$\gamma j \otimes jj$	$12.7^{+1.3}_{-1.3}$ $14.5^{+3.3}_{-5.3}$	D0 [175]	1.96 TeV Tevatron	8.1 fb^{-1}
$jj \otimes jj$	$16.1^{+6.4}_{-7.0}$	ATLAS [172]	7 TeV LHC	37.3 pb^{-1}
$\gamma\gamma \otimes jj$	$19.3^{+7.9}_{-7.9}$	D0 [176]	1.96 TeV Tevatron	8.7 fb^{-1}
$J/\Psi \otimes J/\Psi$	$4.80^{+2.55}_{-2.55}$	D0 [188]	1.96 TeV Tevatron	8.1 fb^{-1}
$J/\Psi \otimes J/\Psi$	$14.4^{+4.9}_{-4.9}$ $9.2^{+3.9}_{-3.9}$ $11.3^{+1.5}_{-1.5}$	LHCb [184]	13 TeV LHC	5 fb^{-1}

Table 4.1: Overview of the principal measurements of σ_{eff} performed by different experiments at various energies. Different values quoted by the same experimental analysis refer to different different decay modes [182], different models [184], or different data samplings [175]. Table from ref. [185].

The double parton scattering in same-sign W boson pair production is considered one of the most promising process for the measurements of DPS thanks to its clear signature. It has been studied extensively in [177,189–192] and finally measured in [180]. The price to pay, for such an ideal process from the theory point of view, is that the DPS cross section is very small and therefore quite some effort has been put in the extraction [180]. We will examine in more details the production of W^+W^+ in Section 4.5.

4.4 Parton correlations in double parton scattering

As previously mentioned, the pocket formula (4.7) and the concept of a universal value for σ_{eff} are based on the assumptions that all the interparton correlation effects are not relevant. In reality, the question about how important correlations in DPS can be is currently open, and this problem has been tackled from different perspectives (for a review of the state of the art of parton correlation in DPS see, e.g., [193]). The potential importance of quantum and kinematic correlations are confirmed by numerous model calculations, at least at low scales and in the valence region [162,163]. For instance, spin correlations are studied in [162,163,166] and they are predicted to be sizable at the higher scales as well. Kinematic correlations, i.e. those which would be responsible for the violation of (4.5) (related to the longitudinal correlations and longitudinal-transverse correlations) are treated in [161–166], with the conclusions that they can be relevant. As largely acknowledged in most of the theoretical works, the characterization of all kind of correlations would shed light on the proton structure at a more fundamental level.

4.4.1 Spin correlations

The cross section formula in eq. (2.38) is quite general because both the hard scattering parts H_i and the correlators Φ depend in principle on all possible indices (such as parton-type, spin, color, fermion and flavor number).

Similarly to the decompositions of the single parton correlators in Chapter 3, also the double parton correlator can be decomposed in different structures that explicitly contain the dependence on the quantum numbers. In addition to the degrees of freedom typical of the parton-hadron system, the extension from the single to the double parton description introduces new degrees of freedom linked to the parton-parton system. This fact leads to the definition of a big number of DPDs, especially when the spin of the target and intrinsic parton momenta are included. As a matter

of fact, not all the DPDs contribute significantly to the physical processes. For this reason, we restrict ourselves to the collinear DPDs in unpolarized targets, which can in principle be accessed in the near future experiments. We refer to [31, 32, 194] for further information.

Quarks and gluons carry spin, and they can have a definite polarization when they enter the hard scatterings. In eq. (2.38) we omitted all the indices that H_i and Φ depend on. Now the parton spin indices will be reinserted, while the others are left out. The i-th (with $i = 1, 2$) hard scattering matrices H_i and the correlators Φ ($\bar{\Phi}$) are matrices in the Dirac space. Showing the indices, one has the following contraction:

$$\Phi_{\alpha_1\beta_1,\alpha_2\beta_2}\bar{\Phi}_{\bar{\alpha}_1\bar{\beta}_1,\bar{\alpha}_2\bar{\beta}_2}H_{1,\alpha_1\bar{\alpha}_1,\beta_1\bar{\beta}_1}H_{2,\alpha_2\bar{\alpha}_2,\beta_2\bar{\beta}_2}, \tag{4.8}$$

We consider one hard scattering at a time, focusing on the contraction between the indices labeled as "1" and we further restrict ourselves to the lower part of the graph in Fig. 2.5, i.e., the left-moving proton (all the other indices are dropped for simplicity). One can decompose $H_{1,\alpha_1\beta_1}$ in terms of Dirac structures and an analogous decomposition can be used for $\Phi_{\alpha_1\beta_1}$.We select the dominant terms in the correlators that, in exact analogy with the single parton case, correspond to the plus-components in the correlator $\Phi_{\alpha_1\beta_1}$.The contraction between the correlator of the left-moving proton and the hard scattering reads:

$$\begin{aligned} H_{i,\beta_1\alpha_1}\Phi_{\alpha_1\beta_1} = &\operatorname{Tr}\left(\frac{1}{2}\gamma^- H_i\right)\operatorname{Tr}\left(\frac{1}{2}\gamma^+\Phi\right) + \operatorname{Tr}\left(\frac{1}{2}\gamma^-\gamma_5 H_i\right)\operatorname{Tr}\left(\frac{1}{2}\gamma^+\gamma_5\Phi\right) \\ &+ \operatorname{Tr}\left(\frac{1}{2}i\sigma^{j-}\gamma_5 H_i\right)\operatorname{Tr}\left(\frac{1}{2}i\sigma^{j+}\gamma_5\Phi\right) + \{\text{higher-twist terms}\}. \end{aligned} \tag{4.9}$$

The different terms in (4.9) corresponds to the scattering of quarks that are respectively unpolarized, longitudinally polarized and transversely polarized [195]. Accordingly, we denote:

$$\Phi^{[\Gamma]} = \frac{1}{2}\operatorname{Tr}(\Phi\Gamma) \tag{4.10}$$

and identify three different Γ structures responsible for selecting unpolarized (q), longitudinally (Δq), and transversely polarized (δq) quarks in the proton:

$$\Gamma_q = \frac{1}{2}\gamma^+, \quad \Gamma_{\Delta q} = \frac{1}{2}\gamma^+\gamma_5, \quad \Gamma^j_{\delta q} = \frac{1}{2}i\sigma^{j+}\gamma_5. \tag{4.11}$$

The same considerations hold true for the polarization of the antiquark coming from the right-moving proton.

We recall the definition of the double parton correlator (2.33) and relabel the fermion fields as $\psi \to q$ in the correlator. The DPDs for two quarks are:

$$F_{a_1 a_2}(x_1, x_2, \boldsymbol{y}) = 2P^+ \int \frac{dz_1^- dz_2^-}{(2\pi)^2} dy^- \, e^{ix_1 z_1^- P^+ + ix_2 z_2^- P^+} \left\langle P \right| \mathcal{O}^{\Gamma_{a_1}}(0, z_2) \mathcal{O}^{\Gamma_{a_2}}(y, z_1) \left| P \right\rangle \Big|_{\substack{z_1^+ = z_2^+ = y^+ = 0, \\ \boldsymbol{z}_{T1} = \boldsymbol{z}_{T2} = \boldsymbol{0}_T.}}, \tag{4.12}$$

where:

$$\mathcal{O}^{\Gamma_a}(y, z) = \bar{q}(y - \frac{1}{2}z)\Gamma_a q(y + \frac{1}{2}z). \tag{4.13}$$

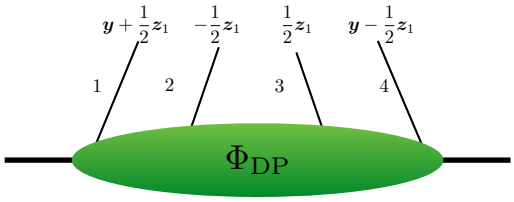

Figure 4.2: Graphic explanation for the notation in eq. (4.14)-(4.16)

We now use the enumeration on the quark fields as in Fig. 4.2, and we drop the dependence of the spinors on the variables z and y. The double parton distribution for two quarks, quarks and antiquarks, and two antiquarks are written as ($\mathcal{FT}$ briefly indicates Fourier transforms and integration over y as in eq. (4.12)):

$$F_{a_1 a_2} = \mathcal{FT} \left\langle P \right| (\bar{q}_3 \Gamma_{a_2} q_2)(\bar{q}_4 \Gamma_{a_1} q_1) \left| P \right\rangle, \tag{4.14}$$

$$F_{a_1 \bar{a}_2} = \mathcal{FT} \left\langle P \right| (\bar{q}_2 \Gamma_{a_2} q_3)(\bar{q}_4 \Gamma_{a_1} q_1) \left| P \right\rangle, \tag{4.15}$$

$$F_{\bar{a}_1 \bar{a}_2} = \mathcal{FT} \left\langle P \right| (\bar{q}_2 \Gamma_{a_2} q_3)(\bar{q}_1 \Gamma_{a_1} q_4) \left| P \right\rangle, \tag{4.16}$$

with the relations:

$$F_{a_1 a_2}(x_1, x_2, \boldsymbol{y}) = \eta_{a_2} F_{a_1 \bar{a}_2}(x_1, -x_2, \boldsymbol{y}), \tag{4.17}$$

$$F_{a_1 a_2}(x_1, x_2, \boldsymbol{y}) = F_{\bar{a}_1 \bar{a}_2}(-x_1, -x_2, \boldsymbol{y}), \tag{4.18}$$

with $\eta_q = \eta_{\delta q} = 1$ and $\eta_{\Delta q} = -1$. One can, therefore, decompose the F further

into [31]:

$$
\begin{aligned}
&F_{qq}(x_1, x_2, \boldsymbol{y}) = f_{qq}(x_1, x_2, y),\\
&F_{\Delta q\Delta q}(x_1, x_2, \boldsymbol{y}) = f_{\Delta q\Delta q}(x_1, x_2, y),\\
&F^{j}_{q\delta q}(x_1, x_2, \boldsymbol{y}) = \epsilon^{j\boldsymbol{y}} M f_{q\delta q}(x_1, x_2, y) = \epsilon^{j\boldsymbol{y}} h_{q\delta q}(x_1, x_2, y),\\
&F^{j}_{\delta qq}(x_1, x_2, \boldsymbol{y}) = \epsilon^{j\boldsymbol{y}} M f_{\delta qq}(x_1, x_2, y) = \epsilon^{j\boldsymbol{y}} h_{\delta qq}(x_1, x_2, y),\\
&F^{jj'}_{\delta q\delta q}(x_1, x_2, \boldsymbol{y}) = \delta^{jj'} f_{\delta q\delta q}(x_1, x_2, y) + (2\boldsymbol{y}^j\boldsymbol{y}^{j'} - \boldsymbol{y}^2\delta^{jj'})M^2 f^t_{\delta q\delta q}(x_1, x_2, y)\\
&\qquad\qquad = \delta^{jj'} h_{\delta q\delta q}(x_1, x_2, y) + (2\boldsymbol{y}^j\boldsymbol{y}^{j'} - \boldsymbol{y}^2\delta^{jj'}) h^t_{\delta q\delta q}(x_1, x_2, y)
\end{aligned}
\tag{4.19}
$$

Some combinations are not present as they violate parity ($q\Delta q$) and time reversal ($\Delta q\delta q$). In fact, we only want to deal with the cases for which time reversal odd collinear DPDs vanish because of the gauge link structure [31]. We denote all the distributions that contain transverse spin (helicity flip) with h as in the single parton case. In the production of double W bosons, the two bosons only couple with left-handed (right-handed) particles (antiparticles), therefore no helicity flip is allowed.

Gathering all the information in a compact form, the cross section can be written in the following factorized form [31]:

$$
\frac{d\sigma}{\prod_{i=1,2} dx_i d\bar{x}_i} = \frac{1}{C} \sum_{\substack{q,\Delta q,\delta q\\ \bar{q},\Delta\bar{q},\delta\bar{q}}} \int d^2\boldsymbol{y}\, \hat{\sigma}_{1,a_1,b_1}\hat{\sigma}_{2,a_2,b_2} F_{a_1,a_2}(x_1, x_2, \boldsymbol{y}) F_{b_1,b_2}(\bar{x}_1, \bar{x}_2, \boldsymbol{y}),
\tag{4.20}
$$

where the indices a_1, a_2, b_1, b_2 run over all polarizations of quarks and antiquarks, and implicitly over flavors. The dependence of the partonic cross section on $x_i\bar{x}_i s \approx q_i^2$ is understood and the symmetry factor C equals 2 if the produced final states are the same, while it is set to 1 when the two hard scatterings produce different particles. This form will be used to calculate the cross section of the W^+ pair production in pp collision.

Interpretation of the functions and positivity bounds

The collinear double parton correlator is, in the very same way as the single one, a positive semidefinite matrix. In fact, it can be shown that it is a diagonal operator,

namely:

$$\Phi(x_1,x_2,\boldsymbol{y}) = \int \frac{dz_1^- dz_2^-}{(2\pi)^2} dy^-\, e^{ik_1^+ z_1^- + ik_2^+ z_2^-} \times \langle P|\, \bar{q}(-\frac{1}{2}z_2) q(\frac{1}{2}z_2) \bar{q}(y-\frac{1}{2}z_1) q(y+\frac{1}{2}z_1)\, |P\rangle \Big|_{\substack{z_1^+=z_2^+=y^+=0;\\ \boldsymbol{z}_{T1}=\boldsymbol{z}_{T2}=\boldsymbol{0}_T.}} \tag{4.21}$$

$$= \int dy^- \sum_X \langle P_X|\, q(0)q(y)\, |P\rangle^* \langle P_X|\, q(0)q(y)\, |P\rangle\, \delta(P_X^+ - (1-x_1-x_2)P^+)\Big|_{y^+=0}, \tag{4.22}$$

where we have inserted a complete set of momentum eigenstates $|P_X\rangle$. In order to derive positivity bounds, which would provide the relations between the DPDs, one has to construct the relevant density matrix. In this case, being the spin of the proton not involved, the density matrix will be a 4×4 matrix defined in the parton$_1\otimes$ parton$_2$ spin space. Each entry of this matrix would accordingly contain the combined information about the polarization of each parton.

The value of the operator Γ_a in (4.13) is chosen as in eq (4.11), and it is responsible for selecting the spin structure of each parton. This structure is the same as the single parton case, and the interpretation of the DPD functions as spin densities (or combination of spin densities) can be found in a very similar way. We can use the knowledge acquired on the good and bad components of the fermion fields to make the meaning of the DPDs more apparent. We recall the well-known procedure for the PDFs, and treat the DPDs as a straightforward extansions.

The contraction of the correlator with the appropriate structures as in (4.11), leads to the definition of the single parton PDFs as follows:

$$\Phi_{SP}^{[\Gamma]} = \frac{1}{2}\,\mathrm{Tr}(\Phi_{SP}\Gamma), \tag{4.23}$$

one has:

$$f_1(x) = \Phi_{SP}^{[\gamma^+]} = \frac{1}{2}\int \frac{d\xi^-}{2\pi} e^{ik\cdot\xi}\, \langle P|\, \bar{\psi}(0)\not{n}\psi(\xi)\, |P\rangle\big|_{\xi^+=\boldsymbol{\xi}_T=0}, \tag{4.24}$$

$$g_1(x) = \Phi_{SP}^{[\gamma^+\gamma_5]} = \frac{1}{2}\int \frac{d\xi^-}{2\pi} e^{ik\cdot\xi}\, \langle P,S_L|\, \bar{\psi}(0)\not{n}\gamma_5\psi(\xi)\, |P,S_L\rangle\big|_{\xi^+=\boldsymbol{\xi}_T=0}, \tag{4.25}$$

$$h_1(x) = \Phi_{SP}^{[\sigma^{i+}\gamma_5]} = \frac{1}{2}\int \frac{d\xi^-}{2\pi} e^{ik\cdot\xi}\, \langle P,S_T|\, \bar{\psi}(0)\left[\not{S}_T,\not{n}\right]\psi(\xi)\, |P,S_T\rangle\big|_{\xi^+=\boldsymbol{\xi}_T=0}. \tag{4.26}$$

It can be shown [97, 196] that all the above contractions automatically reduce to a bilocal operator with only good fields, going in fact from a 4-dimensional to a 2-dimensional space. For instance:

$$\overline{\psi}(0)\not{n}\psi(\xi) \to \phi^\dagger(0)\phi(\xi), \tag{4.27}$$

and similarly for the others. One can use different spin basis to unravel the meaning of the above distributions. One can construct the *helicity basis*, where γ_5 and the matrix of the spin rotation along z-direction $\Sigma^3 = \frac{i}{2}\left[\gamma^1, \gamma^2\right]$ are diagonal [97]. We define the Dirac field only in terms of good field as:

$$\phi_h = \begin{pmatrix} \phi_+ \\ \phi_- \\ 0 \\ 0 \end{pmatrix}, \tag{4.28}$$

where the components of ϕ_h are related to $\pm$ helicity states. This is also eigenstate of the chirality operator γ_5 (which commutes with $P_\pm$) in the massless limit, namely:

$$\gamma_5\phi_h = \begin{pmatrix} +\phi_+ \\ -\phi_- \\ 0 \\ 0 \end{pmatrix} = \begin{pmatrix} \phi_R \\ -\phi_L \\ 0 \\ 0 \end{pmatrix}. \tag{4.29}$$

Alternatively one can use the *transversity basis*, by defining the "transverse-spin-up" and "transverse-spin-down" states as follows

$$\phi_T = \begin{pmatrix} \phi_\uparrow \\ \phi_\downarrow \\ 0 \\ 0 \end{pmatrix} = \frac{1}{\sqrt{2}} \begin{pmatrix} \phi_R + \phi_L \\ \phi_R - \phi_L \\ 0 \\ 0 \end{pmatrix}, \tag{4.30}$$

which is an eigenstate of the operator $\gamma^1\gamma_5$ (or equivalently $\gamma^2\gamma_5$) that selects the transverse components of the parton spin. In this framework the functions have a clear interpretation as densities:

- Helicity basis:

$$\begin{aligned} f_1 &\sim \langle P|\, \phi_R^\dagger\phi_R + \phi_L^\dagger\phi_L\, |P\rangle\,, \\ g_1 &\sim \langle P, S_L|\, \phi_R^\dagger\phi_R - \phi_L^\dagger\phi_L\, |P, S_L\rangle\,, \end{aligned} \tag{4.31}$$

$$h_1 \sim \langle P, S_T |\, \phi_L^\dagger \phi_R \,| P, S_T \rangle \,.$$

- Transversity basis:

$$\begin{aligned} f_1 &\sim \langle P |\, \phi_\uparrow^\dagger \phi_\uparrow + \phi_\downarrow^\dagger \phi_\downarrow \,| P \rangle \,, \\ g_1 &\sim \langle P, S_L |\, \phi_\uparrow^\dagger \phi_\downarrow \,| P, S_L \rangle \,, \\ h_1 &\sim \langle P, S_T |\, \phi_\uparrow^\dagger \phi_\uparrow - \phi_\downarrow^\dagger \phi_\downarrow \,| P, S_T \rangle \,. \end{aligned} \tag{4.32}$$

The unpolarized distribution has the obvious meaning of an average over polarization states, in both basis. The function g has, in the helicity basis, the interpretation as the number density of partons with a neat polarization along the direction of the proton spin, and h_1 represents in the transversity basis the number density of partons with polarization along a direction transverse to the proton spin.

As far as the double parton correlator is concerned, the generalization is direct, and the interpretation of the DPDs as linear combination of two-parton densities follows straightforwardly. The DPDs in the helicity basis are defined as:

$$\begin{aligned} F_{qq} \sim &(\phi_{1R}^\dagger \phi_{1R})(\phi_{2R}^\dagger \phi_{2R}) + (\phi_{1L}^\dagger \phi_{1L})(\phi_{2L}^\dagger \phi_{2L}) \\ &+ (\phi_{1L}^\dagger \phi_{1L})(\phi_{2R}^\dagger \phi_{2R}) + (\phi_{1R}^\dagger \phi_{1R})(\phi_{2L}^\dagger \phi_{2L}), \end{aligned} \tag{4.33}$$

$$\begin{aligned} F_{\Delta q \Delta q} \sim &(\phi_{1R}^\dagger \phi_{1R})(\phi_{2R}^\dagger \phi_{2R}) + (\phi_{1L}^\dagger \phi_{1L})(\phi_{2L}^\dagger \phi_{2L}) \\ &- (\phi_{1L}^\dagger \phi_{1L})(\phi_{2R}^\dagger \phi_{2R}) - (\phi_{1R}^\dagger \phi_{1R})(\phi_{2L}^\dagger \phi_{2L}), \end{aligned} \tag{4.34}$$

and analogous expression for $F_{\delta q \delta q}$ in the transversity basis:

$$\begin{aligned} F_{\delta q \delta q} \sim &(\phi_{1\uparrow}^\dagger \phi_{1\uparrow})(\phi_{2\uparrow}^\dagger \phi_{2\uparrow}) + (\phi_{1\downarrow}^\dagger \phi_{1\downarrow})(\phi_{2\downarrow}^\dagger \phi_{2\downarrow}) \\ &- (\phi_{1\downarrow}^\dagger \phi_{1\downarrow})(\phi_{2\uparrow}^\dagger \phi_{2\uparrow}) - (\phi_{1\uparrow}^\dagger \phi_{1\uparrow})(\phi_{2\downarrow}^\dagger \phi_{2\downarrow}). \end{aligned} \tag{4.35}$$

The connection between F_{qq}, $F_{\Delta q \Delta q}$, and $F_{\delta q \delta q}$ to the single case is a convenient illustrative procedure. However, one shoud bear in mind that the physical meaning of the quantities is completely different, being the DPDs densities (or interference) of two-parton polarizations that can be defined irrespective of the presence of the proton spin.

In order to finally build the two-parton density matrix, we single out the operators

projecting the helicity state of the good components of the fields into [197]:

$$\Gamma_{++} = \gamma^+ \frac{(1+\gamma_5)}{4}, \quad \text{with} \quad \bar{\psi}\Gamma_{++}\psi = \frac{1}{\sqrt{2}}\bar{\phi}_L\phi_L, \tag{4.36}$$

$$\Gamma_{-+} = \frac{i\sigma^{+1}}{4}(1-\gamma_5), \quad \text{with} \quad \bar{\psi}\Gamma_{-+}\psi = \frac{1}{\sqrt{2}}\bar{\phi}_R\phi_L, \tag{4.37}$$

$$\Gamma_{+-} = \frac{-i\sigma^{+1}}{4}(1+\gamma_5), \quad \text{with} \quad \bar{\psi}\Gamma_{+-}\psi = \frac{1}{\sqrt{2}}\bar{\phi}_L\phi_R, \tag{4.38}$$

$$\Gamma_{--} = \gamma^+ \frac{(1-\gamma_5)}{4}, \quad \text{with} \quad \bar{\psi}\Gamma_{--}\psi = \frac{1}{\sqrt{2}}\bar{\phi}_R\phi_R, \tag{4.39}$$

Using this basis, one can write the correlator as:

$$\Phi = \Phi_{++,++} + \Phi_{++,+-} + \Phi_{++,-+} + \Phi_{++,--} + \text{etc..}, \tag{4.40}$$

where

$$\Phi_{++,++} \sim \langle P| \left(\bar{\psi}\Gamma_{++}\psi\right)\left(\bar{\psi}\Gamma_{++}\psi\right)|P\rangle\,. \tag{4.41}$$

Using the functions defined in (4.19), one reads:

$$\rho = \frac{1}{4}\begin{pmatrix} f_{qq}+f_{\Delta q\Delta q} & -ie^{i\varphi}yh_{q\delta q} & -ie^{i\varphi}yh_{\delta qq} & 2e^{2i\varphi}y^2h^t_{\delta q\delta q} \\ ie^{-i\varphi}yh_{\delta qq} & f_{qq}-f_{\Delta q\Delta q} & 2h_{\delta q\delta q} & -ie^{i\varphi}yh_{q\delta q} \\ ie^{-i\varphi}yh_{q\delta q} & 2h_{\delta q\delta q} & f_{qq}-f_{\Delta q\Delta q} & -ie^{i\varphi}yh_{\delta qq} \\ 2e^{-2i\varphi}y^2h^t_{\delta q\delta q} & ie^{-i\varphi}yh_{q\delta q} & ie^{-i\varphi}yh_{\delta qq} & f_{qq}+f_{\Delta q\Delta q} \end{pmatrix}, \tag{4.42}$$

with $\boldsymbol{y} = y(\cos\varphi, \sin\varphi)$. A basis transformation can be performed to simplify the expression of the matrix as in [32]. In every basis, the diagonal elements are positive semidefinite and can be interpreted as probabilities of finding the two partons with the same helicities ($f_{qq}+f_{\Delta q\Delta q}$) or opposite helicities ($f_{qq}-f_{\Delta q\Delta q}$). This constraint leads to the first bound:

$$|f_{\Delta q\Delta q}| \leq f_{qq}. \tag{4.43}$$

The other bounds follow from the diagonalization of the 2×2 sub matrices and they read:

$$2y^2\,\left|h^t_{\delta q\delta q}\right| \leq f_{qq}+f_{\Delta q\Delta q}, \tag{4.44}$$

$$2\,|h_{\delta q\delta q}| \leq f_{qq}-f_{\Delta q\Delta q}, \tag{4.45}$$

$$y^2\,h^2_{q\delta q} \leq (f_{qq}+f_{\Delta q\Delta q})(f_{qq}-f_{\Delta q\Delta q}), \tag{4.46}$$

$$y^2\,h^2_{\delta qq} \leq (f_{qq}+f_{\Delta q\Delta q})(f_{qq}-f_{\Delta q\Delta q}). \tag{4.47}$$

More strict bounds are derived from the diagonalization of 3×3 submatrices and the eigenvalues of the whole matrix. As extensively discussed in Chapter 3, positivity bounds can be powerful tools to derive information about quantities that are mostly unknown, and whose magnitude and behavior is otherwise difficult to access without any experimental information. For instance, the bound (4.43) is used to have an low-scale ansatz about the size of the longitudinally polarized DPDs compared to the unpolarized ones [32].

4.4.2 Other quantum correlations

We reinsert the indices of the correlator and consider the decomposition in color structures. The basis of the $SU(3)$ color space is used, and correspondent projections in color space select whether the quark in the amplitude and its partner in the conjugate amplitude are in a singlet or octet representation. We define the correlator as $\Phi_{jj',kk'}$ and use a color Fierz transformation to decompose it in terms of the singlet and octet color structures, weighted with the singlet (^1F) and octet (^8F) DPDs, i.e.:

$$\Phi_{jj'kk'} = \frac{1}{N^2}\left(\delta_{jj'}\delta_{kk'}\,{}^1F + \frac{2N}{\sqrt{N^2-1}} t^A_{jj'} t^A_{kk'}\,{}^8F\right), \tag{4.48}$$

where t^A are the generators of the color algebra $SU(3)$, satisfying $[t^A, t^B] = if^{ABC}t_C$, with f_{ABC} structure constants. The structures which project the singlet and the octet out from Φ are respectively:

$$\delta_{j'j}\delta_{k'k}\Phi_{jj'kk'} = {}^1F, \quad \frac{2N}{\sqrt{N^2-1}} t^A_{j'j} t^A_{k'k}\Phi_{jj'kk'} = {}^8F. \tag{4.49}$$

Following the notation used for spin correlations in (4.12), one reads:

$$ {}^cF_{a_1a_2}(x_1, x_2, \boldsymbol{y}) = \tag{4.50}$$

$$\int \frac{dz_1^- dz_2^-}{(2\pi)^2} dy^-\, e^{ix_1 z_1^- P^+ + ix_2 z_2^- P^+} \left\langle P\right|{}^c\,\mathcal{O}_{a_1}(0,z_2)^c\mathcal{O}_{a_2}(y,z_1)\left|P\right\rangle \Big|_{\substack{z_1^+=z_2^+=y^+=0,\\ \boldsymbol{z}_{T1}=\boldsymbol{z}_{T2}=\boldsymbol{0}_T,}}, \tag{4.51}$$

where c is the label that indicates whether the selected part is the singlet ($c = 1$) or the octet ($c = 8$) and:

$${}^1\mathcal{O}_a(y,z) = \bar{q}_{j'}(y - \frac{1}{2}z)\delta_{jj'}q_j(y + \frac{1}{2}z), \tag{4.52}$$

$$^{8}\mathcal{O}_a(y,z) = \bar{q}_{j'}(y-\frac{1}{2}z)t^A_{jj'}q_j(y+\frac{1}{2}z). \tag{4.53}$$

When color singlets are produced in the hard process, the singlet (octect) representations from each hadron have to match to produce a color singlet final state. For a thorough study of color correlations and color effects in double parton scattering one can refer to [31,52,198,199] and references therein, where is shown that they are suppressed by Sudakov logarithms at high energy scales.

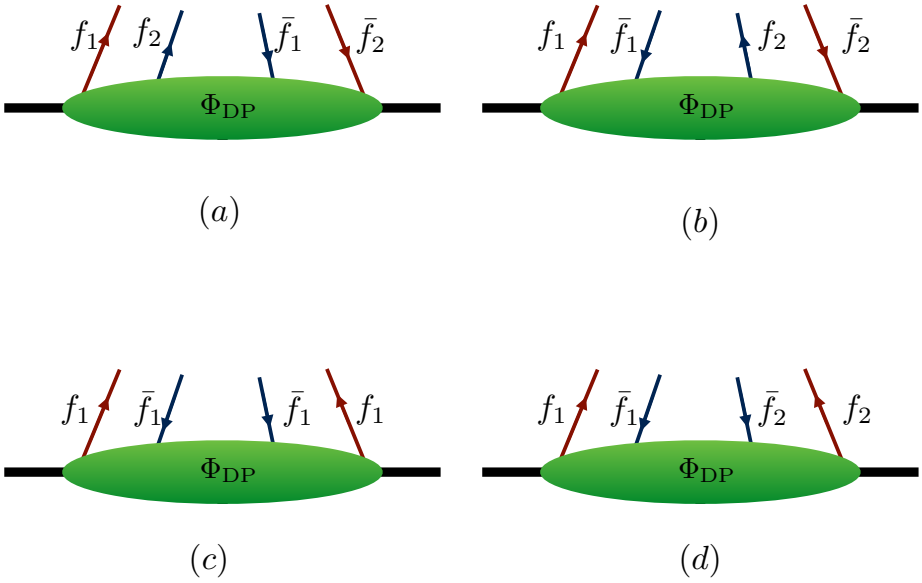

Figure 4.3: Flavor and fermion number interference diagrams. Diagrams in (a) and (b): flavor interference; diagram (c): fermion number interference; diagram (d): combination of both types.

The are other quantum numbers that one can consider: parton-type, fermion and flavor number. They can be responsible for interference diagrams [194,200]. The concept of quantum interference is remarkable and regards the fact that quantum numbers, such as the fermion and flavor number, have to be conserved globally (within the parton pair) in the amplitude and the conjugate one, but not necessarily along each parton leg. Interference terms of this sort would be forbidden in single parton

scattering because of quantum number violation. To summarize the situation one can look at Fig 4.3, where a variety of diagrams with interference terms are displayed. Flavor interference terms are those where two quarks of flavors f, f' in the amplitude are paired up with their conjugate partners with interchanged flavors. This kind of process does not bring any flavor number violation in DPS, and it is, therefore, a valid term in the correlator. The same holds with fermion number interference and parton-type interference (quark/gluons). The combined flavor- and fermion-number interference is also allowed, and it is shown in Fig. 4.3(d). Similarly to color correlations, they also become small at high energy scales due to the presence of the Sudakov factor [199].

Gluons

Double parton distribution involving one or two gluons have been defined and studied in [31, 32, 194, 201]. The case of double gluon distributions is quite analog to the case of quarks as far as the polarization correlations are concerned. Gluons have polarization states which can modify final-state distributions [201]. The starting point is the realization that both the hard part and the double gluon correlator $\Gamma^{ij,i'j'}$ are Lorentz tensors, whose indices are only transverse (i.e. $i, j, i', j' = 1, 2$). The decompositions are analog to (4.9), where the Lorentz basis is used instead of the Dirac one [31]. The relevant structures that select the gluon polarization are:

$$\Pi_g^{ij} = \delta^{ij}, \quad \Pi_{\Delta g}^{ij} = i\epsilon^{ij}, \quad \Pi_{\delta g}^{ij,kl} = \tau^{ij,kl}, \tag{4.54}$$

with:

$$\tau^{ij,kl} = \frac{1}{2}(\delta^{ik}\delta^{jl} + \delta^{il}\delta^{jk} - \delta^{ij}\delta^{kl}), \tag{4.55}$$

that is a symmetric traceless tensor. The three structures above select respectively unpolarized, circularly polarized and linearly polarized gluons. The DPDs are defined as in (4.12) with the operators defined as:

$$\mathcal{O}^{[\Pi_a]}(y, z) = \Pi_a^{ij} F^{+j}(y - \frac{1}{2}z_2)F^{+i}(y + \frac{1}{2}z_1). \tag{4.56}$$

Finally, a comment on the color correlations is in order. The case of two gluon DPDs, or one quark and one gluon DPD, is more complex than the one for two-quarks. In fact, many more representations arise when combining two color octets in the $8 \otimes 8$ representation (two gluons), or one color octet and a color singlet in the $8 \otimes 3$ representations (mixed gluon-quark distributions) [31, 194]. It is possible to establish positivity bounds for color DPDs [194] and study evolution effects. In [199] is showed

that color correlation is washed out by evolution in the quark case. Suppression of the same kind is expected to happen in the gluons, and the mixed quark-gluon sectors, even though the precise expression has not been studied.

4.4.3 Kinematic correlations

As previously mentioned, the factorized ansatz (4.7) has been used with success in the earliest attempts of measuring signals of DPS. Despite its limitations, there are motivations behind the existence and usage of this formula. They are based on the argument that, even though the product of single PDFs naively violates the DPS momentum sum rule for large-x, double parton scattering occurs in a region of small-x values which would be safely away from the thread. Early experimental results did not contradict this arguments, as the measurements of σ_{eff} were compatible with the x-independence statement over a quite wide range [173, 174].

On a theoretical ground, there are many reasons to discard the factorized ansatz. The first source of violation would be the effect of evolution. In fact, even if one assumes the factorized ansatz to hold at a specific energy scale, this cannot be preserved at any other scale due to double DGLAP (dDGLAP) evolution equations [202, 203].

The latter involve two independent evolutions, one for each parton[2] [31, 194]. For the unpolarized DPD it reads explicitly:

$$\begin{aligned}\frac{\partial f_{q_1q_2}(x_1,x_2,y;\mu)}{\partial \log \mu^2} = \frac{\alpha_s}{2\pi}\,[&P_{q_1q_1}\otimes_1 f_{q_1q_2} + P_{q_2q_2}\otimes_2 f_{q_1q_2} \\ &+ P_{q_1g}\otimes_1 f_{gq_2} + P_{q_2g}\otimes_1 f_{q_1g}]\,,\end{aligned} \tag{4.57}$$

where the convolution is defined as:

$$P_{ab}(\cdot)\otimes_1 f(\cdot,x_2,y;\mu) = \int_{x_1}^{1-x_2}\frac{du_1}{u_1}\left(\frac{x_1}{u_1}\right) f_{q_1q_2}(u_1,x_2,y;\mu), \tag{4.58}$$

and analogously for the $\otimes_2$. The splitting functions P_{ab} are the same as for the standard DGLAP equations. From the integral in (4.58) it follows immediately that the $x_1 - x_2$ kinematic correlation is present at any scale different from the initial one.

The second relevant problem regards the theoretical requirement of respecting sum rules. The issue was first studied in [161]. Even in lack of a first-principle procedure, the authors derive momentum and number sum rules, that are general enough and are

[2]There are subtleties related to the region of small $\boldsymbol{y}$ that also receives single parton-like of contributions. This problem can affect the evolution of multiparton distribution in a non trivial way, see, e.g., [159].

valid at all order. Accordingly, momentum sum rules for DPDs have to account for the fact that $x_1 + x_2$ cannot exceed 1, and that extracting a parton with momentum x reduces the probability of extracting the second parton with the same fraction of momentum. Also, extracting a parton with a certain flavor reduces the probability of extracting the second parton with the same flavor. In the factorized ansatz these requirements are violated, and the problem is circumvented with the argument that, at small values of x, the number of partons is high and the joint probabilities factorize. Since the factorized ansatz violates the sum rules, one needs to build new DPDs that respect them at all order and simultaneously preserve the advantage of using the single PDFs.

The authors of [161] proposed a phase-space factor that multiplies the product of single PDF at an initial energy scale and it reads[3]:

$$X_{\text{corr}}(x_1, x_2) = (1 - x_1 - x_2)^2 (1 - x_1)^{-2} (1 - x_2)^{-2}. \tag{4.59}$$

This choice accounts for momentum sum rule and valence quark number conservation, and ensures that they are preserved during evolution. The chosen input DPDs are built from single PDFs with modified MSTW2008lo distributions [204], multiplied by the phase factor (4.59) at an initial scale Q_0. Then the dDGLAP evolution up to a scale Q is implemented. This approach introduces a double source of longitudinal correlation: one that is due to the phase-space factor, and a further source that is introduced by the dDGLAP effect. The transverse part is still factored out and the kinematic correlations introduced are purely longitudinal. This is to say, the DPDs are the ones parametrizing the correlator as in the first part of (4.5), i.e. $\Phi(x_1, x_2, \boldsymbol{y}) \approx \Phi(x_1, x_2) G(\boldsymbol{y})$. We will analyze the effect of this type of correlations in the context of W^+W^+ production through DPS at the LHC. In addition, also polarization can be added and we will investigate the combined.

Transverse separation and longitudinal momenta

Assuming the absence of correlations between the longitudinal momenta and the parton separation is not realistic. It is reasonable to think that the partons inside the proton are subjected to an interplay between their momenta and the transverse separation, connected to the fact that they are confined to the proton [161]. Many model calculations (Bag model, constituent quark model, light-cone models) confirm that, in principle, the factorization between the longitudinal and the transverse part should

[3] An improved version of this factor has been proposed in the same work [161]. However, this will not be objective of our study.

not hold. The previous types of correlations we presented were purely longitudinal, so they regarded the first part of (4.5). On the other hand, the interplay between x and $\boldsymbol{y}$ is expressed by (4.4), by making use of single parton quantities. In particular, the picture according to which DPDs are generated from the product of GPDs can already suggest a nontrivial interplay between x and $\boldsymbol{y}$, in the very characteristic way known from the study of the GPDs [166, 205]. The fact that $\boldsymbol{y}$ is integrated over is a complication, because the dependence on $\boldsymbol{y}$ has to be indirectly inferred, and only consists in a numerical factor after integration. All longitudinal and longitudinal-transverse correlations reflect their presence on the fact that σ_{eff} must exhibit an x-dependence, but distinguishing the source of correlation would need much more extensive knowledge on the distributions.

To summarize, as a general strategy, since the shape and the magnitude of the DPDs is not known, the identifications of the different type of correlations should rely on a qualitative change in suitable quantities (such as final state distributions or asymmetries). Such variables should used to detect signs of correlations. The study presented in Section 4.5 aims at this goal. Ideally, an increasingly better knowledge of the distributions will allow for a proper evaluation of each type of correlations.

4.5 Polarization in same-sign W boson pair productions

The theory of double parton scattering is rich and can predict a large number of effects. Unfortunately, the suppressed nature (see Section 2.4.2) of most of double parton process makes it challenging to identify to which extent they are measurable in real experiments. One of the most promising processes to access double parton scattering is the production of a pair of W bosons of the same electric charge. This process was described in [206, 207] as a special case of the *double Drell-Yan* process. Its relevance has later been pointed out, for instance, in [32, 191], and recently the CMS collaboration has presented the first measurement of the cross section [180]. This is an example of a process where double parton scattering observables, both inclusive and less inclusive cross sections, are not suppressed compared to to the single parton scattering. In Fig. 4.4 one possible diagram for the production of two W bosons through single parton scattering process is depicted (left side), together with the correspondent DPS process (right side). The SPS diagram is of order $\alpha\alpha_s^2$ and implies the production, together with the lepton pair, of two high energetic quarks in the final state. This feature makes it possible to distinguish between the signature

of the two processes and to impose limits on the number of produced jets in order to suppress the contribution of the single parton scattering [180, 191]. The DPS signal also competes with other background processes which produce a muon pair and need to be taken into account.

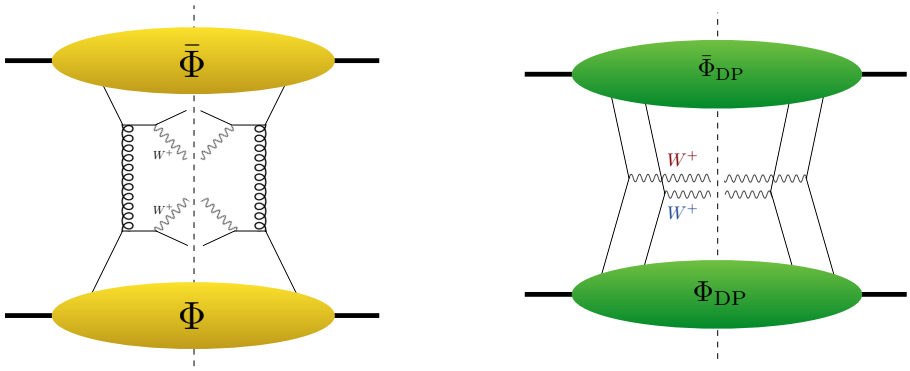

Figure 4.4: Pictorial representation of the production of two W^+ bosons. Part (a): SPS mechanism called $WWjj$ in the text; part (b): DPS process.

In this Section, we exploit the information on the production of two W^+ bosons through DPS to analyze different types of two-parton correlations inside the proton at the LHC. The primary focus is to study the effect of these interparton correlations at the level of the partonic cross sections, by modeling the DPDs at an initial low scale. Subsequently, we study the effect of correlations on final-state distributions, eventually adding the analysis of the relevant background processes. We identify two main observables (the distribution of the product of the muon rapidities and the asymmetry number, that will be defined later) that are a proxy of the presence of correlations.

4.5.1 Parton level result: cross section

Let us consider the process in which the two W^+ bosons are produced with positive charges. The signature of the process is the detection of two muons μ^+ (or electrons) in the final states as result of the leptonic decay of each W^+, and missing energy due to the invisibility of the neutrinos. Quarks exclusively initiate the DPS process, and we study the tree-level results from quark-antiquark annihilation for the flavors

u, d, c, s. Each hard process is then of the kind:

$$q\bar{q} \to W^+ + X \to \mu^+\nu_\mu + X. \tag{4.60}$$

We assume factorization between the hard part and the correlators in every correlation scenario that we present. The starting point is the investigation of polarization effects. The cross section for double W^+ production (integrated over the transverse momenta of the bosons) can be calculated from (4.20). In this special case, only the unpolarized (f_{qq}) and longitudinally polarized ($f_{\Delta q \Delta q}$) distributions for quarks and antiquarks enter the cross section. The transverse quark polarization does not contribute since this is given by the operator that corresponds to a chirality flip for the quark in the amplitude and the conjugate one, and this is prevented by the impossibility for a right-handed (left-handed) quark (antiquark) to couple to the W^+. The expression of the polarized cross section can already be found in [32], expressed in the rest frame of the W boson. Starting from this, we obtain an equivalent expression for the cross section in the laboratory frame, fully differential in the transverse momenta of the muons and rapidities of the muons and neutrinos.

$$\begin{aligned}
\frac{d\sigma}{\prod_{i=1}^{2} d\eta'_{\mu_i} dk_{Ti}{}^2 d\eta'_{\nu_i}} &= \left(\frac{4\pi}{s}\right)^2 \frac{1}{C} \sum_{q_1 q_2 q_3 q_4} K_{q_1\bar{q}_3} K_{q_2\bar{q}_4} \\
&\times \Big\{ \left(\omega_1^- \omega_2^-\right)^2 \int d^2\boldsymbol{y} (f_{q_1 q_2} + f_{\Delta q_1 \Delta q_2})(\bar{f}_{\bar{q}_3\bar{q}_4} + \bar{f}_{\Delta\bar{q}_3\Delta\bar{q}_4}) \\
&\quad + \left(\omega_1^- \omega_2^+\right)^2 \int d^2\boldsymbol{y} (f_{q_1\bar{q}_4} - f_{\Delta q_1 \Delta\bar{q}_4})(\bar{f}_{\bar{q}_3 q_2} - \bar{f}_{\Delta\bar{q}_3\Delta q_2}) \\
&\quad + \left(\omega_1^+ \omega_2^-\right)^2 \int d^2\boldsymbol{y} (f_{\bar{q}_3 q_2} - f_{\Delta\bar{q}_3\Delta q_2})(\bar{f}_{q_1\bar{q}_4} - \bar{f}_{\Delta q_1\Delta\bar{q}_4}) \\
&\quad + \left(\omega_2^+ \omega_2^+\right)^2 \int d^2\boldsymbol{y} (f_{\bar{q}_3\bar{q}_4} + f_{\Delta\bar{q}_3\Delta\bar{q}_4})(\bar{f}_{q_1 q_2} + \bar{f}_{\Delta q_1\Delta q_2}) \Big\} \\
&\quad + \{\text{flavor interference}\},
\end{aligned} \tag{4.61}$$

where $\omega_i^\pm = 1 \pm \tanh\left(\frac{1}{2}(\eta'_{\mu_i} - \eta'_{\nu_i})\right)$. The quantities η'_{μ_i} and η'_{ν_i} are the pseudorapidities of the produced leptons (muons and neutrinos). The superscript "prime" indicates that η' is the transformed quantity of the pseudorapidity η after a boost from the rest frame of the W boson to the laboratory frame. We recall the definition of the pseudorapidity, namely:

$$\eta = -\ln\tan\left(\frac{\theta_{\rm cm}}{2}\right), \tag{4.62}$$

where $\theta_{\rm cm}$ is the polar angle between the lepton plane and the z-direction, measured in the W boson rest frame. From this moment onwards, we will refer to the muon pseudorapidity in the laboratory reference simply as rapidity, and we drop the superscript from all the variables.

The k_{T_i} are the muons transverse momenta, C is the symmetry factor which is set to 2 because of the indistinguishability of the two particles in the final state and $\sqrt{s}$ is the center of mass energy. The fractions of longitudinal momenta x_i, $\bar{x}_i$ read:

$$x_i = \frac{k_T}{\sqrt{s}}(e^{\eta_{\mu_i}} + e^{\eta_{\nu_i}}); \quad \bar{x}_i = \frac{k_T}{\sqrt{s}}(e^{-\eta_{\mu_i}} + e^{-\eta_{\nu_i}}), \tag{4.63}$$

and the arguments of the distributions read $f(x_1, x_2, \boldsymbol{y}; Q)$ and $\bar{f}(\bar{x}_1, \bar{x}_2, \boldsymbol{y}; Q)$, where Q will be set to the W^+ boson mass for both hard processes. We notice that the inclusion of the longitudinally polarized distributions contributes to the change both in magnitude and shape of the final state distributions. The cross section formula (4.61) is useful for applications once it is fed with different input DPDs at an arbitrary scale Q. In particular, given a form for the DPDs at an initial energy scale Q_0 we implement (un)polarized double DGLAP evolution equations to obtain the results at a higher scale Q, which is typically equal to the mass of the produced particle. Unless otherwise specified, the dependence of the functions on the final scale Q will be understood.

Since the leptons are the result of the decay of a W boson with mass M and width Γ_W, we introduce the factors $K_{q_i\bar{q}_j}$ given by:

$$K_{q_i\bar{q}_j} = \frac{\alpha^2}{4N_c}\frac{|V_{q_iq_j}|^2}{(2\sin\theta_w)^4}\frac{q_i^2}{(q_i^2 - m_W^2)^2 + m_W^2\Gamma_W^2}, \quad (e_{q_i} - e_{q_j} = 1), \tag{4.64}$$

where $N_c = 3$ is the number of colors, $V_{q_iq_j}$ a CKM matrix element, θ_w the weak mixing angle, α the electromagnetic fine structure constant and e_{q_i} the charge of quark q_i. The relevant elements in the CKM matrix are V_{ud}, V_{ub}, V_{cd}, V_{cs}, V_{cb} [208]. Finally, by exploiting eq. (4.63) and the relation $q_i^2 = x_i\bar{x}_i s$ in Section 2.4.1, one has:

$$q_i^2 = 2k_T^2[1 + \cosh(\eta_{\mu_i} - \eta_{\nu_i})]. \tag{4.65}$$

If $\Gamma \ll M$ we can use the narrow-width approximation (NWA), i.e. the limit in which W is on the mass-shell:

$$\frac{1}{\pi}\lim_{\Gamma\to 0}\frac{m\Gamma}{(q_i^2 - m_W^2)^2 + m_W^2\Gamma_W^2} = \delta(q_i^2 - m_W^2). \tag{4.66}$$

The (4.64) becomes:

$$K_{q_i\bar{q}_j}^{NWA} \approx \frac{\alpha^2}{4N_c} \frac{|V_{q_iq_j}|^2}{(2\sin\theta_w)^4} \frac{\pi q_i^2}{m_W\Gamma} \delta(q_i^2 - m_W^2). \tag{4.67}$$

When useful, we will make use of this approximation in the following.

4.5.2 Spin and kinematic correlations

In order to study how correlations affect the cross section calculations, we implement different model-based scenario for the DPDs at the initial scale. These different DPDs are supposed to encode the correlations and are used as input to the cross section formula (4.61). In the first part of this analysis, we will calculate the interaction of pointlike partons extracted from the proton (this is what we will call parton level results). The evolution equations account for gluon radiation that is absorbed in the definition of the DPDs. Other initial state radiations, that are the main contributions to be added when interested in the final-state distributions, will be considered in Section 4.5.3. The parton level results on the differential cross sections will then be recalculated after accounting for initial and final state radiations and compared to background processes, whose signatures are the same of, or can be misinterpreted as, the leptonic decay of two W^+.

The type of correlations under investigations are shortly described. While presenting the four main DPD models used for studying correlations we also include the case where correlations are absent.

No correlation

The input DPDs are defined as the product of single PDFs at any scale, that is:

$$f(x_1, x_2, \boldsymbol{y}; Q) = f(x_1; Q) f(x_2; Q) G(\boldsymbol{y}), \tag{4.68}$$

with $\int d^2\boldsymbol{y} G(\boldsymbol{y}) = \sigma_{\text{eff}}^{-1}$. If the two hard processes are independent, the single PDFs evolve separately under unpolarized single DGLAP evolution equation. The factorized form (4.69) is then valid across all energy scales, and the (separate) evolution of the two single PDFs does not create correlations.

Minimal correlation

The input DPDs are defined as the product of single PDFs at the initial scale, that is:

$$f(x_1, x_2, \boldsymbol{y}; Q_0) = f(x_1; Q_0) f(x_2; Q_0) G(\boldsymbol{y}). \tag{4.69}$$

The eq. (4.69) implies that all kind of correlations are set to zero at the initial scale. As a first step, a minimal source of correlation is introduced by the use of the double DGLAP evolution equations. The longitudinal correlations arise at higher scales as the result of evolution. In fact, even if the form (4.69) holds at the initial scale, evolution creates correlation between x_i, and the factorized form is no longer valid. We will call this scenario "minimally correlated" and the cross section $\sigma_{\text{min-corr}}$ is given by (4.61) in which the polarized distributions are set to zero.

Polarization

The cross section σ_{pol} is the expression (4.61) in which, in addition to the unpolarized distributions, we include polarization in the max-scenario, i.e. the polarized distributions individually saturate the positivity bound (4.43) and equal the unpolarized ones at the initial scale [166, 209]. The factorized form (4.69) is still valid but only at the initial scale, while at higher scales the polarized double DGLAP evolution equation introduces the correlations as previously described. One has:

$$f_{\Delta q \Delta q}(x_1, x_2, \boldsymbol{y}; Q_0) = f_{qq}(x_1, x_2, \boldsymbol{y}; Q_0) = f(x_1; Q_0) f(x_2; Q_0) G(\boldsymbol{y}). \tag{4.70}$$

Kinematic correlations

Longitudinal kinematical correlations are explicitly introduced. The product of single PDFs used as initial ansatz is corrected by the x_i-dependent factor in (4.59), to account for the kinematical constraint of double parton scattering as explained in [161]. The factorized form (4.69) is no longer valid at the initial scale:

$$f(x_1, x_2, \boldsymbol{y}; Q_0) = f(x_1; Q_0) f(x_2; Q_0) X_{\text{corr}}(x_1, x_2) G(\boldsymbol{y}), \tag{4.71}$$

with $\int d^2\boldsymbol{y} G(\boldsymbol{y}) = \sigma_{\text{eff}}^{-1}$ and $X_{\text{corr}}(x_1, x_2)$ is defined in (4.59). Longitudinal correlations are present at the initial scale thanks to the factor explicitly introduced, and they travel towards smaller momentum fractions during evolution. The cross section $\sigma_{\text{x-corr}}$ is given by (4.61) without any polarized distributions.

Polarization and kinematic correlations

This scenario assembles all the above mentioned correlations: we include the polarized distributions on top of the ansatz (4.71) and we evolve them up to the final scale with the polarized dDGLAP evolution equations. The cross section $\sigma_{\text{x-corr pol}}$ is given by the full expression of (4.61).

Except for the total cross section results, we will not, in general, include the "no correlation" scenario in our results, obtained by neglecting all correlations between the two partons inside each proton. One should bear in mind that imposing separately $x_1 < 1$ and $x_2 < 1$ does not ensure $x_1 + x_2 < 1$, as required in the case of two partons coming from the same parent hadron. However, in the kinematical region we are interested in, the routine for numerical integration Vegas does not significantly enter the unphysical region (in the context of NWA the latter is an exact statement).

The scenario with no correlation differs from a theoretical viewpoint from the minimal correlated one. In practice, the correction introduced by the use of unpolarized double DGLAP evolution rather than two DGLAP evolution kernels are minimal, such that the minimally correlated scenario is equivalent to the uncorrelated one at this level of accuracy of our results.

Let us specify the relevant quantities that will be used in this study. As previously mentioned, we first address the calculation of the inclusive cross section, using the different inputs for the DPDs outlined above. We set the initial scale $Q_0 = 1\,\text{GeV}$ and implement double DGLAP evolution (unpolarized and polarized) to a final scale $Q = m_W$ [31]. The single parton PDFs used are the leading-order MSTW2008lo distributions [204]. The choice of the initial scale Q_0 and the specific PDF set used can, in principle, have an effect on the parton level and final-state results. This aspect is currently under investigation, but it will not be discussed further in this thesis. The numerical integration is performed with the Vegas routine within the Cuba Library [210]. The results are obtained either through fully numerical integration with Vegas or employing a combination of Vegas and analytical integrations using the NWA. We will specify each time when the NWA approximation is used. Throughout the rest of this Chapter we fix the value of σ_{eff} (4.6) and the CM energy $\sqrt{s}$ as follows:

$$\sigma_{\text{eff}} = 15\,\text{mb}, \qquad \sqrt{s} = 13\,\text{TeV}. \tag{4.72}$$

We define the relevant ratios, that will be used in the following, each time with the obvious substitutions:

$$R_S = \frac{\text{[Polarization]}}{\text{[Minimal correlation]}}, \quad R_I = \frac{\text{[No correlations]}}{\text{[Minimal correlation]}}, \tag{4.73}$$

$$R_X = \frac{\text{[Polarization x-correlation]}}{\text{[x-correlation]}}, \quad R_{XS} = \frac{\text{[x-correlation]}}{\text{[Minimal correlation]}}[1pt] \tag{4.74}$$

Unless otherwise specified, all the parton level results of this Section are calculated using the following cuts on the variables ("zeroth selection"):

$$4\,\text{GeV} \leq k_{T_i} \leq 45.5\,\text{GeV}, \quad |\eta_{\mu_i}| \leq 3.3, \quad |\eta_{\nu_i}| \leq 10. \tag{4.75}$$

The neutrino rapidity range is chosen such that in essence no cuts are imposed. This implies that, for intervals $|\eta_\nu| \leq \eta_\nu^{\max}$ with $\eta_\nu^{\max} \geq 10$, all our parton level results are independent on $\eta_\nu^{\max}$. Similarly, the constraint $k_{T_i} \leq 45.5\,\text{GeV}$ does not produce any change in the results, because the amount of the cross section that would be included by extending further the upper value for k_T is negligible. The range of η_μ is chosen wider than the experimental acceptance typical of the LHC and it will be tightened later on to match the detector ranges. This selection of values serves as starting point for the study of final-state distributions in Section 4.5.3.

We now turn to the presentation and discussion of the numerical results. In the second column of Table 4.2 we summarize all the results for the total cross section, for all correlation types including $\sigma_{\text{no-corr}}$. We observe that the presence of polarization increases the cross section with respect to the unpolarized case, while the x-dependent factor (which is always smaller than 1) is responsible for its decrease.

The results for less inclusive quantities are now in turn, in order to examine to which extent these quantities are sensitive to the DPS correlations effects. At this stage we can still label the muons as μ_1 and μ_2, implying that they originate from the first and second hard interactions. They are equivalent, as we do not assume any hierarchy in magnitude between the hard scales. However, in the real analysis of the data on final muons, there is in no longer knowledge about the origin of the lepton pairs, as discussed in Section 4.5.3.

With numerical integrations, we calculate the cross section differential in the rapidity and transverse momentum of the muon. The results are shown in Fig. 4.5. The muon k_T-distributions in Fig. 4.5(b) are all peaked around $k_T^{\text{peak}} \in [39.72, 40.75]$ GeV, i.e.around the value $k_T = m_W/2$. The cross section value, for all the curves, decreases of nearly two orders of magnitude from the value at the peak and $k_{T\max} = 45$ GeV, which indicates that the interval of transverse momenta in (4.75) only excludes negligible portion of cross section. A different situation is represented in Fig. 4.5(a).

	cross section [fb]	Asymmetry
$\sigma_{\text{no-corr}}$	1.77	0.00
$\sigma_{\text{min-corr}}$	1.74	0.00
σ_{pol}	1.90	-0.05
$\sigma_{\text{x-corr}}$	1.37	0.01
$\sigma_{\text{x-corr Pol}}$	1.48	-0.03
$R_S = \frac{\sigma_{\text{pol}}}{\sigma_{\text{min-corr}}}$	1.09	-
$R_I = \frac{\sigma_{\text{no-corr}}}{\sigma_{\text{min-corr}}}$	1.02	-
$R_X = \frac{\sigma_{\text{x-corr pol}}}{\sigma_{\text{x-corr}}}$	1.07	-
$R_{XS} = \frac{\sigma_{\text{x-corr}}}{\sigma_{\text{min-corr}}}$	0.78	-

Table 4.2: Results for the full cross sections and asymmetry values (4.77) in the different four DPDs scenarios as described in the text, with cuts as in (4.75). The cross section values and relevant ratios (4.73) are shown in the second column. All the values of the table are obtained by numerical integration performed with Cuba Library [210]. We made no use of NWA for these results. The third column contain the values of the asymmetry parameter (4.77) calculated with NWA.

The muon rapidity range selected in (4.75) leaves out a non negligible portion of the total (theoretical) cross section. The distribution is symmetric under $\eta_{\mu_i} \to -\eta_{\mu_i}$ for all the correlations, as expected upon noticing that the cross section formula (4.61) is invariant under the exchange of $\eta \to -\eta$. The maximum values of the cross section are reached at $\eta_{\mu_1} \in [1.8, 2.1]$. For all curves, the cross section decreases both towards central and peripheral values of the rapidity interval. At the bottom part of the panels we also include the ratio as defined in (4.74). The ratios $R_{\{S,X,XS\}}(k_T)$ and $R_{\{S,X,XS\}}(\eta_\mu)$, as defined in (4.73), are displayed over the entire range of k_T and η_μ. From the ratios we notice that for these two observables, there is a hardly visible shape difference between the different correlations.

By employing a combination of Vegas and NWA, we calculate the cross section differential in the sum and absolute value of the difference of the muon rapidities. They are displyed in Fig 4.6, considering once more the four different scenarios and

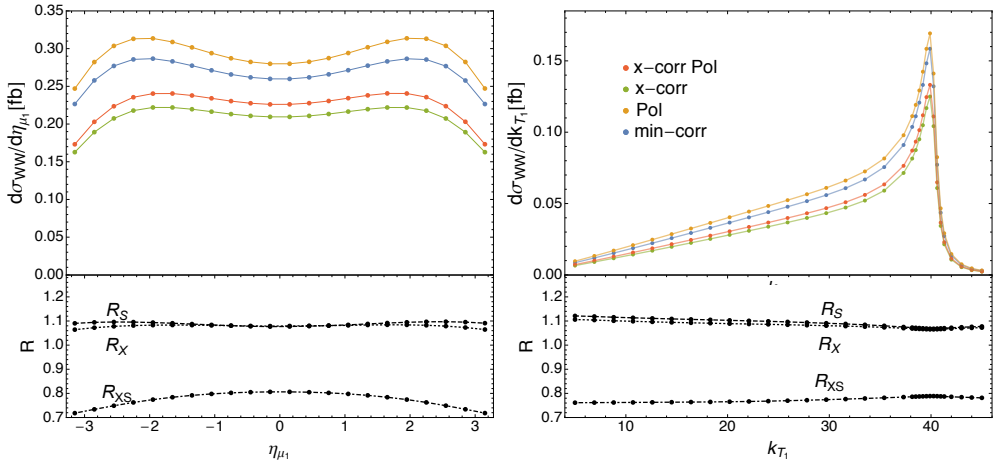

Figure 4.5: Results for the rapidity (left panel), transverse momentum (right panel) profiles of the muon, and relevant ratios as in (4.73), with cuts as in (4.75). The results are obtained by numerical integration performed with Cuba Library [210] with no use of the NWA. The four different scenarios and the definition of the ratios are as described in the text.

the relevant ratios. Both panels of the figure show symmetric curves, reaching the maximum at zero value of the sum (Fig 4.6(a)) and difference (Fig 4.6(b)) of muon rapidities. The cross section differential with respect to the rapidity difference $(\eta_{\mu_1} - \eta_{\mu_2})$ is not observable experimentally and such a difference of rapidity can only be defined theoretically. Therefore, we shall rather consider the absolute value of the difference $|\eta_{\mu_1} - \eta_{\mu_2}|$. However, since the information about the origin of muons is lost in real experiment, one should define different criteria for labeling the detected muons and constructing an analogous observable to Fig 4.6(b), as discussed in Section 4.5.3.

Thus far, the distributions we presented are not manifestly changed by the presence of correlations. In practice, these observables are not ideal for discriminating the change of shape related to polarization and longitudinal correlations.

A very promising observable we want to draw attention to is the cross section differential in the the rapidity product:

$$\frac{d\sigma}{d(\eta_{\mu_1} \times \eta_{\mu_2})}. \tag{4.76}$$

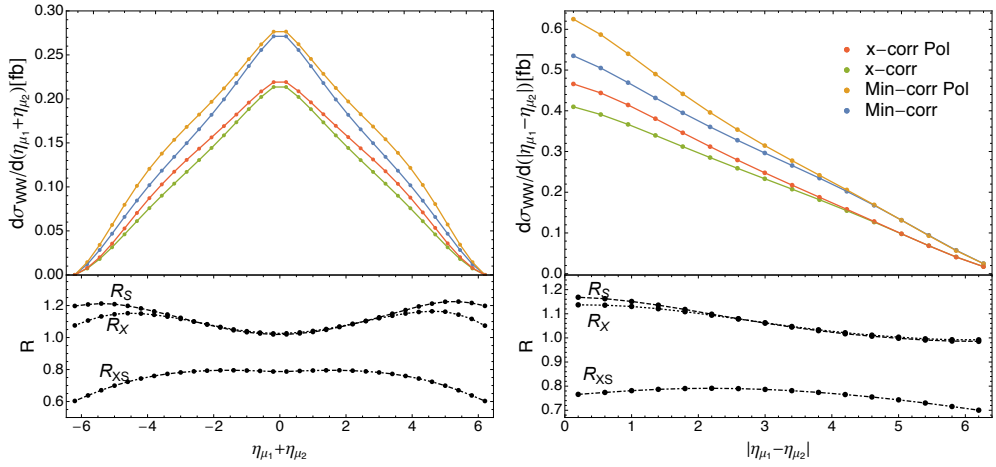

(a) (b)

Figure 4.6: Summary plots for the difference (left), sum (right) of muon rapidities, and relevant ratios as in (4.73), with cuts as in (4.75). Plots (a) and (b) contain the comparison between the four scenarios as defined in the text. The results are obtained by using the NWA.

This quantity gives the probability that the final state muons are detected in the same or different hemisphere. The amount of cross section correspondent to the region where the muons are detected in the same hemisphere ($\eta_{\mu_1} \times \eta_{\mu_2} > 0$) equals the cross section for the muons detected in the opposite one ($\eta_{\mu_1} \times \eta_{\mu_2} < 0$) in absence of any correlations. We stress that this is a very convenient observable to look at correlations, because any deviation from this symmetric picture is a footprint of correlations. In particular, generalizing the definition of [191] for all kind of correlations under study, we define the asymmetry:

$$A = \frac{\sigma(\eta_{\mu_1} \times \eta_{\mu_2} < 0) - \sigma(\eta_{\mu_1} \times \eta_{\mu_2} > 0)}{\sigma(\eta_{\mu_1} \times \eta_{\mu_2} < 0) + \sigma(\eta_{\mu_1} \times \eta_{\mu_2} > 0)}. \tag{4.77}$$

Its value must be exactly zero when the partonic cross section is calculated in the fully uncorrelated scenario. A non-zero value represents the unbalance in the direction of muons detected (same/opposite hemisphere) occurring in any scenario when correlation effects are included, as shown in Fig. 4.7.

The Fig. 4.7 shows the observable in (4.76) calculated with the four different input

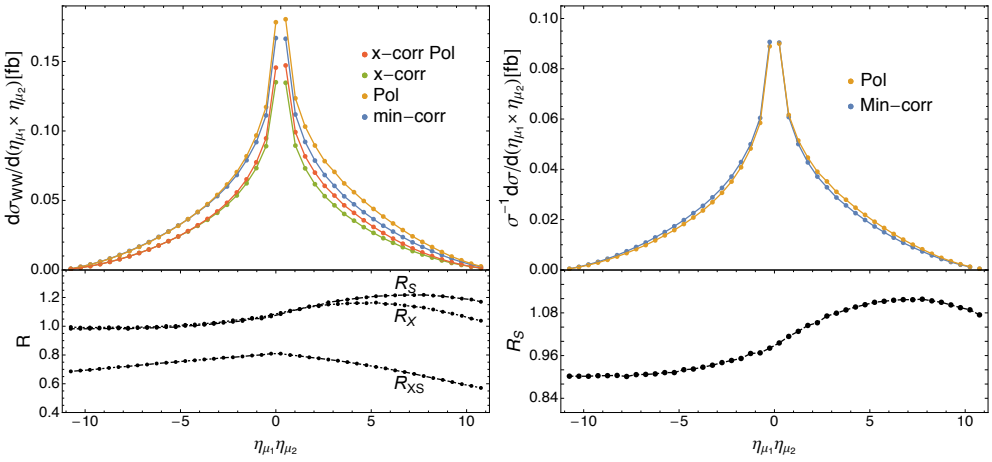

Figure 4.7: Cross section differential in the product of muon rapidities for the different types of correlations, and relevant ratios as defined in (4.73), with cuts as in (4.75). (a): comparison between the four scenarios as described in the text and relevant ratios R_S, R_X, R_{XS}; (b): comparison between the normalized cross section in the minimally correlated case and the polarization case in the max scenario.

for the DPDs that contain correlations. The distribution is symmetric, as expected, in the minimal correlated case (blue line) which plays the role of a truly uncorrelated case, while it loses its symmetry when including the polarized and kinematic correlated terms (orange, red, and green lines). In particular, the "amount" of cross section appears to be shifted towards the positive value of the product for all scenario, i.e., the two muons would prefer to travel towards the detector along the same direction rather than opposite directions. The Fig. 4.8 displays the same situation in the $\eta_1 - \eta_2$ plane. The plot (a) is symmetric with respect to the origin, while the others are distorted. In the polarized cases (b) and (d), there is a clear pattern showing the increase of the cross section in the quadrants 1 and 4 (same hemisphere). In the unpolarized x-dependent case this shift does not occur in the same way, although a small distortion from the symmetric pattern is also visible.

The asymmetry values are listed in the third column of Table 4.2. The values vary from zero, which are the effectively uncorrelated scenario, to values different from zero, which refer to the correlated situations. In all polarized cases, the asymmetry number

migrates towards negative values, corresponding to an increase of the amount of cross section of two muons in the same hemisphere. The longitudinal correlations exhibit an asymmetry different from zero even in the absence of polarization, as expected. However, the distortion occurs in the opposite direction (i.e., towards positive values). In the next Section 4.5.3 we show how much this situation changes as effects of the initial and final state radiations and when the background is included.

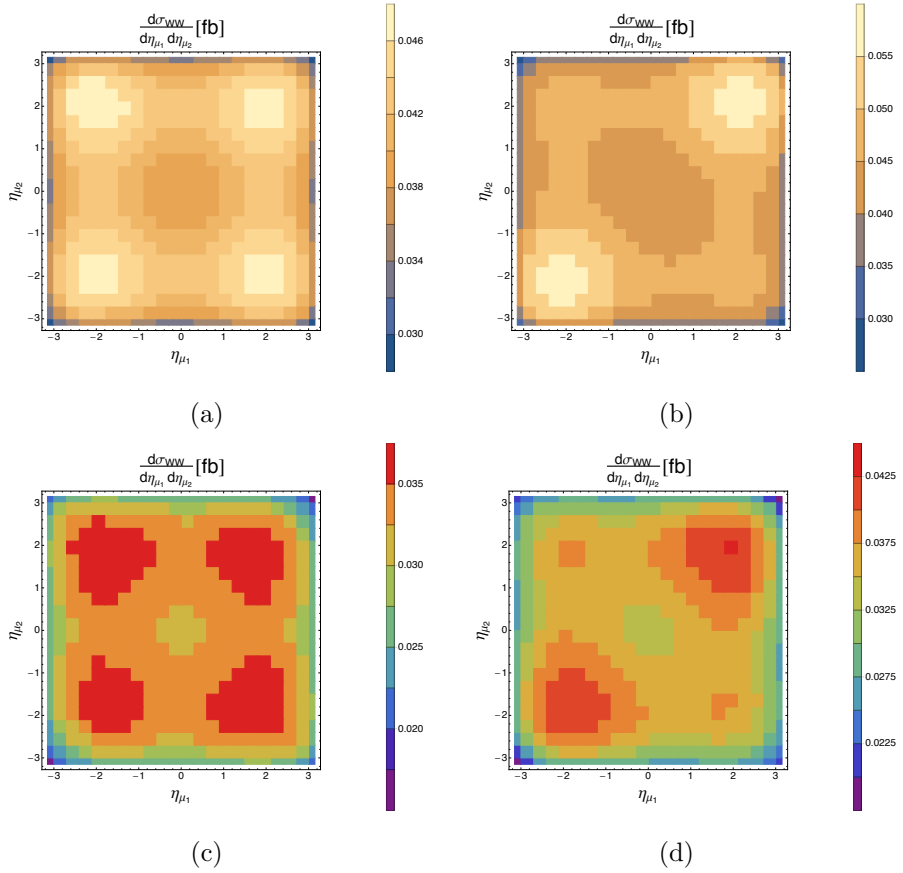

Figure 4.8: Density plots for the cross section as a function of muon rapidities, with cuts as in (4.75). Different correlations are displayed: (a) minimal correlation; (b) polarization; (c) x correlation; (d) polarization x correlation.

4.5.3 Final-state analysis

With the parton level results at hand, we now turn into the analysis at the hadron level, which mainly corresponds to initial state radiations for the W boson production. The ultimate aim is the identification of the kinematic region where the signal process is measurable and enhanced compared to the background processes. In essence, one needs to distinguish the same-sign muon pair originated in DPS by the two W^+ boson decays from the same-sign muons that make up (part of) the signature of other processes in pp collisions. To suppress these unwanted contributions one needs information on the underlying event (UE) surrounding the actual process.

In this Section, we discuss how to embed the results on correlations presented in Section 4.5.2 into the study of the final-state particle distributions. We use general-purpose Monte Carlo generators of pp collisions, namely Herwig 7 and Pythia 8 [211, 212], and we show a selection of preliminary results on this type of analysis. The results of this section and the previous section will be presented in a more definitive form in [213].

Signal process

The first part of the final-state study is performed by using the Monte-Carlo event generator Herwig 7.1.2 (in the following called H7) [211]. The Herwig program produces the full information on proton-proton collisions at the hadron level, providing the four-momenta of all particles in the final state (FS). In particular, it generates the elementary hard scatterings (matrix element – ME), parton showers for initial- and final- state QCD radiations (ISR and FSR), heavy object decays, and hadronization processes.

Herwig is in principle fully capable of generating double W production events. However, in its default setting, it is not tailored to produce entirely independent hard scatterings (more details will be given later and in [213]). Our method for preparing the hadron level event datasets is based on a re-weighting procedure. We initially calculate the partonic cross section differential in four variables (k_{T_1}, k_{T_2}, η_{μ_1}, η_{μ_2}) using the different DPDs and the integration methods as explained in Section 4.5.2. We chose 495616 ($32 \times 32 \times 22 \times 22$) points in the phase space region (4.75) with unequal spacing. The same four times differential cross section is then obtained from the event generator using the same grid of points and the outputs are compared. The advantage of using the Herwig program is the possibility of accessing the information about the outgoing partons directly from the matrix element (ME) before the hard matrix element correction is applied on their momenta. We, therefore, change the

weights (equal to one by default in the Herwig generation) of the DPS WW events into *new* weights according to our results for the cross section. We repeat the same procedure for all type of correlations.

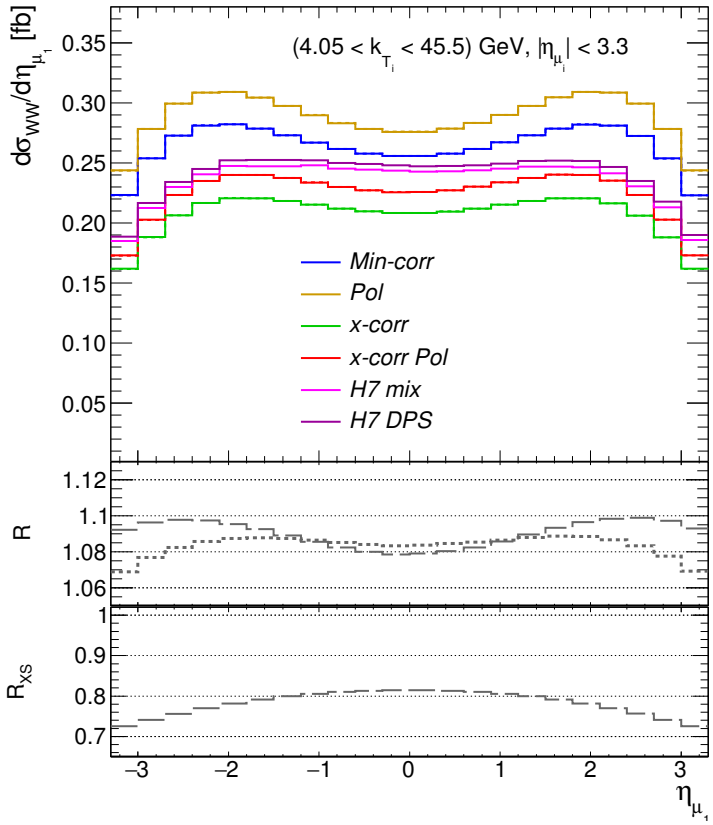

Figure 4.9: Comparison between the calculated distributions (dashed lines, same as in Fig. 4.5(a)) and the reweighted distributions from Herwig generator at ME level (solid lines) with cuts as in (4.75). These distributions are identical so the dashed lines are not visible. The two lines in the middle (pink and purple) represent the two types of Herwig events (explained in the text). Ratio plots at the bottom of the panel, with R: R_S (dashed line), R_X (dotted)

After the reweighting process, the distributions generated by Herwig at the ME level are identical to the ones we have calculated in Section 4.5.2, as shown in Fig. 4.9, where the two types of distributions are compared in each correlation scenario. Solid lines represent the Herwig results after the reweighting procedure, while the results

of the distributions calculated in Section 4.5.2 are included with dashed lines (not visible in the plot). The distributions are identical and the curves overlap (see e.g. Fig. 4.5 (a)for comparison). This validates the procedure of reweighting, which has been found sufficient and fully reliable. The hadron level distributions that we obtain from the reweighted generator, produce FS as we had showers and hadronizations directly from the *new* parton events.

Two additional solid lines are included in Fig. 4.9, that serve as a comparison between the results generated by Herwig before and after the reweighting procedure. As previously mentioned, the Herwig generator can in principle be used to generate this type of DPS events (resulting in fact in the independent production of two W^+). However, an event is discarded when it violates momentum conservation. This event veto effectively modifies the distributions, producing a difference between the first and second production of W^+, although the generation tries to prepare them independently at first. These results are indicated as "H7 DPS" in Fig. 4.9. This dataset is eventually compared to a random combination of two single W events together (line labeled as "H7 mix"). The solid lines for H7 DPS and H7 mix are very similar and differ only in normalization, as mixed events are more likely not to pass the phase space cuts (4.75)

To demonstrate the quantitative effect of the generator correction, i.e. the differences between parton and final-state distributions, we first have to reduce the phase-space with respect to (4.75). The larger zeroth selection is needed because the momenta of the leptons (and partons from UE) are modified during the generation process, so the values of the rapidities and transverse momenta can migrate out of or into the new phase space. However, we need to define an experimentally accessible region, which correspond to a narrower interval of rapidity (e.g. ATLAS and CMS experiments have their tracker acceptance within $|\eta| < 2.5$). At this stage we keep the transverse momenta as low as possible to demonstrate the gradual effect of the phase space restriction on the studied distributions. The following "first selection" is considered:

$$k_{T_i} \geq 5\,\mathrm{GeV}, \quad |\eta_{\mu_i}| \leq 2.5, \quad |\eta_{\nu_i}| \leq 10. \tag{4.78}$$

The Table 4.3 summarizes the total cross sections and asymmetry values for all four types of correlations. We can observe a 40% decrease in the cross section with respect to zeroth selection due to the significant reduction of rapidity range (see Fig. 4.5(a) for comparison).

Fig. 4.10 shows the results for the transverse momentum and rapidity profile, obtained from sharpening the cuts from (4.75) to (4.78). The left-side panels corresponds to ME level events while the right-panels show the effect of the full event generator (FS

	cross section [fb]	ME Asymmetry	FS Asymmetry
$\sigma_{\text{min\_corr}}$	1.06	0.00	0.00
σ_{pol}	1.15	-0.04	-0.04
$\sigma_{\text{x\_corr}}$	0.85	0.00	0.00
$\sigma_{\text{x\_corr\_pol}}$	0.92	-0.03	-0.03

Table 4.3: Results for the full cross section and asymmetry values in the different four DPDs scenarios as described in the text, with cuts as in (4.78). The third and fourth columns contain the values of the asymmetry in the different scenarios before (ME) and after (FS) the parton showers from Herwig.

level) [4]. The ratios R_S, R_X and R_{XS} are also displayed. We can observe a significant smearing of the sharp transverse momenta peak, and small statistical fluctuations in the rapidity distributions.

In Fig. 4.11 we show the cross section as a function of the sum (a), absolute difference (b), and product (c)-(d) of final-state muon rapidities. The cuts in (4.78) are responsible, at the ME level, both for the decrease of the total cross section and for the change in the asymmetry values (4.77) (see Table 4.3, in comparison to Table 4.2). In general, we observe that the distortions introduced by correlations, quantitatively indicated by the asymmetry values in Table 4.2, are not washed out by the effects of the parton showers. In particular, in the presence of polarization correlations, the muons would be more probably detected in the same rather than the opposite hemisphere, and this remains true also when the FS distributions are considered. In Fig. 4.11(c) one can observe more closely the ratio $R_S(\eta_{\mu_1}\eta_{\mu_2})$ between uncorrelated and polarized distribution. It is shown in Fig. 4.11(c) that there is a clear change in the shape of the distribution towards positive values of $\eta_{\mu_1} \times \eta_{\mu_2}$ in the presence of correlations.

An additional promising observable to look at is the slope of the $\eta_{\mu_1} \times \eta_{\mu_2}$ distribution. As will be explained while discussing the background, an advantage related to this variable is that selecting the events corresponding to having both muons in the opposite hemispheres of the detector can help to distinguish the correlated DPS scenarios from the background processes. We postpone this discussion to the appropriate next Section.

[4] These data samples contain around 2 millions of events, a number that allows to illustrate the results as smooth functions. The real measured distributions will only have few thousands of events.

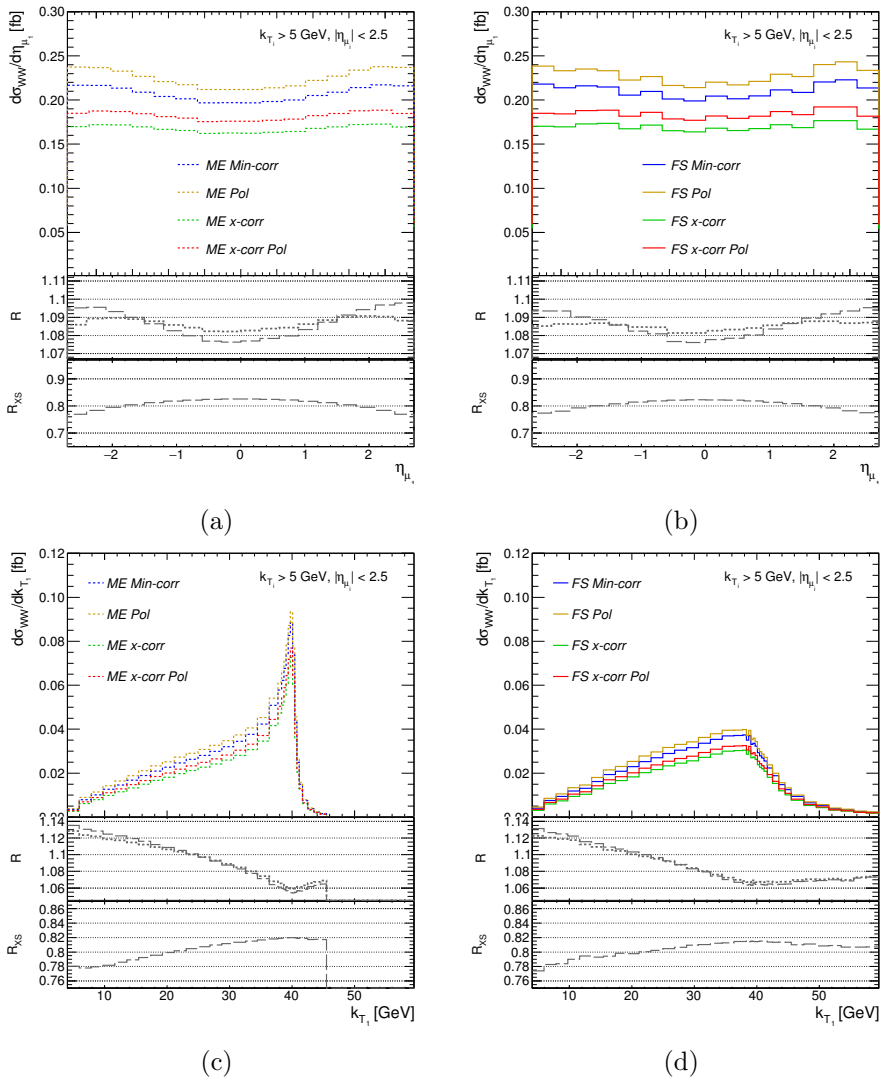

Figure 4.10: Transverse momentum and rapidity profile at the ME level events (left-side panels) and after the effect of the full event generator (FS level), with phase space selection (4.78) in all correlation scenarios. Ratio plots at the bottom of each panel, with R: R_S (dashed line), R_X (dotted). Top left: rapidity profile of the muon at the level of ME . Top right: rapidity profile of the muon at the FS level with selection (4.78). Bottom left: Transverse momentum of the muon at the level of ME with selection (4.78). All the four scenario of correlations are displayed and relevant ratios. Bottom right: transverse momentum profile at the FS level with selection (4.78) .

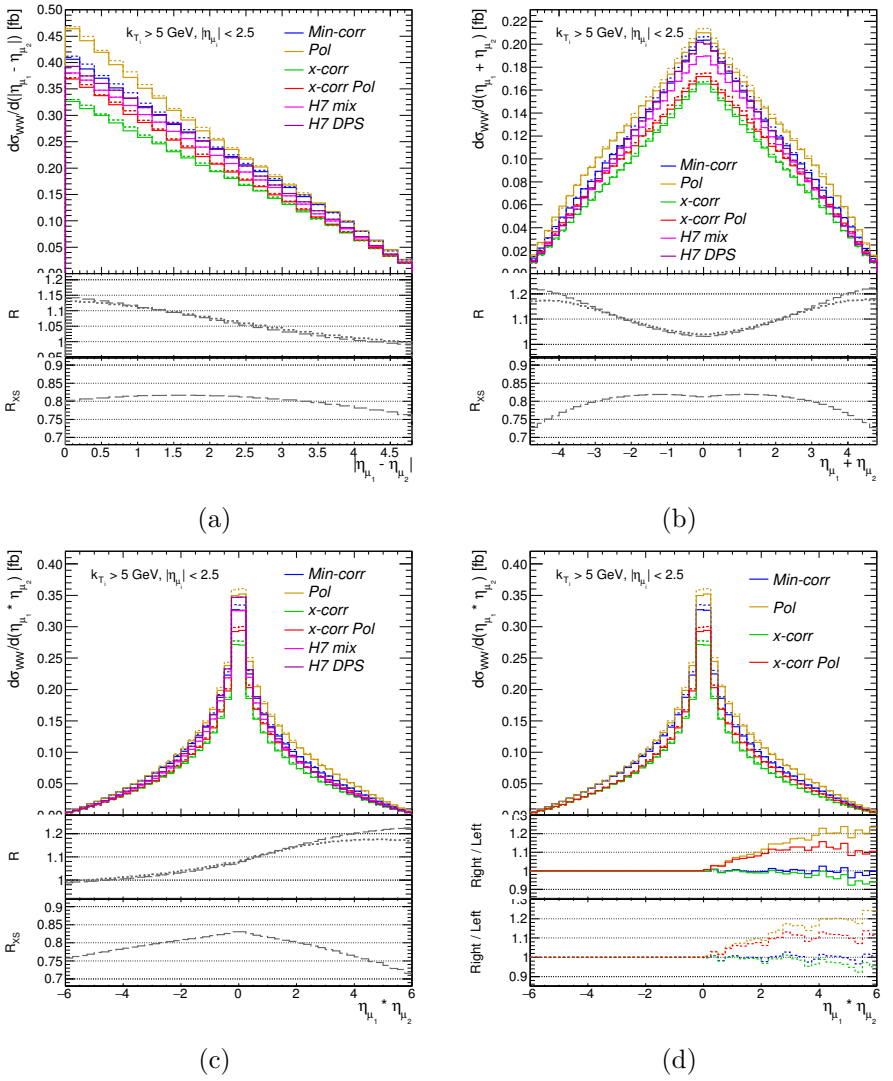

Figure 4.11: Final-state distributions with phase-space cuts as in (4.78) in all correlation scenarios. Ratio plots at the bottom of panels (a),(b), and (c), with R: R_S (dashed line), R_X (dotted). Left/right asymmetry is displayed at the bottom in panel(d). Top left: FS distribution of the absolute value of the difference of muon rapidities. Top right: distribution of the sum of muon rapidities. Left bottom: FS distribution of the product of rapidities. Bottom right: FS distribution of the product of rapidities and left/right asymmetry at the bottom.

Finally, to gain a better intuition about the modifications introduced by initial- and final-state radiations, we display in Fig. 4.12 the results for the cross section double differential in the muon rapidities. These figures are related to the previous Fig. 4.8. Thanks to the reweighting procedure, the ME level results (which we do not show for semplicity), corresponding to the FS results shown in Fig. 4.12, are the same as the ones in Fig. 4.8 but with the reduced phase-space. We observe that, both at the ME and the FS level, passing from the uncorrelated to the correlated cases always causes a drift towards an asymmetric pattern.

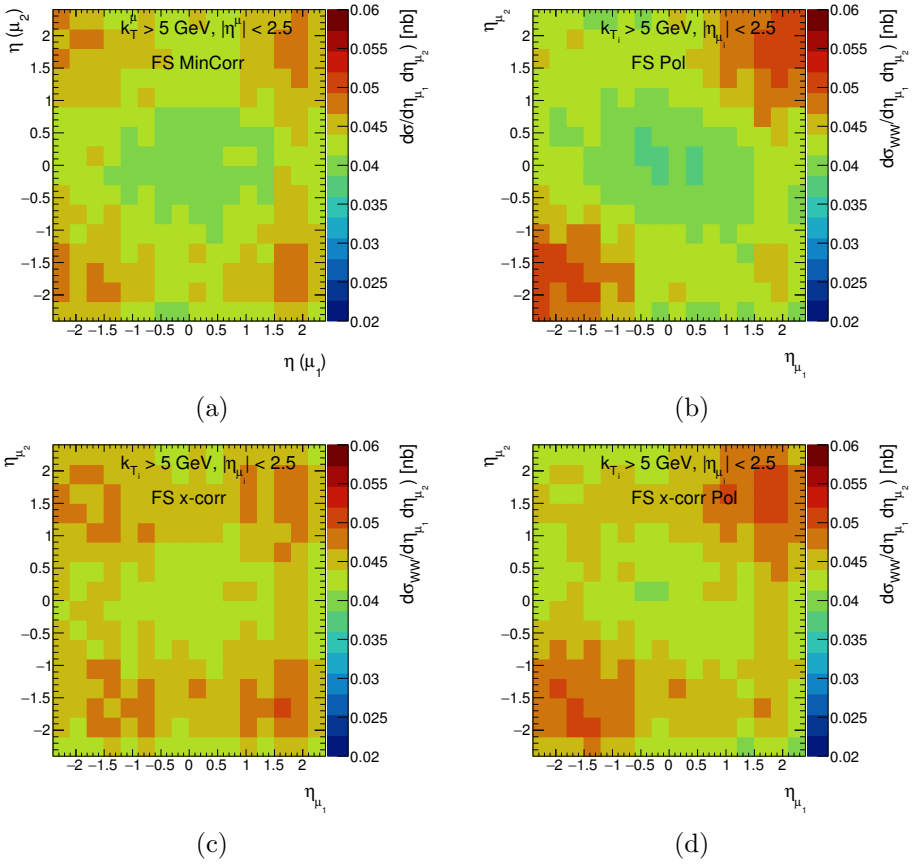

Figure 4.12: FS results for the cross section double differential in η_{μ_1} and η_{μ_2}, with selection (4.78). Different correlation scenario: (a) minimal correlatation, (b) polarization, (c)x-correlation, and (d)x-correlation polarization .

A clarification on the different ways of collecting muons is in order. Thus far, the muons are still distinguishable and can be labeled as μ_1 and μ_2, implying that they are originated from the first or second interaction respectively. They are equivalent, i.e., give rise to identical distributions upon interchange $\mu_1 \leftrightarrow \mu_2$. This is true both at the ME and FS level. In reality, there is no possibility of distinguishing the two muons. Therefore, a second type of muon collection can be created. The two hardest muons among the final states are selected every time, and marked as *leading* and *subleading*, μ_{lead} μ_{sub}. We will need to switch to this type of muon collection technique for the analysis of the background events.

Background processes

We now turn into the analysis of the processes whose signature contains a pair of muons, which constitute the relevant background for the double W production in DPS. The ultimate goal will be to find the ideal selection of cuts and the best theoretical framework that will allow for the measurement of the two-parton correlations in DPS, in the future era of LHC. The results we now present are in a preliminary form, and therefore they will serve as an illustration of the current stage of the analysis, rather than as concluding results. Therefore we point to an upcoming work [213] for the complete discussion of the final results.

The major contributions to the background of a same-sign muon-pair production come from SPS processes such as:

- Heavy flavor production, represented by the (dominant) $t\bar{t}$ process. In this process, one lepton is generated in the first top decay and another lepton, with the same sign, arises from a bottom quark emitted by the other top quark. Since we aim to remove these type of events as much as possible, there is no real need to go through all possible flavors, as the top quark has the largest chance to produce a muon.
- Diboson production. The SPS processes producing a pair of gauge bosons are the most direct background processes. We distinguish three types of processes: ZZ, WZ and WW. The latter is strongly suppressed by the presence of two additional strong vertices at the lowest order diagram and we mark it as $WWjj$ process. We note that Z stands for both Z boson and virtual photon.
- Single Drell-Yan. It belongs to a class of background processes in which the muon charge is mis-measured. We do not provide any quantitative prediction for this background and assume it negligible.

As previously mentioned, we stress that the parton level cuts for the event generation were chosen wide enough to allow the secure reduction of the final state phase space restriction. For simplicity, in comparison with the background processes, we only show the FS level results of the minimally correlated scenario. We use the PDF set MSTW2008 and a combination of the Monte-Carlo event generators Herwig and Pythia. For the diboson process also MadGraph5_aMC@NLO is used [214].

The production of a pair of W-boson with the same electric charge in DPS has been measured for the first time by the CMS collaboration very recently in [180]. Accordingly, in the hunt for the optimal event selection, we will try to preserve the CMS definitions as much as possible. In the second column of Table 4.4 we show the value of the cross section for the signal (DPS WW) calculated with the cuts in 4.78, and the initial cross section values for the background processes ($WWjj$, WZ, ZZ, and $t\bar{t}$). The complete set of cuts used for a first look at the background data is labeled as "second selection" (these are CMS-based):

$$\begin{aligned} &|\eta_{\mu_i}| < 2.4, \quad k_T^{\mu_{\rm lead}} > 20\,{\rm GeV} \quad k_T^{\mu_{\rm sub}} > 20\,{\rm GeV}, \\ &k_T^{\mu_3} < 5\,{\rm GeV}, \quad \not{E}_T > 20\,{\rm GeV}, \quad dR(\eta_{\mu_i}, \phi_i) > 0.1, \end{aligned} \tag{4.79}$$

where $\not{E}_T$ is the missing energy in the transverse plane due to the presence of the elusive neutrinos, and dR is the distance of the two muons in the plane formed by their rapidities η_{μ_i} and the azimuthal scattering angles ϕ_i (see, e.g., [208]). The constraint on dR is imposed in order to prevent the muons to be too close to each other. The effect of the above selection is shown in the third columns of Table 4.4 and Fig. 4.13. In the former, the values for the cross section are displayed. We mention that the veto to the third muon transverse momentum particularly reduce the WZ decay and almost completely removes ZZ events. The situation is sketched in the two upper panels of Fig. 4.13, where the distribution of the muon transverse momenta (leading muon in panel (a) and subleading muon in panel (b)) are plotted for all the processes. We include the ratio R defined as:

$$R = \frac{[\text{Total (Background + DPS signal)}]}{[\text{Background}]}. \tag{4.80}$$

Jet vetoes can further constrain the $WWjj$ and $t\bar{t}$ contributions, i.e., a constraint on the maximal allowed k_T value for jets is imposed. In the lower part of Fig. 4.13 (panel (c) and (d)) the transverse momentum distribution of the first two leading jets is represented. A value of k_T lower than 25 GeV is applied on the second leading

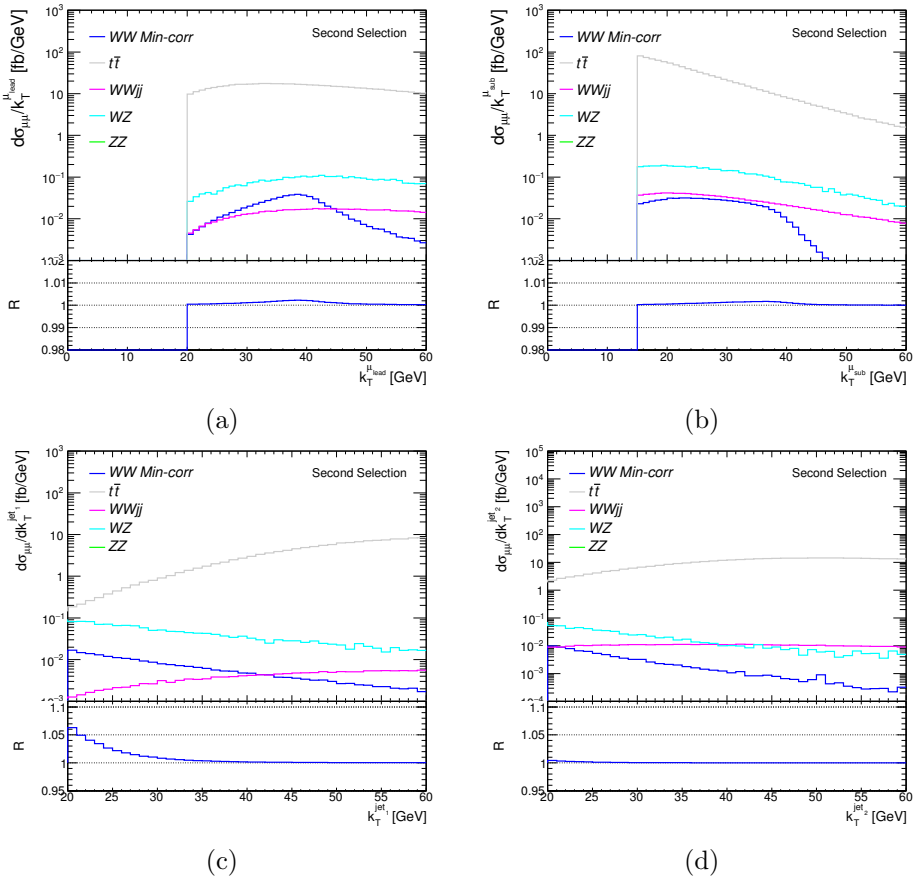

Figure 4.13: Results for the distributions of the transverse momenta of the muons and the jets calculated with cuts as in (4.79), for the signal and background processes (with different colors in the plot). Ratio plots at the bottom show the comparison between the total (background + signal) and the background processes. From top to bottom: (a) leading muon, (b) subleading muon, (c) first leading jet, and (d) second leading jet

jet (jet_2) to suppress the most significant part of $WWjj$ events and another relevant portion of $t\bar{t}$ events. The cut on jet_1 is instead left less strict and a maximum value of 50 GeV is chosen. Moreover, in the seek for an active suppression of the $t\bar{t}$ background, a widely used procedure is the reconstruction of b-jets, i.e., jets containing hadrons deriving from the fragmentation of b-quarks (see, for instance [215, 216] and [213] for the extra information on the adopted procedure and efficiency). The assumed

		2nd selection	3rd selection	final selection
DPS WW	1.06	0.67	0.48	0.11
$WWjj$	2.32	1.30	0.03	0.00
WZ	148.2	4.93	1.77	0.08
ZZ	59.1	0.00	0.00	0.00
$t\bar{t}$	3.6×10^6	939.	2.51	0.08

Table 4.4: Cross section values in fb for the DPS signal and the relevant background processes described in the text. The results of each column are calculated with phase space cuts. Columns from left to right: type of process; cross section values in the first generation of backgrounds ($WWjj$, WZ, ZZ, $t\bar{t}$) and for signal DPS WW with selection (4.78); cross section value for the second selection (4.79); cross section value for the third selection (4.81); cross section value for the and "temporarily" final selection (4.82)

efficiency of the b-jet tagging procedure is: 75% for $k_T^{\rm jet} \in [25-30]$ GeV, 80% for $k_T^{\rm jet} \in [30-40]$ GeV, and 85% for $k_T^{\rm jet} \in [40-50]$ GeV [213].

Another basic part of the selection is to restrict the allowed transverse momenta of muons to a smaller window. We can see in Fig 4.13 that the DPS signal is well located around 38 GeV (25 GeV) for a leading muon (sub-leading muon). Gathering together the above considerations, we define the "third selection" as follows:

$$\begin{aligned} &|\eta_{\mu_i}| < 2.4, \quad 25\,\text{GeV} < k_T^{\mu_{\rm lead}} < 50\,\text{GeV}, \quad 15\,\text{GeV} < k_T^{\mu_{\rm sub}} < 40\,\text{GeV}, \\ &k_T^{\mu_3} < 5\,\text{GeV}, \quad \not{E}_T > 20\,\text{GeV}, \quad dR(\eta_\mu, \phi_\mu) > 0.1, \\ &k_T^{\rm jet_1} < 50\,\text{GeV}, \quad k_T^{\rm jet_2} < 25\,\text{GeV} \quad + \quad \text{jet b-tagging}. \end{aligned} \tag{4.81}$$

The results on the cross section are reported in the fourth column of Table 4.4, where the successful suppression of the $WWjj$ background is apparent. On the other hand, we notice that both $t\bar{t}$ and WZ backgrounds are still dominant with respect to the signal.

The optimal strategy to eventually achieve the suppression is still under investigation. We outline a possible direction and temporarily call it "final selection". Generally speaking, the $t\bar{t}$ process might be reduced below the signal by imposing veto cuts on charged particle multiplicities (tracks). This step has to be considered very carefully from a theoretical point of view because selecting particles introduces a theoretical uncertainty that we have not estimated. However, in the current stage, the checks performed on how much this procedure affects the signal and the background show that

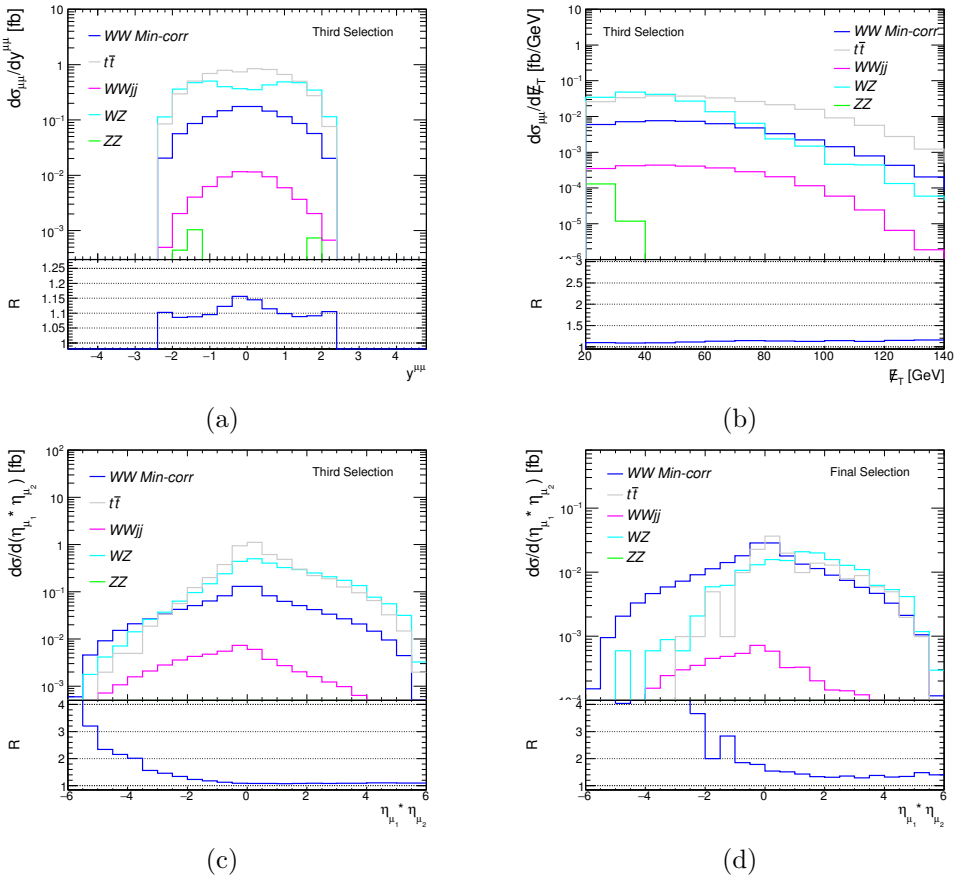

Figure 4.14: Comparison between results obtained with the phase space cuts as in (4.81) (upper panels) and (4.82) (lower panels) for all processes. Ratio as defined in (4.80) is displayed. Panel (a) distribution of the rapidity of the muon pair with third selection (4.81), panel (b) missing transverse energy with cuts (4.81). Panels (c) and (d): product of rapidities for the third selection (4.81) and final selection (4.82), respectively.

the signal is not significantly affected, while the $t\bar{t}$ process is massively reduced [213]. The theoretical validity of the track selection procedure remains to be understood. We present the results obtained by vetoes on the track transverse momentum of 1, 5, and 15 GeV, even though future investigations are needed.

The suppression of the WZ process remains complex because its signature is very close to the signal one. In Fig 4.14 we show two possibilities that can be explored.

The upper left panel shows the rapidity of muon pair and on the right we display the missing transverse energy. In practice, one could for instance attempt to impose cuts on the rapidity of the combined muon system, or require a minimal transverse energy. We explore the latter possibility and define a temporarily "final selection". This contains, in addition to (4.81), the above mentioned selection of tracks and the requirement of minimal transverse energy. Namely:

$$(4.81) \quad + \quad \text{track selection} \quad + \quad \not{E}_T > 70\,\text{GeV}. \tag{4.82}$$

We observe that the background suppression is remarkable compared to the third selection (see the last column of Table 4.4), and the signal process represents the prominent value, as desired. To further underline the improvement produced by the final choices (4.82), we display in the lower panels of Fig. 4.14 the rapidity product distributions for the third selection (left) and the final selection (right). We notice that the selection (4.82) works well for negative values of $\eta_{\mu_1} \times \eta_{\mu_2}$, where the suppression of background is more satisfactory.

Final results and promising directions

Fig. 4.15 contains the final results for the FS product and the difference of muon rapidities, in all four correlation scenarios including background, using the final selection (4.82). An outstanding signal of correlation is still missing, as reported in Table 4.5. Discriminating any variations in the asymmetry values is probably of hard experimental reach at the present stage of our study.

Fig. 4.14 (d) shows that the remaining background is manifestly asymmetric towards the positive values of the rapidity product. Because of this, the asymmetry value will be primarily determined by the non-DPS background rather than the DPS

	σ [fb]	Asymmetry (Total)	Asymmetry (DPS only)
Min-corr	0.105	-0.307	0.003
Pol	0.112	-0.314	-0.033
x-corr	0.092	-0.329	0.005
x-cor Pol	0.086	-0.333	-0.028

Table 4.5: Results for the cross section and asymmetry values for the DPS process in the four different correlation scenarios. The results are calculated with the final selection (4.82) to appropriately suppress background as outlined in the text.

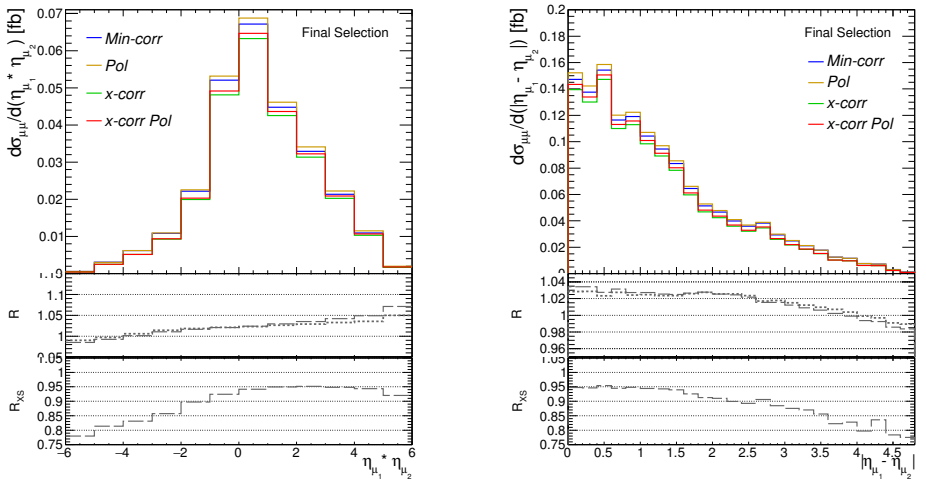

(a) (b)

Figure 4.15: Final results for the FS distributions for all correlation scenarios, using the final selection (4.82), and relevant ratios, with R: R_S (dashed line), R_X (dotted), as defined in (4.74). Left-side panel: DPS cross section differential with respect to the product of rapidities of the muon. Right-side panel: cross section differential with respect to the absolute value of the difference of muon rapidities

signal and will be shifted towards large negative values, as shown in Fig. 4.15(a) and Table 4.5. This is the main reason to argue that measuring the slope of the distribution is in principle a valuable alternative, as the signal entirely dominates the measurement for only negative values of $\eta_{\mu_1} \times \eta_{\mu_2}$. A measurement of the slope consists of counting the total number of events (signal plus background) of muons going to the opposite hemisphere. Such a measurement would demand a great accuracy in the modeling of the signal and background processes, and the main sources of theoretical uncertainties should be carefully evaluated. These considerations are still open and under investigation.

As a concluding remark, we discuss the strategy under investigation to obtain a decisive improvement on the background suppression, and we outline a possible new scenario on spin correlations that can be measured at the LHC. If we resume our analysis after the third selection (4.81), we are left with two prominent background processes: WZ and $t\bar{t}$ production. In order to avoid to perform the track selection,

one can rather use the theoretical calculations combined with data-driven methods to efficiently suppress these processes. The fact that the WZ process is relatively well understood from the theoretical point of view makes it possible to assume that this contribution can be effectively subtracted, leaving a theoretical uncertainty to be added to the signal. Not as simple as the WZ is the case of the $t\bar{t}$ process, for which the status of the theoretical calculations is not as good. In this case, one can adopt methods of muon isolations which are proven to be extremely efficient in separating the prompt muons from the muons produced by meson decays [217]. In this ideal background-free situation, a remaining question would be whether one can push the theoretical assumptions further in order to create a scenario where correlations are detectable. Within what is allowed by the positivity bounds, we can build new longitudinally polarized DPDs that still saturate the bound (4.43) but with difference signs, depending on the type of parton entering the distributions (two quarks, two antiquarks or a mixture of quark-antiquark). By modifying the sign of the polarized distributions at the initial scale as will be explained in [213] we observe an increase of the absolute value of the asymmetry up to the capabilities of the LHC (in our preliminary investigations we could observe an increase of about 3-4 times compared to the numbers in Table 4.2). This direction is promising and the new scenario on spin correlations could be tested through the asymmetry measurement quite directly.

4.6 Discussion and conclusions

We conclude the Chapter with a brief summary and some comments.

The concept of double parton scattering has been attracting theoretical and experimental interest for several years. It is a generalization of the single parton scatterings that potentially creates a very rich phenomenology. In fact, extending the description from a single to a double parton description is a unique opportunity to grasp the structure of the hadrons with nonstandard (multipartonic) eyes. In particular, one can study, in a complementary framework, a bigger number (and different in nature) of correlations, especially in comparison to standard single parton PDFs. The addition of extra degrees of freedom is practically similar, even though conceptually very different, to the extension of the description from the collinear to the transverse space: the presence of the transverse momenta is crucial to introduce quantum and kinematical correlations that are responsible for the manifestation of fundamental properties of QCD: color entanglement, gauge invariance, and universality. The theory of DPS is in this sense younger, even though several of the single parton theory concepts have been developed and are becoming part of the DPS theory as well (such as TMD and

collinear factorization, QCD evolution, description of universality). In addition, very peculiar of DPS is the concept of quantum interference and correlations.

In this Chapter, we have discussed two-parton correlations, a type of correlation that is already included in the double parton correlator from its very first definition. The spin correlation of two partons, also in an unpolarized proton, is a particularly interesting type of correlation. In fact, it is the only correlation which gives a direct (calculable in the hard part of the cross section) effect on the distributions of final states. The other types of correlations are responsible for the interplay between the kinematic variables x_i in a way that is not exactly specified. Since the dependence of the unpolarized DPDs on x_i and $\boldsymbol{y}$ separately is also currently unknown, the predictions are to be taken with care.

We have presented a study of the production of same-sign W-boson pair production in presence of correlations. The analysis has been carried out on the partonic and final-state level, including the relevant background processes. We also identify the key observables that would allow the discrimination of correlations in DPS. The results on the final-state distributions including background are presented, although in a preliminary form. The optimal phase-space portion that would need to be used to detect correlations is still under examination, and a definitive response on the feasibility of measuring correlations in DPS has not been determined. Nevertheless, theoretical and experimental improvements are currently under investigations.

Chapter 5

Quarks in unpolarized targets in AdS/QCD correspondence

5.1 Introduction

In this Chapter, we introduce the main features of the AdS/QCD correspondence, where "AdS" stands for anti-de Sitter space. Through this approach, we derive the LFWFs of mesons and employ it to the study of the pion structure. The pion was theoretically predicted by Yukawa in 1935 [218] as the mediator of the short-range nuclear force, and it was observed experimentally for the first time in 1947 [219]. Across the decades, formidable developments have been achieved in the theory of the strong force. Nowadays the pion has been recognized as having a crucial role in many aspects of the standard model and in the study of QCD and confinement. It is the Goldstone boson of the chiral symmetry breaking, a mechanism which is responsible for dynamically creating most of the visible mass of the universe [220, 221]. On the other hand, it is the simplest hadron in nature: it is the lightest QCD bound state, made up of u and d valence (anti)quarks, and its spin is zero. Thus, no target spin degrees of freedom enter the description.

These complementary pictures emerge when we study different properties of the pion's interior, such as elastic and transition electromagnetic form factors (see e.g. [222–

226]), distribution amplitude (see e.g. [227, 228]), PDFs (see e.g. [229–232]), GPDs (see e.g. [233–239]), TMDs (see e.g. [62,240,241]), and Fragmentation Functions (see, e.g., [242–245]). The comparison with experiment is crucial to draw definitive conclusions, and the experiments planned at JLab 12 [246], and the new mesonic Drell-Yan measurements at modern facilities [247, 248] can provide valuable information.

Since there are no spin states available in the target, a big simplification arises in the description of the distribution functions. Focusing on the quark TMDs at leading-twist, only two functions are involved: the unpolarized f_1 and the Boer-Mulders $h_1^\perp$. However, the absence of experimental information on the TMD structure of the pion prevents us from a direct comparison between theory and experiments, conferring an exploratory connotation to this study.

The internal structure of the pion, as well as other hadrons, can be studied by using different approaches, such as constituent quark models (see e.g. [62, 240]), covariant models and Schwinger-Dyson equations [221, 249], lattice QCD methods [34, 54, 56], and the formulation of the AdS/QCD correspondence [250]. We investigate the opportunities offered by the latter, as being an appealing approach from the theoretical point of view.

The AdS/QCD correspondence in the form of the light-front holography was formulated in 2006 by Brodsky and de Teramond [251, 252]. It has a number of features that will be briefly reviewed in Section 5.2.1. Among those, there is the capability of providing an expression for the LFWF of the valence state of the mesons. As shown later in the Chapter, it has a very simple form and, in its original version, only one free parameter. In essence, very little modification is needed in order to employ it in a phenomenological study. We aim to study quark TMDs in this framework, and discuss some aspects that arise from the transition from the nonperturbative nature of the AdS/QCD description and the perturbative regions.

5.2 Meson LFWF from AdS/QCD

In this Section, we first review the main properties of the LFWFs and we show that the knowledge of such quantities is important in the seek of a unifying framework to describe simultaneously hadronic and partonic observables, since quantities such as TMDs, PDFs, and electromagnetic form factors, can be written as overlap of LFWFs.

With these concepts at hand, we can turn to the actual use of the LFWF for the pion derived in the AdS/QCD correspondence.

In the context of QCD, LFWFs are not known and not calculable perturbatively. They have for example been constructed within the framework of light-front con-

stituent quark models [59,253–256] and used in the calculations of TMDs, GPDs, and GTMDs. As we shall see shortly, the AdS/QCD approach provides an expression for the meson LFWFs directly. The limitation is that the complexity of the hadron spin structure remains unexplored, as the LFWFs has a very simple, spin-independent form. We thus continue this dissertation by looking more closely at unpolarized quantities. On the other hand, this offers the opportunity to look simultaneously at many observable within a unified formalism.

LFWFs overlap representation

The observables under investigation in this Chapter are the electromagnetic form factor, the valence quark PDF and the TMD of the pion. Electromagnetic form factors are measurable quantities in elastic processes. Those processes are quite different from the ones we have been dealing with so far, at least in their much less energetic nature. In fact, a very moderate Q^2 value is needed to investigate the electromagnetic property of the hadrons without resolving the partonic nature (the data on the pion form factor that will be analyzed have a maximum value smaller than $Q^2 \sim 10$ GeV^2).

In terms of operators, the form factors parametrize a non-forward matrix element containing a local current operator, i.e. $\langle P| J^\mu(0) |P'\rangle$. The kinematic is space-like and the virtual photon of momentum q^μ can be chosen such that $q^+ = 0$, with $Q^2 = -q^2$. This choice is useful because in LF quantization, where plus momenta cannot be negative, only processes with the same number of initial and final particles are allowed. The relevant component of the current is the plus component $J^+(0) = \sum_q e_q \bar{\psi}_q(0) \gamma^+ \psi_q(0)$, where e_q is the electric charge of the constituent. This is the only contribution because it contains the good components of the fields, while J^- contains bad components and it is not a one-body contribution. For a spin-1/2 hadron the parametrization of the transition matrix element reads:

$$\langle P', \Lambda'| J^+(0) |P, \Lambda\rangle = \bar{u}_{LF}(P', \Lambda') \left[F_1\left(Q^2\right) \gamma^+ + F_2\left(Q^2\right) \frac{i}{2M} \sigma^{+\alpha} q_\alpha \right] u_{LF}(P, \Lambda), \tag{5.1}$$

where $u_{LF}(\bar{u}_{LF})$ are the LF Dirac spinors as in Appendix A. The form factors F_1 and F_2 are called Dirac and Pauli form factors respectively, and they are a measure of the electric and magnetic charge distributions in the hadron. The hadron initial and final momenta are chosen as [257]:

$$P = \left(P^+, P^-, \boldsymbol{P}_T\right) = \left(P^+, \frac{M^2}{2P^+}, \mathbf{0}_T\right), \tag{5.2}$$

$$P' = \left(P'^{+}, P'^{-}, \boldsymbol{P}'_{T}\right) = \left(P^{+}, \frac{M^2 + \boldsymbol{q}_T^2}{2P^{+}}, \boldsymbol{q}_T\right), \tag{5.3}$$

$$q = \left(q^{+}, q^{-}, \boldsymbol{q}_T\right) = (0, 0, \boldsymbol{q}_T)\,. \tag{5.4}$$

We can write the form factors of eq. (5.1) in terms of helicity conserving and helicity flip amplitudes as follows:

$$F_1\left(Q^2\right) = \langle P+q,\, +| \frac{J^{+}(0)}{2P^{+}} |P,\, +\rangle = \frac{1}{2P^{+}} \mathcal{F}_{++}, \tag{5.5}$$

$$-\left(q^1 - iq^2\right) \frac{F_2\left(Q^2\right)}{2M} = \langle P+q,\, +| \frac{J^{+}(0)}{2P^{+}} |P,\, -\rangle = \frac{1}{2P^{+}} \mathcal{F}_{+-}, \tag{5.6}$$

where

$$\mathcal{F}_{\Lambda'\Lambda}(Q^2) = \langle P', \Lambda'| J^{+}(0) |P, \Lambda\rangle = \sum_q e_q \langle P', \Lambda'| \bar{\psi}_q(0)\, \gamma^{+} \psi_q(0) |P, \Lambda\rangle\,, \tag{5.7}$$

with Λ, Λ' light-front helicity states of the initial and final state of the hadron. After inserting the expression (2.90) for the hadron state in the matrix element (5.7), one has:

$$\mathcal{F}_{\Lambda\Lambda'}\left(Q^2\right) = 2P^{+} \sum_{j=1}^{N} \sum_{q} \sum_{\beta=\beta'} e_q \delta_{s_j q} \int [dx]_N \left[d^2\boldsymbol{k}_T\right]_N \Psi^{*\Lambda'}_{N,\beta'}(r')\, \Psi^{\Lambda}_{N,\beta}(r)\,, \tag{5.8}$$

where N is the number of particles in the n-th Fock state and the integrations measures are defined as in (2.93) and (2.94). The expression (5.8) allows one to compute the form factors once the form of the LFWF $\Psi^{\Lambda}_{N,\beta}(r)$ is known. In the case of a spin-0 particle, like the pion, only the form factor F_1 exists and reds:

$$F\left(Q^2\right) \equiv F_1\left(Q^2\right) = \sum_{j=1}^{N} \sum_{q} \sum_{\beta=\beta'} e_q \delta_{s_j q} \int [dx]_N \left[d^2\boldsymbol{k}_T\right]_N \Psi^{*\Lambda'}_{N,\beta'}(r')\, \Psi^{\Lambda}_{N,\beta}(r)\,, \tag{5.9}$$

With the same logic as for the form factor, one can plug in the expansion (2.90) in operator definition of the TMDs and PDFs and find an expression for the unpolarized TMD $f_1(x, \boldsymbol{k}_T^2)$ and the PDF $f_1(x)$ as:

$$f_1(x, \boldsymbol{k}_T) = \sum_{\beta'} \sum_{j=1}^{N} \int [dx']_N^{(j)} \left[d^2\boldsymbol{k}'_T\right]_N^{(j)} \left|\Psi^{\Lambda}_{N,\beta'}\left(x, \boldsymbol{k}_T; r'^{(j)}\right)\right|^2, \tag{5.10}$$

$$f_1(x) = \sum_{\beta'} \sum_{j=1}^{N} \int [dx']_N^{(j)} \left| \Psi^{\Lambda}_{N,\beta'} \left(x; r'^{(j)} \right) \right|^2, \tag{5.11}$$

where the following notations are used:

$$\begin{cases} [dx']_N^{(j)} = \prod_{\substack{l=1 \\ l \neq j}}^{N} dx'_l \delta \left(x - x'_j \right), \\ \left[d^2 \boldsymbol{k}'_T \right]_N^{(j)} = \frac{1}{(16\pi^3)^{N-1}} \prod_{\substack{l=1 \\ l \neq j}}^{N} d^2 \boldsymbol{k}'_T \delta^{(2)} \left(\boldsymbol{k}_T - \boldsymbol{k}'_{Tj} \right), \\ \Psi^{\Lambda}_{N,\beta'} \left(r; r'^{(j)} \right) = \Psi^{\Lambda}_{N,\beta'} \left(\ldots, r_{j-1}, r, r_{j+1}, \ldots \right). \end{cases} \tag{5.12}$$

The AdS/QCD correspondence provides an expression for the meson valence state, i.e. only the $|q\bar{q}\rangle$ first Fock state is present in the expansion. The above expressions will be then extremely simplified and they become as shortly defined in eq. (5.25), (5.27), and (5.24).

5.2.1 The AdS/QCD correspondence

With the name AdS/CFT correspondence [258,259] (also called gauge/gravity duality or Maldacena conjecture) we refer to the connection between a string theory defined in a d dimensional anti-de Sitter (AdS) space, and a conformal field theory (CFT) defined in a flat space with $d-1$ dimension. This represents a realization of the holographic principle, because the relation involves theories defined in spaces with different dimensions. In particular, the conjecture states that it is possible to relate a gauge theory in standard $(3+1)$ Minkowski space-time to a gravitational theory in five dimension, with the remarkable advantage that the two theories have inverse couplings. The line element in the AdS metric reads:

$$ds^2 = \frac{R^2}{z^2} \left(\sum_{i=0}^{3} dx_i dx^i - dz^2 \right), \tag{5.13}$$

where R is the AdS curvature radius. The 5-th coordinate z is called holographic variable. The Anti-de Sitter AdS space is is a maximally symmetric Lorentzian manifold with constant negative scalar curvaturethe and a four dimensional boundary. Due to the high number of symmetries on the gravity side, the correspondent dual gauge theory consists in a conformal and supersymmetric Yang-Mills theory.

Bottom-up approach and LF Holography

The idea expressed by the gauge/gravity duality is certainly intriguing, and during the past twenty years people have been devoting a lot of work in developing AdS/CFT methods. The aspiration of applying such a conjecture (or a modified version of it) to a strongly-coupled theory existing in nature, such as QCD, has grown. The underlying logic is to match the nonperturbative observables of QCD to other observables that would be calculable in the gravity theory with perturbative methods. However, as soon as the role of the supersymmetric Yang-Mills theory is played by QCD, one should desist from any attempt of implementing AdS/CFT in its original formulation. Since a gravity dual to QCD is not known, one needs to modify the gravitational theory on the AdS side. In this bottom-up approach, the dual gravitational theory is constructed such that all the characteristics of QCD would be implemented: conformality in the massless quarks limit, asymptotic freedom for small distances and confinement in the large distance domain.

The implementation of the AdS/QCD correspondence in the form of Light-Front Holography (LFH) is inspired by these principles [251,252]. In the so-called "soft-wall" version of AdS/QCD correspondence [260], conformal invariance is broken thanks to the effect of a harmonic confining potential (whose strength is determined by a mass parameter κ), producing a distortion of the AdS geometry near a large infrared value of z. If one identifies this value with $z \sim 1/\Lambda_{QCD}$, the scale of the strong interactions can be found. The soft-wall is realized by the insertion of a scalar dilaton field $\varphi(z) = \kappa^2 z^2$ in the 5-dimensional action, namely:

$$S = \int d^4x dz \sqrt{|g|} e^{\varphi(z)} \left(g^{MN} \partial_M \Phi(x,z) \partial_N \Phi(x,z) - m^2 \Phi^2(x,z) \right), \tag{5.14}$$

where uppercase indices M and N run from 1 to 5, g^{MN} is the metric tensor of the AdS space such that $ds^2 = g_{MN} dx^M dx^N$ with $x^M = (x^\mu, z)$ and m is an arbitrary mass parameter. The scalar normalizable modes in AdS can be written as $\Phi(x,z) = e^{-iP\cdot x}\phi(z)$, i.e. plane waves along Minkowski coordinates x_μ and a profile function $\phi(z)$ along the holographic coordinate z.

It can be shown that the equation of motion of $\phi(z)$, derived from the modified AdS action, corresponds to the equation for the transverse part of the LFWF [250], with a non-vanishing harmonic potential and with the identification of z with the impact parameter coordinate in LF [261]. Therefore, the connection established holds between the 5-dimensional gravity theory in modified AdS space and LF formulation of QCD [250]. The consistency of the choice of the harmonic oscillator is supported by several arguments [250]. It is relevant to mention that this is, for instance, consistent

with the fact that a harmonic shape of the potential in LF corresponds to a linear potential in usual IF [262].

Hadronic physics in the AdS/QCD approach

Light-front holographic QCD methods (see [250] and references therein for a complete review on the topic) have been employed in a number of recent works to obtain new insights into the structure of hadrons [250–252, 260, 263, 264].

For instance, the approach leads to linear Regge trajectories [260] for light mesons and baryon, one of the major success of the approach. From the light meson and baryon mass spectra one can extract a possible value of the universal parameter κ, as discussed later in the Chapter and extensively in [250].

Most relevant to our purposes is the achievements of light-front holographic QCD in providing a theory-based expression for the light-front wave function (LFWF) for the valence Fock-state component of mesons. This makes it possible to obtain direct information about many hadronic observables, which can be expressed in terms of overlaps of LFWFs.

Once the correspondence has been found, one can proceed in building the dictionary of the LF Holography. Brodsky and de Teramond in [261], inspired by the work of Polchinski and Strassler [265, 266], matched the spinless string modes in five-dimensional AdS space with the meson LFWFs. The original procedure carried out by Brodsky and de Teramond is extensively explained in, e.g., [261] and will not be repeated here. The matching involves the following quantities:

$$\int d^4x \int dz \sqrt{g}\; A^M\left(x,z\right) \Phi^*_{P'}\left(x,z\right) \overleftrightarrow{\partial}_M \Phi_P\left(x,z\right) \tag{5.15}$$

$$\Updownarrow$$

$$\left(2\pi\right) \delta^{(4)}\left(P'-P-q\right) \epsilon_\mu \left(P'+P\right)^\mu F\left(Q^2\right), \tag{5.16}$$

where the top line (5.15) represents the expression for the transition matrix element of the free electromagnetic current $A^M(x,z)$ propagating in the AdS space, evaluated between five-dimensional AdS modes $\Phi(x,z)$ that correspond to the incoming (P) and outgoing (P') meson states in a soft-wall model effective potential. The bottom line (5.16) represents the same transition amplitude in the physical Minkowski space-time, i.e. $\langle P'|\, J^\mu(0)\,|P\rangle = (P+P')^\mu F(Q^2)$. The meson momentum changes from P to P' as the result of the interaction with a photon with space-like momentum q^μ and polarization vector ϵ^μ. As previously explained in this Section, one can conveniently choose a frame where the photon momentum is only in the transverse direction. The $F(Q^2)$ in (5.16) is then the form factor of the meson expressed in terms of the impact

parameter coordinates $\boldsymbol{b}_T$, Fourier transform of the transferred momentum $\boldsymbol{q}_T$, rather than in momentum space as in (5.9). The matching provides the expression for the LFWFs for the valence state $q\bar{q}$ of a meson h in the impact parameter space[1]:

$$F\left(Q^2\right) = \sum_q e_q \int dx d^2\boldsymbol{b}_T \exp\left(i\boldsymbol{q}_T \cdot (1-x)\boldsymbol{b}_T\right) \left|\psi_{q\bar{q}/h}\left(x, \boldsymbol{b}_T\right)\right|^2 . \tag{5.17}$$

The identification is openly valid only for the first Fock state and the LFWF derived has the form that we will write in eq. (5.18).

The procedure in [261] was based on the correspondence between a free current propagating in AdS and the LFWF overlap representation of the form factor, and it would be exact if one included all the infinite number of Fock states. Later in [267], the mapping with a "dressed current" incorporating non valence Fock state was developed, which led to the expression in eq. (5.22). This wave function is supposed to *effectively* describe the hadron.

The two forms for the LFWF obtained have been used as the starting point to calculate collinear and transverse-momentum dependent parton distributions (PDFs and TMDs, respectively), generalized parton distributions (GPDs) and other parton densities both for mesons and nucleons (see for instance [167, 268–284]).

In Section 5.3 we will review the characteristics of these two forms and we will investigate the phenomenological implications on the simplest mesonic state: the pion.

5.3 The pion in AdS/QCD correspondence

In this Section, we present the results from [66], where we used the LFWFs from the AdS/QCD correspondence to study the 3D internal structure and dynamics of the pion in momentum space.

5.3.1 Pion LFWFs

As previously mentioned, studying the structure of the pion has attracted interest since the pion was predicted and detected experimentally. It can be seen as the simplest realization of a QCD bound state of quark and anti-quark as well as the Nambu-Goldstone boson of the dynamically broken Chiral Symmetry in QCD.

The expressions of the LFWFs coming from the soft-wall model of the AdS/QCD correspondence were originally derived in two different matching procedures [261,267]. Brodsky and de Teramond in [261], inspired by [265, 266], perform the matching

[1] The matching only provides the s-wave contribution to the LFWFs.

procedure taking into account only the two-parton valence component. The explicit expression for the pion LFWF reads

$$\psi^V_{q\bar{q}/\pi}\left(x,\ \boldsymbol{k}_T\right) \sim \frac{1}{\kappa\sqrt{(1-x)\,x}} e^{-\frac{1}{2}\frac{\boldsymbol{k}_T^2}{\kappa^2 x(1-x)}}, \tag{5.18}$$

where the superscript V indicates that we are considering the LFWF for the *pure-valence* state of the pion. The quark masses in the pion LFWF are included following the prescription suggested in [285], i.e. by completing the invariant mass of the system as

$$M^2 = \sum_i \frac{m_i^2 + \boldsymbol{k}_{Ti}^2}{x_i} = \frac{m^2 + \boldsymbol{k}_T^2}{x(1-x)}, \tag{5.19}$$

where $m = m_1 = m_2$ and, from momentum conservation, $\boldsymbol{k}_T = \boldsymbol{k}_{T1} = -\boldsymbol{k}_{T2}$ and $x = x_1 = 1 - x_2$. As a result, the expression (5.18) becomes

$$\psi^V_{q\bar{q}/\pi}\left(x,\ \boldsymbol{k}_T\right) = A\frac{4\pi}{\kappa\sqrt{(1-x)\,x}} e^{-\frac{1}{2\kappa^2}\left(\frac{m^2}{x(1-x)} + \frac{\boldsymbol{k}_T^2}{x(1-x)}\right)}, \tag{5.20}$$

where A is a normalization constant fixed by the condition

$$\int_0^1 dx \int_{-\infty}^{+\infty} \frac{d^2\boldsymbol{k}_T}{16\pi^3} \left|\psi^V_{q\bar{q}/\pi}\left(x,\ \boldsymbol{k}_T\right)\right|^2 = 1. \tag{5.21}$$

An alternative expression for the LFWF has been derived in [267], considering the mapping of the matrix element of a confined electromagnetic current propagating in a warped AdS space to the pion form factor. In this case, one obtains a LFWF which provides the expected pole structure for the form factor in the time-like region. Furthermore it incorporates the effects due to non-valence higher-Fock states generated by the "dressed" confined current and represents an *effective* two-parton state of the pion. It reads

$$\psi^E_{q\bar{q}/\pi}\left(x,\ \boldsymbol{k}_T\right) \sim \frac{\sqrt{\log\left(\frac{1}{x}\right)}}{\kappa\,(1-x)} e^{-\frac{\log(1/x)}{(1-x)^2}\frac{\boldsymbol{k}_T^2}{2\kappa^2}}, \tag{5.22}$$

where the superscript E indicates that we are considering an "effective-valence" component of the LFWF. At variance with the pure-valence LFWF, the effective-valence LFWF is not symmetric in the longitudinal variables x and $1-x$ of the active and spectator quark, respectively. Introducing the quark mass dependence as outlined

above, the effective-valence LFWF becomes

$$\psi^{E}_{q\bar{q}/\pi}(x,\ \boldsymbol{k}_T) = 4\pi A \frac{\sqrt{\log\left(\frac{1}{x}\right)}}{\kappa\,(1-x)} e^{-\frac{\log(1/x)}{(1-x)^2}\frac{\boldsymbol{k}_T^2+m^2}{2\kappa^2}}, \tag{5.23}$$

where the parameter A is once more fixed by demanding the validity of (5.21).

5.3.2 PDF and Form Factor

Using the LFWF overlap representation of the PDF and form factor for the first Fock state in the expansion, in the valence case (5.20), we obtain

$$f_1^V(x;Q_0) = \int_{-\infty}^{+\infty} \frac{d^2\boldsymbol{k}_T}{16\pi^3} |\psi^V_{q\bar{q}/\pi}(x,\ \boldsymbol{k}_T)|^2 = A^2 e^{\left(-\frac{m^2}{\kappa^2 x}-\frac{m^2}{\kappa^2(1-x)}\right)}, \tag{5.24}$$

$$\begin{aligned} F_\pi^V(Q^2) &= \\ &\int_{-\infty}^{+\infty} \frac{d^2\boldsymbol{k}_T}{16\pi^3} dx\, \psi^{*V}_{q\bar{q}/\pi}(x,\ \boldsymbol{k}_T + (1-x)\boldsymbol{q}_T)\, \psi^V_{q\bar{q}/\pi}(x,\ \boldsymbol{k}_T) \\ &= \int_0^1 dx A^2 e^{\left(-\frac{m^2}{\kappa^2 x}-\frac{m^2}{\kappa^2(1-x)}-\frac{Q^2(1-x)}{4\kappa^2 x}\right)}, \end{aligned} \tag{5.25}$$

where $|\boldsymbol{q}_T|^2 = Q^2$. The condition (5.21) implies that $\int_0^1 dx f_1^V(x;Q_0) = F_\pi^V(Q^2 = 0) = 1$. Throughout this analysis $f_1^q(x) = f_1^{\bar{q}}(x)$ is always consistently understood and we discuss results for the π^+ hadron, as the distributions for the π^0 and π^- can be related by isospin and charge conjugation symmetry.

The corresponding expressions for the PDF and the form factor using (5.23) are given by

$$\begin{aligned} f_1^E(x;Q_0) &= A^2 e^{-\frac{\log(1/x)}{(1-x)^2}\frac{m^2}{\kappa^2}}, \\ F_\pi^E(Q^2) &= \int_0^1 dx A^2 e^{-\frac{\log(1/x)}{4\kappa^2}\left(Q^2+\frac{4m^2}{(1-x)^2}\right)}. \end{aligned} \tag{5.26}$$

We fix the parameters of the LFWFs (5.20) and (5.26) by fitting the available experimental data for the pion electromagnetic form factor [286–288][2] and the parametrization of the pion PDF in [289]. For the fit of the PDF, we apply the DGLAP evolution

[2]We point out the difference with our publication [66], where the bibliographic indications for the used data points was not given correctly.

equations at next-to-leading-order (NLO) to evolve the PDF from the (low) scale of the model Q_0 to the scale $Q = 5$ GeV of the parametrization, using the HOPPET code [290]. We leave in the initial scale Q_0 as an additional free parameter to be fitted with the data. Starting from the functional form of the parametrization [289], we select 61 equally-spaced points from $x = 0.2$ to $x = 0.8$ and for each of them we construct error bars by propagation of the errors on the individual parameters. Summing the PDF points and the 58 form factor points (45 data points from [286], 5 data points from [287], and 8 from [288], which includes the reanalized points of [291,292]), we perform the fit using in total 119 points. In the case of the pure-valence LFWF we consider two different fitting strategies: either we fix the quark mass to a constant value ("current quark" mass $m = 0.005$ GeV and "constituent quark" mass $m = 0.2$ GeV) or, alternatively, we let the quark mass entering as an additional fit parameter. For the effective-valence LFWF, we fix the quark mass to the same values as before, but we include also the limit of massless quarks (leaving the quark mass as a free parameter in this case leads anyway to a vanishing mass). The results of the fit are summarized in Tab. 5.1. In the following we discuss the results for two sets of parameters in Tab. 5.1 corresponding with the lowest value of the total $\chi^2_{\text{d.o.f.}}$ for non-vanishing quark mass.

In Fig. 1 we show the results for the form factor of the pure-valence (solid curve) and effective-valence (dashed curve) LFWF. The corresponding results for the PDF are shown in the upper and lower panel, respectively. The solid lines show the results at the hadronic scale, and the dashed lines are obtained after NLO evolution to $Q = 5$ GeV. The shaded band corresponds to the results from the parametrization at $Q = 5$ GeV of Ref. [289].

The results from the pure-valence LFWF are in good agreement with the available experimental and phenomenological information, while a worst comparison, especially for the form factor, is obtained in the case of the effective-valence LFWF.

The mass parameter κ plays a very important role, as it is originally the only free parameter of the theory and it is related to the strength of the confining harmonic potential in the soft-wall model [252, 262]. The value $\kappa \approx 0.37$ GeV obtained in the pure-valence LFWF case is similar to what was obtained in Ref. [261], whereas in the study of the effective-valence LFWF we obtain smaller values, $\kappa \approx 0.26$ GeV, compared to previous analyses [270, 274].

A larger value of κ, namely $\kappa = 0.54$ GeV, is needed in order to describe the hadronic mass spectra and the Regge trajectories [293–295] and this value has been quite extensively used (see [250, 272] for a more complete overview). Recent works [296–299] quote a larger value of approximately $\kappa = 0.5\,\text{GeV}$ to reproduce Regge

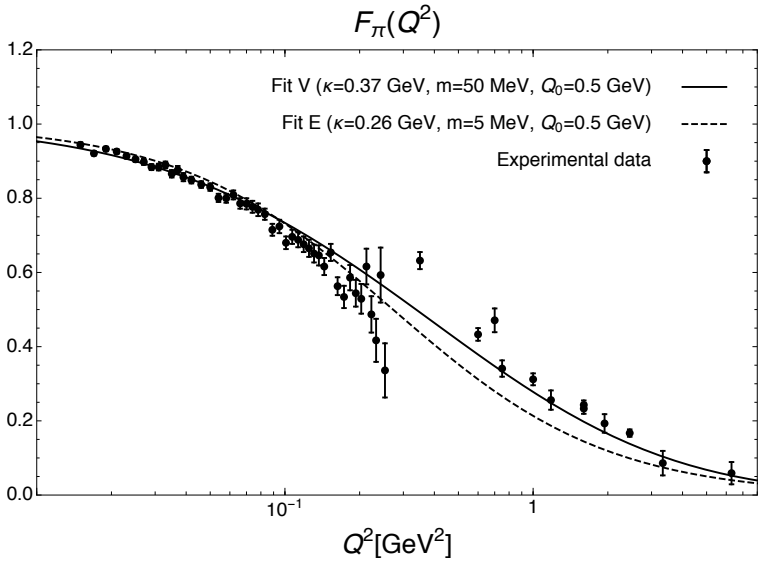

Figure 5.1: Results for the pion electromagnetic form factor from the pure-valence LFWF (solid curve) and the effective-valence LFWF (dashed curve) with the two sets of parameters in Tab. 5.1 corresponding with the lowest values of $\chi^2_{\text{d.o.f.}}$ for non-vanishing quark mass. The experimental data are from Refs. [286–288].

slopes for mesons and baryons and to realize the transition from the non-perturbative (described by light-front holography) and the perturbative regimes, which occurs at an energy scale of about 1 GeV. However, as outlined in [250], the scale κ is systematically lower for form factors, as compared with the values required to account for the mass spectrum. In fact, even though the effective model for the LFWF at zero quark masses reproduces the pole structure of the form factor in the time-like region, the position of the poles does not correspond to the one in the vector meson spectra. Thus, for a meaningful comparison with experimental data, one needs to shift the poles to their physical locations, meaning in fact an extension of the effective model. For the valence Fock state of the pion this simply consists of a rescaling of the κ towards lower values which are compatible with our results. The inclusion of higher Fock states implies the shift of a series of poles to their physical mass and a simple rescaling of the parameter is no longer possible.

Our result for the initial scale is $Q_0 \sim 0.5$ GeV in the pure-valence case and is consistent with the values obtained in different phenomenological quark models [62,238], where the scale is fixed by requiring that the model results for the momentum

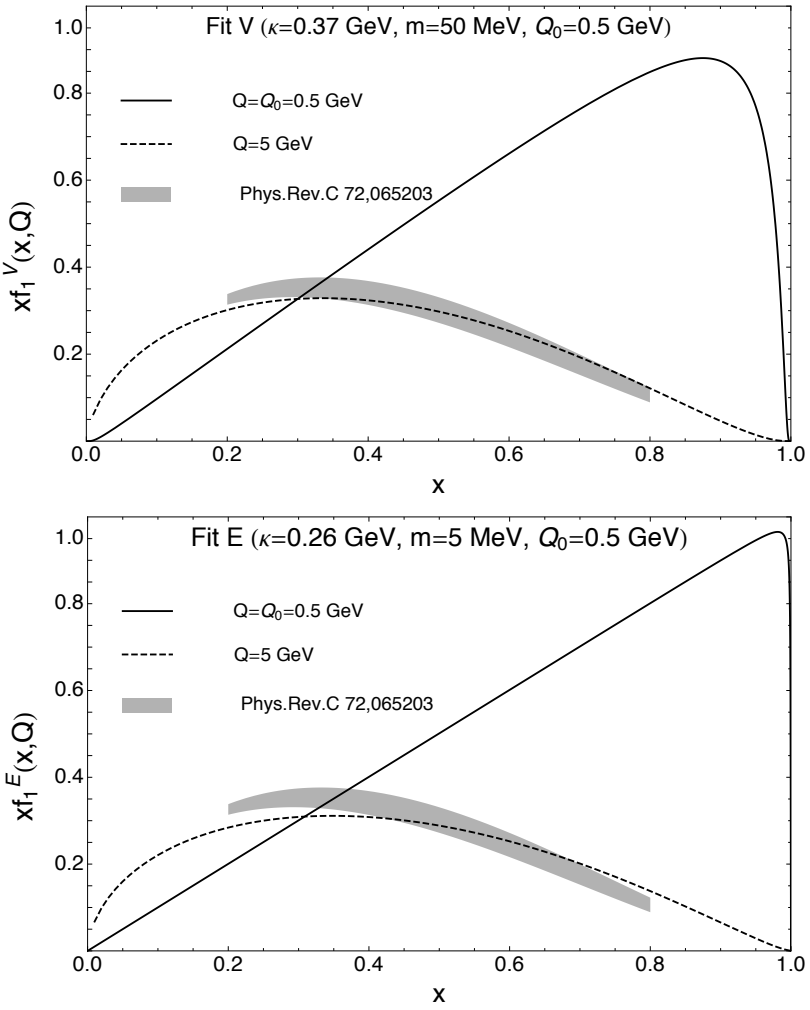

Figure 5.2: Results for the quark PDF of the pion as function of x from the pure-valence LFWF (upper panel) and the effective-valence LFWF (lower panel), with the two sets of parameters in Tab. 5.1 corresponding with the lowest values of $\chi^2_{\text{d.o.f.}}$ for non-vanishing quark mass. Solid curves: results at the initial scale of the model. Dashed curves: results after NLO evolution to $Q = 5$ GeV. Dashed band: parametrization at $Q = 5$ GeV from Ref. [289].

carried by the valence quarks match the experimental value, after DGLAP evolution, but it disagree with the LFH results. We will further comment on this result more

LFWF	m (GeV)	κ (GeV)	Q_0 (GeV)	$\chi^2_{\text{d.o.f.}}\left(\frac{\chi^2_{\text{FF}}+\chi^2_{\text{PDF}}}{N-N_{\text{par}}}\right)$
$\psi^V_{q\bar{q}/\pi}$	0.005 (fixed)	0.397 ± 0.003	0.500 ± 0.003	3.15
	0.200 (fixed)	0.351 ± 0.003	0.491 ± 0.003	11.76
	0.0500 ± 0.00004	0.371 ± 0.002	0.498 ± 0.002	2.25
$\psi^E_{q\bar{q}/\pi}$	0.005 (fixed)	0.261 ± 0.002	0.498 ± 0.003	5.44
	0.200 (fixed)	0.322 ± 0.002	0.630 ± 0.008	12.96
	0. (fixed)	0.262 ± 0.002	0.498 ± 0.003	5.38

Table 5.1: Results from the fit of the pure- and effective-valence LFWFs in different quark mass scenarios. In the last column $\chi^2_{\text{d.o.f.}}$ indicates the sum of the FF and PDF total values divided by the total degrees of freedom (total number of points N minus the number of free parameters N_{par}).

extensively in Section 5.4.

We also notice that the fit of the quark mass provides a value that is quite close to the average effective light-quark mass obtained in LF holographic QCD from the meson spectrum [250]. In the case of the effective-valence LFWF, we expect that the inclusion of the effects of higher-order Fock state components should correspond to a higher hadronic scale. This is the case when comparing the results between the effective-valence and pure-valence LFWF with $m = 200$ MeV and similar values of κ. However, for the other quark-mass scenarios we find similar values of Q_0 in the two models, which are compensated by much lower values for the parameter κ in the case of the effective-valence LFWF. Both the values of κ and the initial scale Q_0 differ with respect to [296–299].

5.3.3 Unpolarized TMD and effect of evolution

At leading twist, the pion transverse momentum dependent quark-quark correlator consists of two functions, the unpolarized TMD function $f_1(x, \boldsymbol{k}_T^2)$ and the Boer-Mulders TMD function $h_1^\perp(x, \boldsymbol{k}_T^2)$. We restrict ourselves to discuss the unpolarized TMD, since the Boer-Mulders function would require to construct a spin-dependent LFWF, which is not naturally present in the original AdS/QCD approach (see for example the phenomenological pion LFWF of [270] and [272]).

The unpolarized TMD $f_1(x, \boldsymbol{k}_T^2)$ can be obtained from the following LFWF overlap [62]

$$f_1(x, \boldsymbol{k}_T^2; Q_0) = \frac{1}{16\pi^3} |\psi_{q\bar{q}/\pi}(x,\ \boldsymbol{k}_T)|^2, \tag{5.27}$$

which reduces to the PDF in Eq. (5.24) after integration over $\boldsymbol{k}_T$. Using the expressions in Eqs. (5.20) and (5.23), one finds that the TMD in both models is a Gaussian distribution in $\boldsymbol{k}_T$, with an x-dependent mean square transverse momenta, i.e.

$$\begin{aligned} f_1^V(x, \boldsymbol{k}_T^2; Q_0) &= \frac{A^2}{\pi\kappa^2 x(1-x)} e^{-\frac{\boldsymbol{k}_T^2+m^2}{\kappa^2 x(1-x)}}, \\ \langle k_T^2(x; Q_0)\rangle^V &= \kappa^2 x(1-x), \end{aligned} \tag{5.28}$$

$$\begin{aligned} f_1^E(x, \boldsymbol{k}_T^2; Q_0) &= \frac{A^2 \log\left(\frac{1}{x}\right)}{\pi\kappa^2 (1-x)^2} e^{-\log\left(\frac{1}{x}\right)\frac{\boldsymbol{k}_T^2+m^2}{\kappa^2(1-x)^2}}, \\ \langle k_T^2(x; Q_0)\rangle^E &= \frac{\kappa^2(1-x)^2}{\log(1/x)}, \end{aligned} \tag{5.29}$$

where $k_T = |\boldsymbol{k}_T|$ and

$$\langle k_T^2(x; Q_0)\rangle^{V/E} = \frac{\int d^2\boldsymbol{k}_T \boldsymbol{k}_T^2 f_1^{V/E}(x, \boldsymbol{k}_T^2; Q_0)}{\int d^2\boldsymbol{k}_T f_1^{V/E}(x, \boldsymbol{k}_T^2; Q_0)}, \tag{5.30}$$

is the width of the distribution at Q_0. In Fig. 5.3 we show the results for the TMD in the two models, as function of x and k_T^2. As in the case of the PDF, the pure-valence model is symmetric under the exchange of $x \to 1-x$, while this symmetry is lost when including effects beyond the valence sector in the effective-valence LFWF. The fall-off in k_T^2 is Gaussian in both models.

The width of the distribution $\langle k_T^2(x)\rangle$ is shown as function of x in Fig. 5.4. It is slightly larger in the pure-valence model, with a maximum at $x = 0.5$ and the characteristic symmetric behaviour around the maximum. Integrating over x, one obtains $\langle k_T^2\rangle^V = 0.023\,\text{GeV}^2$. In the case of the effective-valence LFWF the maximum is shifted at lower values of x, i.e. $x = 0.28$, and the result after x-integration is $\langle k_T^2\rangle^E = 0.020\,\text{GeV}^2$.

As explained before, the AdS/QCD LFWF and the resulting TMDs are obtained at a scale of about 0.5 GeV. In order to be able to compare with data or extractions, TMDs need to be evolved according to TMD evolution equations (see, e.g., Ref. [300]). These equations describe the broadening of the initial TMD due to gluon radiation.

TMD evolution implementation

Even though TMD evolution equations are based on perturbative QCD calculations, their implementation requires the introduction of some prescriptions to avoid extending the calculations outside their region of validity. In general, such prescriptions have

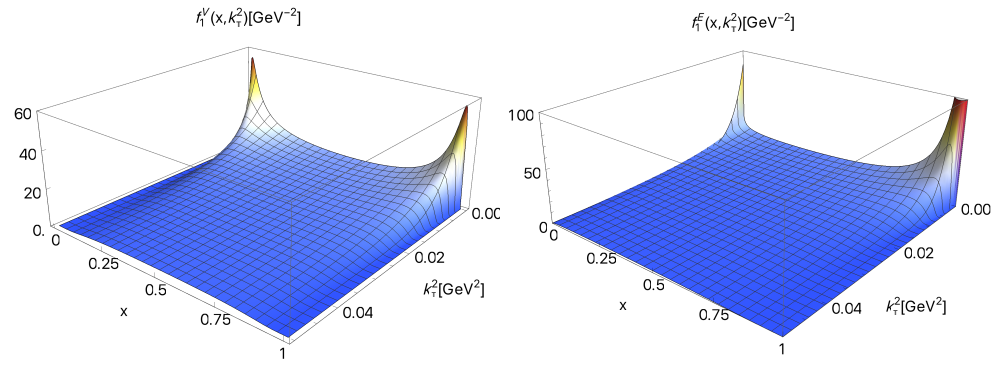

(a) (b)

Figure 5.3: Results for the quark TMD of the pion as function of x and k_T^2 from the pure-valence LFWF (left) and the effective-valence LFWF (right) with the two sets of parameters in Tab. 5.1 corresponding with the lowest values of $\chi^2_{\text{d.o.f.}}$ for non-vanishing quark mass.

the effect of inhibiting perturbative gluon radiation at low transverse momentum and at low Q, but must be complemented with an additional component of gluon radiation, usually referred to as nonperturbative component of TMD evolution [301]. This component cannot be predicted by perturbative QCD, but has to be extracted from experimental measurements, taking advantage of the fact that it is highly universal (i.e., it is independent of the quark's flavor and spin, the parent hadron, the type of process, and whether one considers TMD distribution and fragmentation functions). A recent example of a computation of the behavior of the nonperturbative component of TMD evolution can be found in [302].

Several prescriptions have been proposed in the literature (see, e.g. [14, 106, 108, 301, 303–305]). In principle, if complemented with the appropriate nonperturbative components, they should lead to compatible results for the evolved TMDs. However, there is still considerable uncertainty on the nonperturbative components and systematic studies of these uncertainty are still lacking. We therefore choose a specific implementation of TMD evolution equations, which has been successfully applied to the description of data in the range 1.2 GeV $\lesssim Q \lesssim$ 80 GeV. Details of this implementation are discussed in Ref. [108]. We summarize here the most important points.

TMD evolution is implemented in the space Fourier-conjugate to $k_\perp$. Therefore, we first define the Fourier-transformed TMDs

$$\widetilde{f}_1(x, b_\perp^2; \mu) = \int_0^\infty dk_\perp k_\perp J_0\big(b_\perp k_\perp\big) f_1(x, k_\perp^2; \mu) \tag{5.31}$$

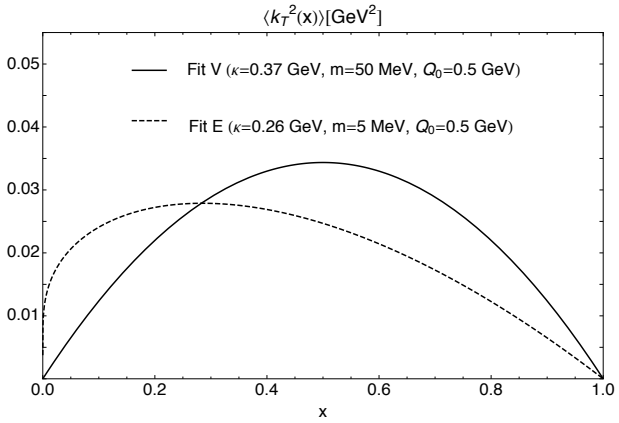

Figure 5.4: Results for the width $\langle k_T^2(x)\rangle$ as a function of x for the pure-valence LFWF (solid curve) and the effective-valence LFWF (dashed curve), with the two sets of parameters in Tab. 5.1 corresponding with the lowest values of $\chi^2_{\text{d.o.f.}}$ for non-vanishing quark mass.

and we use the following form for the evolved TMDs in $b_\perp$ space (see Refs. [15, 306])

$$\widetilde{f}_1^a(x, b_\perp^2; \mu) = \sum_{i=q,\bar{q},g} \left(\tilde{C}_{a/i} \otimes f_1^i\right)(x; \mu_b) e^{\tilde{S}(\bar{b}_*; \mu_b, \mu)} e^{g_K(b_\perp) \ln \frac{\mu}{Q_0}} \widetilde{f}_1^a(x, b_\perp^2; Q_0), \tag{5.32}$$

where the label a indicates the parton type. We consider the above equation at Next-to-Leading Logarithmic (NLL) approximation and at leading order in α_s. In this case, the convolution at the beginning of the evolved formula reduces simply to

$$\sum_{i=q,\bar{q},g} \left(C_{a/i} \otimes f_1^i\right)(x; \mu_b^2) \approx f_1^a(x; \mu_b^2), \tag{5.33}$$

and the expression for the Sudakov form factor $\tilde{S}(\bar{b}_*; \mu_b, \mu)$ can be found, e.g., in Ref. [307, 308]. We further use

$$\mu_b = \frac{2e^{-\gamma_E}}{\bar{b}_*}, \qquad g_K = -g_2 b_\perp^2/2, \qquad Q_0 = 0.5 \text{ GeV}. \tag{5.34}$$

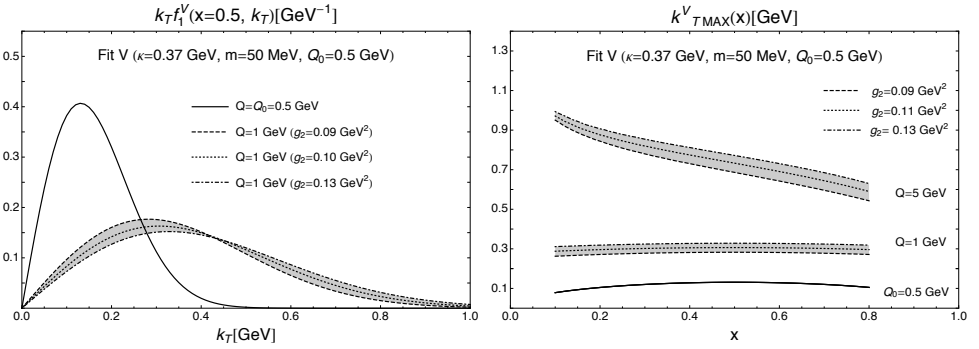

(a) (b)

Figure 5.5: Left panel: results for the quark TMD of the pion, multiplied by k_T, from the pure-valence LFWF for the $m = 50$ MeV scenario, as function of $k_\perp$ and at fixed $x = 0.5$. The solid line shows the result at the scale of the model, $Q_0 = 0.5$ GeV, corresponding with the initial scale for the TMD evolution. The shaded band gives the spread of the results after evolution of the TMD to 1 GeV with three different values of g_2: 0.09 GeV^2 (dashed curve), 0.11 GeV^2 (dotted curve) and 0.13 GeV^2 (dashed-dotted curve). Right panel: results for k_{TMAX} as function of x, at the scale of the model (solid curve) and after TMD evolution to $Q = 1$ GeV (lower band) and $Q = 5$ GeV (upper band) with three different values of g_2: 0.09 GeV^2 (dashed curve), 0.11 GeV^2 (dotted curve) and 0.13 GeV^2 (dashed-dotted curve).

We introduced the following variable

$$\bar{b}_* \equiv b_{\max}\left(\frac{1-e^{-b_\perp^4/b_{\max}^4}}{1-e^{-b_\perp^4/b_{\min}^4}}\right)^{1/4}, \tag{5.35}$$

with

$$b_{\max} = 2e^{-\gamma_E}/Q_0 = 2.246\ \text{GeV}^{-1}, \qquad b_{\min} = 2e^{-\gamma_E}/Q\ . \tag{5.36}$$

The above choice guarantee that at the initial scale $Q = Q_0$ any effect of TMD evolution is absent. The model results are thus preserved and in particular the relation between TMD and collinear PDF is maintained.

The value of the g_2 parameter should be extracted from experimental data, keeping all other choices fixed. In a recent analysis, the parameter was found to be 0.13 ± 0.01 GeV^2 in combination with a $b_{\max}$ that was half of the value we assume here. Since $b_{\max}$ and g_2 are in general anticorrelated, we choose for the present analysis the following three values

$$g_2 = 0.09,\ 0.11,\ 0.13\ \text{GeV}^2. \tag{5.37}$$

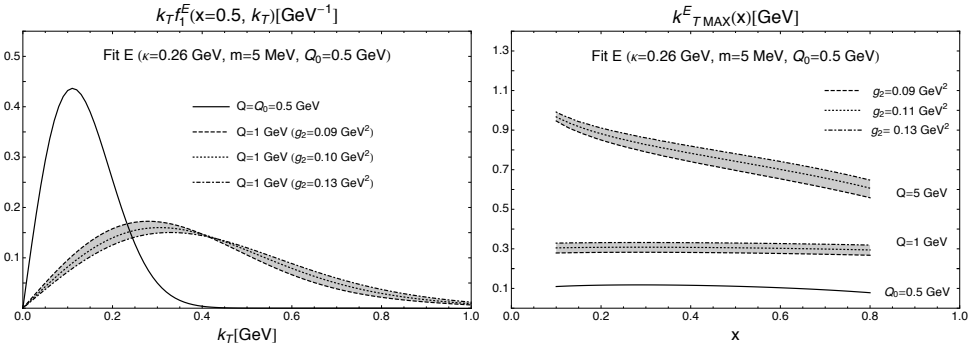

(a) (b)

Figure 5.6: Left panel: results for the quark TMD of the pion, multiplied by k_T, from the effective-valence LFWF for the $m = 50$ MeV scenario as function of $k_\perp$ and at fixed $x = 0.5$. The solid line shows the result at the scale of the model, $Q_0 = 0.5$ GeV, corresponding with the initial scale for the TMD evolution. The shaded band gives the spread of the results after evolution of the TMD to 1 GeV with three different values of g_2: 0.09 GeV^2(dashed curve), 0.11 GeV^2 (dotted curve) and 0.13 GeV^2 (dashed-dotted curve). Right panel: results for k_{TMAX} as function of x, at the scale of the model (solid curve) and after TMD evolution to $Q = 1$ GeV (lower band) and $Q = 5$ GeV (upper band) with three different values of g_2: 0.09 GeV^2 (dashed curve), 0.11 GeV^2 (dotted curve) and 0.13 GeV^2 (dashed-dotted curve).

Figures 5.5(a) and 5.6(a) show the effect of TMD evolution when going from the model scale to 1 GeV and 5 GeV (at an illustrative value of $x = 0.5$). The value of k_T corresponding to the position of the peak of the distributions $k_T f_1(x, k_T^2)$ can be used as a measure of the width of the TMDs. The peak moves from about 0.1 to 0.3 GeV, showing that there is a broadening of the width of the distributions. Even if this not evident from the plot, the distributions are no longer Gaussian.

Figures 5.5(b) and 5.6(b) show the position of the peak for x between 0.1 and 0.8 and for three values of Q. At the scale of the model, this is an analytic function which reads:

$$k_{TMAX}(x) = \sqrt{\frac{\langle k_T^2(x)\rangle}{2}}. \tag{5.38}$$

After evolution to 1 GeV, as already observed, the width of the TMD increases to about 0.3 GeV in both versions of the model. The x dependence of the TMD width is rather flat. The symmetry about $x = 0.5$ of the pure-valence model is lost. The two models become quite similar to each other: the position of the peak is the same within a 5% error. At 5 GeV, the width of the TMD increases to about 0.7 GeV at $x = 0.5$ and increases at low x, and is again very similar in the two versions of the

model. We do not display the functions at 5 GeV in the left panels of Figures 5.5 and 5.6 for simplicity. The distributions $k_T\, f_1^{V/E}(x = 0.5; k_T; Q = 5\,\text{GeV})$ are very wide in k_T and they loose any Gaussian shape.

In summary, TMD evolution from the model scale (0.5 GeV) to a typical experimental scale of 5 GeV increases the width of the TMD of almost one order of magnitude and leads to an x dependence of the width that is different from the original one, with no strong difference between the two versions of the model.

5.3.4 Summary of the results

We took into consideration two different versions of the pion LFWFs: pure-valence and effective-valence. For each version, the model contains three free parameters: the mass parameter κ (expressing the strength of the confining harmonic potential that breaks conformal invariance), the quark mass, and the scale of the model. We fix the parameters by comparison to experimental information on pion form factors and PDFs.

We obtain a value of κ in agreement with previous estimate [261], for the pure-valence version of the model. For the effective-valence version, we obtain a smaller value [270, 274]. These values are both different from the ones obtained from the mass spectra.

In order to achieve a fair agreement with the pion PDF at 5 GeV, the model scale has to be set to about 0.5 GeV. This turns out to be true both for the pure-valence and the effective-valence LFWF. We further comment on this results in the next Section.

The sets of parameters obtained have then been used to study the unpolarized TMD of the pion. At the model scale, the resulting TMD has a Gaussian shape with a width (defined as the position of the peak of the distributions $k_T f_1(x, k_T^2)$) of about 0.1 GeV at $x = 0.5$. The x dependence of this width is different in the two versions of the model: in the pure-valence model the TMD attains its maximal width at $x = 0.5$; in the effective model, this happens at $x = 0.28$. After the TMD is evolved to a typical experimental scale of about 5 GeV, its width increases by almost one order of magnitude. The x dependence is different from the one at the model scale: the width grows monotonically as x decreases, and the differences between the two versions of the model fade away.

5.4 The QCD running coupling

A crucial ingredient of our calculation is to identify the energy scale where the model is valid. In our work, we have assumed that the transition between the nonperturbative regime (where the model is applicable) and the perturbative regime (where pQCD is applicable) occurs at a precise scale, which we define as the model scale. We fix this scale by fitting the pion PDF to available phenomenological parametrizations, after applying DGLAP evolution equations [309,310]. The value for the initial scale Q_0 is set uniquely from the DGLAP evolution to the low scale $Q_0 = 0.5$ GeV, a value which is needed in order to reach the agreement with the parametrization. One should take this outcome cautiously, as we are stretching the validity of the perturbative calculations down to an energy scale where these methods do not in principle hold (the value of α_s in the $\overline{\rm MS}$ scheme is larger than 1 for this Q value).

In Table 5.2 we show the values of the best fit parameters when the initial scale is instead fixed to some values Q_h, with $Q_h > 0.5$ GeV. The description of the PDF data becomes substantially worse. One can see that the $\chi^2_{\rm PDF}$ and the total $\chi^2_{\rm d.o.f}$ increase of almost one order of magnitude with respect to the best values we obtained from the fitting strategy explained in the text (see Table 5.1 and the Table 1 in [66]). That is, fixing a higher model scale by hand would lead to a very unsatisfactory description of the data at the energy scale of the parametrization.

To solve this, one can interpret the result as an indication about the fact that the model must be valid at a scale lower than $Q^2 \approx 0.75\,{\rm GeV}^2$, assuming a "grey area" where the transition from the perturbative to the nonperturbative physics described by the AdS/QCD correspondence occurs.

Describing a smooth transition at a fixed calculable Q_0 value is also possible from

LFWF	m (GeV)	κ (GeV)	Q_0(fixed) (GeV)	$\chi^2_{\rm PDF}$	$\chi^2_{\rm d.o.f.}$
$\psi^V_{q\bar{q}/\pi}$	0.00 ± 0.6	0.397 ± 0.004	0.86	3465	31.8
	0.00 ± 0.6	0.40 ± 0.2	1.00	4665	42.2
$\psi^E_{q\bar{q}/\pi}$	0.180 ± 0.003	0.30 ± 0.002	0.86	645	16.6
	0.201 ± 0.003	0.310 ± 0.002	1.00	1014.6	20.3

Table 5.2: Results from the fit of the pure- and effective-valence LFWFs with fixed values of the initial scale. In the last column $\chi^2_{\rm d.o.f.}$ is defined as in Table 5.1. In the fifth column we now display explicitly the χ^2 of the PDF fit.

a theoretical viewpoint, and it has been recently presented in [298, 299]. The value of the mass parameter used is $\kappa = 0.51 \pm 0.04$ GeV, derived from the linear Regge slope of the ρ meson and the nucleon[3]. The expression of the coupling constant in the LF holographic theory is given by the coupling of the AdS theory modified by the soft-wall:

$$\alpha_{\rm LFH}(Q^2) = \alpha_{\rm LFH}(0) e^{-Q^2/4\kappa^2}. \tag{5.39}$$

[3]Deriving the parameter κ from a Renormalization Scheme (RS) invariant quantity would be preferable, but the values obtained with this methods do not manage to describe the PDF values.

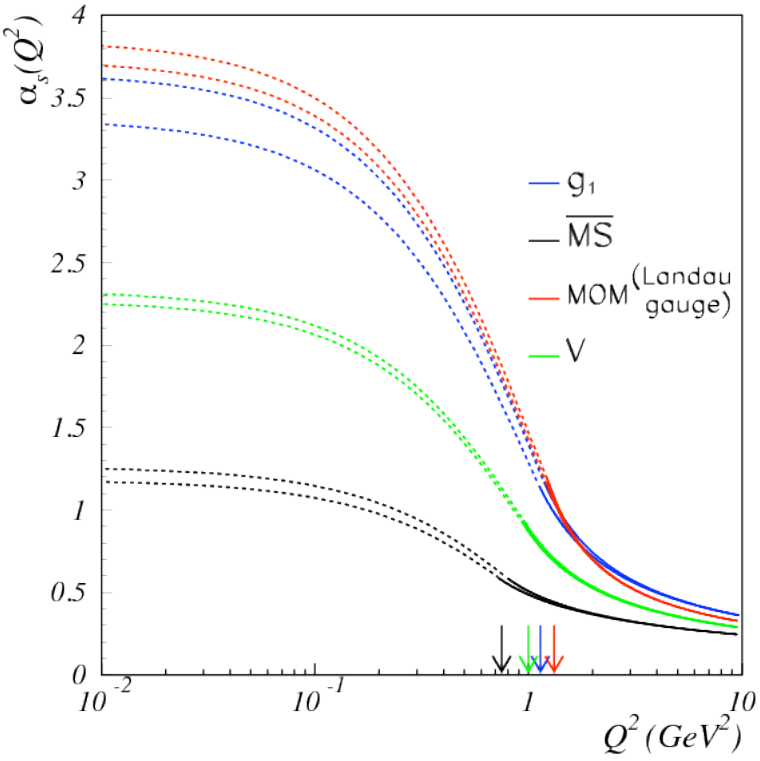

Figure 5.7: Figure from [298]. Strong coupling α_s as defined in eq. (5.42) over all range of Q. The procedure performs the matching between the pQCD coupling constant in the $\overline{\rm MS}$ scheme at N^{3}LO and NNLO (continue black lines) and the LF Holography description (dashed black line). The transition point, calculated as explained in [298], is $Q_0^2 = 0.75$ GeV^2 for $\overline{\rm MS}$ scheme and it is indicated by a black arrow. A value of $\kappa = 0.51$ GeV is used. The green, blue, and red lines are the similar results for different renormalization schemes. In particular the blue line represents the effective Bjorken coupling α_{g_1} for which the matching procedure was originally devised [311, 312].

According to [298], the coupling (5.39) represents the nonperturbative extension of the α_s defined in a specific scheme, e.g. the $\overline{\text{MS}}$ scheme. In order for (5.39) to be the smooth extension of the pQCD expression these conditions must hold:

$$\begin{cases} \alpha_{\text{LFH}}(Q_0) = \alpha_{\overline{\text{MS}}}(Q_0) \\ \beta_{\text{LFH}}(Q_0) = \beta_{\overline{\text{MS}}}(Q_0), \end{cases} \tag{5.40}$$

which fix the value of Q_0, $\alpha(0)$. The β function is defined in terms of the coupling constant α (pQCD and LFH) as:

$$\beta(\alpha_s) = Q^2 \frac{\partial \alpha_s}{\partial Q^2}. \tag{5.41}$$

For the $\overline{\text{MS}}$ scheme at three loop level the transition occur at the scale $Q_0^2 = 0.75$ GeV [298]. The strong coupling constant can be then defined over all ranges of Q as:

$$\alpha_s(Q) = \begin{cases} \alpha_{\text{LFH}}(Q) & Q \leq Q_0 \\ \alpha_{\overline{\text{MS}}}(Q) & Q > Q_0, \end{cases} \tag{5.42}$$

This result is obtained at a fixed order in pQCD, regardless the possible variations that different values of the initial conditions can produce at lower scales (e.g. input values of α_s or $\Lambda_{\overline{\text{MS}}}$). The transition has been studied for different definitions of the coupling in [298], and this method was originally tailored for describing the effective coupling $\alpha_{g_1} = g_1^2/4\pi$ defined from the Bjorken sum rule [313] (see also [263, 299, 311, 312] for more details on the topic). The situation is displayed in Figure 5.7, where other schemes besides $\overline{\text{MS}}$ are included and compared.

Using our values of κ and the scale Q_0, that are most suitable for the description of PDF and Form Factor (see Table 5.1), the smooth matching is a too rigid procedure

However, one can still attempt to describe the transition in the same way, by relaxing the condition (5.40), only imposing the continuity of the coupling at the matching point $\alpha_{\text{LFH}}(Q_0) = \alpha_{\overline{\text{MS}}}(Q_0)$. The situation obtained is displayed in Figure 5.8. We vary the values of α_s at the Z boson mass and eventually display the results for $\alpha_s(M_Z) = 0.118$. The solid lines on the pQCD side (right side of the plot) correspond to LO and NLO results and they are continuously joined to the LFH curves. We use the two values of κ that correspond to our best results for the fit procedures. The stability of the perturbative calculation is arguable at such lower scales, but, as already stressed earlier, it is necessary to use such a low scale to provide a good agreement with the collinear PDF.

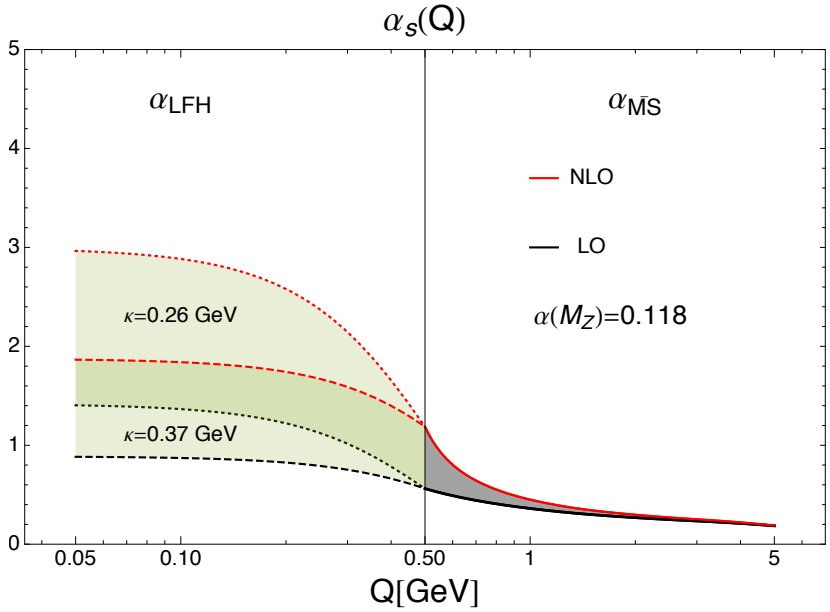

Figure 5.8: Right part of the plot: the continue line represents the value of α_s in pQCD at LO (black) and NLO (red) extracted by the HOPPET [290] routine with input value of 0.118 at the Z-boson mass. Left part: matching LFH lines with the values of κ from Section 5.3.2, and $\alpha(0)$ fixed by the first of the conditions in (5.40). The dashed lines refer to $\kappa = 0.37$ GeV and match the LO (dashed black) and NLO (dashed red) calculations in pQCD. The dotted lines refer to $\kappa = 0.26$ GeV and match the LO (dotted black) and NLO (dotted red) calculations in pQCD.

5.5 Discussion and conclusions

In this Chapter we developed the study of the pion, a spin-zero hadron. An explicit form for the LFWFs is a very powerful tool in order to study several hadronic observables simultaneously. The LFWFs, when all the Fock states are included, contain in principle a complete information of the internal dynamics of the hadron in terms of all quantum numbers of the partons and their intrinsic momentum and spatial coordinates, .

We choose to analyze the phenomenological implications resulting from the LFWFs provided by the AdS/QCD correspondence, in the context of the LF Holography formulation. This approach has some advantages: the derivation and the idea underlying the LFWF matching procedure is quite simple and attractive. It is based on a modified version of the gauge/gravity duality that was specifically tailored to the study

of QCD in the nonperturbative region. There is only one free parameter, which is in principle universal and it can be extracted from different observables.

Despite its attractive theoretical simplicity, the approach is however suitable to only account for a few degrees of freedom. Phenomenology-based modifications are possible and have been attempted in the literature. However, the choice of this work was to use the original functional forms with as little modifications as possible. We deliberately do not attempt to build a phenomenological LFWF starting from the original form and therefore we need to restrict ourselves to the study of unpolarized quarks in an unpolarized meson.

On the phenomenological side, with small changes from the original version of the LFWF and with some caveats, we obtained a qualitatively good description of the pion form factors and PDF, and we predicted pion TMD. We also studied the behavior of α_s in the nonperturbative regime and we found encouraging results.

Chapter 6

Summary, conclusions, and outlook

This thesis has been mainly devoted to the study of (single and double) parton distributions, with particular attention to the transverse momentum dependent parton distribution functions (TMDs) and the collinear double parton distributions (DPDs). They are of utmost importance for the present understanding of the hadron structure, as they contain rich information about the spin-spin and spin-orbit correlations between the partons and the hadron, and they play an essential role in the phenomenology of azimuthal and spin asymmetries. Moreover, DPDs are the ideal tool to investigate the internal structure of hadrons from a different perspective: rather than exploring the correlations between the parton and the parent hadron, they shed light on the quantum and kinematic correlations between partons.

In the following we summarize the contributions of this thesis to each of the topic mentioned above and we discuss some possible future directions.

Transverse-momentum dependent parton distributions for gluons in polarized hadrons

The full three-dimensional image of hadrons in momentum space is encoded in the quark and gluon TMDs, which appear in the transverse-momentum dependent corre-

lator. In the case of gluons, the latter is a nonlocal matrix element containing the gluon field operators and Wilson lines (also called gauge links), bridging the nonlocality to guarantee color gauge invariance. The gauge link structure of the correlators depends on the specific process and can lead to a universality breaking of the TMDs [39,40,42]. In Chapter 3, we parametrized the gluon-gluon correlator in terms of gluon TMDs and we considered targets that are unpolarized, vector polarized (relevant for spin-1/2 and spin-1), and tensor polarized (relevant for hadrons and nuclei of spin-1). We derived positivity bounds, i.e. model-independent inequalities, that help to relate and estimate the magnitude of the gluon TMDs about which very little, or almost nothing, is currently known. In fact, the gluon observables are typically much smaller than the valence quark ones, as far as present experimental facilities are concerned. However, at higher energies, the gluon distributions become the dominant ones and they need to be studied in detail. As a generalization of the previous results in the literature [47, 131], we found that in the kinematical region of low parton momentum x, the gluon correlator with a specific gauge link structure (called *dipole-type*) reduces to the matrix element of a single closed Wilson loop operator, where explicit gluon fields are absent [88]. The gluon TMDs are either suppressed or they become proportional to the functions appearing in the parametrization of the Wilson loop correlator. The gluonic contributions to the internal structure of hadrons, as well as nuclei, could be studied at the experiments planned in the context of the 12GeV program at Jefferson Lab, as well as at the Large Hadron Collider (LHC), and in the future at AFTER@LHC [133] and Electron-Ion Collider (EIC) [126].

Opportunities for gluon TMDs

A novel physics program will become possible at the future EIC [126]. The use of (un)polarized nuclear targets will shed light on the nuclear structure as well as fundamental QCD concepts. Outstanding questions concern, for instance, the spin-orbit and azimuthal asymmetries in scattering with ions and nuclei, and the role of these experiments in revealing non-nucleonic degrees of freedom, i.e., related to the partons which are not confined within one single nucleon. In the kinematical region probed by these future experiments, the gluon observables become accessible and this would pave the way to study the gluonic content of nuclei and hadrons of spin higher than 1/2. Consequently, it is important to investigate further the gluon TMDs and PDFs studied in [88,93] for spin-1 targets, and devote theoretical effort in implementing for the first time model calculations on these functions, as it has been already partially done for the quark case.

Double parton distributions and parton correlations at the LHC

The production of a pair of W bosons with the same charge at the LHC is one of the clearest processes to look at while hunting for DPSs, as the equivalent single parton contribution at the same order is forbidden in the Standard Model [191]. DPDs involve correlations between two partons extracted simultaneously from a proton and participating in two hard scatterings. They depend on the momentum fractions of the two extracted quarks, their transverse separation, and the quark quantum numbers, i.e. spin, flavor, and color [31]. In Chapter 4, we focused on the characterization of quark-quark correlations at the parton level, exploring various different correlation scenarios. We considered the production of a pair of W bosons at the LHC and performed a final-state analysis of the partonic results, with the inclusion of the relevant background processes. We referred to the asymmetry value as the key measurement for identifying double parton correlations in DPS. This observable is extremely attractive from the theoretical point of view: any value of the asymmetry different from zero would unequivocally be a sign of parton correlations in double parton scattering. The results were presented in a preliminary form, and a conclusive verdict on the possibility of measuring correlations in DPS could not be stated but promising directions have been identified [213]. Although the current results of our analysis would not allow us to observe a clear sign of parton correlations, it contributes in setting the stage for a fruitful interplay of theory and experiments in the field of multiparton interactions. At present, all DPDs are almost unknown. However, the experimental effort to measure DPS is growing and the number of experimental analysis on DPS processes is increasing. This will soon open up the possibility of boosting the field of DPS phenomenology towards a more precise level.

Light-front wave functions in AdS/QCD correspondence

In 2006 a new way of looking at QCD had been proposed by Brodsky and de Teramond [251, 252]. The use of the AdS/QCD correspondence based on the light-front formalism has provided a remarkable tool to access the hadron mass spectra and several hadronic observables. Moreover, a particular form for the valence-state light-front wave function (LFWF) of the mesons has been derived. This allows one to compute nonperturbative observables, including form factors and parton distributions, e.g., collinear parton distributions functions PDFs, generalized parton distributions GPDs, TMDs and DPDs DPDs [250]. In Chapter 5, based on the work done in [66,282] we used this meson LFWF and performed a phenomenological analysis on the pion. The purpose was to treat the functional form provided by the Light-front holography

approach as a non-perturbative starting point and then conduct an analysis on the transition to the perturbative one, by studying the pion form factor (FF) and the evolution of the pion PDF in the framework of collinear factorization and DGLAP evolution equations. By fitting the free parameters to the available experimental information, we found the best value for the energy scale at which the transition from the holographic description to the perturbative QCD occurs. In the analysis of the pion TMD (for which experimental data are not available yet) we used such a value as the lowest scale in the implementation of the TMD evolution equations. As expected, the resulting effect is a considerable increase of the transverse-momentum width of the distributions and a change in the shape of TMDs.

The many unanswered questions regarding TMDs and DPDs, and their importance in our understanding of the proton structure will benefit from the dedicated experiments planned for the next future at the LHC and the upcoming EIC. It is therefore essential to theoretically identify the processes where these distributions are sizeable and to drive the experimental searches. Only with a synergic effort between theory and experiments, physicists can aim at unravelling the numerous remaining open questions in the field.

Appendix A

Notation, conventions, and useful relations

Light-cone spinors in standard representation

The free light-front Dirac spinor $u_{LF}(k,\lambda)$ and antispinor $v_{LF}(k,\lambda)$ are given by (light-cone standard representation):

$$u_{LF}(k,+) = \frac{1}{\sqrt{2^{3/2}k^+}} \begin{pmatrix} \sqrt{2}k^+ + m \\ k^1 + ik^2 \\ \sqrt{2}k^+ - m \\ k^1 + ik^2 \end{pmatrix}, \quad u_{LF}(k,-) = \frac{1}{\sqrt{2^{3/2}k^+}} \begin{pmatrix} -k^1 + ik^2 \\ \sqrt{2}k^+ + m \\ k^1 - ik^2 \\ -\sqrt{2}k^+ + m \end{pmatrix},$$

$$v_{LF}(k,+) = -\frac{1}{\sqrt{2^{3/2}k^+}} \begin{pmatrix} -k^1 + ik^2 \\ \sqrt{2}k^+ - m \\ k^1 - ik^2 \\ -\sqrt{2}k^+ + m \end{pmatrix}, \quad v_{LF}(k,-) = -\frac{1}{\sqrt{2^{3/2}k^+}} \begin{pmatrix} \sqrt{2}k^+ - m \\ k^1 + ik^2 \\ \sqrt{2} + m \\ k^1 + ik^2 \end{pmatrix}.$$

The "good" components of the light-cone spinors and antispinors are given by $P_+ u_{LF}(k,\lambda) = u_+(k,\lambda)$ and $P_+ v_{LF}(k,\lambda) = v_+(k,\lambda)$. In standard representation

(Dirac), the projector operator P_+ is defined as:

$$P_+ = \frac{1}{2}\gamma^-\gamma^+ = \begin{pmatrix} 1 & 0 & 1 & 0 \\ 0 & 1 & 0 & -1 \\ 1 & 0 & 1 & 0 \\ 0 & -1 & 0 & 1 \end{pmatrix}. \tag{A.1}$$

The LF spinors explicitly read:

$$u_+(k,+) = \sqrt{\tfrac{k^+}{2^{1/2}}} \begin{pmatrix} 1 \\ 0 \\ 1 \\ 0 \end{pmatrix}, \quad u_+(k,-) = \sqrt{\tfrac{k^+}{2^{1/2}}} \begin{pmatrix} 0 \\ 1 \\ 0 \\ -1 \end{pmatrix}, \tag{A.2}$$

$$v_+(k,+) = \sqrt{\tfrac{k^+}{2^{1/2}}} \begin{pmatrix} 0 \\ -1 \\ 0 \\ 1 \end{pmatrix}, \quad v_+(k,-) = \sqrt{\tfrac{k^+}{2^{1/2}}} \begin{pmatrix} -1 \\ 0 \\ -1 \\ 0 \end{pmatrix}. \tag{A.3}$$

Good fields

At a given light-cone time, say $x^+ = 0$, the independent dynamical components (*good field*) of the free quark fields have Fourier expansion in momentum space:

$$\phi(x)\Big|_{x^+=0} = \int \frac{dk^+ d^2\boldsymbol{k}_T}{2k^+(2\pi)^3}\theta(k^+)\left[b(k^+,\boldsymbol{k}_T)u_+(k^+,\boldsymbol{k}_T,\lambda)e^{-ik\cdot x}\right. \tag{A.4}$$

$$\left. + d^\dagger(k^+,\boldsymbol{k}_T)v_+(k^+,\boldsymbol{k}_T,\lambda)e^{ik\cdot x}\right]\Big|_{x^+=0}, \tag{A.5}$$

where u_+, v_+ are the good components of the spinors as earlier defined, and $\lambda = \pm 1/2$ denotes the helicity of the quarks. The operators b and $d^\dagger$ are respectively the annihilation of the good components of the quark fields and the creation operator of the good component of the antiquark fields. The anticommutation relations for the quark (antiquark) creation and annihilation operators are:

$$\left\{b(k^+,\boldsymbol{k}_T), b^\dagger(k'^+,\boldsymbol{k}'_T)\right\} = 2k^+(2\pi)^3\delta(k^+ - k'^+)\delta^{(2)}(\boldsymbol{k}_T - \boldsymbol{k}'_T)\delta_{\lambda\lambda'}, \tag{A.6}$$

and the same holds for $d, d^\dagger$.

The free gluon field reads:

$$A^i(x)\Big|_{x^+=0} = \int \frac{dkd^2\boldsymbol{k}_T}{2k^+(2\pi)^3}\theta(k^+)\sum_\alpha \left[a_\alpha(k^+,\boldsymbol{k}_T)\epsilon^i_\alpha(k^+,\boldsymbol{k}_T)e^{-ik\cdot x}\right. \tag{A.7}$$

$$\left. +a^\dagger_\alpha(k^+,\boldsymbol{k}_T)\epsilon^{i*}_\alpha(k^+,\boldsymbol{k}_T)e^{ik\cdot x}\right]\Big|_{x^+=0}, \tag{A.8}$$

where ϵ is the transverse component of the gluon polarization vector, $\alpha = \pm 1$ denotes the gluon polarization states. The creation and annihilation operators for the gluon fields a, $a^\dagger$ obey commutation relations:

$$\left[a_\alpha(k), a^\dagger_{\alpha'}(k')\right] = 2k^+(2\pi)^3\delta(k^+ - k'^+)\delta^{(2)}(\boldsymbol{k}_T - \boldsymbol{k}'_T)\delta_{\alpha\alpha'}. \tag{A.9}$$

Poicaré algebra in LF

The four-momentum P^μ and angular-momentum $M^{\mu\nu} = x^\mu P^\nu - x^\nu P^\mu$ obey standard commutation relations which define the Poincaré group:

$$\begin{aligned}
&[P^\rho, M^{\mu\nu}] = i\left(g^{\rho\mu}P^\nu - g^{\rho\nu}P^\mu\right),\\
&[P^\rho, P^\mu] = 0,\\
&[M^{\rho\sigma}, M^{\mu\nu}] = i\left(g^{\rho\nu}M^{\sigma\mu} + g^{\sigma\mu}M^{\rho\nu} - g^{\rho\mu}M^{\sigma\nu} - g^{\sigma\nu}M^{\rho\mu}\right).
\end{aligned} \tag{A.10}$$

with the basic commutator $[x^\mu, p^\nu] = \delta^{\nu\mu}$.

In the front-form the matrix $M_{\mu\nu}$ takes the form:

$$M_{\mu\nu} = \begin{pmatrix}
0 & K_3 & -\frac{1}{\sqrt{2}}(K_1 - J_2) & -\frac{1}{\sqrt{2}}(K_2 + J_1)\\
-K_3 & 0 & -\frac{1}{\sqrt{2}}(K_1 + J_2) & -\frac{1}{\sqrt{2}}(K_2 - J_1)\\
\frac{1}{\sqrt{2}}(K_1 - J_2) & \frac{1}{\sqrt{2}}(K_1 + J_2) & 0 & J_3\\
\frac{1}{\sqrt{2}}(K_2 + J_1) & -\frac{1}{\sqrt{2}}(K_2 - J_1) & -J_3 & 0
\end{pmatrix} \tag{A.11}$$

and defining:

$$B_1 = \frac{1}{\sqrt{2}}(K_1 + J_2); \qquad B_2 = \frac{1}{\sqrt{2}}(K_2 - J_1); \tag{A.12}$$

$$S_1 = \frac{1}{\sqrt{2}}(K_1 - J_2); \qquad S_2 = \frac{1}{\sqrt{2}}(K_2 + J_1) \tag{A.13}$$

$$M_{\mu\nu} = \begin{pmatrix} M_{++} & M_{+-} & M_{+1} & M_{+2} \\ M_{-+} & M_{--} & M_{-1} & M_{-2} \\ M_{1+} & M_{1-} & M_{11} & M_{12} \\ M_{2+} & M_{2-} & M_{21} & M_{22} \end{pmatrix} = \begin{pmatrix} 0 & K_3 & -S_1 & -S_2 \\ -K_3 & 0 & -B_1 & -B_2 \\ S_1 & B_1 & 0 & J_3 \\ S_2 & B_2 & -J_3 & 0 \end{pmatrix} \tag{A.14}$$

The seven generators $P^-, P^+, P^1, P^2, J_3, B_1$ and B_2 are mutually commutant and satisfy different commutation relations, namely:

$$\begin{aligned} &\left[P^- \boldsymbol{P}_T\right] = \left[P^-, P^+\right] = \left[\boldsymbol{P}_T, P^+\right] = 0 \\ &\left[J_3, P^-\right] = \left[J_3, P^+\right] = \left[\boldsymbol{B}_T, P^+\right] = 0; \\ &[J_3, P_k] = i\epsilon_{kl} P_l, \;\; [J_3, B_k] = i\epsilon_{kl} B_l, \;\; \left[B_k, P^+\right] = -iP^k, \;\; [B_k, P_l] = -i\delta_{kl} P^+. \end{aligned} \tag{A.15}$$

where $(B_1, B_2) = \boldsymbol{B}_T$. The subgroup of the Poincare group generated by P^μ, J_3 and $\boldsymbol{B}_T$ in the light-front is isomorphous to the non-relativistic Galilean group.

Appendix B

Definitions of gluon TMDs

In this appendix the definitions of the various TMDs are given in terms of the coefficients A_i and B_i that have been introduced in the parametrizations at the level of the unintegrated correlators.

B.1 The gluon-gluon correlator

As we are only interested in leading twist functions, we omit the terms containing n (the situation is analogous to the quark case, see ref. [128]). We split the following results in terms of target polarization, i.e. unpolarized, vector, and tensor polarized.

$$\begin{aligned}\Gamma^{[U,U']\,\mu\nu;\rho\sigma}(k;P) = {} & M^2 A_1\, \epsilon^{\mu\nu\alpha\beta}\epsilon^{\rho\sigma}{}_{\alpha\beta} + A_2\, P^{[\mu}g^{\nu][\rho}P^{\sigma]} + A_3\, k^{[\mu}g^{\nu][\rho}k^{\sigma]} \\ & + (A_4 + iA_5)\, P^{[\mu}g^{\nu][\rho}k^{\sigma]} + (A_4 - iA_5)\, k^{[\mu}g^{\nu][\rho}P^{\sigma]} \\ & + (A_6/M^2)\, P^{[\mu}k^{\nu]}P^{[\rho}k^{\sigma]}, \end{aligned} \tag{B.1}$$

$$\begin{aligned}\Gamma^{\mu\nu;\rho\sigma}(k;P,S) = {} & -2MA_7\, \epsilon^{\mu\nu\rho\sigma}k{\cdot}S + iMA_8\left(\epsilon^{\mu\nu P[\rho}S^{\sigma]} - \epsilon^{\rho\sigma P[\mu}S^{\nu]}\right) \\ & + iMA_9\left(\epsilon^{\mu\nu S[\rho}P^{\sigma]} - \epsilon^{\rho\sigma S[\mu}P^{\nu]}\right)\end{aligned}$$

$$
\begin{aligned}
&+ iMA_{10}\left(\epsilon^{\mu\nu k[\rho}S^{\sigma]} - \epsilon^{\rho\sigma k[\mu}S^{\nu]}\right)\\
&+ iMA_{11}\left(\epsilon^{\mu\nu S[\rho}k^{\sigma]} - \epsilon^{\rho\sigma S[\mu}k^{\nu]}\right)\\
&+ \frac{iA_{12}}{M}\left(\epsilon^{\mu\nu P[\rho}P^{\sigma]} - \epsilon^{\rho\sigma P[\mu}P^{\nu]}\right)k{\cdot}S\\
&+ \frac{iA_{13}}{M}\left(\epsilon^{\mu\nu k[\rho}k^{\sigma]} - \epsilon^{\rho\sigma k[\mu}k^{\nu]}\right)k{\cdot}S\\
&+ \frac{iA_{14}}{M}\left(\epsilon^{\mu\nu P[\rho}k^{\sigma]} - \epsilon^{\rho\sigma P[\mu}k^{\nu]}\right)k{\cdot}S\\
&+ \frac{iA_{15}}{M}\left(\epsilon^{\mu\nu k[\rho}P^{\sigma]} - \epsilon^{\rho\sigma k[\mu}P^{\nu]}\right)k{\cdot}S + \frac{A_{16}+iA_{17}}{M}\,\epsilon^{\mu\nu PS}k^{[\rho}P^{\sigma]}\\
&+ \frac{A_{16}-iA_{17}}{M}\,\epsilon^{\rho\sigma PS}k^{[\mu}P^{\nu]} + \frac{A_{18}+iA_{19}}{M}\,\epsilon^{\mu\nu kS}k^{[\rho}P^{\sigma]}\\
&+ \frac{A_{18}-iA_{19}}{M}\,\epsilon^{\rho\sigma kS}k^{[\mu}P^{\nu]} + \frac{A_{20}+iA_{21}}{M}\,\epsilon^{\mu\nu kP}P^{[\rho}S^{\sigma]}\\
&+ \frac{A_{20}-iA_{21}}{M}\,\epsilon^{\rho\sigma kP}P^{[\mu}S^{\nu]} + \frac{A_{22}+iA_{23}}{M}\,\epsilon^{\mu\nu kP}k^{[\rho}S^{\sigma]}\\
&+ \frac{A_{22}-iA_{23}}{M}\,\epsilon^{\rho\sigma kP}k^{[\mu}S^{\nu]} + \frac{A_{24}+iA_{25}}{M^3}\,\epsilon^{\mu\nu kP}k^{[\rho}P^{\sigma]}k{\cdot}S\\
&+ \frac{A_{24}-iA_{25}}{M^3}\,\epsilon^{\rho\sigma kP}k^{[\mu}P^{\nu]}k{\cdot}S,
\end{aligned}
\tag{B.2}
$$

$$
\begin{aligned}
\Gamma^{\mu\nu;\rho\sigma}(k;P,T) = {}& A_{26}\,k^{[\mu}T^{\nu][\rho}k^{\sigma]} + A_{27}\,P^{[\mu}T^{\nu][\rho}P^{\sigma]} + (A_{28}+iA_{29})\,k^{[\mu}T^{\nu][\rho}P^{\sigma]}\\
&+ (A_{28}-iA_{29})\,P^{[\mu}T^{\nu][\rho}k^{\sigma]} + \frac{A_{30}+iA_{31}}{M^2}\,k_\alpha T^{\alpha[\mu}k^{\nu}k^{[\rho}P^{\sigma]}\\
&+ \frac{A_{30}-iA_{31}}{M^2}\,k_\alpha T^{\alpha[\rho}k^{\sigma]}k^{[\mu}P^{\nu]} + \frac{A_{32}+iA_{33}}{M^2}\,k_\alpha T^{\alpha[\mu}P^{\nu]}k^{[\rho}P^{\sigma]}\\
&+ \frac{A_{32}-iA_{33}}{M^2}\,k_\alpha T^{\alpha[\rho}P^{\sigma]}k^{[\mu}P^{\nu]} + M^2A_{34}\left(g^{\mu[\rho}T^{\sigma]\nu} - g^{\nu[\rho}T^{\sigma]\mu}\right)\\
&+ (A_{35}+iA_{36})\,k_\alpha T^{\alpha[\mu}g^{\nu][\rho}k^{\sigma]} + (A_{35}-iA_{36})\,k_\alpha T^{\alpha[\rho}g^{\sigma][\mu}k^{\nu]}\\
&+ (A_{37}+iA_{38})\,k_\alpha T^{\alpha[\mu}g^{\nu][\rho}P^{\sigma]} + (A_{37}-iA_{38})\,k_\alpha T^{\alpha[\rho}g^{\sigma][\mu}P^{\nu]}\\
&+ A_{39}\,k_\alpha k_\beta T^{\alpha\beta}\epsilon^{\mu\nu\kappa\lambda}\epsilon^{\rho\sigma}{}_{\kappa\lambda} + \frac{A_{40}}{M^2}\,k_\alpha k_\beta T^{\alpha\beta}P^{[\mu}g^{\nu][\rho}P^{\sigma]}\\
&+ \frac{A_{41}}{M^2}\,k_\alpha k_\beta T^{\alpha\beta}k^{[\mu}g^{\nu][\rho}k^{\sigma]} + \frac{(A_{42}+iA_{43})}{M^2}\,k_\alpha k_\beta T^{\alpha\beta}P^{[\mu}g^{\nu][\rho}k^{\sigma]}\\
&+ \frac{(A_{42}-iA_{43})}{M^2}\,k_\alpha k_\beta T^{\alpha\beta}k^{[\mu}g^{\nu][\rho}P^{\sigma]}
\end{aligned}
$$

$$+\frac{A_{44}}{M^4}\,k_\alpha k_\beta T^{\alpha\beta}P^{[\mu}k^{\nu]}P^{[\rho}k^{\sigma]}, \tag{B.3}$$

where $A_i = A_i(k{\cdot}n, k{\cdot}P, k^2)$. Terms with coefficients A_5, A_7, A_{16}, A_{18}, A_{20}, A_{22}, A_{24}, A_{29}, A_{31}, A_{33}, A_{36}, A_{38}, A_{43} are T-odd, and we note that the ones with coefficients A_8 up to A_{15} are slightly different from those in ref. [86].

Let us now denote by $\Gamma(k)$ the gluon-gluon correlator for any type of polarization, then the light-front correlator is defined as

$$\Gamma(x, \boldsymbol{k}_T) \equiv \int dk{\cdot}P\,\Gamma(k) = \frac{M^2}{2}\int [d\sigma d\tau]\,\Gamma(k), \tag{B.4}$$

where we have introduced the shorthand notation

$$[d\sigma d\tau] \equiv d\sigma d\tau\,\delta\left(\tau - x\sigma + x^2 + \frac{\boldsymbol{k}_T^2}{M^2}\right), \tag{B.5}$$

with the dimensionless invariants σ and τ given by

$$\sigma \equiv \frac{2k{\cdot}P}{M^2}, \quad \tau \equiv \frac{k^2}{M^2}, \tag{B.6}$$

spanning regions in remnant mass $M_R^2 \equiv (P-k)^2$ and in the partonic virtuality k^2. For both of these, the main contribution comes from small (hadronic) values (i.e. σ and τ of order one).

The (leading twist) TMDs that occur in the parametrization of the gluon-gluon correlator for the various types of polarization in eqs. (3.29)-(3.34), are related to the coefficients A_i as follows:

$$xf_1(x, \boldsymbol{k}_T^2) \equiv M^2\int [d\sigma d\tau]\left(A_2 + 2xA_4 + x^2A_3 + \frac{\boldsymbol{k}_T^2}{2M^2}\,A_6\right), \tag{B.7}$$

$$xh_1^\perp(x, \boldsymbol{k}_T^2) \equiv M^2\int [d\sigma d\tau]\,A_6, \tag{B.8}$$

$$\begin{aligned} xg_1(x, \boldsymbol{k}_T^2) \equiv 2M^2\int [d\sigma d\tau]\Bigg\{ & A_8 + A_9 + x\,(A_{10} + A_{11}) \\ & + \left(\frac{\sigma}{2} - x\right)\left[A_{12} + x\,(A_{14} + A_{15}) + x^2A_{13}\right] \\ & + \frac{\boldsymbol{k}_T^2}{2M^2}\left[A_{19} + A_{23} + \left(\frac{\sigma}{2} - x\right)A_{25}\right]\Bigg\}, \end{aligned} \tag{B.9}$$

$$xh_{1L}^\perp(x, \boldsymbol{k}_T^2) \equiv -2M^2\int [d\sigma d\tau]\left[A_{18} + A_{22} + \left(\frac{\sigma}{2} - x\right)A_{24}\right], \tag{B.10}$$

$$xf_{1T}^{\perp}(x,\boldsymbol{k}_T^2) \equiv M^2 \int [d\sigma d\tau]\,[A_{16} - A_{20} + x\,(A_{18} - A_{22})]\,, \tag{B.11}$$

$$xg_{1T}(x,\boldsymbol{k}_T^2) \equiv -M^2 \int [d\sigma d\tau] \Bigg[2A_{12} + A_{17} + A_{21} + 2x\,(A_{14} + A_{15}) + x\,(A_{19} + A_{23}) + 2x^2 A_{13} + \frac{\boldsymbol{k}_T^2}{M^2}\,A_{25}\Bigg]\,, \tag{B.12}$$

$$xh_1(x,\boldsymbol{k}_T^2) \equiv 2M^2 \int [d\sigma d\tau] \left[A_{16} + A_{20} + x\,(A_{18} + A_{22}) + \frac{\boldsymbol{k}_T^2}{2M^2}\,A_{24}\right], \tag{B.13}$$

$$xh_{1T}^{\perp}(x,\boldsymbol{k}_T^2) \equiv 2M^2 \int [d\sigma d\tau]\,A_{24}, \tag{B.14}$$

$$\begin{aligned} xf_{1LL}(x,\boldsymbol{k}_T^2) \equiv \frac{M^2}{3} \int [d\sigma d\tau] \Bigg\{ & A_{27} - 2A_{34} + 2xA_{28} + x^2 A_{26} \\ & + 2(\sigma - 2x)\,(A_{37} + xA_{35}) \\ & + \frac{(\sigma - 2x)^2}{2}\,\left(A_{40} + 2xA_{42} + x^2 A_{41}\right) \\ & - \frac{\boldsymbol{k}_T^2}{M^2}\Bigg[A_{26} - A_{32} + A_{40} + 2xA_{42} + x^2 A_{41} + \\ & (\sigma - 3x)A_{30} - \left(\frac{(\sigma - 2x)^2}{4} - \frac{\boldsymbol{k}_T^2}{2M^2}\right) A_{44}\Bigg]\Bigg\}\,, \end{aligned} \tag{B.15}$$

$$\begin{aligned} xh_{1LL}^{\perp}(x,\boldsymbol{k}_T^2) \equiv -\frac{2M^2}{3} \int [d\sigma d\tau] \Bigg[& A_{26} - A_{32} + (\sigma - 3x)A_{30} \\ & - \left(\frac{(\sigma - 2x)^2}{4} - \frac{\boldsymbol{k}_T^2}{2M^2}\right) A_{44}\Bigg]\,, \end{aligned} \tag{B.16}$$

$$\begin{aligned} xf_{1LT}(x,\boldsymbol{k}_T^2) \equiv -M^2 \int [d\sigma d\tau] \Bigg\{ & A_{37} + xA_{35} + \left(\frac{\sigma}{2} - x\right)\left(A_{40} + 2xA_{42} + x^2 A_{41}\right) \\ & - \frac{\boldsymbol{k}_T^2}{4M^2}\left[A_{30} + \left(x - \frac{\sigma}{2}\right) A_{44}\right]\Bigg\}\,, \end{aligned} \tag{B.17}$$

$$xg_{1LT}(x,\boldsymbol{k}_T^2) \equiv -\frac{M^2}{2} \int [d\sigma d\tau] \left[A_{29} + \left(x - \frac{\sigma}{2}\right)(A_{33} + xA_{31})\right], \tag{B.18}$$

$$\begin{aligned} xh_{1LT}(x,\boldsymbol{k}_T^2) \equiv \frac{M^2}{2} \int [d\sigma d\tau] \Bigg\{ & A_{28} + xA_{26} + \left(\frac{\sigma}{2} - x\right)(A_{32} + xA_{30}) \\ & + \frac{\boldsymbol{k}_T^2}{2M^2}\left[A_{30} + \left(x - \frac{\sigma}{2}\right) A_{44}\right]\Bigg\}\,, \end{aligned} \tag{B.19}$$

$$xh_{1LT}^{\perp}(x,\boldsymbol{k}_T^2) \equiv -M^2 \int [d\sigma d\tau] \left[A_{30} + \left(x - \frac{\sigma}{2}\right) A_{44}\right], \tag{B.20}$$

$$xf_{1TT}(x,\boldsymbol{k}_T^2) \equiv \frac{M^2}{2}\int [d\sigma d\tau]\left(A_{40}+2xA_{42}+x^2A_{41}+\frac{\boldsymbol{k}_T^2}{6M^2}A_{44}\right), \tag{B.21}$$

$$xg_{1TT}(x,\boldsymbol{k}_T^2) \equiv \frac{M^2}{2}\int [d\sigma d\tau]\left(A_{33}+xA_{31}\right), \tag{B.22}$$

$$xh_{1TT}(x,\boldsymbol{k}_T^2) \equiv -\frac{M^2}{2}\int [d\sigma d\tau]\left[A_{27}+2xA_{28}+x^2A_{26}+\frac{\boldsymbol{k}_T^2}{M^2}\left(A_{32}+xA_{30}\right) - \frac{\boldsymbol{k}_T^4}{4M^4}A_{44}\right], \tag{B.23}$$

$$xh_{1TT}^{\perp}(x,\boldsymbol{k}_T^2) \equiv \frac{M^2}{2}\int [d\sigma d\tau]\left(A_{32}+xA_{30}-\frac{\boldsymbol{k}_T^2}{3M^2}A_{44}\right), \tag{B.24}$$

$$xh_{1TT}^{\perp\perp}(x,\boldsymbol{k}_T^2) \equiv \frac{M^2}{2}\int [d\sigma d\tau]\, A_{44}. \tag{B.25}$$

B.2 The Wilson loop correlator

For the Wilson loop correlator, translation invariance in the $\xi{\cdot}P$ direction forces $k{\cdot}n = x$ to be zero and the integration over x is actually naturally the first to be done, even before the integration over $k{\cdot}P$. The remaining dependence is on the invariant k^2, which for vanishing x is just $k^2 = k_T^2 = -\boldsymbol{k}_T^2$. The parametrization of the Wilson loop correlator for the various types of polarization in Eq. (3.47) depend on $t = k^2$ and reads:

$$\begin{aligned}\Gamma_0^{[U,U6\prime]}(k;P,S,T,n) =& \frac{B_1}{M^2}+\frac{B_2}{M^3}\epsilon^{nPkS}+\frac{B_3}{M^4}k_\mu k_\nu T^{\mu\nu} \\ &+ B_4 n_\mu n_\nu T^{\mu\nu}+\frac{B_5}{M^4}k_\mu n_\nu T^{\mu\nu}.\end{aligned} \tag{B.26}$$

The TMDs in the parametrization are related to the coefficients B_i as follows:

$$e(\boldsymbol{k}_T^2) \equiv \frac{M^2}{2\pi L}\int dx\, d\sigma\, B_1, \tag{B.27}$$

$$e_T(\boldsymbol{k}_T^2) \equiv \frac{M^2}{2\pi L}\int dx\, d\sigma\, B_2, \tag{B.28}$$

$$e_{LL}(\boldsymbol{k}_T^2) \equiv -\frac{M^2}{4\pi L}\int dx\, d\sigma\left[2B_4+(\sigma-2x)B_5+\left(\frac{(\sigma-2x)^2}{2}-\frac{\boldsymbol{k}_T^2}{M^2}\right)B_3\right], \tag{B.29}$$

$$e_{LT}(\boldsymbol{k}_T^2) \equiv -\frac{M^2}{4\pi L}\int dx\, d\sigma\left[B_5+(\sigma-2x)B_3\right], \tag{B.30}$$

$$e_{TT}(\boldsymbol{k}_T^2) \equiv \frac{M^2}{4\pi L} \int dx\, d\sigma\, B_3. \tag{B.31}$$

Appendix C

Summary

No problem is too small or too trivial if you can really do something about it.
R. Feynman

The great challenge of modern physics is to discover the fundamental constituents of the universe and explain how they behave and interact to eventually build the world in the form we see it. Since the earliest days of the modern science history (which dates back to the beginning of the 17th century when Galileo Galilei established the scientific methods and started the scientific revolution), the interest for examining deeper and deeper inside every object, in order to reach their building blocks, has never stopped. The first tools constructed to zoom in an object were simple systems of two curved lenses, but they soon were replaced by more sophisticated arrangements of lenses that led to the first optical microscopes.

When people became able to almost "observe" the atoms, it was soon realized that microscopes would have not allowed to diving into the subatomic matter, and some other tools were needed to enter the scene. Scattering processes between molecules and atoms were found to be perfect for accessing subatomic structures. The experiment of Rutherford, in the first decade of the 20th century, is the first of this type and it led to the discovery of the structure of the atom. Nowadays, a century after the Rutherford experiments, the scattering of particles off a target and the collisions between particles are still the best magnifiers ever devised by mankind and the most used tool to access

subatomic and subnuclear structures.

In this dissertation, we want to contribute to the field of *hadronic* physics by studying the internal structure of subatomic particles called *hadrons*. They are not elementary particles but they are built from elementary (point-like) constituents: *quarks* and *gluons*. Despite being extremely small (about a hundred of million times smaller than a human blood cell, for instance), in the landscape of the subatomic particles hadrons are "large" objects and their internal structure deserves to be studied. At least, we want to study hadrons such as protons and neutrons because they constitute the nuclei and the great majority of the visible matter.

What is special about hadrons is that their "macroscopic" properties are determined by the elementary constituents in a way that is not directly calculable. Interestingly enough, the mass of the proton originates from a rather complex interplay of different dynamical contributions and cannot be explained as a simple "sum" of the masses of its substructures. Quarks and gluons are *confined* inside their hadronic box and they have never been observed experimentally as free particles.

The difficulty in describing the proton and the other hadrons in high-energy scattering processes is due to the unicity of the interaction that governs its constituents. The theory that describes this interaction is called Quantum ChromoDynamics (QCD). Loosely speaking, QCD describes the interaction between quarks and gluons inside the hadrons, collectively called *partons*, through their *color charge*. This is conceptually similar to describing the interactions between electrons by means of their *electric charge*. The peculiarity of QCD is that the strength of the interaction varies considerably with the distances, being large at large distances and progressively becoming smaller as the distance decreases. If we could directly look inside the hadrons at very small distances, we would see an infinite number of almost free partons, that are oblivious of each other because their interaction is very weak. This regime of QCD is called *asymptotic freedom*. As soon as the distance gradually increases, asymptotically free partons are replaced by strongly coupled constituents, and because the intensity of the interaction is very strong, the partons remain confined inside the hadrons and they cannot escape. This phenomenon is called *confinement*.

The concept according to which a "macroscopic" object can manifest itself differently depending on the length scale at which it is observed is something that scientists have always been familiar with. For instance, if we zoom in molecules and atoms (the main objects studied by chemistry and atomic physics) new pictures can be resolved in terms of electrons and nuclei. These constituents can be observed and measured and they become the main elements in terms of which we can describe atoms and molecules. Proceeding towards smaller distances inside the nuclei, we eventually en-

counter the protons and nucleons, solid containers of the color interaction. Differently from the cases in which the substructures are free and can be observed through more and more powerful magnifiers, in the case of QCD the partons live freely only inside the hadrons and cannot manifest themselves as free particles in the experiments. When a scattering process occurs, the partons get kicked out from the parent hadron very energetically, but as soon as they start interacting with each other they immediately recombine themselves into new hadrons. Reading out the information about the hadronic structure from the results of the experiments is a bit of an art: one needs an optimal interplay between the theoretical predictions and the experimental results, and these two aspects feed each other continuously.

The fact that the information about the hadron internal structure is not easily and readily accessible does not mean that we cannot do something about it. Building a theoretical framework from first-principles and symmetry arguments allows the physicists to characterize the hadrons and establish which portion of their internal space is being probed in the high-energy process.

The quantities that contain the information about a specific portion of the hadron space are *multidimensional* functions that depend on the kinematical variables of the partons. For instance, the information about the momentum carried by each parton along the direction of motion of the parent hadron is encoded in the *parton distribution functions* (PDFs), while the complete information on the motion of each parton in the three-dimensional momentum-space is contained in the *transverse-momentum-dependent parton distributions* (TMDs). The above-mentioned functions contain *single parton* information, and they neglect aspects deriving from looking at multiple partons at the same time. The latter information is typical of the *double parton distributions* (DPDs), which also take into account the distribution and correlation between pairs of partons. DPDs are accessible in experiments in which two partons from the same hadron are kicked out simultaneously to participate into two distinct high-energetic scatterings.

Parton distributions also account for the fact that partons have quantum properties other than color charge. Most importantly for the purposes of this thesis, partons carry *spin*, one of the most intriguing quantum mechanical properties of each particle. The spin of an elementary particle does not refer to any property in the physical space (there is no actual rotation involved), but to the intrinsic nature of the particle. However, with some caution one can visualize quarks and gluons inside the hadrons as a bunch of "spinning" toys as in Fig. C.1. When they all spin randomly, no preferred rotational direction can be selected and the spin states are averaged out as if none of the parton carried spin. On the other hand, when there is a neat majority of

Figure C.1: A basket full of tops, like the partons that carry spin inside the proton. Their velocity distributions in the three-dimensional basket space is described by the Transverse-momentum dependent distribution functions (TMDs). The probability of being extracted pairwise from the basket is described by the double parton distributions (DPDs)

partons whose spin states "point" towards a specific direction, i.e. they are *polarized*, then their distributions and dynamics inside the parent hadron are actually modified. The effect of spin can generate distortions and asymmetries that can be studied and characterized.

In this thesis, we focused on the TMDs and DPDs to study the properties of the polarized quarks and gluons inside the hadrons. Throughout the chapters we have presented our original results and in the following we summarize the most relevant ones.

- TMDs: we have studied the TMD functions that describe the gluons inside the hadrons. The quantities that are related to gluons are difficult to study thoroughly because the experimental information on them is currently very limited. They become the dominant entities only when the energy increases. At present, none of the existing facilities around the world is tailored to access this regime of energies. For the first time, we have defined the TMD functions that describe polarized gluons inside hadrons that have spin-1 (for example the deuteron, which is a system of a proton and a neutron) and derived the relations between these functions that will be useful for future experiments. We have also predicted and shown that, when the energy drastically increases, only a few of the numerous gluon functions survive and become relevant.

- DPDs: we have studied the correlations between pairs of quarks inside the proton. Extending the description from a single to a double parton description is a unique opportunity to grasp the structure of the hadrons with nonstandard (multipartonic) eyes. Also in this case, the experimental information on the double parton scattering processes is still very limited. We have focused on the theoretical framework that describes inter-parton correlation and we have carefully analyzed the possibility of measuring for the first time quantities that will be a clear sign of parton correlations at the Large Hadron Collider (LHC) in the near future.

The result of the combination of different parton distributions is similar to a mosaic: each piece comes from a different place and occupies a relevant position on its own, but the final picture is complete only once all the tiles are combined.

Appendix D

Riassunto

Nessun problema è troppo piccolo o troppo irrilevante
se possiamo fare qualcosa per risolverlo.
R. Feynman

La grande missione della fisica moderna è quella di individuare i costituenti fondamentali dell'universo, descrivere la loro natura e le loro mutue interazioni, al fine di spiegare l'origine del mondo nella forma in cui lo percepiamo. Sin da quando la scienza moderna ha mosso i primi passi (ovvero quando Galileo Galilei nel diciassettesimo secolo formulò il metodo scientifico e sancì l'inizio della rivoluzione scientifica) il tentativo dell'uomo di studiare sempre più approfonditamente la composizione degli oggetti per conoscerne la loro struttura interna non si è mai fermato. Se inizialmente i primi strumenti atti a questo scopo erano semplici lenti curve che riuscivano a ingrandire gli oggetti della vita quotidiana, ben presto vennero realizzati sistemi di lenti molto più complessi, e i primi microscopi iniziarono ad essere utilizzati per osservare oggetti non accessibili dall'occhio umano. Tuttavia, sebbene i microscopi ottici divennero sempre più potenti, si capì che per raggiungere la struttura dell'atomo e la materia subatomica sarebbero stati necessari altri strumenti, e si sentì la necessit di fare nuovi esperimenti che consentissero di addentrarsi sempre più a fondo nella materia. Il primo di questi esperimenti fu condotto da Rutherford agli inizi del 1900. Esso ha portato alla scoperta della struttura dell'atomo mediante un processo di collisione tra le particelle di una sorgente radioattiva e gli atomi di una lamina d'oro. Ancora

oggi, a più di cento anni dall'esperimento di Rutherford, i processi di collisione tra particelle rappresentano le più potenti lenti di ingrandimento mai realizzate dall'uomo per accedere allo studio delle strutture subatomiche e subnucleari.

L'obiettivo di questa tesi è proprio quello di fornire un contributo alla fisica subnucleare e precisamente al campo della fisica *adronica*, branca che studia delle particelle chiamate *adroni*. Si tratta di particelle non elementari che hanno una estensione nello spazio (anche se molto limitato) e contengono delle sottostrutture che sono invece particelle elementari e puntiformi: i *quark* e i *gluoni*. Sebbene gli adroni siano la cosa più piccola che ognuno di noi possa sforzarsi di immaginare (centinaia di milioni di volte più piccoli di una cellula di sangue umano), se considerati nella rosa delle particelle subnucleari, essi sono "grandi" e spaziosi e la loro struttura, ancora misteriosa, merita di essere studiata attentamente. D'altra parte, studiare la struttura interna degli adroni assume grande rilevanza se si considera che il protone e il neutrone, che costituiscono la maggior parte della materia ordinaria e che formano tutti i nuclei atomici, sono essi stessi adroni. La peculiarità di dette particelle è che le loro caratteristiche macroscopiche non sono direttamente riconducibili ai loro costituenti elementari. Ne un esempio la massa del protone che viene originata dai sui costituenti interni grazie a dei complessi meccanismi che governano la dinamica del sistema e non può essere ricavata dalla semplice somma delle masse dei suoi costituenti.

Questa difficoltà nello studio degli adroni è in primo luogo riconducibile al fatto che quark e gluoni, collettivamente chiamati *partoni*, interagiscono in modo alquanto singolare. La teoria che descrive questa interazione fondamentale è chiamata CromoDinamica Quantistica (QCD). La QCD descrive essenzialmente la capacità dei partoni di interagire tra loro grazie ad una proprietà chiamata *colore*. La situazione è analoga alla capacità delle particelle elettricamente cariche di interagire tra di loro perché dotate di una proprietà detta *carica elettrica*. La particolarità della QCD risiede nel fatto che l'intensità della interazione di colore dipende dalla distanza: in particolare le particelle colorate interagiscono in modo molto forte quando sono lontane e in modo debole quando si trovano a breve distanza. Se potessimo direttamente guardare tanto in profondità da raggiungere distanze piccolissime all'interno degli adroni vedremmo un numero enorme di partoni praticamente liberi e non interagenti tra loro. Infatti a queste distanze l'intensità dell'interazione di colore è talmente blanda da rendere i partoni delle entità indipendenti e isolate, incuranti dei propri vicini. Questo regime della QCD è chiamato *libertà asintotica*. Tuttavia, non appena le distanze crescono l'interazione si incrementa moltissimo e i partoni interagiscono intensamente tra loro, tanto da non riuscire ad allontanarsi oltre una certa distanza all'interno dell'adrone stesso, restandone intrappolati. Questo fenomeno per cui i quark e gluoni rimangono

imprigionati dentro la loro scatola adronica è chiamato *confinamento* ed è responsabile del fatto che nessuna di queste particelle possa raggiungere i rivelatori di particelle ed essere direttamente misurata in laboratorio.

Il principio secondo cui un oggetto si palesa in modo differente a seconda di quanto vicino lo si guarda non è affatto nuovo ai fisici, che hanno sempre avuto a che fare con strutture che contengono al loro interno delle sottostrutture. Basti pensare alle molecole e gli atomi (studiati in chimica e fisica atomica): quando li si guarda da una certa distanza essi appaio come oggetti compatti, ma appena ci si avvicina la loro sottostruttura, composta di elettroni e nuclei, viene rivelata e la loro descrizione fisica cambia. Se si fa un'ulteriore zoom sui nuclei atomici ci si imbatte immediatamente nei protoni e i neutroni, ovvero i contenitori ermetici dell'interazione di colore. Al contrario del caso precedente, in cui le sottostrutture sono accessibili e misurabili, nel caso del protone e del neutrone i costituenti vivono unicamente dentro le scatole adroniche e non possono essere osservati come particelle libere. Durante gli esperimenti di collisione con gli adroni, i partoni vengono sbalzati fuori energeticamente ma non appena tentano di sfuggire e allontanarsi la loro interazione di colore diventa talmente forte da fare in modo che essi si assemblino immediatamente sotto forma di nuovi adroni. Interpretare e usare le informazioni che vengono da questi esperimenti è un'operazione molto delicata, in quanto è necessario possedere una ottima conoscenza teorica per fare predizioni dei risultati sperimentali e, allo stesso tempo, bisogna estrarre continuamente informazioni dagli esperimenti per ottenere predizioni più affidabili. Ne consegue che una conoscenza teorica il più completa possibile ci permette di capire quale porzione dello spazio interno degli adroni può essere studiata in un certo esperimento.

Le quantità che definiamo per descrivere le informazioni sulla struttura interna delle particelle sono delle funzioni *multidimensionali* che dipendono dalle variabili cinematiche dei partoni stessi. Per esempio, la distribuzione della velocità dei partoni lungo la direzione del moto del protone è descritta dalle *funzioni di distribuzione partoniche* (PDF), mentre la stessa informazione estesa a uno spazio tridimensionale delle velocità è contenuta nelle *funzioni di distribuzioni partoniche dipendenti dal momento transverso* (TMD). Le PDF e TMD sono dunque quantità che descrivono l'interno del protone in termini di un *singolo partone* alla volta e ignorano gli effetti derivanti dall'analisi di due o più partoni contemporaneamente. Quest'ultima informazione è tipica delle *funzioni di distribuzioni a due partoni* (DPD), che tengono in considerazione proprio le coppie di partoni, aprendo di fatto la strada allo studio delle correlazioni tra i partoni. Le DPD, inoltre, sono misurabili in esperimenti in cui due partoni vengono sbalzati fuori dal protone contemporaneamente e partecipano a due

Figure D.1: Un cesto di trottole, che simboleggiano i partoni con spin all'interno del protone. La distribuzione delle velocità delle trottole nello spazio tridimensionale è descritto dalle funzioni TMD. La probabilità che una coppia di trottole con un certo spin venga estratta dal cesto è descritta dalle funzioni DPD.

processi indipendenti di collisione ad alta energia.

Le funzioni di distribuzione partonica tengono anche conto delle proprietà quantistiche dei partoni (e degli adroni). Oltre alla carica di colore, i partoni hanno anche lo *spin*, una delle proprietà più affascinanti della descrizione quantistica delle particelle. A dispetto del nome (che suggerirebbe una rotazione), lo spin non ha in realtà nulla a che vedere con una rotazione fisica della particella, ma, al contrario, si riferisce a una sua proprietà intrinseca. Con un po' di cautela nell'interpretazione, possiamo tuttavia immaginare le particelle con spin come fossero delle trottole come in Fig. D.1; del resto la descrizione puramente matematica dello spin è in effetti analoga a quella dei momenti angolari. Per capire il ruolo dello spin dei partoni nello studio della struttura degli adroni basti considerare la seguente situazione. Quando i partoni ruotano in maniera casuale non c'è nessuna direzione di rotazione preferenziale nella collettività dei partoni e una media sugli stati di spin equivale a dire che lo spin dei partoni non ha globalmente alcun effetto nel loro moto interno. Al contrario, quando la rotazione delle trottole predilige una direzione anziché un'altra, allora si ha una *polarizzazione* netta dei partoni all'interno dell'adrone e questa proprietà modifica effettivamente la distribuzione dei costituenti, generando ad esempio delle distorsioni e delle asimmetrie che possono essere studiate e caratterizzate di volta in volta.

In questa tesi ci siamo concentrati proprio sullo studio dei partoni polarizzati

tramite lo studio delle funzioni TMD e DPD. Nel corso dei capitoli abbiamo presentato i risultati originali, di cui nel seguito riassumiamo i passi pi importanti:

- TMDs: abbiamo studiato le funzioni TMD che descrivono i gluoni all'interno degli adroni. Le quantità relative ai gluoni sono complesse da studiare perché le informazioni che ricaviamo dagli esperimenti sono molto limitate. Queste quantità diventano rilevanti quando si va ad alte energie, ma a tutt'oggi nessuno degli acceleratori esistenti è in grado di dare accesso alle regioni dove i gluoni sono più "visibili". Abbiamo per la prima volta definito le funzioni TMD che descrivono i gluoni all'interno degli adroni con spin uguale a 1 (ad esempio il deutone, che è un nucleo atomico formato da un protone e un neutrone). Abbiamo derivato delle relazioni tra le TMD dei gluoni che saranno utili per le future estrazioni sperimentali di alcune di queste funzioni. Infine, abbiamo mostrato che, ad energie molto elevate, non tutte le TMD dei gluoni sono importanti, ma soltanto alcune tra queste.

- DPDs: abbiamo studiato le correlazioni di coppia tra partoni, cosa possibile grazie al formalismo delle DPDs. Questa informazione a due partoni permette di guardare al protone con uno sguardo meno standard rispetto che alle funzioni di singolo partone. Anche in questo caso i dati sperimentali a disposizione sono molto limitati. Abbiamo quindi studiato una strategia ottimale per osservare le correlazioni a due partoni dovute allo spin in un prossimo futuro all'acceleratore LHC di Ginevra.

Concludendo, il processo di raccolta di informazione sulla struttura interna degli adroni tramite le funzioni di distribuzione partoniche è paragonabile alla creazione di un mosaico: ogni funzione arriva da un posto diverso ed occupa una posizione a sé stante, ma l'opera finale sarà completa solo quando tutti i tasselli verranno messi insieme.

Acknowledgements

I would like to thank all the people that have been involved in the realization of this thesis and those who have contributed in different ways to my growing as a scientist.

I want to thank my supervisor Piet Mulders, for his precious guidance and continuous encouragements. Thank you very much Piet, I am very grateful for the time you devoted discussing and explaining things to me. I have been sincerely inspired by your knowledge and expertise and I admire your great passion and enthusiasm.

Thanks to the members of the reading committee Daniël Boer, Eric Laenen, Cédric Lorcé, Tomas Kasemets, Barbara Pasquini, and Gerhard Raven for the time they spent in reviewing my manuscript, for the valuable feedback and comments.

Thanks to all the people I had the pleasure to collaborate with during the past years, especially Tomas Kasemets, Miroslav Myska, Alessandro Bacchetta, Barbara Pasquini, Daniël Boer, Andrea Signori, Tom van Daal, Yajin Zhou, and for the fruitful discussions with Cristian Pisano, Guy de Teramond, Cédric Lorcé, Elena Petreska, Maarten Buffing, Marco Radici, Miguel G. Echevarria.

I am especially grateful to Alessandro Bacchetta and Barbara Pasquini for the help and the support over the years and across the countries.

Thanks to all the members of the Theory Group at Nikhef for the warm atmosphere and the recharging coffee breaks.

Finally, I want to thank my paranimphs, colleagues, friends and family for sharing with me all the highs and lows of the past four years.

Bibliography

[1] D. J. Gross and F. Wilczek, *Ultraviolet Behavior of Nonabelian Gauge Theories*, *Phys. Rev. Lett.* **30** (1973) 1343–1346.

[2] D. J. Gross and F. Wilczek, *Asymptotically Free Gauge Theories - I*, *Phys. Rev.* **D8** (1973) 3633–3652.

[3] Y. Ne'eman, *Derivation of strong interactions from a gauge invariance*, *Nucl. Phys.* **26** (1961) 222–229.

[4] M. Gell-Mann, *A Schematic Model of Baryons and Mesons*, *Phys. Lett.* **8** (1964) 214–215.

[5] CMS collaboration, V. Khachatryan et al., *Measurement of the inclusive 3-jet production differential cross section in protonproton collisions at 7 TeV and determination of the strong coupling constant in the TeV range*, *Eur. Phys. J.* **C75** (2015) 186, [1412.1633].

[6] S. J. Brodsky, H.-C. Pauli and S. S. Pinsky, *Quantum chromodynamics and other field theories on the light cone*, *Phys.Rept.* **301** (1998) 299–486, [hep-ph/9705477].

[7] R. L. Jaffe and A. Manohar, *The G(1) Problem: Fact and Fantasy on the Spin of the Proton*, *Nucl. Phys.* **B337** (1990) 509–546.

[8] X.-D. Ji, *Gauge-Invariant Decomposition of Nucleon Spin*, *Phys. Rev. Lett.* **78** (1997) 610–613, [hep-ph/9603249].

[9] R. P. Feynman, *Very high-energy collisions of hadrons*, *Phys. Rev. Lett.* **23** (1969) 1415–1417.

[10] J. D. Bjorken and E. A. Paschos, *Inelastic Electron Proton and gamma Proton Scattering, and the Structure of the Nucleon*, *Phys. Rev.* **185** (1969) 1975–1982.

[11] H. D. Politzer, *Power Corrections at Short Distances*, *Nucl. Phys.* **B172** (1980) 349.

[12] CTEQ collaboration, R. Brock et al., *Handbook of perturbative QCD: Version 1.0*, *Rev. Mod. Phys.* **67** (1995) 157–248.

[13] J. C. Collins, D. E. Soper and G. Sterman, *Factorization for one loop corrections in the drell-yan process*, *Nucl. Phys.* **B223** (1983) 381.

[14] J. C. Collins, D. E. Soper and G. F. Sterman, *Transverse Momentum Distribution in Drell-Yan Pair and W and Z Boson Production*, *Nucl. Phys.* **B250** (1985) 199.

[15] J. Collins, *Foundations of perturbative QCD*. Cambridge University Press, 2011.

[16] X.-d. Ji, J.-p. Ma and F. Yuan, *Qcd factorization for semi-inclusive deep-inelastic scattering at low transverse momentum*, *Phys. Rev.* **D71** (2005) 034005, [hep-ph/0404183].

[17] J. Collins and J.-W. Qiu, *kt factorization is violated in production of high-transverse-momentum particles in hadron-hadron collisions*, *Phys. Rev.* **D75** (2007) 114014, [arXiv:0705.2141 [hep-ph]].

[18] D. Boer, S. J. Brodsky, P. J. Mulders and C. Pisano, *Direct Probes of Linearly Polarized Gluons inside Unpolarized Hadrons*, *Phys.Rev.Lett.* **106** (2011) 132001, [1011.4225].

[19] T. C. Rogers and P. J. Mulders, *No Generalized TMD-Factorization in Hadro-Production of High Transverse Momentum Hadrons*, *Phys. Rev.* **D81** (2010) 094006, [1001.2977].

[20] P. J. Mulders and T. C. Rogers, *Gauge Links, TMD-Factorization, and TMD-Factorization Breaking*, 1102.4569.

[21] T. C. Rogers, *Extra spin asymmetries from the breakdown of transverse-momentum-dependent factorization in hadron-hadron collisions*, *Phys. Rev.* **D88** (2013) 014002, [1304.4251].

[22] M. Diehl, J. R. Gaunt, D. Ostermeier, P. Plößl and A. Schäfer, *Cancellation of Glauber gluon exchange in the double Drell-Yan process*, *JHEP* **01** (2016) 076, [1510.08696].

[23] M. G. A. Buffing, M. Diehl and T. Kasemets, *Transverse momentum in double parton scattering: factorisation, evolution and matching*, *JHEP* **01** (2018) 044, [1708.03528].

[24] J. C. Collins and A. Freund, *Proof of factorization for deeply virtual Compton scattering in QCD*, *Phys. Rev.* **D59** (1999) 074009, [hep-ph/9801262].

[25] S. Drell and T.-M. Yan, *Massive Lepton Pair Production in Hadron-Hadron Collisions at High-Energies*, *Phys.Rev.Lett.* **25** (1970) 316–320.

[26] F. Pijlman, *Single Spin Asymmetries and Gauge Invariance in Hard Scattering Processes*. PhD thesis, Ph.D. thesis at VU University (Amsterdam), 2006.

[27] D. Boer and C. Pisano, *Polarized gluon studies with charmonium and bottomonium at LHCb and AFTER*, *Phys. Rev.* **D86** (2012) 094007, [1208.3642].

[28] W. J. den Dunnen, *Polarization effects in proton-proton collisions within the Standard model and beyond*. PhD thesis, Vrije U., Amsterdam, 2013.

[29] C. Pisano, D. Boer, S. J. Brodsky, M. G. Buffing and P. J. Mulders, *Linear polarization of gluons and photons in unpolarized collider experiments*, *JHEP* **1310** (2013) 024, [1307.3417].

[30] D. Boer, P. J. Mulders, C. Pisano and J. Zhou, *Asymmetries in Heavy Quark Pair and Dijet Production at an EIC*, 1605.07934.

[31] M. Diehl, D. Ostermeier and A. Schäfer, *Elements of a theory for multiparton interactions in QCD*, *JHEP* **03** (2012) 089, [1111.0910].

[32] T. Kasemets, *Double parton scattering - a tale of two partons*. PhD thesis, Hamburg U., 2013.

[33] M. Diehl and A. Schäfer, *Theoretical considerations on multiparton interactions in QCD*, *Phys. Lett.* **B698** (2011) 389–402, [1102.3081].

[34] K. G. Wilson, *Confinement of Quarks*, *Phys. Rev.* **D10** (1974) 2445–2459.

[35] Y. Aharonov and D. Bohm, *Significance of electromagnetic potentials in the quantum theory*, *Phys. Rev.* **115** (1959) 485–491.

[36] M. Peskin and D. Schroeder, *An introduction to Quantum Field Theory*. Westview Press, 1995.

[37] A. V. Efremov and A. V. Radyushkin, *Field theoretic treatment of high momentum transfer processes. 3. Gauge theories*, *Theor. Math. Phys.* **44** (1981) 774.

[38] X.-d. Ji and F. Yuan, *Parton distributions in light-cone gauge: Where are the final-state interactions?*, *Phys. Lett.* **B543** (2002) 66–72, [hep-ph/0206057].

[39] A. V. Belitsky, X. Ji and F. Yuan, *Final state interactions and gauge invariant parton distributions*, *Nucl. Phys.* **B656** (2003) 165–198, [hep-ph/0208038].

[40] D. Boer, P. J. Mulders and F. Pijlman, *Universality of T-odd effects in single spin and azimuthal asymmetries*, *Nucl. Phys.* **B667** (2003) 201–241, [hep-ph/0303034].

[41] C. J. Bomhof, P. J. Mulders and F. Pijlman, *Gauge link structure in quark quark correlators in hard processes*, *Phys. Lett.* **B596** (2004) 277–286, [hep-ph/0406099].

[42] C. J. Bomhof, P. J. Mulders and F. Pijlman, *The construction of gauge-links in arbitrary hard processes*, *Eur. Phys. J.* **C47** (2006) 147–162, [hep-ph/0601171].

[43] C. J. Bomhof and P. J. Mulders, *Non-universality of transverse momentum dependent parton distribution functions*, *Nucl. Phys.* **B795** (2008) 409–427, [0709.1390].

[44] M. Buffing and P. Mulders, *Gauge links for transverse momentum dependent correlators at tree-level*, *JHEP* **1107** (2011) 065, [1105.4804].

[45] M. Buffing, A. Mukherjee and P. Mulders, *Generalized Universality of Higher Transverse Moments of Quark TMD Correlators*, *Phys.Rev.* **D86** (2012) 074030, [1207.3221].

[46] M. G. A. Buffing, P. J. Mulders and A. Mukherjee, *Universality of Quark and Gluon TMD Correlators*, *Int. J. Mod. Phys. Conf. Ser.* **25** (2014) 1460003, [1309.2472].

[47] F. Dominguez, C. Marquet, B.-W. Xiao and F. Yuan, *Universality of Unintegrated Gluon Distributions at small x*, *Phys. Rev.* **D83** (2011) 105005, [1101.0715].

[48] M. G. A. Buffing, A. Mukherjee and P. J. Mulders, *Generalized Universality of Definite Rank Gluon Transverse Momentum Dependent Correlators*, *Phys. Rev.* **D88** (2013) 054027, [1306.5897].

[49] C. J. Bomhof, *Azimuthal Spin Asymmetries in Hadronic Processes*. PhD thesis, Ph.D. thesis at VU University (Amsterdam), 2007.

[50] M. G. A. Buffing, *Color and TMD Universality in Hadronic Interactions*. PhD thesis, NIKHEF, Amsterdam, 2015-09-02.

[51] D. Boer and P. J. Mulders, *Time-reversal odd distribution functions in leptoproduction*, *Phys. Rev.* **D57** (1998) 5780–5786, [hep-ph/9711485].

[52] M. Mekhfi and X. Artru, *Sudakov Suppression of Color Correlations in Multiparton Scattering*, *Phys. Rev.* **D37** (1988) 2618–2622.

[53] G. Martinelli and C. T. Sachrajda, *A Lattice Study of Nucleon Structure*, *Nucl. Phys.* **B316** (1989) 355–372.

[54] P. Hagler, *Hadron structure from lattice quantum chromodynamics*, *Phys. Rept.* **490** (2010) 49–175, [0912.5483].

[55] B. U. Musch, P. Hagler, J. W. Negele and A. Schäfer, *Exploring quark transverse momentum distributions with lattice QCD*, *Phys. Rev.* **D83** (2011) 094507, [1011.1213].

[56] H.-W. Lin et al., *Parton distributions and lattice QCD calculations: a community white paper*, *Prog. Part. Nucl. Phys.* **100** (2018) 107–160, [1711.07916].

[57] B. Yoon, M. Engelhardt, R. Gupta, T. Bhattacharya, J. R. Green, B. U. Musch et al., *Nucleon Transverse Momentum-dependent Parton Distributions in Lattice QCD: Renormalization Patterns and Discretization Effects*, *Phys. Rev.* **D96** (2017) 094508, [1706.03406].

[58] A. Bacchetta, F. Conti and M. Radici, *Transverse-momentum distributions in a diquark spectator model*, *Phys. Rev.* **D78** (2008) 074010, [0807.0323].

[59] B. Pasquini, S. Cazzaniga and S. Boffi, *Transverse momentum dependent parton distributions in a light-cone quark model*, *Phys. Rev.* **D78** (2008) 034025, [0806.2298].

[60] S. Boffi, A. V. Efremov, B. Pasquini and P. Schweitzer, *Azimuthal spin asymmetries in light-cone constituent quark models*, *Phys. Rev.* **D79** (2009) 094012, [0903.1271].

[61] C. Lorcé, B. Pasquini and M. Vanderhaeghen, *Unified framework for generalized and transverse-momentum dependent parton distributions within a 3Q light-cone picture of the nucleon*, *JHEP* **05** (2011) 041, [1102.4704].

[62] B. Pasquini and P. Schweitzer, *Pion TMDs in light-front constituent approach, and Boer-Mulders effect in the pion-induced Drell-Yan process*, *Phys.Rev.* **D90** (2014) 014050, [1406.2056].

[63] A. V. Efremov, P. Schweitzer, O. V. Teryaev and P. Zavada, *The relation between TMDs and PDFs in the covariant parton model approach*, *Phys. Rev.* **D83** (2011) 054025, [1012.5296].

[64] H. Avakian, A. V. Efremov, P. Schweitzer and F. Yuan, *The transverse momentum dependent distribution functions in the bag model*, *Phys. Rev.* **D81** (2010) 074035, [1001.5467].

[65] Y. Ninomiya, W. Bentz and I. C. Cloët, *TMDs of Spin-one Targets: Formalism and Covariant Calculations*, 1707.03787.

[66] A. Bacchetta, S. Cotogno and B. Pasquini, *The transverse structure of the pion in momentum space inspired by the AdS/QCD correspondence*, *Phys. Lett.* **B771** (2017) 546–552, [1703.07669].

[67] R. Angeles-Martinez et al., *Transverse Momentum Dependent (TMD) parton distribution functions: status and prospects*, *Acta Phys. Polon.* **B46** (2015) 2501–2534, [1507.05267].

[68] J. Collins, *The non-triviality of the vacuum in light-front quantization: An elementary treatment*, 1801.03960.

[69] P. A. Dirac, *Forms of Relativistic Dynamics*, *Rev.Mod.Phys.* **21** (1949) 392–399.

[70] S. Weinberg, *Dynamics at infinite momentum*, *Phys.Rev.* **150** (1966) 1313–1318.

[71] L. Susskind, *Model of selfinduced strong interactions*, *Phys.Rev.* **165** (1968) 1535–1546.

[72] S.-J. Chang and S.-K. Ma, *Feynman rules and quantum electrodynamics at infinite momentum*, *Phys.Rev.* **180** (1969) 1506–1513.

[73] K. Bardakci and M. Halpern, *Theories at infinite momentum*, *Phys.Rev.* **176** (1968) 1686–1699.

[74] J. B. Kogut and D. E. Soper, *Quantum Electrodynamics in the Infinite Momentum Frame*, *Phys. Rev.* **D1** (1970) 2901–2913.

[75] S. Drell, D. J. Levy and T.-M. Yan, *A Theory of Deep Inelastic Lepton-Nucleon Scattering and Lepton Pair Annihilation Processes. 1.*, *Phys.Rev.* **187** (1969) 2159–2171.

[76] S. Drell, D. J. Levy and T.-M. Yan, *A Theory of Deep Inelastic Lepton Nucleon Scattering and Lepton Pair Annihilation Processes. 2. Deep Inelastic electron Scattering*, *Phys.Rev.* **D1** (1970) 1035–1068.

[77] S. Drell, D. J. Levy and T.-M. Yan, *A Theory of Deep Inelastic Lepton-Nucleon Scattering and Lepton Pair Annihilation Processes. 3. Deep Inelastic electron-Positron Annihilation*, *Phys.Rev.* **D1** (1970) 1617–1639.

[78] J. C. Collins, *Light cone variables, rapidity and all that*, `hep-ph/9705393`.

[79] D. D. Dietrich, P. Hoyer and M. Jarvinen, *Boosting equal time bound states*, *Phys.Rev.* **D85** (2012) 105016, [`1202.0826`].

[80] D. Müller and D. S. Hwang, *The concept of phenomenological light-front wave functions – Regge improved diquark model predictions*, `1407.1655`.

[81] P. Hoyer, *Bound states – from QED to QCD*, 2014. `1402.5005`.

[82] M. Diehl, T. Feldmann, R. Jakob and P. Kroll, *The Overlap representation of skewed quark and gluon distributions*, *Nucl.Phys.* **B596** (2001) 33–65, [`hep-ph/0009255`].

[83] P. Mulders and R. Tangerman, *The complete tree level result up to order 1/Q for polarized deep inelastic leptoproduction*, *Nucl.Phys.* **B461** (1996) 197–237, [`hep-ph/9510301`].

[84] A. Bacchetta and P. J. Mulders, *Deep inelastic leptoproduction of spin-one hadrons*, *Phys. Rev.* **D62** (2000) 114004, [hep-ph/0007120].

[85] A. Bacchetta, *Probing the Transverse Spin of Quarks in Deep Inelastic Scattering*. PhD thesis, Ph.D. thesis at VU University (Amsterdam), 2002.

[86] P. J. Mulders and J. Rodrigues, *Transverse momentum dependence in gluon distribution and fragmentation functions*, *Phys. Rev.* **D63** (2001) 094021, [hep-ph/0009343].

[87] S. Meißner, A. Metz and K. Goeke, *Relations between generalized and transverse momentum dependent parton distributions*, *Phys. Rev.* **D76** (2007) 034002, [hep-ph/0703176].

[88] D. Boer, S. Cotogno, T. van Daal, P. J. Mulders, A. Signori and Y.-J. Zhou, *Gluon and Wilson loop TMDs for hadrons of spin $\leq$ 1*, *JHEP* **10** (2016) 013, [1607.01654].

[89] W. Detmold and P. E. Shanahan, *Gluonic Transversity from Lattice QCD*, *Phys. Rev.* **D94** (2016) 014507, [1606.04505].

[90] F. Winter, W. Detmold, A. S. Gambhir, K. Orginos, M. J. Savage, P. E. Shanahan et al., *First lattice QCD study of the gluonic structure of light nuclei*, *Phys. Rev.* **D96** (2017) 094512, [1709.00395].

[91] J. Maxwell et al., *Search for Exotic Gluonic States in the Nucleus, A Letter of Intent to Jefferson Lab PAC 44*, 1803.11206.

[92] S. Cotogno, *Parametrization of the Transverse Momentum Dependent Light-Front Correlator for Gluons*, *Few Body Syst.* **58** (2017) 92.

[93] S. Cotogno, T. van Daal and P. J. Mulders, *Positivity bounds on gluon TMDs for hadrons of spin $\leq$ 1*, *JHEP* **11** (2017) 185, [1709.07827].

[94] E. Leader, *Spin in particle physics*, *Camb. Monogr. Part. Phys. Nucl. Phys. Cosmol.* **15** (2011) pp.1–500.

[95] A. Signori, *Flavor and Evolution Effects in TMD Phenomenology*. PhD thesis, Vrije U., Amsterdam, 2016.

[96] K. G. Wilson, *Nonlagrangian models of current algebra*, *Phys. Rev.* **179** (1969) 1499–1512.

[97] R. L. Jaffe, *Spin, twist and hadron structure in deep inelastic processes*, hep-ph/9602236.

[98] T. van Daal, *Quark and gluon TMD correlators in momentum and coordinate space*, in *22nd International Symposium on Spin Physics (SPIN 2016) Urbana, IL, USA, September 25-30, 2016*, 2016. 1612.06585.

[99] P. Hoodbhoy, R. L. Jaffe and A. Manohar, *Novel Effects in Deep Inelastic Scattering from Spin 1 Hadrons*, *Nucl. Phys.* **B312** (1989) 571–588.

[100] M. Boglione and A. Prokudin, *Phenomenology of transverse spin: past, present and future*, *Eur. Phys. J.* **A52** (2016) 154, [1511.06924].

[101] HERMES collaboration, A. Airapetian et al., *Multiplicities of charged pions and kaons from semi-inclusive deep-inelastic scattering by the proton and the deuteron*, *Phys. Rev.* **D87** (2013) 074029, [1212.5407].

[102] J. Ball et al., *On the large COMPASS polarized deuteron target*, *Czech. J. Phys.* **56** (2006) F295–F305.

[103] CDF collaboration, T. Aaltonen et al., *Transverse momentum cross section of e^+e^- pairs in the Z-boson region from $p\bar{p}$ collisions at $\sqrt{s} = 1.96$ TeV*, *Phys. Rev.* **D86** (2012) 052010, [1207.7138].

[104] A. Signori, A. Bacchetta, M. Radici and G. Schnell, *Investigations into the flavor dependence of partonic transverse momentum*, *JHEP* **11** (2013) 194, [1309.3507].

[105] M. Anselmino, M. Boglione, J. O. Gonzalez Hernandez, S. Melis and A. Prokudin, *Unpolarised Transverse Momentum Dependent Distribution and Fragmentation Functions from SIDIS Multiplicities*, *JHEP* **04** (2014) 005, [1312.6261].

[106] U. D'Alesio, M. G. Echevarria, S. Melis and I. Scimemi, *Non-perturbative QCD effects in q_T spectra of Drell-Yan and Z-boson production*, *JHEP* **11** (2014) 098, [1407.3311].

[107] M. G. Echevarria, A. Idilbi, Z.-B. Kang and I. Vitev, *QCD Evolution of the Sivers Asymmetry*, *Phys. Rev.* **D89** (2014) 074013, [1401.5078].

[108] A. Bacchetta, F. Delcarro, C. Pisano, M. Radici and A. Signori, *Extraction of partonic transverse momentum distributions from semi-inclusive deep-inelastic*

scattering, Drell-Yan and Z-boson production, *JHEP* **06** (2017) 081, [1703.10157].

[109] I. Scimemi and A. Vladimirov, *Analysis of vector boson production within TMD factorization*, *Eur. Phys. J.* **C78** (2018) 89, [1706.01473].

[110] D. W. Sivers, *Hard scattering scaling laws for single spin production asymmetries*, *Phys. Rev.* **D43** (1991) 261–263.

[111] J. C. Collins, *Fragmentation of transversely polarized quarks probed in transverse momentum distributions*, *Nucl. Phys.* **B396** (1993) 161–182, [hep-ph/9208213].

[112] S. J. Brodsky, D. S. Hwang and I. Schmidt, *Final-state interactions and single-spin asymmetries in semi-inclusive deep inelastic scattering*, *Phys. Lett.* **B530** (2002) 99–107, [hep-ph/0201296].

[113] J. C. Collins, *Leading-twist single-transverse-spin asymmetries: Drell-Yan and deep-inelastic scattering*, *Phys. Lett.* **B536** (2002) 43–48, [hep-ph/0204004].

[114] HERMES collaboration, A. Airapetian et al., *Single-spin asymmetries in semi-inclusive deep-inelastic scattering on a transversely polarized hydrogen target*, *Phys. Rev. Lett.* **94** (2005) 012002, [hep-ex/0408013].

[115] E.-C. Aschenauer et al., *The RHIC SPIN Program: Achievements and Future Opportunities*, 1501.01220.

[116] L. D. Isenhower et al., *Polarized Drell-Yan measurements with the Fermilab Main Injector*, .

[117] C. Brown et al., *Letter of Intent for a Drell-Yan Experiment with a Polarized Proton Target*, .

[118] A. Bacchetta, A. Courtoy and M. Radici, *First extraction of valence transversities in a collinear framework*, *JHEP* **03** (2013) 119, [1212.3568].

[119] HERMES collaboration, A. Airapetian et al., *First measurement of the tensor structure function b(1) of the deuteron*, *Phys. Rev. Lett.* **95** (2005) 242001, [hep-ex/0506018].

[120] S. Kumano, *Tensor-polarized quark and antiquark distribution functions in a spin-one hadron*, *Phys. Rev.* **D82** (2010) 017501, [1005.4524].

[121] H. Khan and P. Hoodbhoy, *Convenient parametrization for deep inelastic structure functions of the deuteron*, *Phys. Rev.* **C44** (1991) 1219–1222.

[122] G. A. Miller, *Pionic and Hidden-Color, Six-Quark Contributions to the Deuteron b1 Structure Function*, *Phys. Rev.* **C89** (2014) 045203, [1311.4561].

[123] W. Cosyn, Y.-B. Dong, S. Kumano and M. Sargsian, *Tensor-polarized structure function b_1 in standard convolution description of deuteron*, *Phys. Rev.* **D95** (2017) 074036, [1702.05337].

[124] K. Slifer, *The Deuteron Polarized Tensor Structure Function b_1*, *J. Phys. Conf. Ser.* **543** (2014) 012003.

[125] D. Boer et al., *Gluons and the quark sea at high energies: Distributions, polarization, tomography*, 1108.1713.

[126] A. Accardi et al., *Electron Ion Collider: The Next QCD Frontier*, *Eur. Phys. J.* **A52** (2016) 268, [1212.1701].

[127] S. Abeyratne et al., *MEIC Design Summary*, 1504.07961.

[128] K. Goeke, A. Metz, P. V. Pobylitsa and M. V. Polyakov, *Lorentz invariance relations among parton distributions revisited*, *Phys. Lett.* **B567** (2003) 27–30, [hep-ph/0302028].

[129] R. L. Jaffe and A. Manohar, *Nuclear gluonometry*, *Phys. Lett.* **B223** (1989) 218.

[130] X. Artru and M. Mekhfi, *Transversely Polarized Parton Densities, their Evolution and their Measurement*, *Z. Phys.* **C45** (1990) 669.

[131] D. Boer, M. G. Echevarria, P. Mulders and J. Zhou, *Single spin asymmetries from a single Wilson loop*, *Phys. Rev. Lett.* **116** (2016) 122001, [1511.03485].

[132] D. Boer, T. Van Daal, P. J. Mulders and E. Petreska, *Directed flow from C-odd gluon correlations at small x*, 1805.05219.

[133] S. J. Brodsky, F. Fleuret, C. Hadjidakis and J. P. Lansberg, *Physics Opportunities of a Fixed-Target Experiment using the LHC Beams*, *Phys. Rept.* **522** (2013) 239–255, [1202.6585].

[134] L. Massacrier et al., *Physics perspectives with AFTER@LHC (A Fixed Target ExpeRiment at LHC)*, *EPJ Web Conf.* **171** (2018) 10001, [1712.01740].

[135] D. Kikola, M. G. Echevarria, C. Hadjidakis, J.-P. Lansberg, C. Lorcé, L. Massacrier et al., *Feasibility Studies for Single Transverse-Spin Asymmetry Measurements at a Fixed-Target Experiment Using the LHC Proton and Lead Beams (AFTER@LHC)*, *Few Body Syst.* **58** (2017) 139, [1702.01546].

[136] D. Boer, W. J. den Dunnen, C. Pisano and M. Schlegel, *Determining the Higgs spin and parity in the diphoton decay channel*, *Phys. Rev. Lett.* **111** (2013) 032002, [1304.2654].

[137] M. G. Echevarria, T. Kasemets, P. J. Mulders and C. Pisano, *QCD evolution of (un)polarized gluon TMDPDFs and the Higgs q_T-distribution*, *JHEP* **07** (2015) 158, [1502.05354].

[138] D. Boer, W. J. den Dunnen, C. Pisano, M. Schlegel and W. Vogelsang, *Linearly Polarized Gluons and the Higgs Transverse Momentum Distribution*, *Phys. Rev. Lett.* **108** (2012) 032002, [1109.1444].

[139] J.-W. Qiu, M. Schlegel and W. Vogelsang, *Probing Gluonic Spin-Orbit Correlations in Photon Pair Production*, *Phys. Rev. Lett.* **107** (2011) 062001, [1103.3861].

[140] W. J. den Dunnen, J. P. Lansberg, C. Pisano and M. Schlegel, *Accessing the Transverse Dynamics and Polarization of Gluons inside the Proton at the LHC*, *Phys. Rev. Lett.* **112** (2014) 212001, [1401.7611].

[141] J.-P. Lansberg and H.-S. Shao, *Double-quarkonium production at a fixed-target experiment at the LHC (AFTER@LHC)*, *Nucl. Phys.* **B900** (2015) 273–294, [1504.06531].

[142] J.-P. Lansberg, C. Pisano and M. Schlegel, *Associated production of a dilepton and a $\Upsilon(J/\psi)$ at the LHC as a probe of gluon transverse momentum dependent distributions*, *Nucl. Phys.* **B920** (2017) 192–210, [1702.00305].

[143] D. Boer, C. Lorcé, C. Pisano and J. Zhou, *The gluon Sivers distribution: status and future prospects*, *Adv. High Energy Phys.* **2015** (2015) 371396, [1504.04332].

[144] J.-W. Qiu and G. Sterman, *Single transverse spin asymmetries*, *Phys. Rev. Lett.* **67** (1991) 2264–2267.

[145] J.-W. Qiu and G. Sterman, *Single transverse-spin asymmetries in hadronic pion production*, *Phys. Rev.* **D59** (1999) 014004, [hep-ph/9806356].

[146] R. D. Ball, V. Bertone, M. Bonvini, S. Marzani, J. Rojo and L. Rottoli, *Parton distributions with small-x resummation: evidence for BFKL dynamics in HERA data*, *Eur. Phys. J.* **C78** (2018) 321, [1710.05935].

[147] Y. V. Kovchegov and E. Levin, *Quantum chromodynamics at high energy*, vol. 33. Cambridge University Press, 2012.

[148] X. Artru, M. Elchikh, J.-M. Richard, J. Soffer and O. V. Teryaev, *Spin observables and spin structure functions: inequalities and dynamics*, *Phys. Rept.* **470** (2009) 1–92, [0802.0164].

[149] W. Detmold, R. Jaffe, J. Maxwell, R. Milner, D. Crabb, D. Day et al., *Letter of intent*, *Jefferson Lab* **LOI12-14-001** (2014) .

[150] A. Bacchetta, M. Boglione, A. Henneman and P. J. Mulders, *Bounds on transverse momentum dependent distribution and fragmentation functions*, *Phys. Rev. Lett.* **85** (2000) 712–715, [hep-ph/9912490].

[151] A. Bacchetta and P. J. Mulders, *Positivity bounds on spin one distribution and fragmentation functions*, *Phys. Lett.* **B518** (2001) 85–93, [hep-ph/0104176].

[152] D. Boer, M. G. A. Buffing and P. J. Mulders, *Operator analysis of p_T -widths of TMDs*, *JHEP* **08** (2015) 053, [1503.03760].

[153] J. Soffer, *Positivity constraints for spin dependent parton distributions*, *Phys.Rev.Lett.* **74** (1995) 1292–1294, [hep-ph/9409254].

[154] W. Vogelsang, *Next-to-leading order evolution of transversity distributions and Soffer's inequality*, *Phys. Rev.* **D57** (1998) 1886–1894, [hep-ph/9706511].

[155] C. Bourrely, J. Soffer and O. V. Teryaev, *The Q**2 evolution of Soffer inequality*, *Phys. Lett.* **B420** (1998) 375–381, [hep-ph/9710224].

[156] O. Martin, A. Schäfer, M. Stratmann and W. Vogelsang, *Soffer's inequality and the transversely polarized Drell-Yan process at next-to-leading order*, *Phys. Rev.* **D57** (1998) 3084–3090, [hep-ph/9710300].

[157] M. G. Echevarria, A. Idilbi and I. Scimemi, *Unified treatment of the QCD evolution of all (un-)polarized transverse momentum dependent functions: Collins function as a study case*, *Phys. Rev.* **D90** (2014) 014003, [1402.0869].

[158] S. Abeyratne et al., *Science Requirements and Conceptual Design for a Polarized Medium Energy Electron-Ion Collider at Jefferson Lab*, 1209.0757.

[159] M. Diehl, J. R. Gaunt and K. Schönwald, *Double hard scattering without double counting*, *JHEP* **06** (2017) 083, [1702.06486].

[160] M. Diehl and J. R. Gaunt, *Double parton scattering theory overview*, 1710.04408.

[161] J. R. Gaunt and W. J. Stirling, *Double Parton Distributions Incorporating Perturbative QCD Evolution and Momentum and Quark Number Sum Rules*, *JHEP* **03** (2010) 005, [0910.4347].

[162] H.-M. Chang, A. V. Manohar and W. J. Waalewijn, *Double Parton Correlations in the Bag Model*, *Phys. Rev.* **D87** (2013) 034009, [1211.3132].

[163] M. Rinaldi, S. Scopetta and V. Vento, *Double parton correlations in constituent quark models*, *Phys. Rev.* **D87** (2013) 114021, [1302.6462].

[164] M. Rinaldi, S. Scopetta, M. Traini and V. Vento, *Double parton correlations and constituent quark models: a Light Front approach to the valence sector*, *JHEP* **12** (2014) 028, [1409.1500].

[165] M. Rinaldi, S. Scopetta, M. Traini and V. Vento, *Double parton scattering: a study of the effective cross section within a Light-Front quark model*, *Phys. Lett.* **B752** (2016) 40–45, [1506.05742].

[166] M. Diehl, T. Kasemets and S. Keane, *Correlations in double parton distributions: effects of evolution*, *JHEP* **05** (2014) 118, [1401.1233].

[167] M. Traini, M. Rinaldi, S. Scopetta and V. Vento, *The effective cross section for double parton scattering within a holographic AdS/QCD approach*, *Phys. Lett.* **B768** (2017) 270–273, [1609.07242].

[168] Axial Field Spectrometer collaboration, T. Akesson et al., *Double Parton Scattering in pp Collisions at $\sqrt{s} = 63$-GeV*, *Z. Phys.* **C34** (1987) 163.

[169] UA2 collaboration, J. Alitti et al., *A Study of multi - jet events at the CERN anti-p p collider and a search for double parton scattering*, *Phys. Lett.* **B268** (1991) 145–154.

[170] CDF collaboration, F. Abe et al., *Study of four jet events and evidence for double parton interactions in $p\bar{p}$ collisions at $\sqrt{s} = 1.8$ TeV*, *Phys. Rev.* **D47** (1993) 4857–4871.

[171] CMS collaboration, S. Chatrchyan et al., *Measurement of four-jet production in proton-proton collisions at* $\sqrt{s} = 7\,TeV$, *Phys. Rev.* **D89** (2014) 092010, [1312.6440].

[172] T. A. collaboration, *Study of hard double parton scattering in four-jet events in pp collisions at* $\sqrt{s} = 7$ TeV *with the ATLAS experiment at the LHC*, .

[173] CDF collaboration, F. Abe et al., *Measurement of double parton scattering in* $\bar{p}p$ *collisions at* $\sqrt{s} = 1.8$ *TeV*, *Phys. Rev. Lett.* **79** (1997) 584–589.

[174] CDF collaboration, F. Abe et al., *Double parton scattering in* $\bar{p}p$ *collisions at* $\sqrt{s} = 1.8\,TeV$, *Phys. Rev.* **D56** (1997) 3811–3832.

[175] D0 collaboration, V. M. Abazov et al., *Double Parton Interactions in* $\gamma + 3$ *Jet and* $\gamma + b/cjet + 2$ *Jet Events in* $p\bar{p}$ *Collisions at* $\sqrt{s} = 1.96$ *TeV*, *Phys. Rev.* **D89** (2014) 072006, [1402.1550].

[176] D0 collaboration, V. M. Abazov et al., *Study of double parton interactions in diphoton + dijet events in* $p\bar{p}$ *collisions at* $\sqrt{s} = 1.96$ *TeV*, *Phys. Rev.* **D93** (2016) 052008, [1512.05291].

[177] M. Myska, *Double Parton Scattering Contribution to the Same-Sign W Boson Pair Production at ATLAS*. PhD thesis, Prague, Tech. U., 2013-03-22.

[178] ATLAS collaboration, G. Aad et al., *Measurement of hard double-parton interactions in* $W(\rightarrow l\nu)$*+ 2 jet events at* $\sqrt{s}$*=7 TeV with the ATLAS detector*, *New J. Phys.* **15** (2013) 033038, [1301.6872].

[179] CMS collaboration, S. Chatrchyan et al., *Study of double parton scattering using W + 2-jet events in proton-proton collisions at* $\sqrt{s} = 7$ *TeV*, *JHEP* **03** (2014) 032, [1312.5729].

[180] CMS collaboration, C. Collaboration, *Measurement of double parton scattering in same-sign WW production in p-p collisions at* $\sqrt{s} = 13$ TeV *with the CMS experiment*, .

[181] ALICE collaboration, B. Abelev et al., J/ψ *Production as a Function of Charged Particle Multiplicity in pp Collisions at* $\sqrt{s} = 7$ *TeV*, *Phys. Lett.* **B712** (2012) 165–175, [1202.2816].

[182] LHCb collaboration, R. Aaij et al., *Observation of double charm production involving open charm in pp collisions at* $\sqrt{s} = 7$ *TeV*, *JHEP* **06** (2012) 141, [1205.0975].

[183] CMS collaboration, V. Khachatryan et al., *Measurement of prompt J/ψ pair production in pp collisions at $\sqrt{s}$ = 7 Tev*, *JHEP* **09** (2014) 094, [1406.0484].

[184] LHCb collaboration, R. Aaij et al., *Measurement of the J/ψ pair production cross-section in pp collisions at $\sqrt{s} = 13$ TeV*, *JHEP* **06** (2017) 047, [1612.07451].

[185] Q.-H. Cao, Y. Liu, K.-P. Xie and B. Yan, *Double parton scattering of weak gauge boson productions at the 13 TeV and 100 TeV proton-proton colliders*, *Phys. Rev.* **D97** (2018) 035013, [1710.06315].

[186] ATLAS collaboration, M. Aaboud et al., *Measurement of the prompt J/ψ pair production cross-section in pp collisions at $\sqrt{s} = 8$ TeV with the ATLAS detector*, *Eur. Phys. J.* **C77** (2017) 76, [1612.02950].

[187] CMS collaboration, C. Collaboration, *Double Parton Scattering cross section limit from same-sign W bosons pair production in di-muon final state at LHC*, .

[188] D0 collaboration, V. M. Abazov et al., *Observation and studies of double J/ψ production at the Tevatron*, *Phys. Rev.* **D90** (2014) 111101, [1406.2380].

[189] A. Kulesza and W. J. Stirling, *Like sign W boson production at the LHC as a probe of double parton scattering*, *Phys. Lett.* **B475** (2000) 168–175, [hep-ph/9912232].

[190] E. Maina, *Multiple Parton Interactions in Z+4j, W+- W+- + 0/2j and W+ W- + 2j production at the LHC*, *JHEP* **09** (2009) 081, [0909.1586].

[191] J. R. Gaunt, C.-H. Kom, A. Kulesza and W. J. Stirling, *Same-sign W pair production as a probe of double parton scattering at the LHC*, *Eur. Phys. J.* **C69** (2010) 53–65, [1003.3953].

[192] F. A. Ceccopieri, M. Rinaldi and S. Scopetta, *Parton correlations in same-sign W pair production via double parton scattering at the LHC*, *Phys. Rev.* **D95** (2017) 114030, [1702.05363].

[193] T. Kasemets and S. Scopetta, *Parton correlations in double parton scattering*, 1712.02884.

[194] T. Kasemets and P. J. Mulders, *Constraining double parton correlations and interferences*, *Phys. Rev.* **D91** (2015) 014015, [1411.0726].

[195] R. D. Tangerman and P. J. Mulders, *Intrinsic transverse momentum and the polarized Drell-Yan process*, *Phys. Rev.* **D51** (1995) 3357–3372, [hep-ph/9403227].

[196] M. Diehl and P. Kroll, *Nucleon form factors, generalized parton distributions and quark angular momentum*, *Eur.Phys.J.* **C73** (2013) 2397, [1302.4604].

[197] M. Diehl, *Generalized parton distributions with helicity flip*, *Eur.Phys.J.* **C19** (2001) 485–492, [hep-ph/0101335].

[198] M. Mekhfi, *Correlations in Color and Spin in Multiparton Processes*, *Phys. Rev.* **D32** (1985) 2380.

[199] A. V. Manohar and W. J. Waalewijn, *A QCD Analysis of Double Parton Scattering: Color Correlations, Interference Effects and Evolution*, *Phys. Rev.* **D85** (2012) 114009, [1202.3794].

[200] T. Kasemets and M. Diehl, *Angular correlations in the double Drell-Yan process*, *JHEP* **01** (2013) 121, [1210.5434].

[201] M. G. Echevarria, T. Kasemets, P. J. Mulders and C. Pisano, *Polarization effects in double open-charm production at LHCb*, *JHEP* **04** (2015) 034, [1501.07291].

[202] R. Kirschner, *Generalized Lipatov-Altarelli-Parisi Equations and Jet Calculus Rules*, *Phys. Lett.* **84B** (1979) 266–270.

[203] V. P. Shelest, A. M. Snigirev and G. M. Zinovev, *The Multiparton Distribution Equations in QCD*, *Phys. Lett.* **113B** (1982) 325.

[204] A. Martin, W. Stirling, R. Thorne and G. Watt, *Parton distributions for the LHC*, *Eur.Phys.J.* **C63** (2009) 189–285, [0901.0002].

[205] M. Diehl, T. Feldmann, R. Jakob and P. Kroll, *Generalized parton distributions from nucleon form-factor data*, *Eur. Phys. J.* **C39** (2005) 1–39, [hep-ph/0408173].

[206] C. Goebel, F. Halzen and D. M. Scott, *Double Drell-Yan Annihilations in Hadron Collisions: Novel Tests of the Constituent Picture*, *Phys. Rev.* **D22** (1980) 2789.

[207] M. Mekhfi, *Multiparton processes: an application to double Drell-Yan*, *Phys. Rev.* **D32** (1985) 2371.

[208] Particle Data Group collaboration, C. Patrignani et al., *Review of Particle Physics*, *Chin. Phys.* **C40** (2016) 100001.

[209] M. Diehl and T. Kasemets, *Positivity bounds on double parton distributions*, *JHEP* **05** (2013) 150, [1303.0842].

[210] T. Hahn, *CUBA: A Library for multidimensional numerical integration*, *Comput. Phys. Commun.* **168** (2005) 78–95, [hep-ph/0404043].

[211] J. Bellm et al., *Herwig 7.0/Herwig++ 3.0 release note*, *Eur. Phys. J.* **C76** (2016) 196, [1512.01178].

[212] T. Sjöstrand:, S. Mrenna and P. Z. Skands, *A Brief Introduction to PYTHIA 8.1*, *Comput. Phys. Commun.* **178** (2008) 852–867, [0710.3820].

[213] S. Cotogno, T. Kasemets and M. Myska, *Parton correlations in same sign W boson pair production at the LHC*, *in preparation* (2018) .

[214] J. Alwall, R. Frederix, S. Frixione, V. Hirschi, F. Maltoni, O. Mattelaer et al., *The automated computation of tree-level and next-to-leading order differential cross sections, and their matching to parton shower simulations*, *JHEP* **07** (2014) 079, [1405.0301].

[215] ATLAS collaboration, *Measuring the b-tag efficiency in a top-pair sample with 4.7 fb^{-1} of data from the ATLAS detector*, .

[216] CMS collaboration, C. Collaboration, *Identification of b quark jets at the CMS Experiment in the LHC Run 2*, .

[217] CMS collaboration, S. Chatrchyan et al., *Performance of CMS muon reconstruction in pp collision events at $\sqrt{s} = 7$ TeV*, *JINST* **7** (2012) P10002, [1206.4071].

[218] H. Yukawa, *On the Interaction of Elementary Particles I*, *Proc. Phys. Math. Soc. Jap.* **17** (1935) 48–57.

[219] G. P. S. Occhialini and C. F. Powell, *Nuclear disintegration produced by slow charged particles of small mass*, .

[220] C. D. Roberts, *Perspective on the origin of hadron masses*, *Few Body Syst.* **58** (2017) 5, [1606.03909].

[221] T. Horn and C. D. Roberts, *The pion: an enigma within the Standard Model*, *J. Phys.* **G43** (2016) 073001, [1602.04016].

[222] J. P. B. C. de Melo, T. Frederico, E. Pace and G. Salmè, *Electromagnetic form-factor of the pion in the space and time - like regions within the front form dynamics*, *Phys. Lett.* **B581** (2004) 75–81, [hep-ph/0311369].

[223] J. P. B. C. de Melo, T. Frederico, E. Pace and G. Salmè, *Space-like and time-like pion electromagnetic form-factor and Fock state components within the light-front dynamics*, *Phys. Rev.* **D73** (2006) 074013, [hep-ph/0508001].

[224] L. Chang, I. C. Cloët, C. D. Roberts, S. M. Schmidt and P. C. Tandy, *Pion electromagnetic form factor at spacelike momenta*, *Phys. Rev. Lett.* **111** (2013) 141802, [1307.0026].

[225] E. Ruiz Arriola and W. Broniowski, *Pion transition form factor in the Regge approach and incomplete vector-meson dominance*, *Phys. Rev.* **D81** (2010) 094021, [1004.0837].

[226] A. E. Dorokhov and E. A. Kuraev, *Pion transition form factor in the constituent quark model*, *Phys. Rev.* **D88** (2013) 014038, [1305.0888].

[227] A. V. Radyushkin, *Shape of Pion Distribution Amplitude*, *Phys. Rev.* **D80** (2009) 094009, [0906.0323].

[228] D. G. Dumm, S. Noguera, N. N. Scoccola and S. Scopetta, *Pion distribution amplitude and the pion-photon transition form factor in a nonlocal chiral quark model*, *Phys. Rev.* **D89** (2014) 054031, [1311.3595].

[229] L. Chang, C. Mezrag, H. Moutarde, C. D. Roberts, J. Rodrguez-Quintero and P. C. Tandy, *Basic features of the pion valence-quark distribution function*, *Phys. Lett.* **B737** (2014) 23–29, [1406.5450].

[230] N. Chouika, C. Mezrag, H. Moutarde and J. Rodrguez-Quintero, *An algebraic model for the pion's valence-quark GPD*, *Few Body Syst.* **58** (2017) 144, [1612.01176].

[231] C. Chen, L. Chang, C. D. Roberts, S. Wan and H.-S. Zong, *Valence-quark distribution functions in the kaon and pion*, *Phys. Rev.* **D93** (2016) 074021, [1602.01502].

[232] P. C. Barry, N. Sato, W. Melnitchouk and C.-R. Ji, *First Monte Carlo global QCD analysis of pion parton distributions*, 1804.01965.

[233] A. Mukherjee, I. V. Musatov, H. C. Pauli and A. V. Radyushkin, *Power law wave functions and generalized parton distributions for pion*, *Phys. Rev.* **D67** (2003) 073014, [hep-ph/0205315].

[234] B. C. Tiburzi and G. A. Miller, *Generalized parton distributions and double distributions for q anti-q pions*, *Phys. Rev.* **D67** (2003) 113004, [hep-ph/0212238].

[235] C.-R. Ji, Y. Mishchenko and A. Radyushkin, *Higher Fock state contributions to the generalized parton distribution of pion*, *Phys. Rev.* **D73** (2006) 114013, [hep-ph/0603198].

[236] T. Frederico, E. Pace, B. Pasquini and G. Salmè, *Pion Generalized Parton Distributions with covariant and Light-front constituent quark models*, *Phys.Rev.* **D80** (2009) 054021, [0907.5566].

[237] A. E. Dorokhov, W. Broniowski and E. Ruiz Arriola, *Generalized Quark Transversity Distribution of the Pion in Chiral Quark Models*, *Phys. Rev.* **D84** (2011) 074015, [1107.5631].

[238] C. Fanelli, E. Pace, G. Romanelli, G. Salmè and M. Salmistraro, *Pion Generalized Parton Distributions within a fully covariant constituent quark model*, *Eur. Phys. J.* **C76** (2016) 253, [1603.04598].

[239] C. Mezrag, L. Chang, H. Moutarde, C. D. Roberts, J. Rodríguez-Quintero, F. Sabatié et al., *Sketching the pion's valence-quark generalised parton distribution*, *Phys. Lett.* **B741** (2015) 190–196, [1411.6634].

[240] C. Lorcé, B. Pasquini and P. Schweitzer, *Transverse pion structure beyond leading twist in constituent models*, *Eur. Phys. J.* **C76** (2016) 415, [1605.00815].

[241] S. Noguera and S. Scopetta, *Pion transverse momentum dependent parton distributions in the Nambu and Jona-Lasinio model*, *JHEP* **11** (2015) 102, [1508.01061].

[242] A. Bacchetta, R. Kundu, A. Metz and P. J. Mulders, *Estimate of the Collins fragmentation function in a chiral invariant approach*, *Phys. Rev.* **D65** (2002) 094021, [hep-ph/0201091].

[243] A. Bacchetta, L. P. Gamberg, G. R. Goldstein and A. Mukherjee, *Collins fragmentation function for pions and kaons in a spectator model*, *Phys. Lett.* **B659** (2008) 234–243, [0707.3372].

[244] H. H. Matevosyan, W. Bentz, I. C. Cloët and A. W. Thomas, *Transverse Momentum Dependent Fragmentation and Quark Distribution Functions from the NJL-jet Model*, *Phys. Rev.* **D85** (2012) 014021, [1111.1740].

[245] S.-i. Nam and C.-W. Kao, *Fragmentation functions and parton distribution functions for the pion with the nonlocal interactions*, *Phys. Rev.* **D85** (2012) 034023, [1111.4444].

[246] J. Dudek et al., *Physics Opportunities with the 12 GeV Upgrade at Jefferson Lab*, *Eur. Phys. J.* **A48** (2012) 187, [1208.1244].

[247] R. J. Holt and P. E. Reimer, *Structure of the Goldstone bosons*, *AIP Conf. Proc.* **588** (2001) 234–239, [nucl-ex/0010004].

[248] COMPASS collaboration, F. Gautheron et al., *COMPASS-II Proposal*, .

[249] P. Maris, C. D. Roberts and P. C. Tandy, *Pion mass and decay constant*, *Phys. Lett.* **B420** (1998) 267–273, [nucl-th/9707003].

[250] S. J. Brodsky, G. F. de Téramond, H. G. Dosch and J. Erlich, *Light-Front Holographic QCD and Emerging Confinement*, *Phys. Rept.* **584** (2015) 1–105, [1407.8131].

[251] S. J. Brodsky and G. F. de Téramond, *Hadronic spectra and light-front wavefunctions in holographic QCD*, *Phys. Rev. Lett.* **96** (2006) 201601, [hep-ph/0602252].

[252] G. F. de Téramond and S. J. Brodsky, *Light-Front Holography: A First Approximation to QCD*, *Phys.Rev.Lett.* **102** (2009) 081601, [0809.4899].

[253] B. Pasquini, M. Pincetti and S. Boffi, *Drell-Yan processes, transversity and light-cone wavefunctions*, *Phys. Rev.* **D76** (2007) 034020, [hep-ph/0612094].

[254] S. Boffi and B. Pasquini, *Generalized parton distributions and the structure of the nucleon*, *Riv.Nuovo Cim.* **30** (2007) 387, [0711.2625].

[255] B. Pasquini and F. Yuan, *Sivers and Boer-Mulders functions in Light-Cone Quark Models*, *Phys. Rev.* **D81** (2010) 114013, [1001.5398].

[256] C. Lorcé, B. Pasquini, X. Xiong and F. Yuan, *The quark orbital angular momentum from Wigner distributions and light-cone wave functions*, *Phys. Rev.* **D85** (2012) 114006, [1111.4827].

[257] M. Diehl, T. Feldmann, R. Jakob and P. Kroll, *Linking parton distributions to form-factors and Compton scattering*, *Eur. Phys. J.* **C8** (1999) 409–434, [hep-ph/9811253].

[258] J. M. Maldacena, *The Large N limit of superconformal field theories and supergravity*, *Int.J.Theor.Phys.* **38** (1999) 1113–1133, [hep-th/9711200].

[259] E. Witten, *Anti-de Sitter space and holography*, *Adv.Theor.Math.Phys.* **2** (1998) 253–291, [hep-th/9802150].

[260] A. Karch, E. Katz, D. T. Son and M. A. Stephanov, *Linear confinement and AdS/QCD*, *Phys. Rev.* **D74** (2006) 015005, [hep-ph/0602229].

[261] S. J. Brodsky and G. F. de Téramond, *Light-Front Dynamics and AdS/QCD Correspondence: The Pion Form Factor in the Space- and Time-Like Regions*, *Phys.Rev.* **D77** (2008) 056007, [0707.3859].

[262] A. P. Trawiński, S. D. Glazek, S. J. Brodsky, G. F. de Téramond and H. G. Dosch, *Effective confining potentials for QCD*, *Phys. Rev.* **D90** (2014) 074017, [1403.5651].

[263] J. Erlich, E. Katz, D. T. Son and M. A. Stephanov, *QCD and a holographic model of hadrons*, *Phys. Rev. Lett.* **95** (2005) 261602, [hep-ph/0501128].

[264] L. Da Rold and A. Pomarol, *Chiral symmetry breaking from five dimensional spaces*, *Nucl. Phys.* **B721** (2005) 79–97, [hep-ph/0501218].

[265] J. Polchinski and M. J. Strassler, *Hard scattering and gauge / string duality*, *Phys. Rev. Lett.* **88** (2002) 031601, [hep-th/0109174].

[266] J. Polchinski and M. J. Strassler, *Deep inelastic scattering and gauge / string duality*, *JHEP* **05** (2003) 012, [hep-th/0209211].

[267] S. J. Brodsky, F.-G. Cao and G. F. de Téramond, *Meson Transition Form Factors in Light-Front Holographic QCD*, *Phys.Rev.* **D84** (2011) 075012, [1105.3999].

[268] J. R. Forshaw and R. Sandapen, *An AdS/QCD holographic wavefunction for the rho meson and diffractive rho meson electroproduction*, *Phys. Rev. Lett.* **109** (2012) 081601, [1203.6088].

[269] A. Vega, I. Schmidt, T. Branz, T. Gutsche and V. E. Lyubovitskij, *Meson wave function from holographic models*, *Phys. Rev.* **D80** (2009) 055014, [0906.1220].

[270] T. Gutsche, V. E. Lyubovitskij, I. Schmidt and A. Vega, *Pion light-front wave function, parton distribution and the electromagnetic form factor*, *J. Phys.* **G42** (2015) 095005, [1410.6424].

[271] R. Swarnkar and D. Chakrabarti, *Meson structure in light-front holographic QCD*, *Phys. Rev.* **D92** (2015) 074023, [1507.01568].

[272] M. Ahmady, F. Chishtie and R. Sandapen, *Spin effects in the pion holographic light-front wavefunction*, *Phys. Rev.* **D95** (2017) 074008, [1609.07024].

[273] D. Chakrabarti and C. Mondal, *Generalized Parton Distributions for the Proton in AdS/QCD*, *Phys. Rev.* **D88** (2013) 073006, [1307.5128].

[274] T. Gutsche, V. E. Lyubovitskij, I. Schmidt and A. Vega, *Light-front quark model consistent with Drell-Yan-West duality and quark counting rules*, *Phys. Rev.* **D89** (2014) 054033, [1306.0366].

[275] C. Mondal and D. Chakrabarti, *Generalized parton distributions and transverse densities in a light-front quarkdiquark model for the nucleons*, *Eur. Phys. J.* **C75** (2015) 261, [1501.05489].

[276] D. Chakrabarti and C. Mondal, *Chiral-odd generalized parton distributions for proton in a light-front quark-diquark model*, *Phys. Rev.* **D92** (2015) 074012, [1509.00598].

[277] T. Liu and B.-Q. Ma, *Baryon properties from light-front holographic QCD*, *Phys. Rev.* **D92** (2015) 096003, [1510.07783].

[278] M. Aghasyan, H. Avakian, E. De Sanctis, L. Gamberg, M. Mirazita, B. Musch et al., *Studies of Transverse Momentum Dependent Parton Distributions and Bessel Weighting*, *JHEP* **03** (2015) 039, [1409.0487].

[279] T. Maji, C. Mondal, D. Chakrabarti and O. V. Teryaev, *Relating transverse structure of various parton distributions*, *JHEP* **01** (2016) 165, [1506.04560].

[280] T. Maji and D. Chakrabarti, *Light front quark-diquark model for the nucleons*, *Phys. Rev.* **D94** (2016) 094020, [1608.07776].

[281] D. Chakrabarti, T. Maji, C. Mondal and A. Mukherjee, *Wigner distributions and orbital angular momentum of a proton*, *Eur. Phys. J.* **C76** (2016) 409, [1601.03217].

[282] A. Bacchetta, S. Cotogno and B. Pasquini, *Internal Structure of the Pion Inspired by the AdS/QCD Correspondence*, *Few Body Syst.* **57** (2016) 443–447.

[283] M. C. Traini, *Generalized Parton Distributions: confining potential effects within AdS/QCD*, *Eur. Phys. J.* **C77** (2017) 246, [1608.08410].

[284] M. Rinaldi, *GPDs at non-zero skewness in ADS/QCD model*, *Phys. Lett.* **B771** (2017) 563–567, [1703.00348].

[285] S. J. Brodsky and G. F. de Téramond, *AdS/CFT and Light-Front QCD*, *Subnucl. Ser.* **45** (2009) 139–183, [0802.0514].

[286] NA7 collaboration, S. R. Amendolia et al., *A Measurement of the Space - Like Pion Electromagnetic Form-Factor*, *Nucl. Phys.* **B277** (1986) 168.

[287] C. J. Bebek et al., *Electroproduction of single pions at low epsilon and a measurement of the pion form-factor up to q^2 = 10-GeV^2*, *Phys. Rev.* **D17** (1978) 1693.

[288] Jefferson Lab collaboration, G. M. Huber et al., *Charged pion form-factor between Q**2 = 0.60-GeV**2 and 2.45-GeV**2. II. Determination of, and results for, the pion form-factor*, *Phys. Rev.* **C78** (2008) 045203, [0809.3052].

[289] K. Wijesooriya, P. E. Reimer and R. J. Holt, *The pion parton distribution function in the valence region*, *Phys. Rev.* **C72** (2005) 065203, [nucl-ex/0509012].

[290] G. P. Salam and J. Rojo, *A Higher Order Perturbative Parton Evolution Toolkit (HOPPET)*, *Comput. Phys. Commun.* **180** (2009) 120–156, [0804.3755].

[291] H. Ackermann, T. Azemoon, W. Gabriel, H. D. Mertiens, H. D. Reich, G. Specht et al., *Determination of the Longitudinal and the Transverse Part in pi+ Electroproduction*, *Nucl. Phys.* **B137** (1978) 294–300.

[292] P. Brauel, T. Canzler, D. Cords, R. Felst, G. Grindhammer, M. Helm et al., *Electroproduction of $\pi^+ n$, $\pi^- p$ and $K^+\Lambda$, $K^+\Sigma^0$ Final States Above the Resonance Region*, *Z. Phys.* **C3** (1979) 101.

[293] T. Branz, T. Gutsche, V. E. Lyubovitskij, I. Schmidt and A. Vega, *Light and heavy mesons in a soft-wall holographic approach*, *Phys. Rev.* **D82** (2010) 074022, [1008.0268].

[294] P. Colangelo, F. De Fazio, F. Giannuzzi, F. Jugeau and S. Nicotri, *Light scalar mesons in the soft-wall model of AdS/QCD*, *Phys. Rev.* **D78** (2008) 055009, [0807.1054].

[295] H. Forkel, M. Beyer and T. Frederico, *Linear square-mass trajectories of radially and orbitally excited hadrons in holographic QCD*, *JHEP* **07** (2007) 077, [0705.1857].

[296] S. J. Brodsky, G. F. de Téramond, H. G. Dosch and C. Lorcé, *Meson/Baryon/Tetraquark Supersymmetry from Superconformal Algebra and Light-Front Holography*, *Int. J. Mod. Phys.* **A31** (2016) 1630029, [1606.04638].

[297] A. Deur, S. J. Brodsky and G. F. de Téramond, *Determination of $\Lambda_{\bar{M}S}$ at five loops from holographic QCD*, *J. Phys.* **G44** (2017) 105005, [1608.04933].

[298] A. Deur, S. J. Brodsky and G. F. de Téramond, *On the Interface between Perturbative and Nonperturbative QCD*, *Phys. Lett.* **B757** (2016) 275–281, [1601.06568].

[299] A. Deur, S. J. Brodsky and G. F. de Téramond, *The QCD Running Coupling*, *Prog. Part. Nucl. Phys.* **90** (2016) 1–74, [1604.08082].

[300] T. C. Rogers, *An overview of transverse-momentumdependent factorization and evolution*, *Eur. Phys. J.* **A52** (2016) 153, [1509.04766].

[301] J. Collins and T. Rogers, *Understanding the large-distance behavior of transverse-momentum-dependent parton densities and the Collins-Soper evolution kernel*, *Phys. Rev.* **D91** (2015) 074020, [1412.3820].

[302] I. Scimemi and A. Vladimirov, *Power corrections and renormalons in Transverse Momentum Distributions*, *JHEP* **03** (2017) 002, [1609.06047].

[303] E. Laenen, G. F. Sterman and W. Vogelsang, *Higher order QCD corrections in prompt photon production*, *Phys. Rev. Lett.* **84** (2000) 4296–4299, [hep-ph/0002078].

[304] A. Bacchetta, M. G. Echevarria, P. J. G. Mulders, M. Radici and A. Signori, *Effects of TMD evolution and partonic flavor on e^+ e annihilation into hadrons*, *JHEP* **11** (2015) 076, [1508.00402].

[305] I. Scimemi and A. Vladimirov, *Systematic analysis of double-scale evolution*, 1803.11089.

[306] S. Aybat and T. C. Rogers, *TMD Parton Distribution and Fragmentation Functions with QCD Evolution*, *Phys.Rev.* **D83** (2011) 114042, [1101.5057].

[307] S. Frixione, P. Nason and G. Ridolfi, *Problems in the resummation of soft gluon effects in the transverse momentum distributions of massive vector bosons in hadronic collisions*, *Nucl. Phys.* **B542** (1999) 311–328, [hep-ph/9809367].

[308] M. G. Echevarria, A. Idilbi, A. Schfer and I. Scimemi, *Model-Independent Evolution of Transverse Momentum Dependent Distribution Functions (TMDs) at NNLL*, *Eur. Phys. J.* **C73** (2013) 2636, [1208.1281].

[309] G. Altarelli and G. Parisi, *Asymptotic Freedom in Parton Language*, *Nucl. Phys.* **B126** (1977) 298–318.

[310] Y. L. Dokshitzer, *Calculation of the Structure Functions for Deep Inelastic Scattering and e+ e- Annihilation by Perturbation Theory in Quantum Chromodynamics.*, *Sov. Phys. JETP* **46** (1977) 641–653.

[311] S. J. Brodsky, G. F. de Teramond and A. Deur, *Nonperturbative QCD Coupling and its β-function from Light-Front Holography*, *Phys. Rev.* **D81** (2010) 096010, [1002.3948].

[312] A. Deur, S. J. Brodsky and G. F. de Téramond, *Connecting the Hadron Mass Scale to the Fundamental Mass Scale of Quantum Chromodynamics*, *Phys. Lett.* **B750** (2015) 528–532, [1409.5488].

[313] A. Deur, V. Burkert, J.-P. Chen and W. Korsch, *Experimental determination of the effective strong coupling constant*, *Phys. Lett.* **B650** (2007) 244–248, [hep-ph/0509113].